NONLINEAR PROPAGATION OF INCOHERENT WHITE LIGHT IN A PHOTOPOLYMERISABLE MEDIUM: FROM SINGLE SELF-TRAPPED BEAMS TO 2-D AND 3-D LATTICES

NONLINEAR PROPAGATION OF INCOHERENT WHITE

LIGHT IN A PHOTOPOLYMERISABLE MEDIUM: FROM

SINGLE SELF-TRAPPED BEAMS TO 2-D AND 3-D

LATTICES

By

KAILASH KASALA, B. Sc., M.Sc.,

A Thesis

Submitted to the School of Graduate Studies

in Partial Fulfillment of the Requirements

for the Degree

Doctor of Philosophy in Chemistry

McMaster University

DOCTOR OF PHILOSOPHY (200512)   McMaster University

(Chemistry)   Hamilton, Ontario

TITLE: Nonlinear propagation of incoherent white light in a photopolymerizable medium: From single self-trapped beams to 2-D and 3-D lattices

AUTHOR: Kailash Kasala, B.Sc, M.Sc. (Indian Institute of Technology Kharagpur, India)

SUPERVISOR: Dr. Kalaichelvi Saravanamuttu

NUMBER OF PAGES: 241

Abstract

Optical beams that travel through a material without undergoing divergence are known as self-trapped beams. Self-trapping occurs when a beam induces a suitable index gradient in the medium that is capable of guiding the original beam. An incoherent white light beam consists of femtosecond scale speckles, due to random phase fluctuations and such beams were not thought to self-trap until recently. In 1997, Mitchell et al., showed that white light beams can self-trap, provided the medium cannot respond fast enough to form index gradients to these speckles individually. However, detailed studies with incoherent beams have been hampered by a lack of suitable materials and strategies for enabling such a response. In 2006, our group showed that a photopolymerizable system is suitable for incoherent self-trapping, since the index change is governed by an inherently slow rate of polymerization (of the order of milliseconds). The demonstration of self-trapping with a single incoherent white light beam in this medium has enabled further studies of various phenomena with white light self-trapping.

The studies here show (i) the first direct experimental evidence of interactions of two incoherent white light self-trapped beams, as well as fission, fusion as well as repulsion. Existence of dark self-trapping beams with incoherent white light was also shown, counter intuitively in a positive nonlinear medium. Corresponding detailed studies of their dynamics including theoretical simulations were done in order to understand the mechanism involved. (iii) 2D and 3D lattices were formed with multiple ordered bright as well as dark self-trapping filaments. These showed rearrangements within lattices and the

ability of dark beams to control bright interstitial regions. (iv) Woodpile-like 3D lattices with bright and dark beams were demonstrated and simulations showed theoretical band gaps. (v) Self-trapping of a co-axial beam of incoherent white light was also shown experimentally and through simulations.

Acknowledgements

Table of Contents

Table of Figures

1. Introduction

1.1. Nonlinear wave propagation

Waves can exist in many different systems – fluid dynamics, acoustics and optics – and form sound, light, water waves, etc. The simplest wave equation is linear and these waves follow a superposition principle (for instance, the net amplitude of two optical waves at a point in space is the sum of the amplitude of each wave at that point). Nonlinear waves are special cases where the superposition principle does not hold, and commonly exist in many of these systems as well, such as tsunami ocean waves or a sonic boom of a jet plane, for instance. These examples are self-reinforcing waves and are described by nonlinear wave equations (such as the nonlinear Schrödinger equation in optics). In optical waves, nonlinearity occurs typically at high intensities and results in a wide range of optical phenomena - higher harmonic generation, optical parametric amplification, self and cross-phase modulation, two photon absorption, modulation instability, bright and dark self-trapping, etc. Of this rich variety of phenomena, optical self-trapping is one of the most fundamental and is also described by the nonlinear Schrödinger equation.

1.1.1. Self-trapped light beams

An optical beam that passes through a medium undergoes natural divergence due to diffraction. Under certain conditions, the diffraction can be suppressed and the beam is said to undergo 'self-trapping'. Self-focusing, a precursor to self-trapping occurs when a medium provides a refractive index gradient (induced by the beam itself) that can act as a

lens causing the beam to focus. This index change is induced by the nonlinear response of a material to an optical field (such as Kerr effect, for instance). Only when the self-focusing tendency of a beam exactly balances out its natural divergence, the beam travels with a steady stationary profile and is called a soliton.[1] Solitons are therefore a special case of self-trapped beams and the term self-trapped beams will be used in the context of the research presented here.

Self-trapping is a common effect in nature, and is seen in any media supporting nonlinear waves such as sound waves or water waves. Optical self-trapping was discovered relatively recently[2,3] – only after the invention of the laser, which made high beam intensities available, enabling significant nonlinear optical response in materials (i.e. their ability to exhibit an intensity dependent refractive index change). Initially, they were observed in glass[2], sodium vapor[4], CS_2. Later, they were also shown to exist in other media such as photorefractive media[5], polymers[6], liquid crystals[7], semiconductors[8] and air.[9] Optical self-trapping has even been predicted to be possible in vacuum.[10] A basic classification of self-trapping is based on the type of supporting medium. Each of these beams can further be classified as bright, or dark depending on their intensity gradient.[11] In the former case, the beam has a higher intensity near the centre, (its intensity profile has a hump) and the surrounding environment is dark. In the latter case, the intensity profile is exactly the opposite, with a dark centre and a bright surrounding environment. Dark beams are discussed in detail later in section 1.4, the next few sections discuss only bright self-trapping for simplicity. Related phenomena such as modulation instability that forms patterned self-trapping beams are also discussed in detail in section 1.5.3.

Self-trapped beams can be generated with different degrees of coherence of a source beam. A spatially coherent beam always has correlation at any instant, in the phases of the wavetrains at any two separate points in the spatial profile of the beam. A temporally coherent beam always has correlation at any point in space, in the phases of the wavetrains at any two distinct times. Spatial self-trapping can be achieved when a beam profile is preserved over space. Separately, a beam profile can be preserved over time for temporal self-trapping. When both occur simultaneously, i.e. when a beam profile is preserved over both space and time simultaneously, then it is a spatiotemporally self-trapped beam.

If a beam does not have spatial correlation, then any two different points of the beam can reach a maximum independently of the other, resulting in the formation of speckles - bright intensity spots that appear at random in the beam. Similarly, a temporally incoherent wave consists of wave trains that are short and uncorrelated –two points of the wavetrain separated in time can maximize independently of one another, i.e. they appear in a random order temporally (Figure 1). If the correlation is not complete, then the beam is partially coherent – such beams can also self-trap. On the other hand, if the beam has neither spatial nor temporal correlation, it can still self-trap[12], to form an *incoherent* self-trapped beam. Such beams are typically generated by incandescent sources, where the radiation is emitted through random relaxations from multiple excited states, giving rise to unsynchronized wave trains. Such a beam therefore has no spatial or temporal coherence, and the constituent wave trains span the full visible spectrum in wavelength.
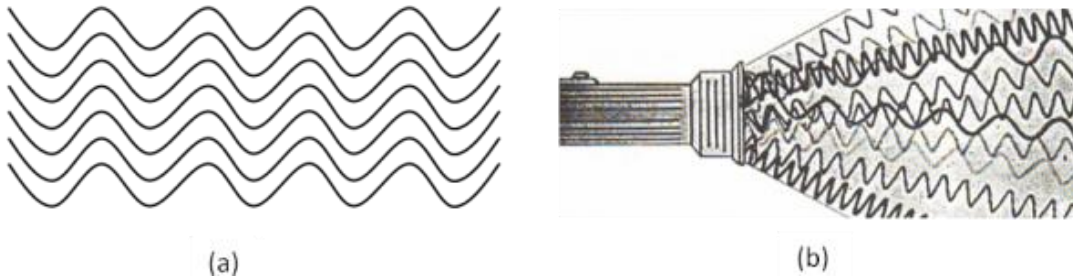
Figure 1.Comparison between constituent waves of (a) a spatially and temporally correlated beam (monochromatic laser light) and (b) a spatially and temporally uncorrelated beam of incandescent white light.

A coherent beam self-traps when the medium it propagates through, responds nonlinearly to incident light intensity to form a light-confining refractive index gradient. The resulting index gradient then confines and guides the light that initially induced it, to form a self-trapped waveguide along its propagation path. Previous studies include both experimental and theoretical research demonstrating coherent self-trapping[13,14] with most recent studies shown in nonlocal media.[15] A partially spatially incoherent beam self-traps when the medium has a response time longer than the lifetime of individual speckles in the beam. The individual speckles that cause incoherence are then masked from the nonlinear response of the medium and can then collectively form a common smooth index gradient, leading to a single self-trapping beam.[16] Several theoretical studies have been made in order to understand how such a beam can self-trap.[17,18,19,20,21,22,23,24] Later studies have shown the underlying equivalence of these separate studies[25,26,27,28] Recently, partially incoherent beams have also been shown to self-trap in nonlocal media[29] and their mechanism has been analyzed theoretically.[30] Incandescently generated spatially and temporally incoherent white light beams that are polychromatic in nature also self-trap.

This happens when additionally each individual frequency self-adjusts its correlation distance (i.e. degree of coherence) so that wave trains spanning the entire spectrum of frequencies can propagate through one single induced waveguide. This self-trapping has been studied in depth theoretically[31,32,33,34,35,36] although experimental studies are relatively few.[12]

This thesis researches exclusively of self-trapping in the spatial domain (not the temporal domain) with an incoherent white light beam. An incoherent self-trapping beam is a special case of self-trapping beams, and is formed only when certain medium-specific requirements are met. Such a beam therefore has two associated aspects – the first is nonlinearity of a material and how it affects a light wave; the second is the collective process of self-trapping an optically incoherent wave consisting of random phase fluctuations. The latter is made possible only if certain special conditions are fulfilled by a nonlinear medium. The next section explains basic aspects of nonlinearity and incoherence with respect to a single propagating beam. The subsequent section reviews coherence in self-trapping.

1.1.2. The Nonlinear Schrodinger equation

The nonlinear Schrödinger equation is the central equation governing most nonlinear optical phenomena and especially optical self-trapping. It is derived from Maxwell equations for the electric field associated with a propagating wave in a nonlinear medium. Nonlinearity of a medium itself can be of several different types – such as Kerr or Pockels or photorefractive effect (these are explained in detail in the next section).

Nonlinearity essentially makes the refractive index of a medium dependent on the intensity of a propagating wave even though individual mechanisms may be very different in each medium. Another important optical phenomenon is the spatial broadening of a light wave through diffraction. A balance of broadening through diffraction and self-reinforcing of a light wave through nonlinearity results in optical self-trapping. A derivation of the nonlinear Schrödinger equation for the specific case of nonlinear light propagation in nonlinear materials with high order susceptibilities is described below.

In such materials, a refractive index change originating from higher order polarization terms of the medium is induced. The polarization in the medium is in turn, induced by the incident beam itself. For an electromagnetic wave (of field strength E) traveling in vacuum, the electric displacement vector D is given by $D = \varepsilon_0 E$ (where ε_0 is the permittivity of free space). In a material however, this is modified to $D = \varepsilon_0 E + P = \varepsilon E$ where P is the polarization in the material and ε is the permeability of the medium. Since polarization modifies the displacement vector D, it can be used in turn, to modify a passing electromagnetic beam through refractive index changes, as follows:

For a linear medium, the polarization (P) in the material is defined as[37] $P = \varepsilon_0 \chi(1) E$, where, $\chi(1)$ is the linear susceptibility of the medium and E is the electric field vector of the wave. However, for a medium with a nonlinear response, this equation is modified to include the higher order susceptibility terms $P = \varepsilon_0 [\chi(1)E + \chi(2)E^2 + \chi(3)E^3 + \ldots]$, where $\chi(2)$ and $\chi(3)$ are the quadratic and cubic susceptibility tensors of the medium. Plugging this

into $\varepsilon_0 E + P = \varepsilon E$ gives an expansion for ε in terms of $\chi(1)$, $\chi(2)$, $\chi(3)$,etc. For the simplest case where $\chi(2)=0$ (centrosymmetric medium), $\varepsilon = \varepsilon_0 + \varepsilon_2 \overline{E^2}$ (and $\varepsilon_2 = \varepsilon_0 \chi(3)$).

Since the refractive index is given by $n = \sqrt{\varepsilon}$, this medium must have an intensity dependent index defined by $n(E) = n_0 + n_2 \overline{E^2}$ (where n_2, is the second-order nonlinear refractive index). The latter term gives the refractive index change that can be induced in a medium by a light beam. For instance, in a Kerr medium, a beam of wavelength λ can induce a refractive index change in the medium given by $\Delta n = \kappa \lambda \overline{E^2}$ (where κ is the Kerr constant). When such a beam passes through the medium, substituting $\varepsilon = \varepsilon_0 + \varepsilon_2 \overline{E^2}$ in Maxwell's equation for an electromagnetic wave,

$$\nabla^2 E = \frac{\varepsilon}{c^2} \frac{\partial^2 E}{\partial t^2}$$

1-1

gives a generalized propagation equation for the beam. For a (1+1)D wave, (with 1 transverse axis (x) and one direction of propagation (z) and separating the time independent part) equation is simplified to

$$i\frac{\partial E}{\partial z} + \frac{1}{2}\frac{\partial^2 E}{\partial x^2} \pm \left| E^2 \right| E = 0$$

1-2

This propagation equation has a solution $E(z,x) = a\ \text{sech}(ax)\exp\left(ia^2 z \middle/ 2\right)$ which describes a beam with a stationary profile, i.e. a self-trapped beam.

Other phenomena also dependent on the nonlinear Schrödinger equation such as dark self-trapping and modulation instability are explained in detail in later (chapters 1.4 onward).

1.1.3. Nonlinearity in a material

A nonlinear medium in this context, is one that provides a refractive index change in response to varying intensity of the input beam. (Through the dielectric polarization P which depends nonlinearly on the electric field E of the light wave). Nonlinearities can arise out of different systems, such as kerr, photorefractive, photopolymerization etc. Each of these media has a different mechanism, but they all result in generating an index change in response to the beam intensity. These media can be classified as instantaneous or non-instantaneous, depending on whether they respond fast on a femtosecond scale or not. A medium can also be local or nonlocal (or partially nonlocal) - depending on whether an index change is confined strictly to the region of illumination or not.

Only a few types of media have emerged that exhibit the specific slow nonlinear response and are capable of supporting incoherent self-trapping beams. One reason is that the widely used conventional nonlinear optical crystals in self-trapping studies have an instantaneous response. The fast response time self-traps each individual speckle into a transient self-trapped filament, resulting in a breakdown of the beam. The only exception using such media involves the use of extremely low nW beam powers in order to slow the material response time.[12] Since then, researchers have migrated to alternative media that

natively support incoherent self-trapping - such as photochemical and nematic liquid crystal media.[63, 29]

Nematic liquid crystals are capable of sustaining incoherent beam self-trapping because they are a nonlocal medium[38,39,36] where index changes in any volume illuminated by an optical beam are distributed over a wider surrounding region. The resulting index gradient in a certain volume is therefore an averaged nonlinear response of all incoherent speckles passing through its neighborhood. This enables an incoherent beam to induce a single averaged smooth index profile, leading to single beam self-trapping in the medium. Several studies have been done to understand the effect of nonlocality on coherent and partially coherent self-trapping and beam interaction in such media.[40,41] These media typically have a reversible index gradient formed in the process. Self-trapping of (coherent) spatial solitons has also been demonstrated in a hybrid polymer stabilized nematic liquid crystal medium, which leads to a permanent index gradient.[42]

A photopolymerizable medium is inherently both, noninstantaneous and nonlocal in its nonlinearity. The noninstantaneous character arises from the inherently slow (millisecond order) rate of photochemical reactions.[63] Nonlocality arises from monomer diffusion in the system, and extends any index gradients formed beyond regions under direct illumination.[43] Taken together, the overall nonlinear response of a photochemical reaction masks incoherent fluctuations from the nonlinearity of the medium, leading to single beam self-trapping. Photochemical media support the formation of permanent waveguide structures through irreversibility of photopolymerization and do not need

external voltages to maintain molecular alignment, unlike liquid crystals. Additionally, the capability of photochemical media to robustly support both coherent and incoherent self-trapping under a range of powers makes it ideally suited for experimental studies on incoherent white light self-trapping and beam interactions.

The basic theoretical mechanisms behind the three main types of nonlinearities frequently used in incoherent self-trapping studies i.e. photorefractive, nonlocal and photochemical nonlinearities, are reviewed below in detail along with relevant experimental developments.

Non-instantaneous media

Incoherent self-trapping was first experimentally demonstrated by Mitchell et al., with partially incoherent light.[16] The beam was generated by passing a coherent laser beam through a rotating diffuser to make it partially spatially incoherent. Next, self-trapping with incoherent white light showed that beams generated with incandescent sources can also self-trap.[12]

An incoherent beam will self-trap when the random femtosecond scale speckles which disrupt collective beam self-trapping do not generate individual refractive index. The strategy for collective self-trapping involves using very low intensity incoherent beams (~nW range) to slow down the index change in photorefractive materials. Screening nonlinearity[5] is commonly used with these photorefractive materials although other types (such as photovoltaic nonlinearity[44]) can also generate self-trapped beams.

The materials are typically non-centrosymmetric crystals (such as barium titanate,

lithium niobate) where an index change is generated via an electro-optic effect, given by

$$\Delta n = -n^3 r_{eff} E_0 / 2 \qquad\qquad 1\text{-}3$$

where E_0 is an externally applied electric field and r_{eff} is an electro-optic

coefficient. The external electric field induces a uniform charge in the material, which is

then screened by the local space charge induced by a passing optical beam. The resulting

non-uniform field induces the necessary refractive index gradient (through the electro

optic effect) for self-trapping.[45]

The photovoltaic effect can also create a refractive index change via a

space charge field, given by:

$$\Delta n \propto [|E|^2 / (|E|^2 + I_{dark})] \qquad\qquad 1\text{-}4$$

Where I_{dark} is a parameter which depends on the material conductivity in the dark.

Non-local media

Although a slow response medium is the most successful strategy for incoherent

beam self-trapping, recently alternative strategies have also been reported. Cohen et al.,

predict an alternative strategy resulting in the self-trapping of incoherent beams by

suppressing the formation of local refractive index gradients using nonlocality.[46] Here,

the material exhibits a nonlocal or diffused refractive index gradient in response to a light

beam. Although the material has a fast response (i.e. instantaneous media), the

delocalization erases speckled refractive index gradients. This allows a beam with the

correct intensity profile to induce a refractive index gradient that acts as a lens. The refractive index change in such a medium is given by

$$\Delta n(x,z,t) \approx \frac{P(t)}{\sqrt{\pi\sigma^2}}\left\{1 - \frac{[x-[a(z,t)]^2}{\sigma^2}\right\} \qquad \text{1-5}$$

where P(t) is the beam power, propagation is along y axis, σ is the range of nonlocality (assumed to be much larger than beam width), a is the 'beam centre'.

Such instantaneous incoherent self-trapped beams form when two conditions are satisfied - the medium self-traps in a time frame faster than the characteristic fluctuation time (i.e. speckles), and the transverse momentum of the beam is invariant with time. (The characteristic fluctuation time can be enhanced by using rotating diffusers with coherent beams).

A theoretical study of nonlocal soliton solutions[39](using a Ritz's variational method) determined that they were identical for any given beam width, irrespective of the strength of nonlocality. It was determined that when the nonlocal response function decays in direct proportion to the mth power of the distance near the source point, the power and the phase constant of the strongly nonlocal soliton vary inversely to the (m+2)[th] power of the beam width.

Self-trapping with incoherent light

An incoherent beam consists of uncorrelated wave trains which appear as random speckles on a femtosecond scale. A medium that responds to each constituent femtosecond scale speckle of such a beam induces transient index gradients that attempt

to self-focus each individual speckle creating many transient randomly oriented waveguides. The resulting mix of crisscrossing waveguides disrupts collective guiding of the entire beam, and such beams were therefore not thought to self-trap until recently. However, in 1997, Mitchell et al., showed that even such a beam can self-trap, provided the medium cannot respond fast enough to form index gradients to each of these speckles individually. Incoherent white light self-trapping was demonstrated using a photorefractive medium where the response time is increased by using extremely low beam powers (nW). Despite this initial demonstration, detailed incoherent white light self-trapping studies, such as beam interactions have not been shown until now. Such studies have been hampered by a lack of suitable materials and difficulties in using this strategy for enabling a slow response from the medium. In 2006, the Saravanamuttu group showed that an entirely different material – a photopolymerizable system – is also capable of self-trapping incoherent white light, at higher powers (mW). This medium also enables a slow response from the media, but with a different strategy - here the index change is governed by an inherently slow rate of polymerization (of the order of milliseconds). This demonstration of incoherent white light self-trapping has for the first time enabled detailed studies such as the interactions between two incoherent white light self-trapped beams. Other phenomena with incoherent white light such as lattice formation using modulation instability and dark self-trapping beams have also been demonstrated by our group and are detailed in subsequent chapters. The following section reviews different types of media that can support incoherent self-trapping beams as well as their individual mechanisms that enable such a response.

1.1.4. Self-trapping of partially spatially incoherent light

Coherence is a measure of the degree of correlation between two points on a wavefront (Figure 2) – the points can be separated either in space (for spatial coherence) or in time (for temporal coherence). When the phase of a point on the wavefront cannot be used to predict the phase of a neighbouring point, the wave is incoherent. The phenomenon of self-trapping of spatially and temporally incoherent white light can be approached by first understanding the self-trapping of partially (spatially) incoherent light. The temporal incoherence aspect is combined with this idea for a theory of spatially and temporally incoherent white light, which is dealt with in the subsequent sections. Partially spatially incoherent beams can be generated by passing a fully coherent beam through a rotating diffuser. The diffuser creates speckles, or random spatial profile fluctuations in the beam. By changing the speed of the diffuser, the degree of incoherence can be increased. Alternately, spatial coherence can be increased by passing a partially coherent beam through a pinhole, as shown in Figure 2c.
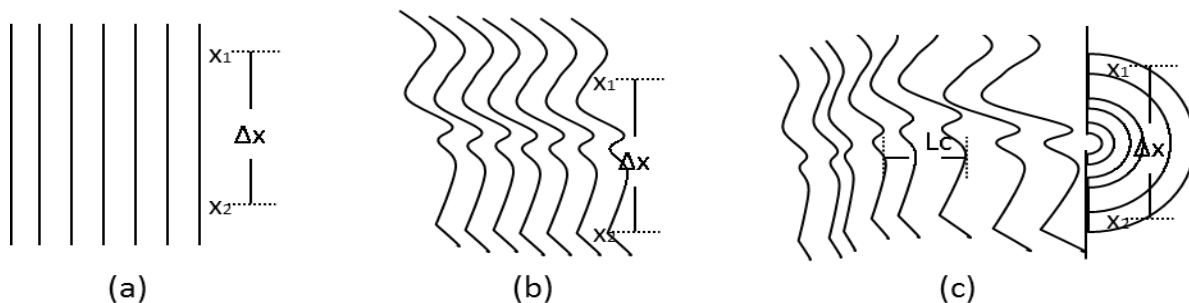
Figure 2. Phase fronts in (a) ideal spatially and temporally coherent plane wave, (b) spatially and temporally coherent wave, but with a distorted profile and (c) a spatially partially coherent wave (the correlation between any two points separated in space (x1 & x2) is poor. This can be converted into a spatially fully coherent wave by passing it

through a narrow pinhole. Any two points separated in space on this wave front will then be fully correlated.

Three main theories were proposed, to explain the phenomenon of spatially incoherent optical self-trapping.[22] These are (a) Coherent Density theory[18], (b) Modal theory[19] and (c) Mutual coherence theory.[20] Later, another simpler theory (d) based on geometric optics[21] was proposed, applicable to large incoherent self-trapped beams without phase information.

Coherent density theory

The coherent density theory models self-trapping of partially spatially incoherent light in a biased photorefractive medium. [17,18] Beams were generated experimentally using coherent laser light passed through a rotating diffuser. The modeling is done with an infinite set of coupled nonlinear Schrödinger-like equations, where the incoherent angular power spectrum of the beam source determines the weightage for each of them. Index change is obtained from $n^2 = n_0^2 + 2n_0\Delta n(I)$. For biased photorefractives,[45] the index change is taken as $\Delta n = -\Delta n_0(1+I_N)$. The beam evolution equation is obtained using a mutual coherence function J_{12} from the coupled equations for nonlinear media. Alternately, this theory demonstrates that for a logarithmic saturable nonlinearity, any strength of nonlinearity has a corresponding limited range of the angular spectrum associated with it that is allowed to self-trap. Further, as this angular spectrum increases, the corresponding self-trapped beam width also increases, up to a certain limit. This model can be applied to any 'slow' nonlinear medium, i.e. where the medium response

time is much longer than the scale of phase fluctuations in the beam. This model showed that the coherence properties of incoherent beams are modified by the self-trapping process, and also predicted the existence conditions for dark incoherent solitons.[47]

Modal theory

The modal theory interprets an incoherent self-trapped beam as a multimode waveguide.[19] The coupled equations of the coherent density theory describe the dynamic evolution of the wave through the medium, but have limited application in identifying static self-trapped solutions. The modal theory solves this problem through a statistical approach and helps identify the conditions determining the existence range of self-trapping. In the analysis, guided modes of a waveguide are populated one-by-one with coherent modes. These are then examined to see if any nonlinearity-induced intensity profiles can recreate the waveguide - it is then self-trapped. The initial resulting guided mode is simply a bright coherent soliton.[23] As higher modes are populated, their mutual interference and different modal propagation velocities result in a varying intensity profile.[24] However, mutually incoherent modes avoid this interference. Their different velocities do not affect their total intensity (because total intensity is now phase independent) and a stationary intensity profile or incoherent self-trapping results.

The theory gives three basic principles essential for incoherent self-trapping (i) a 'slow' nonlinearity is necessary, (i.e. a non-instantaneous nonlinearity) for incoherent self-trapping. This essentially prevents speckled refractive index gradients from forming. (ii) A multimode (i.e. a speckled beam – with many waveguides) beam should be able to induce a multimode waveguide through the nonlinearity. Since saturating nonlinearities

induce multimode waveguides even with coherent input[19] they are well suited to satisfy this criterion. (iii) The multimode waveguide has to guide itself in its induced waveguide – this is known as the self-consistency condition.

Mutual coherence theory

The mutual coherence theory is also known as the radiation transfer approach.[20] It looks at the spatial evolution of an incoherent beam's local angular spectrum for a steady state equation (in terms of a self-consistent differential equation) and its possible self-similar solutions. The radiation transfer equation takes into account refraction at a smooth profile. It views the self-trapping process as the formation of a waveguide that confines light inside it by means of a smooth step refractive index gradient. This is highest at the beam centre and lowest at the periphery. Only when the index gradient is sufficiently strong, total internal reflection holds light in very effectively. Beam evolution is done using a parabolic wave equation applied to Gaussian beams and shows oscillatory behavior. The self-similar solution of an incoherent beam shows that light concentrates in areas of larger susceptibility (i.e. the beam center). Further, it also predicts an anti-guiding effect for regions of negative variations of optical density (i.e. a dark incoherent soliton should also be able to self-trap in a similar system).

Geometric optics approach

The geometric optics approach gives the first classical geometric optics description of incoherent self-trapped beams.[21] Incoherent beams differ significantly from coherent beams in that they diffract due to diffuse irradiance rather than diffraction.[48] Geometric optics can describe both - this diffusely illuminated multimode waveguide[49]

and the incoherent solitons inducing them. This description is accurate when the beam spread by diffraction is insignificant compared to the maximum angle of diffuse irradiation. This is equivalent to a 'big' incoherent soliton or one that is multimode or strongly incoherent.

The incoherent beam is assumed to radiate in a cone, which gets confined when passing through a step profile waveguide by total internal reflection. Similarly, a circularly symmetric uniform intensity beam radiating light in a cone smaller than the critical angle, can induce a uniform waveguide, and is a soliton. This analytical approach yields an expression for the diffuse irradiation (or beam incoherence) necessary for each beam intensity to result in self-trapping. The allowed distribution of rays radiated diffusely from each position in the beam's cross section is characterized by a ray density function.

Wigner formalism

The Wigner formalism is an alternative theoretical approach to describe partially incoherent waves.[25] It starts with the standard Nonlinear Schrödinger (NLS) equation with the slowly varying wave envelope field. The Wigner transform is the form of the Fourier transform of a complex mutual coherence function and the two form a Fourier transform pair, and are equivalent descriptions of partially incoherent light. The evolution of this Wigner distribution function is known as the Wigner-Moyal equation, and is expanded using a Taylor series, ignoring all but the first few terms to result in a geometric optics approximation to yield a Vlasov-like equation for Wigner distribution. This equation corresponds to a geometric optics approximation analysis, and gives its

corresponding ray equations and is identical to the radiative transfer equation of geometric optics.

Equivalence of all above approaches

All the above theoretical approaches were shown to be exactly equivalent to each other[26,27] with the geometric optics theory being applicable in the limit of full incoherence.[28] Theoretically, the mutual coherence function's evolution equation derived from all 3 approaches turns out to be the same. The first two – coherent density theory and mutual coherence are shown to be equivalent through the Van Cittert-Zernike theorem. The third – the multimode theory – is proved to be equivalent using the Karhunen-Loeve expansions.[25]

According to these theories, incoherent self-trapped beams show a dual character – they can be treated theoretically as both self-induced linear waveguides, and as multisoliton complexes. For a multisoliton complex, it has been shown that the beam shape depends on the number of modes.[50] A fundamental soliton is coherent; it only has a single mode with a unique symmetric shape defined by the characteristic sech function. A partially coherent beam has a finite number of modes, and therefore a finite number of parameters controlling the beam shape. A fully incoherent beam can have an arbitrary shape since it has an infinite number of modes.[51] This in turn, results in the fact that any interaction between incoherent beams can alter the modal statistics in each beam, resulting in a modification in the beam shape[52] (such as forming elliptic self-trapped beams[53,54]). This makes shape control possible by interacting incoherent beams with either incoherent beams, partially coherent beams[55], or even with coherent beams.[22,56]

1.1.4.1.   Self-trapping of spatially and temporally incoherent white light

Theories described in the previous section are limited to spatial incoherence. White light consists of both, spatial as well as temporal incoherence simultaneously, and a theory for such beams was developed by Buljan et. al.[31,32] This theory is applicable to the 'slow' (i.e. non-instantaneous) nonlinearities where the refractive index is assumed to respond only to time-averaged intensity. It extends the coherent density theory for spatially incoherent beams to include a temporal incoherence term in the dynamic beam evolution equation. For a saturable media, index change is taken as $\Delta n = -\alpha(1+I)^{-1}$, where I is the time-averaged intensity, n_0 is the linear refractive index, α is a constant. Mutual spectral density at a transverse plane is used to describe the beam evolution and is monitored through two parameters for each temporal constituent - spatial intensity profile and a complex coherence factor. The former gives the temporal spectral density and the latter the spatial coherence for each of these frequencies individually. Mutual spectral density for the beam is given by

$$i(\frac{\partial f^{\omega}}{\partial z} + \theta \cdot \nabla_T f^{\omega}) + \frac{1}{2k_{\omega}} \nabla_T^2 f^{\omega} + k_{\omega} \Delta n(I) f^{\omega} = 0 \qquad \text{1-6}$$

,where f^{ω} represents the coherent density for each frequency of a beam, $k_{\omega} = n_0 \omega/c$.

For Kerr media case, index change is taken as $2n_0 \Delta n = n_2 I$, where I is the time-averaged intensity, n_0 is the linear refractive index, n_2 is the second-order nonlinear refractive index. Since both coherent density and Modal theories are equivalent,[33] the modal theory is used to span the incandescent frequency spectrum in this case. However, to account for temporal incoherence, the modal weights are time averaged.[35] Again, two

parameters – the spatial intensity profile and a complex coherence factor are used to monitor the beam for changes. For Kerr nonlinearity,

$$\frac{\partial^2 U_m{}^{\omega}}{\partial x^2} + 2ik_{\omega}\frac{\partial U_m{}^{\omega}}{\partial z} + \frac{2\Delta n(I)k_{\omega}^2}{n_0}U_m{}^{\omega} = 0 \qquad\qquad 1\text{-}7$$

where $U_m{}^{\omega}$ is the profile of the m mode at frequency ω.

Analysis of the beam evolution reveals that for both types of nonlinearities, the total intensity profile is almost constant, but coherence properties change and self-adjust during the self-trapping process. Self-adjustment results in a larger spatial correlation distance for lower frequencies (i.e. they become more coherent). Incoherent white light self-trapping is a collective phenomenon involving all frequency constituents involved.[34] Since the beam confines all its frequency components within the same sized waveguide their effective diffraction angle θ_0 is ~ constant. Since $\theta_0 \alpha \lambda/l_s(\lambda)$, where l_s is the spatial correlation distance at wavelength λ, this results in $l_s(\lambda) \alpha \lambda$ and therefore, larger correlation distances for longer wavelengths.
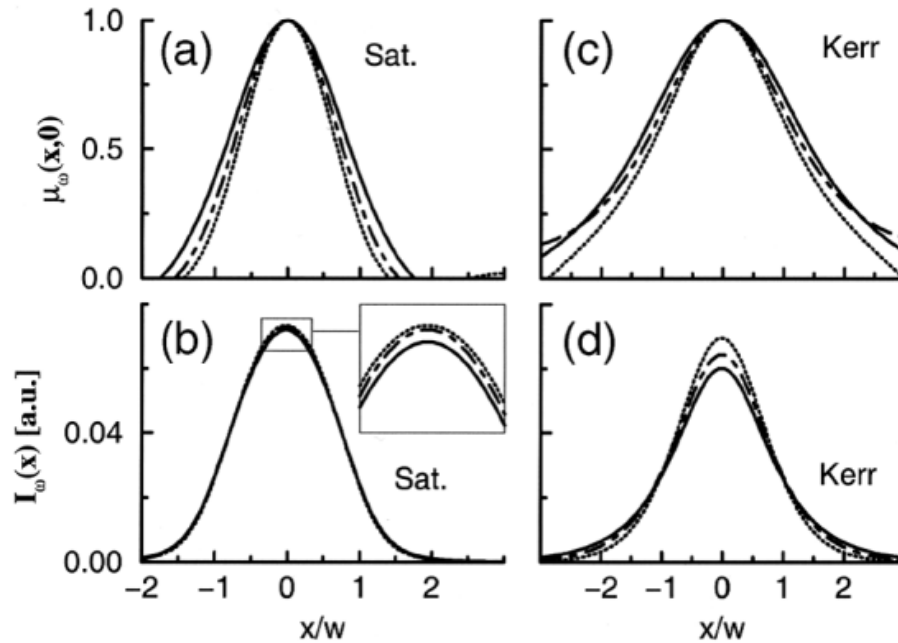
Figure 3.[34] Self-trapping modifies the coherence properties of a partially incoherent beam. Complex coherence factor μ_ω(a) & (c) and the intensity profile I_ω(b) & (d) of a white-light self-trapped beam are shown at three representative frequencies: ω_{min} (solid curve), ω_0 (dotted–dashed curve), and ω_{max} (dotted curve). The self-modification results in a slightly increased coherence for lower frequencies (a) & (c), and a slightly wider intensity profile for higher frequencies (b) & (d). The effects are slightly higher in Kerr media (c) & (d).

1.1.5. Treatment of incoherence and material nonlinearity simultaneously

Partially incoherent white light self-trapped beams in nonlocal media

An alternate theoretical study on "nematicons" [57] combines partial (spatial) incoherence using a modal approach to partially incoherent self-trapping with the nonlocality of a material (such as nematic liquid crystals). Coherence characteristics of

these multi-mode solutions were found to depend on a parameter *e* which is a measure of the medium's nonlocality. The latter ranges between $-\infty$ and -4. At $-\infty$, it approaches the coherent case; the medium nonlocality is higher and results in an index distribution profile that is wider than the beam's intensity profile.

Incoherent white light self-trapped beams in nonlocal media

An additional improved theory by Shen, et al., (2006) accounts for spatial and temporal incoherence in white light self-trapping in *noninstantaneous and nonlocal media*.[30,36] It extends the mutual spectral density theory with non-locality, a beam propagation equation is obtained as

$$\frac{\partial B_\omega}{\partial z} - \left(\frac{i}{2k_\omega}\right)\left[\nabla^2_{\perp 1} - \nabla^2_{\perp 2}\right]B_\omega - \frac{ik_\omega}{n_0}\left\{\delta n(I(r_1,z)) - \delta n(I(r_2,z))\right\}B_\omega(r_1,r_2,z) = 0 \quad \text{1-8}$$

where $B_\omega(r_1, r_2, z)$ is the mutual spectral density function which describes the correlation statistics between r_1 and r_2, $k_\omega = n_0\omega/c$ is the wave vector, δn is the nonlocal index change of the beam, as a function of intensity. A spectral width $\omega_0(1\pm\Delta)$ accounts for a broad spectrum beam (i.e. white light). For the case of a strongly nonlocal medium with Kerr type nonlinearity, the refractive index change is obtained as

$$\delta n(I) = R_0 P_0 - \frac{1}{2}\gamma P_0 r^2 \qquad \text{1-9}$$

where δn is the nonlocal of the index change, as a function of intensity I, R_0 is the maximum value of the circularly symmetric nonlocal response function $R(r)$, γ = - $R_2(r)|_{r=0}$, and P_0 is the total beam power. The nonlocal response function R(r) is given by

$$R(\vec{r}) = \frac{1}{2\pi\sigma^2}e^{\left[\frac{-(x^2+y^2)}{2\sigma^2}\right]} \qquad \text{1-10}$$

which gives $\gamma = 1/2\pi\sigma^4$. In this theory, (as in the previous theory) two parameters – the complex coherence parameter and the spatial coherence distance are monitored for changes in beam evolution. This theory also concludes that self-trapping results in modification of correlation distances for each frequency component – it is larger for lower frequencies and shorter for high frequencies. Further, a critical value of the input power exists for self-trapping in this case, and any variation from this value results in periodic oscillations in the beam profile.

The above theories built upon previous models to simulate spatially and temporally incoherent white light. Material properties such as nonlocality were also incorporated in the simulations subsequently. White light self-trapping in a polymer system involves spatial and temporal incoherence, as well as nonlocality and photopolymerization nonlinearity. A review of photopolymerization and resulting nonlinearity is discussed in the next section.

Theories describing incoherent self-trapping were developed sufficiently to predict existence of other self-trapping phenomena with white light such as the formation of dark solitons[17,47] and modulation instability (MI)[22,28] before they were experimentally demonstrated (dark incoherent solitons,[58,59] and MI[60,61] shown with white light). Dark solitons are defined in section 1.4. Modulation instability (MI) is a nonlinear phenomenon that results in the formation of patterns of individual self-trapped peaks with wide beams or uniform illumination. It is discussed further in section 1.5.3.

1.2. **Self-trapping in a photopolymer**

Coherent beam self-trapping has been demonstrated in free-radical polymerizable media since 1996.[43,62] Our group has demonstrated for the first time the suitability of a photopolymer for incoherent white light self-trapping as well as detailed studies on the phenomenon. [63,64,65] Other related phenomena such as modulation instability and formation of arrays of self-trapping filaments, as well as coherent self-trapping using organosiloxane photopolymer have been studied by our group as well.[66, 180]

Such a medium provides a natural difference in the indices of the monomer and the polymer (typically ~0.04). An index gradient is achieved when the incident beam has an intensity profile that induces a variable amount of photopolymerization across the beam path – which is higher at the beam center and falls smoothly towards the beam periphery. This type of media can also permanently imprint a solid gradient refractive index waveguide through irreversible polymerization, where the surrounding unpolymerized medium acts as a cladding. Such systems differ significantly in comparison to the non-instantaneous photorefractive media (described earlier in section 1.1.3 on nonlinearity), where index changes are induced by physical processes rather than chemical reactions. Photopolymerizable media have been studied in detail, and have been shown to be a robust medium for coherent self-trapping studies. Corresponding theoretical analyses of the self-trapping process were also done for slab waveguides[67,68] and bulk liquids.[69] The studies correlate temporal behavior of coherent self-trapping to stages of photopolymerization and also provide a dynamic explanation of waveguide

formation (in bulk) based on the formation of a moving polymerization centre (called an 'eye' which propagates along the medium).

A photopolymer's property of providing a slow index change (of the order of milliseconds) makes it an ideal medium to study incoherent self-trapping, and was first shown by our group using organosiloxane. Besides an inherently slow index change, organosiloxane also has a certain degree of nonlocality, both of which act together, screening the speckled effect of incoherent white light to form an averaged index gradient. However, the organosiloxane system has certain differences in comparison to other photopolymer systems.

Free monomer systems have a characteristic upper threshold limit for self-trapping intensities.[70] Intensities above this threshold will induce formation of a large number of radicals in a very short time. If this time happens in less time than the radical lifetime, then polymerization occurs completely before the radicals have time to diffuse. Such a system cannot form an index gradient and will not self-trap at this intensity. Therefore lower beam intensities are necessary for self-trapping. In organosiloxane, the medium is already doped with a well dispersed photo initiator before launching a beam, resulting in a higher (maximum intensity) threshold.

1.2.1. The chemical process

Preparation of the photopolymerizable siloxane involves the following basic steps:

Step 1: Condensation of siloxane
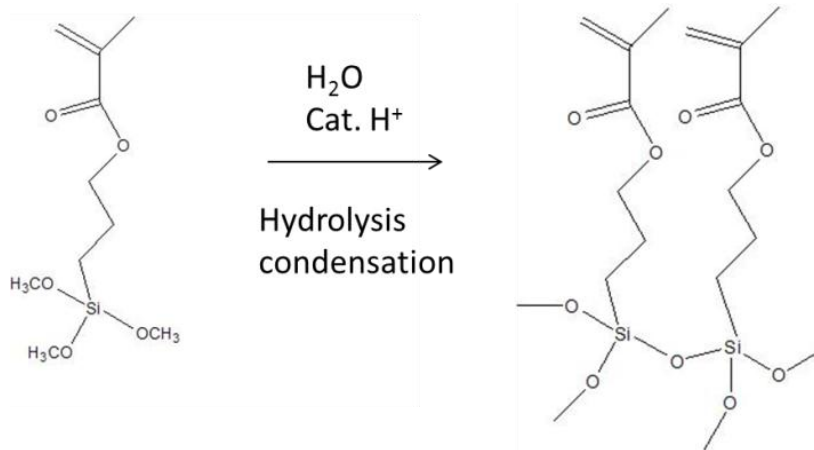
Figure 4. Alkoxysilane (MAPTMS) is condensed into a glass-like material using dilute HCl to induce hydrolysis and condensation.[71]

MAPTMS is stirred with 6.14% (w/w) of 0.05N HCl, resulting in the formation of a clear solution through condensation. Subsequently, 0.05% (w/w) titanocene is added as a photoinitiator and the mixture is kept in the dark and stirred for > 16 hr prior to use. Before placing it in the optical assembly, the organosiloxane is filtered and ~1.5mL is transferred into a plastic or glass cuvette. This cuvette is then illuminated uniformly until it forms a gel (See section 2.1 for experimental details). The sample transforms from a liquid to a partial gel state which limits strong convection & diffusion, besides also providing some mechanical stability to fine polymerized structures (from convection currents).

Step 2: Titanocene is added as a Photoinitiator
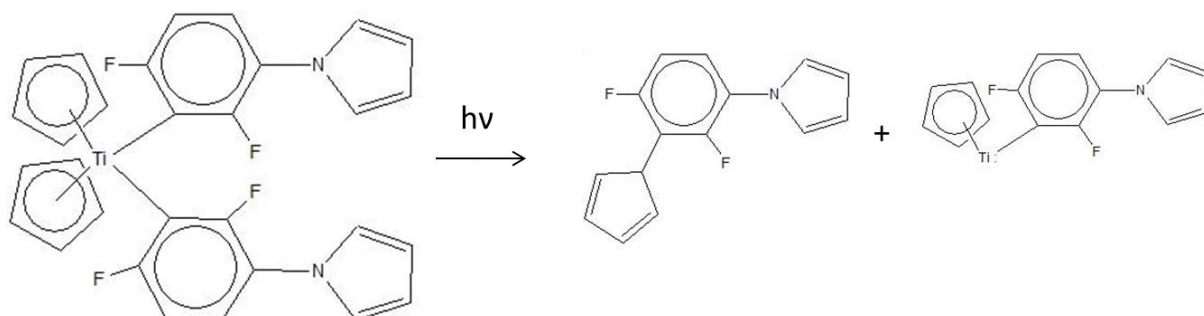
Figure 5. Titanocene photolyzes according to the above reaction into titanium diradicals as shown above.[72]

Step 3: Diradicals derived from titanocene initiate free radical polymerization

The titanocene diradical reacts with free methacrylate siloxane derivative units according to the reaction step shown Figure 6, initiating free radical polymerization.[73] (The referred mechanism has been figured out for a system with diphenyliodonium chloride (DPI) but as this is absent in our system, and it is reasonable to assume that it is the biradical that initiates free-radical polymerization).

Step 4: Chain polymerization continues in the presence of free monomer

When the titanocene reacts with the condensed siloxane instead, photopolymerization takes place as shown below:
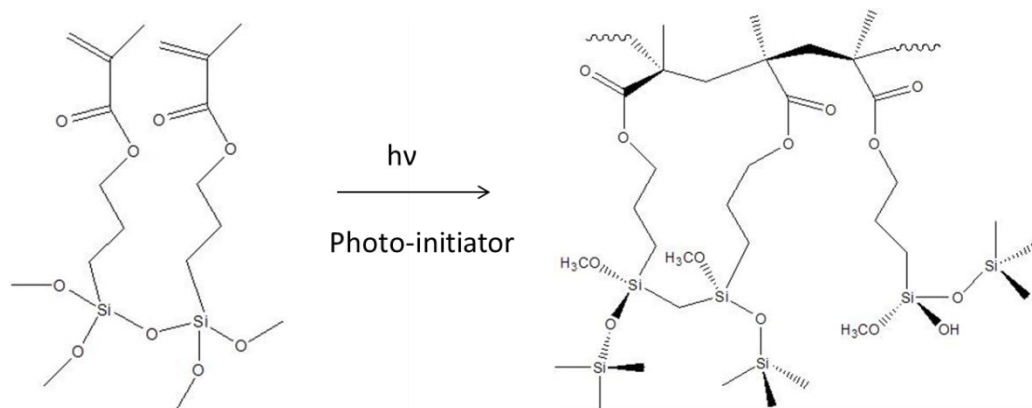
Figure 6. An organosiloxane medium consists of individual polymerizable methacrylate units bound to a cross linked siloxane backbone (formed on condensation with HCl). The backbone strongly limits the diffusion of the monomer units.

Titanocene in the system dissociates to yield titanium diradicals, which then initiate free radical polymerization in methacrylate monomer units. Because the units are themselves bound to the condensed siloxane, they are not very free to diffuse over large regions. Although the photoinitiator units are free to diffuse in the medium, their diffusion is somewhat limited by both, partial polymerization at the initial steps as well as the cross linked mesh network formed by the condensed siloxane.

Another characteristic of free monomer systems is their relatively high degree of nonlocality, due to diffusion of relatively small monomer units. A high nonlocality increases the minimum intensity necessary for self-trapping, since it degrades the induced

refractive index profile even for an intense beam. In organosiloxane, the monomer units are bound to a siloxane backbone, severely limiting their diffusion. Such a system can confine index gradients to less than 0.15 μm – forming features with a very high degree of spatial resolution[74]–which makes it possible to self-trap even low intensities. The net effect of both modifications in siloxane is a wider range of intensities that can provide a refractive index gradient, necessary for self-trapping. Further, such a system provides for tuning the degree spatial localization, by changing the length of the siloxane backbone to control extent of monomer diffusion.

Although the siloxane and free monomer systems are quite different, they have very similar dynamics. In both, the polymerization shows three distinct stages: in the first stage, small diffusible polymeric chains result in small index change with a flat induction period. Larger polymeric molecules form in the second stage with cross-linking, and the index changes are larger (>0.04) – this is the regime of self-trapping. In the third stage, polymerization is almost complete, index changes saturate and monomer diffusion becomes difficult.

The waveguide formation in bulk media has been explained with the concept of an 'eye formation' and its propagation along the medium. An 'eye' is the region where a sufficient index gradient has formed so that self-focusing begins to overcome diffraction. (A primary eye – the starting point - is formed at the interface where the beam enters the bulk medium). When the region in front of the eye polymerizes and develops an index gradient, the eye moves forward. The new position of the eye again begins to polymerize

the region in front of it, and the process continues, eventually resulting in the formation of a channel waveguide in the traversed path. This is again similar to both systems.

1.2.2. Relating photopolymerization with a refractive index change

Kewitsch and Yariv[43] analyzed the wave propagation of a Gaussian beam through a photopolymer liquid by solving the NLSE using the beam propagation method.[75,76] An intensity profile was computed using a transparent boundary condition and the evolution of the refractive index change was incorporated into it ignoring photobleaching and photoinitiator absorption. Index change is modeled on a function of the optical field amplitude E as:

$$\Delta n^{'}(x,y,z,t) = \Delta n_o^{'} \left\{ 1 - \exp\left[-\frac{1}{U_o} \int_0^{t-\tau} \left| E(t^{'}) \right|^2 dt^{'} \right] \right\}$$ 1-11

where $\Delta n_o^{'}$ is the index difference between the monomer and polymer, $\left| E(t') \right|^2$ is the optical field intensity , τ is the monomer radical lifetime and U_0 is the critical exposure needed to initiate polymerization. This index change induces formation of a self-trapped, light guiding polymeric waveguide. Exposure is a measure of total light energy on a surface in a unit time. Only above this required critical exposure, i.e., exposure to minimum light intensity for a certain amount of time, an index change can be induced (Figure 7). Other alternative studies of waveguide formation in a photopolymer[77,78] also support the requirements of a threshold energy requirement. Exposure for short times or with very low intensity of light will not induce significant polymerization. The study was able to correlate qualitative predictions from numerical studies with experimental results.[43] It was able to show that a threshold exposure is needed to initiate self-focusing.

At moderate exposures, a lens like profile of the index change initially occurs due to focusing light at the more intense center of the beam. Later index changes increase linearly with exposure, and mimic the transverse intensity profile closely. At large exposures however, it simply becomes a step index fiber as the center index is saturated and cannot increase further. At very large exposures, light goes beyond the core and polymerizes the entire volume. Diffusion and light scattering effects in the medium were not considered here.
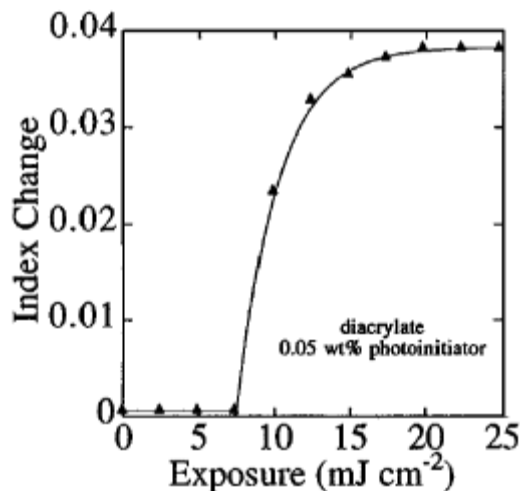
Figure 7. A delay time and critical exposure of the monomer are required (due to diffusion) before actual polymerization begins and an index change is produced.[43] Here, the measured index change (at 589.3 nm) of the diacrylate photopolymer under UV exposure at 325 nm shows a threshold exposure of about 7 mJcm^{-2} in the graph before an index change begins to appear.

1.2.3. Accounting for diffusion within the system

Theoretical studies on diffusion causing gel formation in diffusion-controlled free-radical polymerization reactions have been done previously.[79] Specifically, photopolymer materials have also been previously studied in detail for hologram formation. Diffusion has been accounted for using a partial differential from Fick's law, introduced by Zhao and Mouroulis[80]

$$\frac{\partial u(x,t)}{\partial t} = \frac{\partial}{\partial x}\left[D(x,t)\frac{\partial u(x,t)}{\partial x}\right] - F(x,t)u(x,t) \qquad \text{1-12}$$

where u(x, t) is the monomer concentration, F(x, t) is the polymerization rate, and D(x, t) is the so-called 'diffusion constant', which is not really constant due to the change in polymer concentration and associated change in the mobility of monomers.

The concentration of polymerized monomers N(x, t) after some exposure time t is

$$N(x,t) = \int_0^t F(x,t')u(x,t')dt' \qquad \text{1-13}$$

Hologram formation in dry photopolymers has also been studied for diffusion dependence[81] and was determined to nonlinearly depend on the ratio between diffusion rate and polymerization rate R. Higher order gratings are formed with ~zero amplitude when the diffusion is much higher than the polymerization rate. Higher order harmonics begin to build up as R decreases. Experiments confirm only qualitatively some of the theoretical conclusions of this study. A simple diffusion model was shown to be the first step in understanding grating formation in photopolymers. Diffusion has also been further studied with nonlocality for temporal responses.[82] Accounting for diffusion in polymer waveguiding systems is essential, especially for studies of white light in nonlocal media

(section 1.1.5) since diffusion causes the nonlocality. Monomer units tend to diffuse to regions of increased light intensity to undergo polymerization, and result in removal of material from non-illuminated areas. Further, under prolonged illumination, once polymerization is nearly complete at regions of highest intensity, additional diffusion can lead to complete polymerization even in regions of lower intensity. This may lead to formation of a flat index gradient throughout the waveguide. Besides an index gradient formation, mechanical shrinkage is also known to occur during photopolymerization and has been studied previously.[83] This results from differences in material density and tensile strength between polymerized and unpolymerized regions.

Layout of the thesis

Section 1.1-1.2 reviews basic concepts of nonlinearity, coherence and polymerization. Subsequent sections of this introductory chapter provide a review of previous studies of various nonlinear self-trapping phenomena. They describe new phenomena in various systems with incoherent light – such as (i) interactions between self-trapping beams; (ii) dark beam formation, (iii & iv) dark and bright lattices, as well as embedded (v & vi) dark-in-bright and bright-in-dark self-trapping beams.

1.3. **Interactions of self-trapping beams**

This section focuses on experimental studies in self-trapped beam interactions, with emphasis on incoherent beam interactions. Interaction of two self-trapping beams have been previously studied both theoretically[84] and experimentally,[1,85,86,87,88,89,90] initially with coherent laser beams in a variety of media. Interaction effects such as fission, fusion, annihilation, spiral[91,92,93,94,95] have been shown. Their interactions in nonlocal media have also been studied recently.[41,96,97] Similarly, interaction studies with partially spatially coherent beams have also been done – both experimentally[1,95,98] and theoretically[7,99,100] Corresponding studies on incoherent bright beams have been done only theoretically[101,102,103] but not experimentally.

Because self-trapping beams induce index gradients along their paths, two such beams not launched in parallel simply pass through (by refraction) one another without significant changes. Parallel beams however, can attract or repel and continue to periodically evolve around one another.[1] Coherent self-trapping beams exhibit mutual attraction or repulsion for one another, depending on whether they are in-phase or out-of-phase. Attraction occurs when a higher index is induced by a higher total intensity in the intervening region between beams with an in-phase intensity overlap. This region therefore draws and confines light from either beam and appears as attraction. Conversely, an out-of-phase overlap causes repulsion by inducing a lower index region between the beams that cannot confine light more poorly than either beam. The interaction strength between such beams decays with increasing spacing between them, due to a lowering of their intensity overlap. Two partially spatially incoherent beams can

also similarly interact with one another. If the response time of the medium is significantly larger than the life time of speckles in each beam, the beams become mutually incoherent. Their relative phases then become irrelevant and any overlap always leads to an increase in total average intensity in the region of intersection. This results in their interaction being always attractive (with two notable exceptions[104,105] exhibiting repulsion due to other factors). For the case of spatially and temporally incoherent white light beams, interactions are predicted to be always attractive, for the same reason.

Recent experimental studies on incoherent interactions have used two *dark* solitons to demonstrate mutual attraction between beams.[106] Significant progress has also been made in understanding the influence of incoherence in single beam self-trapping using various medium conditions - such as non-instantaneous and non-local nonlinearities - with both theoretical and experimental studies.[29,30,36,63,57] Interactions between counter propagating beams of various degrees of coherence have been studied as well.[40,107,108,109] Several theoretical simulation studies on interactions between two bright co-propagating self-trapping beams have also been made, with both, partially coherent as well as incoherent white-light.[102,57] These studies predict features in incoherent self-trapping beam interactions similar to the coherent case, in terms of beam paths and orientations. Beams are predicted to exhibit attractive interactions in all cases with periodic intersection if they are initially sufficiently close. The interaction strength is also predicted to decay with increasing spacing between beams, leading to larger periods of intersection.

The following sections review these interaction studies in detail, beginning with Kerr and saturating media, followed by incoherent beam interactions in photorefractive and nonlocal media. The subsequent section concludes with potential applications and the significance of studies in photopolymerizable media.

1.3.1. Interactions of self-trapped beams in a Kerr type nonlinearity

The first self-trapped beams shown experimentally were in Kerr type media.[2,85,110] Later, they were theoretically analyzed[111] and several interesting properties were revealed. It was found that these beams were stable only for the (1+1) D i.e. planar waveguides, and not in bulk (2+1) D media − this was also observed as a catastrophic (unstoppable) self-focusing.[112] Solitons not launched in parallel simply pass through (by refraction) one another with no significant changes. Beams launched in parallel can attract or repel each other, depending on the relative phase between them. These beams exhibit particle like behavior − the solitons retain their trajectories and propagation velocities after collision. This was shown to be a consequence of integrability, so that their power and velocities are conserved, the number of solitons is conserved in collision, and all collision interactions are fully elastic.[113]

For fundamental solitons, in general, the interaction varies between attraction (for absolute phase $<\pi/2$) and repulsive (for absolute phase between $\pi/2$ and $3\pi/2$), and solitons separate as they propagate. Only when the phase difference is zero, the beams do not separate completely; instead they continue to periodically evolve around one

another.[114] Further, the 'interaction potential' decreases with increasing soliton separation.

The attraction of in-phase solitons can be understood as follows: Since the self-trapped beams depend on a refractive index gradient for confinement, the (positive) index gradient of a second soliton in a soliton's neighborhood causes its light to be diverted towards the second beam's path. This diversion also occurs for the second soliton, resulting in the appearance of attraction. If however, the beams were out of phase, there would be a negative index gradient, diverting light away from each other instead. These interactions were demonstrated experimentally in various media.[86,87,110,113]

1.3.2. Interactions of self-trapped beams in a saturating nonlinearity

In contrast to a Kerr medium, a saturating medium can support (2+1)D (i.e. bulk) self-trapped beams (1st shown in sodium vapor[4] - no catastrophic collapse). This is because saturating nonlinearity limits the maximum possible change in refractive index. Once a higher intensity is confined to a narrow region at the beam center, it cannot self-focus further into a smaller region.[85] The beam propagation equations are not integrable here. This makes inelastic collisions possible and the soliton number need not be conserved through the collision and a much richer variety of interaction phenomena are observed. Fusion,[91] fission[92] and annihilation[93,41] of solitons are possible with an associated radiation loss.

These interactions can be understood as follows: The waveguides confine light because the modes within them fall at angles smaller than the critical angle (escape

angle). The solitons interacting at large angles again simply refract through one another like Kerr solitons. However, when the interaction angle is small, some modes of one waveguide can couple into the second one if they enter into it with an angle less than its critical angle. This results in excitation of higher modes in each waveguide, enabling fusion. (Kerr media solitons can support only a single mode, whereas saturating media where index changes are higher can support these higher modes[84]).

Spiraling interactions

Soliton beams spiral around one another when they are launched in different planes rather than in the same plane. Their interaction force bends their trajectories and can make them spiral and drift apart, if repulsive, or can make them fuse if it is sufficiently attractive. A careful balance of this force can also make them spiral indefinitely. This type of interaction resembles forces between rotating or spiraling charged particles where an electric force can balance a centrifugal force.[115] Because of the difficulty of generating two independent solitons side-by-side simultaneously, several alternative strategies were initially used - such as a split vortex soliton or modulation instability[86,116] - to observe such out-of-plane interactions. However, independent phase and spacing control of such soliton beams is extremely difficult and stable indefinite spiraling was not observed experimentally until later.[88] This was made possible only by using an incoherent interaction, where phase control becomes irrelevant.[1] Later, a theory for soliton-spiraling was also developed.[98] The spiraling was shown to involve power exchanges and is controlled by the degree of mutual initial coherence.[95]

1.3.3. Role of incoherence in beam interactions

In contrast to coherent beam interactions which are strongly phase dependent, closely spaced incoherent bright self-trapped beams increase the total intensity in their intervening region (Figure 8). This is because a slow responding medium cannot respond to the instantaneous interferences from the random phase fluctuations of each beam, instead it only responds to the total phase fluctuations averaged over its long response time.[12] This in effect is the superposition of the two incoherent intensities. Since this superposition always results in a higher intensity, the corresponding nonlinearity-induced refractive index is always higher in this region of overlap. Theoretically, this result predicts bright incoherent self-trapped beams always exhibiting an attractive force in general. This interaction force is dependent on the beam separation, orientations and angles of incidence.
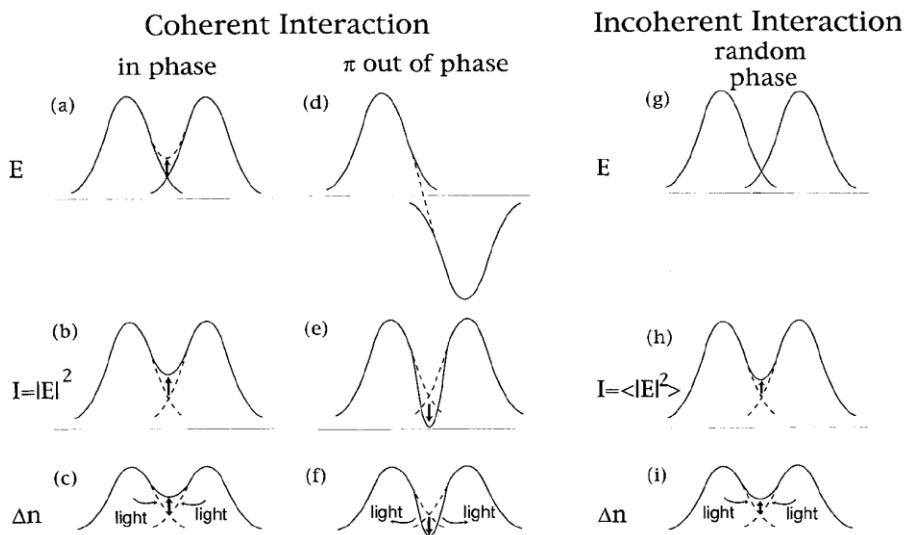
Figure 8.[85] Intensity and refractive index profiles of small-angle collisions between coherent (a)-(f) and incoherent (g)-(i) self-trapped beams are shown in the diagram above.

(a)-(f) show the strong dependence of the outcome of coherent beam collisions on the initial phases. Both, attraction and repulsion are possible. In contrast, (g)-(i) show the phase insensitivity of incoherent collisions.

Several related studies were done in order to explore the nature of interactions between incoherent beams. These were based on either utilizing specific material properties, such as refractive index anisotropy (Figure 9)[105], cross phase modulation[99,117] or with laser-generated beams that were partially coherent or were mutually incoherent to one another or hybrid interactions between coherent and partially incoherent beams. Partially incoherent dark self-trapped beams (with a noninstantaneous nonlinearity) have also been employed to guide and achieve control of coherent self-trapped beams through their ability to switch to MI beyond a certain degree of incoherence.[118,119,120] As a side effect, such beams also influence the coherence character of the guided beams.[121,122] Total partial incoherence of two solitons have been employed to control interactions with tunability from attraction to repulsion[104] (Kerr type nonlinearity) via a coherence parameter, θ_0 that alters their relative phase. Coherent and mutually incoherent counter propagating beams have also been studied theoretically[107,108] as well as experimentally[109] for interactions. One beam was shown to experience attraction, and the other beam repulsion (photorefractive media). Other researchers have studied two beam interactions using incoherent white light, but between dark solitons[106] using a $LiNbO_3$:Fe self-defocusing medium. Mutual beam attraction with decreasing separation and even fusion of the beams was demonstrated.
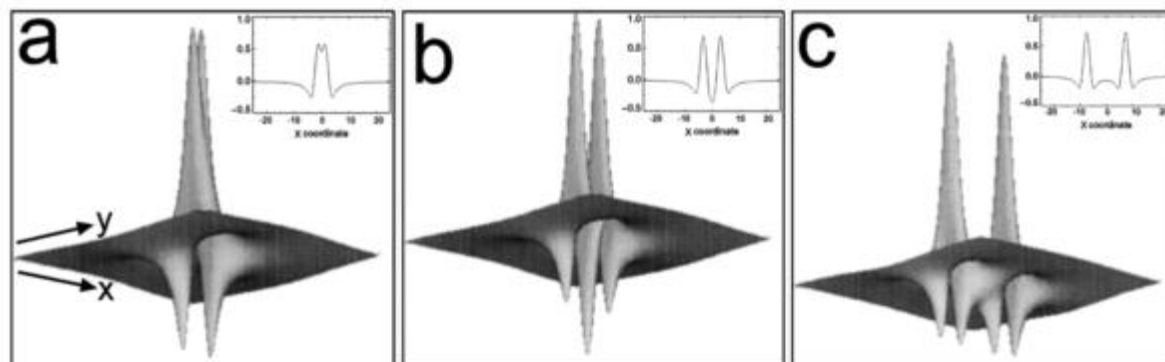
Figure 9.[105] An anisotropic medium has small dips in its refractive index profile, but only along one axis (x), as shown in the inset plots above (c). When the overlap is exactly close enough for these (-ve index profile) dips to overlap, the beams can repel one another (b). If the beams are closer, they can attract (a) (due to a +ve index profile overlap). Above, the refractive index for beam separation (along the x axis) d equal to 3 (a), 7 (b), and 15 (c). The computational window was a square of width 50. The inset plots show the variation of the refractive index in units of 1024 along the x axis.

Nonlocality and interactions in liquid crystalline materials

A separate class of interaction studies involves bright beams in a nonlocal Kerr type nonlinearity (such as nematic liquid crystal materials). A numerical study done via a coherent density approach on interactions of self-trapping spatially incoherent bright beams showed such beams can collide and cross through one another periodically.[103] Numerical studies were further extended to the study of spatially and temporally incoherent white light beams[101] as well as saturating logarithmic nonlinearity (Figure 10).[102] The degree of attraction was found to be strongly influenced by the extent of nonlocality and input power of the beams. Various wavelengths of the white light beam

are predicted to undergo collective self-adjustment according to the coherent density theory. Again, decreasing spatial separation between the beams results in a stronger attraction and consequently shortens collision and crossover periods.

Corresponding experimental studies with coherent sources in liquid crystalline media confirmed these predictions.[41] At lower nonlocality, interactions effectively resemble coherent soliton interactions and depend strongly upon relative phase difference of the beams. Tuning nonlocality effectively changes coherent to partially incoherent interactions. Because a nonlocal medium actually supports incoherent solitons through a high degree of nonlocality, this is particularly relevant to incoherent self-trapping beam interactions. Counter-propagating coherent beams were also studied for interactions in liquid crystal nonlocal media.[40] Lower power, soliton ("probe") were found to be deflected by the higher power one ("pump") and this strength was used to estimate the induced index profile width of the pump beam.
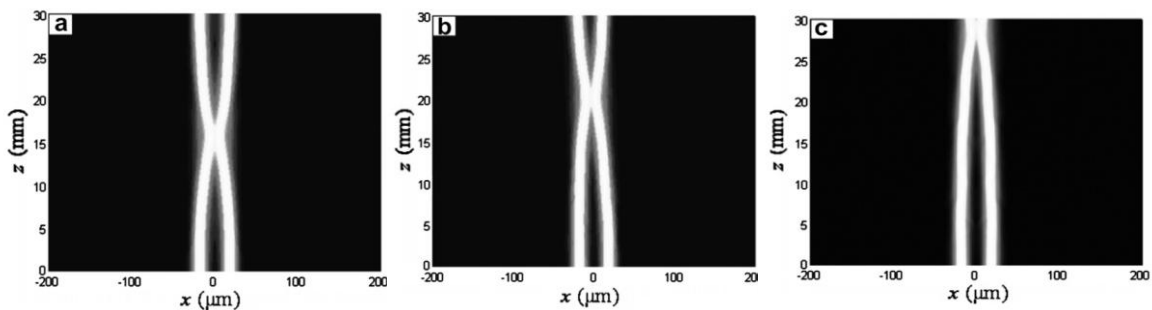
Figure 10. Attractions and crossover between two incoherent white-light solitons propagating along z-axis are simulated with their initial phase differences set to (a) $\varphi = 0$; (b) $\varphi = \pi/2$; (c) $\varphi = \pi$, respectively. In (a) the two beams pass through each other, in (b) even with $\varphi = \pi/2$ there is no significant energy transfer between the two beams. In (c) the two beams again attract and pass through each other. However, the crossover period is

highest at this φ. All these beams crossover periodically, where the period depends on φ [102]

In summary, although there are a number of strategies to study interactions between self-trapped beams, most indirectly study coherently generated beams that are either mutually incoherent or are made partially incoherent. There is a lack of direct experimental evidence of self-trapped beam interactions with each beam generated using incandescent white light sources directly. The next section explains the significance of such a study.

1.3.4. Significance of incoherent beam interaction studies

Single beam incoherent white-light self-trapping is fascinating because it is a counterintuitive collective effect, where all individual speckles and frequencies self-trap into one single waveguide. The resulting index gradient acts as a universal channel waveguide, capable of guiding any individual component(s) irrespective of frequency or degree of coherence.[12] It also enables substitution of broad spectrum incandescent sources[22] (such as LED devices) instead of expensive coherent light sources for use with self-trapping beams.

Self-trapping beam interactions on the other hand, represents a very fundamental physical property of waves - their interaction is analogous to particle collisions and appears in a variety of media with the same universal properties.[45] Beam interactions also are important for practical applications such as all-optical beam control,[123,124] beam steering and guiding,[118,125] optical wiring,[126,127] wiring based devices such as directional

couplers, beam splitters,[128] 'y' junctions,[129] and optical solder.[130] Although coherent self-trapped beams exhibit both attraction and repulsion – interactions that are well suited for applications - they are also extremely phase sensitive, making beam switching and control very difficult in practice.[90] Incoherent interactions therefore assume a special significance, because unlike their coherent counterparts their behavior is insensitive to the relative phase between the beams.

Coherent beam interaction studies

Saturating media have been shown to be well suited for using waveguides to guide and manipulate other waveguides, Beam steering and switching i.e. achieve all-optical beam control.[123,124]It is potentially advantageous over currently used devices because it can avoid fabrication of complex structures and beams can interact directly without the need for electronic controlling devices.

Low power self-guiding waveguides can guide other (higher power) beams at a different wavelength in photorefractive material.[123] However, the induced waveguide vanishes if the self-trapped beam is turned off.[124,131] Such transient waveguides hold potential for devices that require a dynamic manipulation of beams, by using erasable waveguides. Alternately, applications such as optical wiring[126]require the formation of permanent waveguide structures within the material. Several wiring based devices such as a directional coupler, multiple beam splitter[128] and a 'y' junction[129] have been demonstrated in photorefractive media using such permanent waveguides. (These were

inscribed by reorienting ferroelectric domains permanently in the crystal through phase transition[132]).

Incoherent beam interaction studies

Coherent beam interactions studies (mentioned above) have shown that strong phase dependence can be very difficult to deal with experimentally. Unlike coherent self-trapped beams, incoherent self-trapped beams always induce a phase independent refractive index increase. This makes beam control significantly easier. Further, incoherent self-trapped beams can guide beams of multiple wavelengths simultaneously. Devices based on these beams can therefore process several beams all at once for increased performance. These beams also do not need expensive coherent light sources, so they can be combined with broad spectrum incandescent sources[12] (for instance, multicolored LEDs which are cheap, efficient, long lasting).

Incoherent beam interactions in photopolymerizable media

Since photopolymerizable media are capable of both - supporting incoherent self-trapped beams, as well as making permanent waveguides, they hold particularly strong potential in applications such as optical wiring[127], optical solder[130], beam steering and guiding[125] with *incandescent* sources instead of coherent ones. Also, unlike saturating photorefractive media capable of self-trapping only extremely low (nW) powers, this media can support higher power ranges (mW) which is better suited for practical applications.

Another limitation of other media is the fixed nature of material properties such as the nonlinearity. In the case of photopolymerizable media however, the nature of nonlinearity can be tuned chemically. The nonlocal character of its nonlinearity can be varied by altering the diffusion of the monomer radicals. It therefore provides for a very interesting study for the dependence of interactions on the nature of the nonlinearity itself. This makes a strong case for the study of incoherent beam interactions in this medium.

1.4. Review of dark self-trapping beams

A dark soliton is the solution of the nonlinear Schrodinger (NLS) equation that occurs under negative nonlinearity conditions.[133] Bright solitons are the other solution, which occur when the nonlinearity is positive. Both bright and dark solitons have also been demonstrated in a variety of media, such as sodium vapor[134], bulk ZnSe[135], nonlinear optical crystals[136] with various types of nonlinearity, such as photorefractive and photovoltaic types. Although both bright and dark solitons are solutions of the same NLS equation, the physical mechanism behind the generation of each one is very different. In case of dark solitons, self-defocusing balances diffraction of the dark beam whereas in bright solitons, self-focusing balances diffraction.[137]

1.4.1. Mathematical description of dark beams

A fundamental dark soliton solution is obtained from the NLS equation as

$$u(z,x) = u_0 \tanh(u_0 x) e^{iu_o^2 z} \qquad\qquad \text{1-14}$$

This function being anti-symmetric in nature confers a defining feature on dark solitons – they have a *pi phase jump* along with a minimum or zero intensity at their center, unlike

bright solitons. The latter have a sech form and therefore have a constant phase profile with a maximum intensity at the centre.

For an input beam of the form[138]

$$u(0, x) = u_0 \tanh(ax) \qquad \text{1-15}$$

the eigenvalues of the discrete spectrum are given by $\lambda_1 = 0$, and

$$\lambda_{2n} = -\lambda_{2n+1} = \sqrt{u_0^2 - w_n^2} \qquad \text{1-16}$$

Where $n = 1,2,\dots N_0$ and

$$w_n = u_0\left(1 - \frac{na}{u_0}\right) \qquad \text{1-17}$$

And $N_0 < u_o/a$. The first eigenvalue (with value =0) corresponds to the black soliton. The secondary eigenvalues λ_{2n} correspond to gray solitons propagating on either side of the black soliton. If $u_o < a$, then only the black solitons exists as $N_o = 0$.

In order to generate the black soliton, a primary requirement is that the intensity must vanish at some point. If not, the input can be taken as

$$u(0, x) = u_0[I - b\mathrm{sech}^2(ax)] \qquad \text{1-18}$$

where only gray solitons are created. Thus, dark solitons can also be gray (especially so for incoherent beams) where the minimum intensity at the center is non-zero.[139]

A most interesting feature of dark solitons is that they do not need any minimum threshold energy to exist unlike bright solitons. Any arbitrary intensity dip in a continuous wave background is sufficient to give rise to a dark soliton (Figure 11).

Theoretically the two types are treated differently as well: bright solitons have a vanishing intensity profile and are treated as bound modes of the self-induced waveguide. Dark solitons however, have a non-zero intensity at their boundary and can be treated as radiation modes without reflections from a linear waveguide.[140] They are also known to be generally always stable at small amplitudes; in cases where they are unstable, the slope of their renormalized momentum $M_s(v)$ has to be negative.[138]

1.4.2. Generating dark solitons

Experimentally, dark solitons are generated by using an amplitude mask or a phase mask.[134,141,142] In the case of a (1+1) D beam, an amplitude mask can be made out of a thin wire like structure and its shadow is cast on the nonlinear medium while the background is illuminated. Alternately, a phase mask can be used by using a step-like transparent medium, where the path difference at the step causes light from either side to be out of phase with one another. Such a step can be fabricated for instance, by vapor deposition methods.[137]   Uniform illumination through such a step creates a zero intensity at the centre of the step due to the overlap of out of phase parts of light on either side, generating a dark beam.

1.4.3. Grayness of incoherent dark beams

Partially incoherent light (Figure 11-Figure 12) can also be used to generate an incoherent dark beam[58,143] by using a phase or amplitude mask. Such dark beams are known to become gray and do not become completely dark. A modal analysis of the dark soliton formation shows that they contain both − bound states as well as a continuum of

radiation modes.[59] Introducing a phase shift at the center makes odd modes dominant within this dark region of the beam, and is essential for self-trapping. However, grayness of the incoherent dark solitons[137] is caused by the presence of even modes of both types.
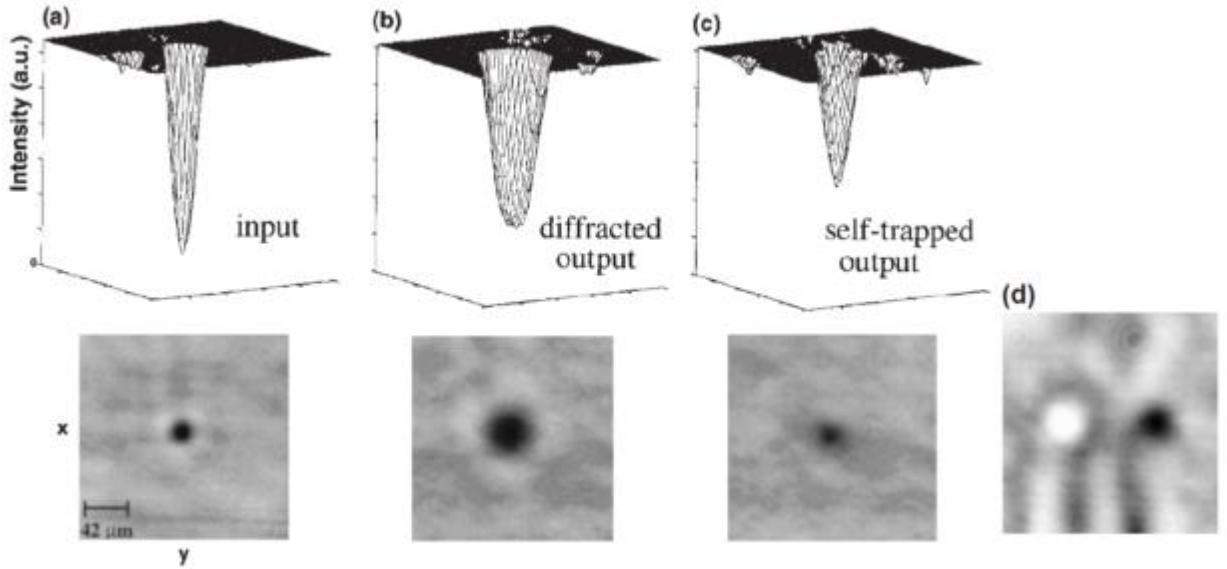
Figure 11. Self-trapping of an optical vortex[58] carried by a partially spatially incoherent beam is shown. In (a) the 3D intensity plots and photographs of the input beam, in (b) diffracted output beam, and in (c) the self-trapped output beam are shown. For better visualization, the 3D intensity plots have been truncated to remove the noise in the carrier beam. The last photograph (d) demonstrates the guidance of the carrier beam (bright spot) into the self-trapped channel of the vortex as the crystal is slightly translated to the left.
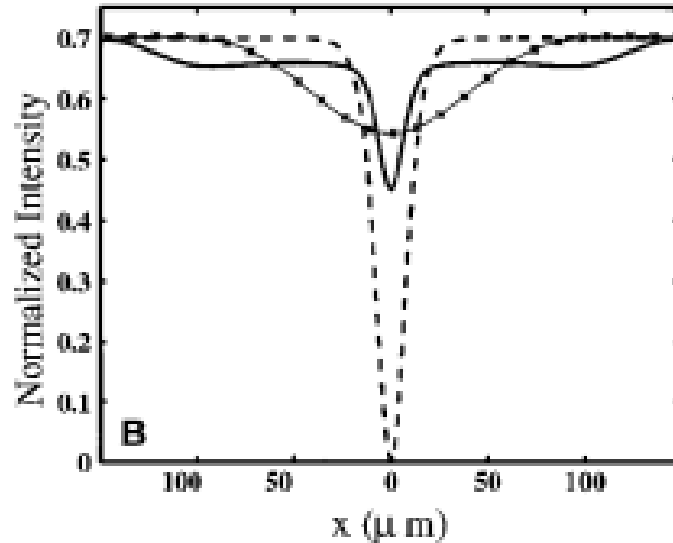
Figure 12. Numerical results[58] showing the intensity profile of the input (dashed curve), diffracted (solid curve with asterisks) and self-trapped (solid curve) incoherent dark beam when the width of the angular power spectrum is 0.3°, similar to the experimental profiles of Figure 11.

1.4.4. Applications of dark beams

Dark soliton beams are also known to show mutual repulsion in close proximity to one other in general. However, under certain non-local conditions they can also exhibit attraction.[144, 145] Dark beams in photorefractive materials have been shown to split and form y-junctions[146] and steerable waveguides[147] under certain conditions. By adjusting the phase relationship of both sides of the step in a phase mask, the waveguide can be steered to either side in the bulk medium. Further, the waveguide has also been shown to persist in the dark, and can also be used to guide other bright beams as well.[141, 148] By using incoherent sources to generate a background beam, it has been suggested that more powerful coherent beams can potentially be guided and steered with simple low-power

incandescent sources.[137] Further, arrays[149] and lattice grids[150] have also been demonstrated with dark solitons. Such structures can potentially be used in photolithography for generating sharp edges and in making periodic structures for photonic crystal lattices.

1.5. Photo-fabrication of periodic structures

1.5.1. Fabricating ordered structures

Patterning and ordering in materials can be achieved through many different methods – either top down or bottom up approaches. Various popular methods include material deposition,[151] etching[152] and lithography, novel chemical methods (self-assembly[153,154]),   mechanical   processing   (such   as   microscopic manipulation,[155]machining[156]) or other methods, such as lithographic layer-by-layer approach[157,158] or holographic lithography[159,160]or wafer fusion bonding,[161] colloidal crystallization.[162,163,164]The resulting ordered structures find many uses in electronic, photonic and many other applications, and each method has a range of applications for which it is best suited. For example, lithography and self-assembly based methods have been very widely employed for fabrication of photonic crystal structures.

Other methods such as instability induced polymer patterning[165] rely on a different approach – a balance between two opposing nonlinear forces, results in the spontaneous formation of order and patterning in the system. This method can involve temperature gradients, surface pressure[166] or electric field gradients[167], which are balanced by opposing forces – typically surface tension/buoyancy, or capillary action to result in an instability and pattern formation. Patterns can also be trapped by techniques such as UV curing in such unstable systems.[168]

1.5.2. Nonlinear 1D & 2D optically-induced lattices

Optical lattices, first theoretically proposed by Efremidis and coworkers[169] are reconfigurable photonic structures fashioned by arrays of waveguides in a nonlinear material. They have been studied in detail for use in guiding and manipulating secondary light beams through their nonlinear arrays, generation of lattice solitons and their role in diffraction management. Optical lattices sometimes mimic photonic crystals in terms of scale and functionality, and have potential applications in beam shaping, light routing, etc., for micro and nano scale devices.[170] However, photonic crystals themselves are a general class of passive materials with permanent 1D, 2D or 3D periodic high index gradients – they do not necessarily involve cylindrical waveguides or nonlinear material response. While photonic crystals are essentially Bragg gratings from 1D to 3D and can be fabricated in a variety of ways ranging from chemical to micro-mechanical to the use of light via lithography, optical lattices are restricted to 1D and 2D and were accessible through only two routes till recently.

Current methods for inducing optical lattices

Optical lattices have traditionally been generated either by (i) interference of multiple plane waves (Figure 13) or alternately by (ii) self-trapping of nonlinear periodic waves (Figure 14). In both methods, optical lattices are induced as a result of a material's nonlinear response to a periodic light intensity gradient.

In the interference method, multiple plane waves interfere to form a light intensity pattern that generates a refractive index lattice via the electro-optic effect of a nonlinear

photorefractive crystal.[169,171] This has been done with bright (in phototorefractive crystals[172]), as well as dark lattices (in liquid crystalline media), in both 1D and 2D. [173] This method requires interference between three correctly oriented laser beams for a optically induced 2D lattice of cylindrical waveguides (Figure 14).
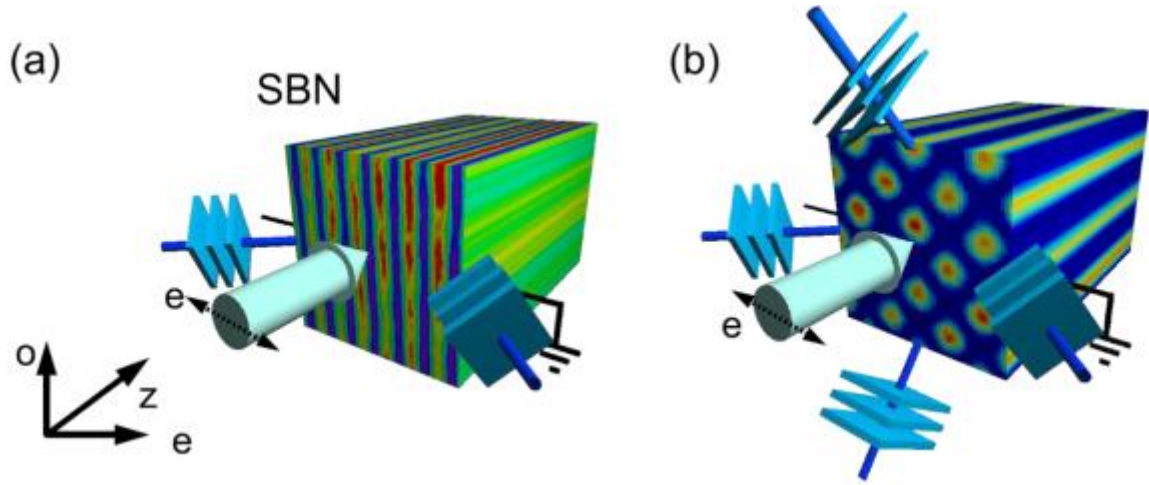
Figure 13. Experimental method of fabricating optical lattices is shown with the interference of multiple coherent beams is shown above. 2 beams can fabricate a 1 D lattice (a), and 3 beams are required to fabricate a 2D lattice (b).[174]

The propagation of light in such a system can be described (isotropic approximation) by the nonlinear Schrödinger equation for the slowly varying amplitude of the electric field,[174]

$$i\frac{\partial E}{\partial z} + D\left(\frac{\partial^2 E}{\partial x^2} + \frac{\partial^2 E}{\partial y^2}\right) - \frac{\gamma V_o}{I_b + I_p(x, y) + |E|^2} E = 0$$

1-19

where (x, y) and z are the transverse and propagation coordinates normalized to the characteristic values respectively, $D = z_8 \lambda/(4\pi n_0 x^2_s)$ is the diffraction coefficient. λ =wavelength in vacuum, n_0=avg refractive index, and V_0=bias voltage

across crystal. $\gamma\,V_0[(I_b + \; I_p(x,\; y) \;+\; /E/^2)]^{-1}$ characterizes the total refractive index modulation induced by the optical lattice and the probe beam, and is proportional to the applied electric field. Here $I_b = 1$ is the normalized constant dark irradiance, and the lattice intensity I_p depends on the specific lattice geometry controlled by the number and position of the lattice forming beams.

In the self-trapping method, a launched beam composed of either periodic waves[175] or filament arrays induces formation of an ordered array of individual solitons or 'pixel-like' beams (Figure 14-Figure 15).[176,178] These are essentially parallel index gradient waveguides within the medium, (section 1.1.1) where the index gradient results from a nonlinear material response. Such optical lattices have been previously demonstrated with an amplitude modulator and coherent light[170,177] as well as with partially incoherent light in photorefractive materials.[178] Various types such as square, diamond, and honeycomb lattices have been studied in detail for their properties (Figure 15).[179] A direct advantage of this method is the ability to launch defect modes within the lattice, creating photonic crystal fiber analogues and guiding secondary coherent probe beams.
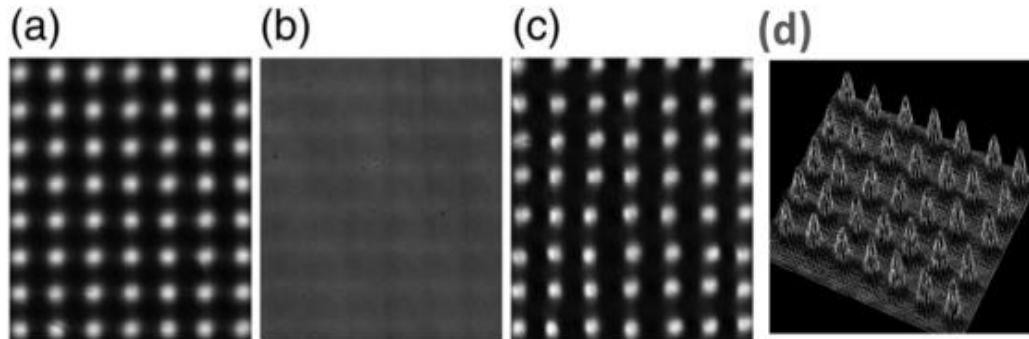
Figure 14. Spatial soliton pixels of partially incoherent light show lattice shaped intensity patterns from (a) input, (b) output with linear diffraction, (c) output with nonlinearity and (d) a 3D intensity plot of (c).[176,178]
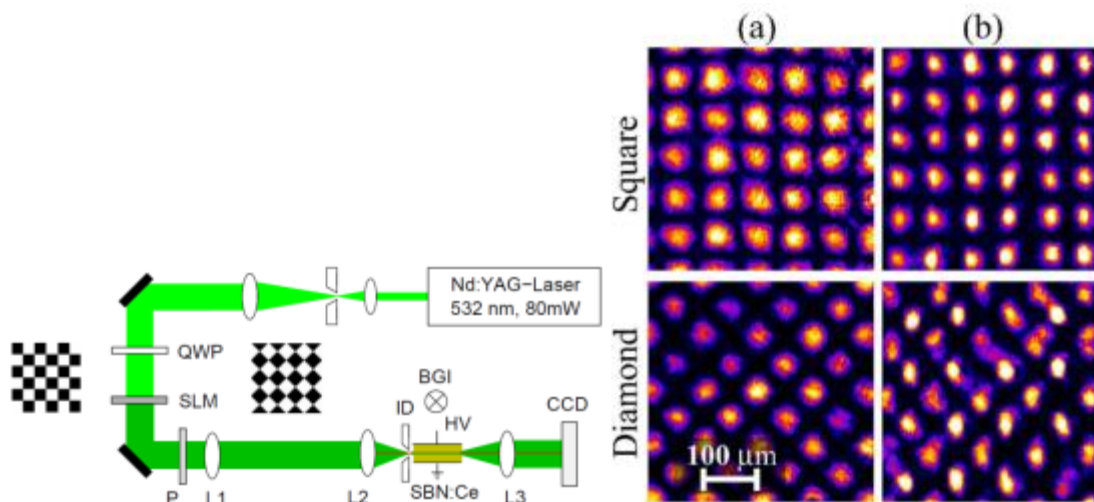
Figure 15. (Left) Complexity of a laser based setup required to generate a lattice of self-trapped beams is shown above. The setup consists of a quarter wave plate (QWP), spatial light modulator (SLM), polarizer (P), lens (L), iris diaphragm (ID), background illumination (BGI), High voltage (HV), CCD camera (CCD). The insets show the chessboard-like phase patterns for square (left) and diamond (right) lattices, phase values are π (black) and 0 (white). (Right) Experimentally generated light intensity patterns with chessboard-like phase: square (upper row) and diamond (lower row). (a) Linear output without applied electric field, (b) nonlinear output with applied electric field.[177]

1.5.3. Modulation Instability induced 3D photopolymer lattices

Our group recently discovered a means to make full 3-Dimensional lattices for the first time using waveguides induced with white light (Figure 16). [180,181] This method relies on modulation instability (MI) through use of a patterened mask to induce 2D square arrays of waveguides in a photopolymer. Modulation instability (MI) is a nonlinear phenomenon that typically occurs in the same parameter ranges as self-trapping. In MI, noise superimposed on a large self-trapping wave becomes unstable. Any existing noise in the system undergoes amplification, resulting in the formation of randomly positioned self-trapped filaments of a characteristic width. When the noise itself is periodic, the resulting filaments can also be organized periodically (Figure 16). Modulation instability occurs when the illuminating bright beam is itself extremely wide and non-uniform. Here, brighter patches of light in the optical field induce polymerization and index changes rapidly while depleting available monomer from the remaining regions, resulting in filamentation. Multiple discrete waveguides are formed as a result. Utilizing two separate white light beams with masks in orthogonal orientations results in intersecting arrays forming a full 3D lattice, with ordered filaments forming along each beam direction. This method has therefore enabled generation and study of 2D and 3D optical lattices induced with incoherent white light through a polymerization-driven approach. This method however is constrained to the formation of only square type 2D lattices with each beam.
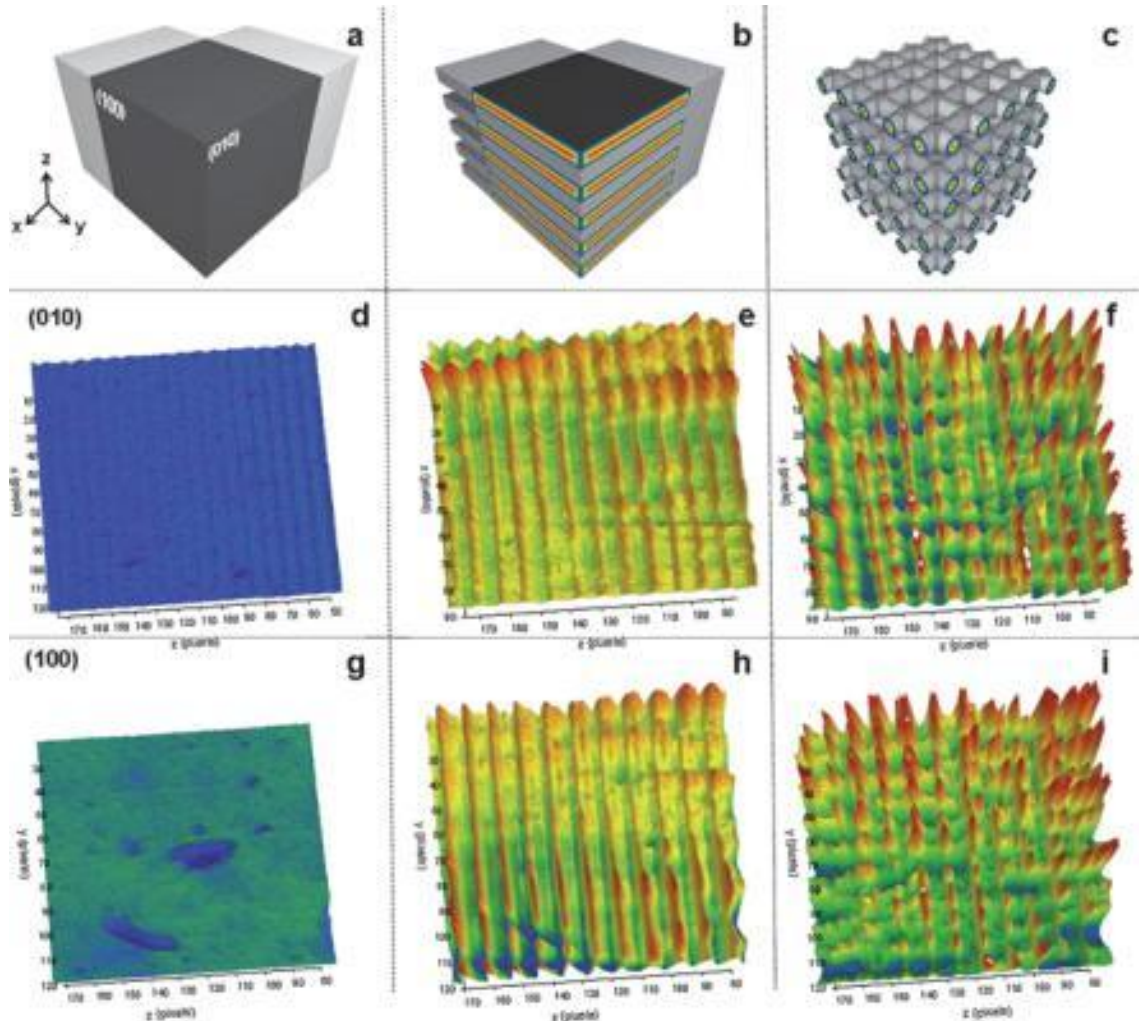
Figure 16. MI induced 3D lattices are formed by intersecting 2D arrays of waveguides in perpendicular planes are shown above induced by beams along configuration X and Y.[181] Schematic representations above show transitions in intensity distribution during lattice formation from (a) isotropic, (b) periodic stack of self-trapped lamellae to (c) 3-D lattice of self-trapped filaments. Actual intensity profiles observed in the [010] plane of the corresponding transitions of beam Y_z from (d) isotropic to (e) 1-D array of bright stripes to (f) 2-D array of bright spots are shown in the middle row. Simultaneously acquired intensity profiles in the [100] plane showed similar transitions of beam X (g–i) at the bottom. (1 pixel = 9 μm; highest (lowest) intensity = red (blue).

1.5.4. Optical lattices for diffraction management & photonic templates

Optical lattices have been studied in detail for use in guiding and manipulating secondary light beams through their nonlinear arrays, generation of lattice solitons and their role in diffraction management,[179] especially through the use of secondary coherent probe beams. Specific studies involving optical lattices are formation of random phase lattice solitons,[182] 'staggered solitons',[174] polychromatic supercontinuum gap solitons and tunability of beam diffraction and refraction via lattice parameters. Fundamental studies of interactions with solitonic launch beams, [183] vortex beams,[184] and incandescent beams have led to the discovery of new types of discrete solitons[185] such as dipole solitons, vertex solitons[186] necklace-like solitons,[187] and even incoherent white light lattice solitons.[188] Interactions have also been found to affect the lattice - the lattice itself undergoes deformation and compression[184] through formation of composite solitons. Interactions between discrete soliton arrays have also been studied theoretically, and incoherent arrays were found to always attract one another. Various types of (lattice based) solitons[174,] and related phenomena[189,] have also been studied in depth using optical lattices.

1.5.5. Basics of photonic bandgap materials

The origin of a photonic bandgap

A periodic dielectric structure exhibits a bandgap. The simplest PBG structure is a 1D periodic dielectric structure, formed by layers of alternating dielectric constants (Figure 17).[190,191] A wave propagating in such a structure can be described by a wavevector k along the z direction, the electric and magnetic fields $E(z)$ and $B(z)$ are

perpendicular to it and can be assumed to be along the x and the y directions. The

dielectric constant ε(z) is defined by ε_A if z is in layer A and by ε_B if z is in layer B.

$$\varepsilon(x) = \varepsilon(x+a)$$
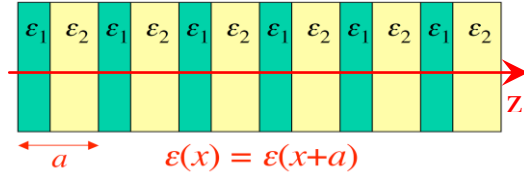
Figure 17.Assuming layers A, B of thickness a_A, a_B with dielectric constants ε_A and ε_B
form such a structure, it will have a lattice periodicity of $a=a_A+a_B$.

$$\varepsilon(z) = \begin{cases} \varepsilon_A & 0 < z < a_A \\ \varepsilon_B & 0 < z < a_B \end{cases} \qquad\qquad 1\text{-}20$$

This function can be expressed as a Fourier series $\varepsilon(z) = \sum_{p=-\infty}^{\infty} \varepsilon_p e^{i\frac{2\pi p}{a}z}$ $\qquad$ 1-21

for (-∞ < z < +∞). In this expansion form, the exponent terms have a periodicity given by

$2\pi p/a$, where p is any integer. These terms form the basis set and the periodicity is the

reciprocal lattice vector. The Fourier coefficient for a basis function is obtained by the

integral taken over the unit cell, given by $\qquad \varepsilon_p = \frac{1}{a}\int_0^a dz \varepsilon(z) e^{-i\frac{2\pi p}{a}z}$ $\qquad$ 1-22

From 1.1, $\qquad\qquad \varepsilon_p = \begin{cases} \varepsilon_A \dfrac{a_A}{a} + \varepsilon_B \dfrac{a_B}{a} & \text{for p=0} \\[2mm] \dfrac{i}{2\pi p}(\varepsilon_A - \varepsilon_B)(e^{-i\frac{2\pi p}{a}a_A} - 1) & \text{for } p \neq 0 \end{cases}$ $\qquad$ 1-23

It's photonic band structure (PBS) can be obtained as follows: The electric field

vector in such a medium can be expressed as $E(z,t) = e^{-i\omega t}E(z)$ by separating the temporal

components. Here, E(z) is obtained from the Bloch theorem, which states that in a

periodic system with a period a, the electric field vector E(z) of a wave can be expressed

as $E(z+a)=e^{ika}E(z)$. Using this for the periodic dielectric layers A,B yields the Fourier expansion,

$$E(z) = \sum_{p=-\infty}^{\infty} c_p e^{i(k+p\frac{2\pi p}{a})z}$$

1-24

This electric field vector E (z,t) passing through the medium satisfies Maxwell's equations,

$$\frac{\partial^2}{\partial z^2} E(z,t) - \frac{1}{c^2} \frac{\partial^2}{\partial t^2} \varepsilon(z)E(z,t) = 0$$

1-25

Substituting its form from 1.1-2 with the Fourier expansion of $\varepsilon(z)$ in this equation and setting the prefactor term of the plane wave $e^{i(k+2\pi p/a)z}$ to zero yields

$$\left(k + \frac{2\pi p}{a}\right)^2 c_p - \sum_{p'=-\infty}^{\infty} \left(\frac{\omega}{c}\right)^2 \varepsilon_{p-p'} c_{p'} = 0 \quad (p=(0,\pm1,\pm2,...))$$

1-26

This gives a system of linear coupled equations where the coefficients can be cast into a determinant D (known as the secular matrix), given by

$$\det \begin{vmatrix} ... & ... & ... & ... & ... \\ ... & (k-\frac{2\pi}{a})^2 - (\frac{\omega}{c})^2\varepsilon_0 & -(\frac{\omega}{c})^2\varepsilon_{-1} & -(\frac{\omega}{c})^2\varepsilon_{-2} & ... \\ ... & -(\frac{\omega}{c})^2\varepsilon_1 & (k)^2 - (\frac{\omega}{c})^2\varepsilon_0 & -(\frac{\omega}{c})^2\varepsilon_{-1} & ... \\ ... & -(\frac{\omega}{c})^2\varepsilon_2 & -(\frac{\omega}{c})^2\varepsilon_1 & (k+\frac{2\pi}{a})^2 - (\frac{\omega}{c})^2\varepsilon_0 & ... \\ ... & ... & ... & ... & ... \end{vmatrix} = 0$$

1-27

It yields a set of solutions $\omega_1(k)$, $\omega_2(k)$,…$\omega_n(k)$ that satisfy the equation D=0, where the subscript n is known as the band index. The solutions are actually continuous functions of k and form the dispersion curves of the photonic bands for this 1D system.

The 2D solution can be extended to 3D structures using

$$\varepsilon(r) = \sum_h \varepsilon_h e^{ih.r}$$

1-28

where h is the reciprocal lattice vector with h=2πp/a for a 1D case. and yields a similar determinant consisting of 3x3 block matrices and $(I_{hh'})_{ij}=\delta_{ij.}$ Again, the solutions for ω^2 of

the secular equation yield the eigenvalues for the photonic band. The band structure is obtained in a plot of the eigenvalues as a function of the wavevector k in the first Brillouin zone.

Besides the 'plane wave expansion method' described above, alternate methods for solving the PBS include (i) Vector Korringa-Kohn-Rostoker (KKR) method[192] (limited to arrays of spheres and cylinders), (ii) Bloch theorem extension of single PC layer scattering data[193] and (iii) Finite-Difference Time-Domain (FDTD) method[194] (which uses explicit periodic boundary conditions on a unit cell). Unit cell defects can introduce defect modes within a bandgap which can also be solved with some modifications such as treating them as a perturbation of the normal modes of the host PC, so that $\varepsilon(r) = \varepsilon_0(r) + \delta\varepsilon(r)$. Alternatives for solving defect modes accurately exist as well.[195,196,197]

The bandgap of a PBG material is independent of the absolute scale of the lattice periodicity in the structure.[190] In other words, a micron scale lattice that possesses a bandgap for much smaller wavelength and a centimeter scale lattice with a bandgap for wavelengths orders of magnitude larger will have identical band structures provided their lattice structures are scaled up in the ratio of the wavelengths.

Common PBG structures

An ideal PC should possess a bandgap in 3D and the larger the gap, the better the light confinement. Only (i) FCC and (ii) diamond structures (or a modification of these two) satisfy this requirement best.[198] The FCC structure actually exhibits a pseudo

bandgap in 3D since the gap does not cover the entire Brillouin zone (BZ), but can be constructed easily by self-assembly, with air spheres in a dielectric ("inverse opal" structure). The diamond structure possesses a complete bandgap in 3D and can be constructed with more difficulty by drilling holes along the 110 direction into an FCC lattice, oriented vertically in the 111 direction. A third design is the "woodpile structure" with four layers of sheets of dielectric gratings form one period. The grating layers are stacked in alternating perpendicular directions so that the structure appears like a "mesh" or woodpile from a vertical viewpoint. The bandgap depends on the refractive index contrasts and the filling ratios f, which in turn depends on the radius r_s of the spheres in the lattice.[191,198]

Applications of PBG structures

The most relevant application of PBG structures to optical self-trapping, is photonic crystal fibers (PCFs) that closely resemble optically induced self-trapped waveguides (Figure 18). Optical fiber analogues made out of PC materials are of three main types[199] (a) holey fiber, (b) PBG fiber and (c) Bragg fiber. They are made by stretching and cooling heated silica fiber structures with preformed air holes in the core. The holey fiber consists of an optical fiber with its core cross section consisting of holes and a dielectric defect at the center whereas the PBG type has an air defect at the center. The Bragg type consists of concentric alternating multilayers, somewhat similar to a step index waveguide. These fibers provide low propagation loss (<0.5dB/km) along with strong optical confinement and other unique features making them useful for dispersion compensation fibers.[200,201]
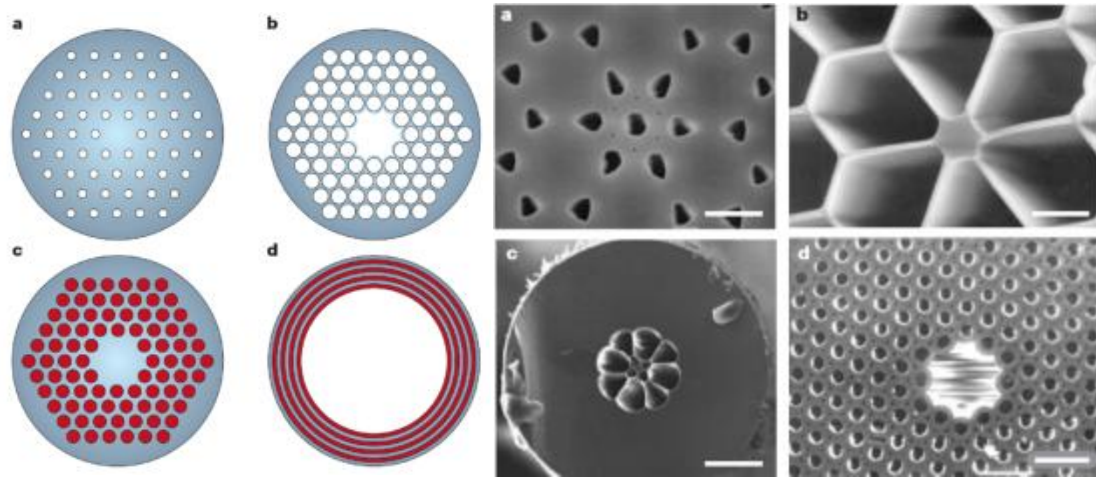
Figure 18. (Above) white= air, blue= low-index silica, red= high-index material. (a) single-mode fibre with silica core & reduced-index PC cladding, (b) air-guiding fibre with hollow core & 2D air–glass PC cladding, (c) silica core with high index liquid cladding filled with holes, (d) hollow cylindrical multilayer fibre with an all-solid cladding. (Right) PCF Electron micrographs show (a) Bandgap guiding fibre - with glass ring around central hole, (b) strongly TIR guiding PCF (O dispersion) around λ= 800 nm, (c) extruded fibre formed from commercial SF6 glass, (d) hollow-core photonic bandgap fibre.[a,c– bar=10µm;   b,d bar=1µm]

1.6. **Review of self-trapped dark ring beams**

Ring dark solitons were studied numerically by Kivshar, et al., in 1994 for a self-defocusing nonlinearity (Figure 19).[202] The NLS equation describes a self-trapped beam in a medium by

$$i\frac{\partial u}{\partial z} + \frac{1}{2}\Delta_\perp u - |u|^2 u = 0 \qquad \text{1-29}$$

Here, Δ is the transverse Laplacian describing spatial broadening and u represents the electric field vector. The last term represents the changes through nonlinearity that balance diffraction. In cylindrical coordinates, Δ is transformed as:

$$\Delta_\perp = \frac{\partial^2}{\partial r^2} + \frac{(D-1)}{r}\frac{\partial}{\partial r} \qquad \text{1-30}$$

For dark-soliton solutions of circular symmetry, with slowly varying parameters, the solution is found to be of the form

$$u(z,r) = e^{-iz}(\cos\phi\,\text{tanh}Z + i\sin\phi) \qquad \text{1-31}$$

Where

$$Z = \cos(\phi)[r - R(z)] \qquad \text{1-32}$$

In this solution form, cos 2Φ is the contrast of the dark soliton (Φ is the soliton angle, 2 Φ is the phase jump across the soliton) and R is the (slowly varying) soliton ring radius. A numerical analysis shows that

$$R_{min} = R(0)[\cos\phi(0)]^{3/(D-1)} \qquad \text{1-33}$$

Further, at $R=R_{min}$, contrast is maximum. The soliton can either collapse to reach R_{min} or diverges to decrease the contrast, depending on the initial value Φ (0).The dark soliton is expected to be always stable, even expanding when the limit length of the ring R_{min} is

smaller than the minimum wavelength $1/Q_{cr}(0)$ for the instability region, i.e., $R_{min}Q_{cr}<1$.(Q_{cr} is the maximum wave number that characterizes an instability band).

Two specific scenarios can occur,(i) when sin Φ (0)>0 the ring soliton simply diverges (ii) when sin Φ (0)<0, it first collapses to reach the minimum value R min before diverging. The equation for the soliton amplitude also turns out to be identical to the common cylindrical KdV equation representing cylindrical and spherical pulse solitons in plasmas and tsunami-shallow water waves.

Dark ring soliton formation was also demonstrated experimentally by Baluschev, et al., using an amplitude mask and a coherent source (Figure 20).[203]Dark self-trapped beams were referred to as odd dark spatial solitons (where as dark self-trapped rings were referred to as even dark spatial solitons), due to the number of phase flips across the soliton. Their experimental setup consisted of using an amplitude mask with dark dots and lines ranging from 50-250 μm. Temporal evolution showed that a dark dot evolves initially as a dark self-trapped beam, which later gives rise to a bright central region and subsequently concentric bright rings. They also demonstrated numerically that the bright central beam formed in the evolution has a higher intensity than the background bright region. However, significant interference lines were also observed from the input and output faces of the sample. Such beams were also shown to support >1 self-trapped ring.

Dark ring solitons were also thought to be useful for real-time reconfigurable applications involving light directing, switching, and multiplexing/demultiplexing for

information transmission purposes. Similar dark rings were also observed in other

environments such as Bose-Einstein condensates.[204,205]
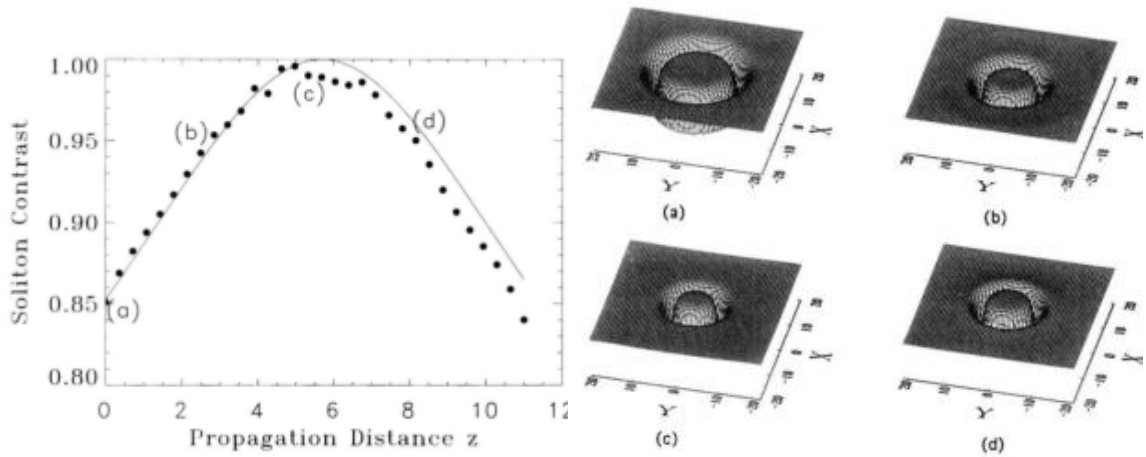
Figure 19. Evolution of a ring dark soliton is shown above. (Left)The soliton contrast $\cos 2\phi$ vs. propagation distance z is shown.[202] (Right) The profiles (a)-(d) display a ring dark soliton (unit-intensity background) at different distances marked on the (left) figure. (a) and (b) correspond to a collapsing soliton whereas (c) and (d) correspond to a divergent soliton.
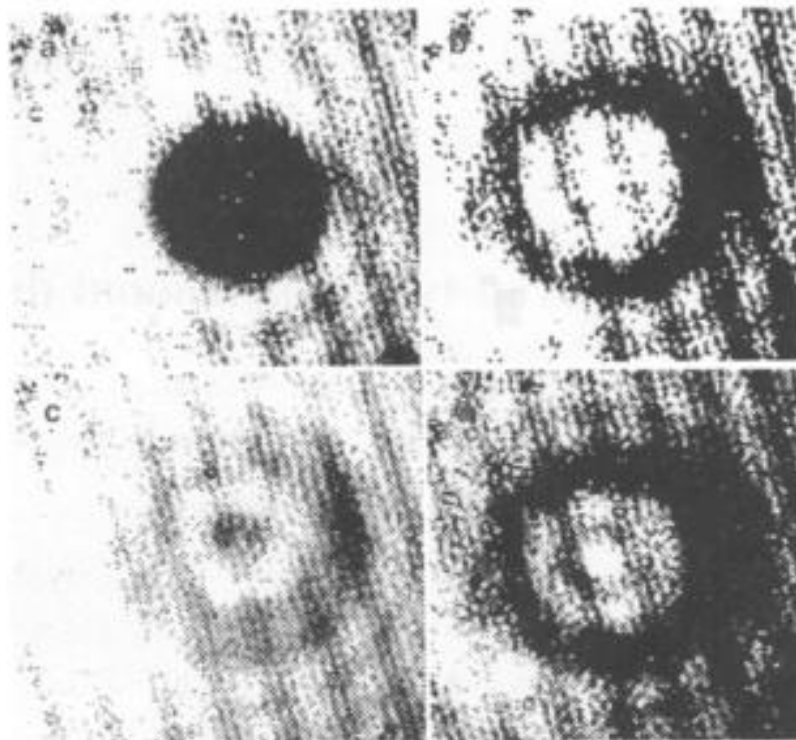
Figure 20. Evolution stages of a 2D EDSS obtained experimentally: (a) diffraction compensated by the medium nonlinearity; (b) first soliton ring; (c) initial stages of a second soliton ring; (d) two soliton rings.[203]

1.7. **Objectives of the doctoral studies**

Self-trapped beams of incandescent white light, which is both spatially and temporally incoherent, was first shown by Mitchell and Segev in 1997.[12] Because it originates from the uncorrelated decay of excited states, white light suffers rapid and random phase fluctuations[33,34] self-trapping of this weakly correlated beam has been theoretically examined in terms of spatial correlation, shape[34], frequency distribution,[31] behavior in media with nonlocalized responses, response to intensity fluctuations, propagation in nonlinear lattices and susceptibility to modulation instability.[33] These studies raise intriguing questions about the interaction dynamics of self-trapped white light beams and consequent changes to their statistical coherence structure. Although their collisions were recently studied for the first time by extending the mutual coherent density approach,[102] there has until now been no experimental study of the interactions of self-trapped white light beams, which can only be generated in materials with a noninstantaneous and saturable photo response. These properties, which respectively smooth (time-average) out phase fluctuations and facilitate growth of a multimode waveguide, are difficult to elicit in materials with ultrafast responses originating from high-order susceptibility tensors and in the first experimental study, were realized at very low intensities (nW) in a photorefractive crystal.[12] Saturability and noninstantaneity however are inherent to refractive index change due to free-radical photopolymerization reactions and our group recently demonstrated that self-trapping over a wide range of intensities in a polymerizable organosiloxane. Refractive index change due to polymerization is expressed through Equation [1-11].[63] By taking advantage of this

accessible experimental route, for the first time, various phenomena with incoherent white light can now be examined in detail.

The primary aim of this study is to explore the viability of known coherent phenomena as well as occurrence of new self-trapping phenomena with incoherent white light. Several phenomena have traditionally been studied using coherent light, and strongly depend on the phase relationship of coherent beams. With incoherent white light, such a phase relationship does not exist and theoretical predictions indicate major differences in them. A primary example is interactions between two self-trapping beams of incoherent white light (section 1.3).

Initial studies (chapter 3) began with a study of the incoherent counterpart of coherent interaction studies (reviewed in section 1.3). Preliminary evidence showed for the first time that incoherent interactions show a rich variety of phenomena such as repulsion between two incoherent beams, not predicted by existing theoretical studies. A careful analysis showed dark regions can form between incoherent bright self-trapping regions and tend to influence their interactions. Further research (chapter 4) clearly indicated dark beams can exist in photopolymer media. Previous studies (reviewed in section 1.4) have always suggested negative nonlinearity is a requirement for a dark beam to self-trap in the medium, which is not the case with our experimental and simulation results. These studies demonstrate dark self-trapping for the first time in a positive nonlinear medium.

Subsequently, dark beams were explored thoroughly, for their properties, and were found to be useful in controlling and directing bright self-trapped beams (chapter 4) 2D as well as 3D lattices of a large variety of patterns were demonstrated using such beams. These studies demonstrate an extremely simplified approach to creating complex 3D lattices previously made through laborious and expensive coherent optical assemblies (reviewed in section 1.5).

However, in order to create woodpile like lattices with such beams, some major modifications were made to the masks and embedded beams (chapter 7) were found to be essential. Because such beams were not demonstrated before with incoherent light and are counterparts of previous coherent studies (reviewed in section 1.6) these were also analyzed in detail. These studies are the first experimental studies of complex ring beams with incoherent white light.

Format and sequence of the thesis

The results of this research can be classified into four major ideas, presented through chapters 3-7 as follows: chapter 3: Interactions of two incoherent white light beams, 4: Dark self-trapping beams with incoherent white light, chapters 5-6: Fabricating lattices using bright and dark incoherent beams and chapter 7: incoherent ring beams involving aspects of both dark and bright self-trapping.

In chapter 3: Interactions of two beams, the primary objective was to experimentally characterize interactions between a pair of parallel propagating self-trapped beams of incoherent white light in photopolymerizable media. Specific objectives

were (i) Parallel beam interactions at varying spatial separation between two beams. Do parallel incoherent beams *always* fuse at close separations, as theoretically predicted? (ii) Angular interactions by varying the angle between two coplanar beams for angular collision phenomena such as fusion, deflections or cross coupling of light. Coherent angular studies range from small angles ($<10^0$), large angles (90^0, 180^0) and non-coplanar beams demonstrating fusion, simple crossing, or even spiraling. (iii) Between the two extreme cases of fusion at small angles and simple refraction at large angles, mutually incoherent beams have a threshold where they can still couple light into each another without fusing. This threshold itself is limited by their total internal reflection angle. A potential objective is to study the existence of such a threshold with white light beams. This may be may be done by using beams which are distinguishable even after interactions (e.g. by using two different polarization filters) to provide a good insight into the coherence behavior of colliding beams.

In chapter 4: dark beams, the objectives were (i) to prove conclusively the existence of incoherent dark self-trapping beams in photopolymer media, as well as (ii) to characterize the new phenomenon. Dark beams are theoretically predicted to exist in self-defocusing media, and existence of dark self-trapped beams in such a positive nonlinear environment cannot be explained by current theory. (iii) Additional studies may include simulation studies of dark self-trapping beams in order to explain their mechanism of formation.

In chapters 5-6: self-assembly and self-organization of lattices, the primary objective of the study was to demonstrate the feasibility of achieving control of bright as

well as dark beams, especially to fabricate a variety of 2D and 3D structures. This can be done by using masks to generate multiple self-trapped beams - dark self-induced arrays as well as bright - in each plane, and can potentially be extended from 2D to 3D. Such lattices can potentially be used as templates for photonic band gap materials as well. Theoretical studies of simulated self-trapped arrays (using BandSolve® software) can reveal potential band gaps. In the future, such optimized structures can be made experimentally as well. Feasibility of fabricating a 3D woodpile lattice can also be explored −a woodpile is significant for its 3D theoretical bandgap.

In chapter 7: Coaxial beams, the objectives were to (i) study the existence of embedded beams and (ii) characterize them experimentally. Embedded bright beams consist of regular bright self-trapped beams with dark core, while embedded dark beams would consist of the converse - dark self-trapped beams with a bright core. Such beams – if they exist in incoherent media, can be studied for their stability, coherence and interaction properties in photopolymer media. (iii) Simulation studies in 2D can also be done for ring beams in order to correlate theory with experimental behavior.

List of Publications

The following is a list of publications that derive from the corresponding chapter:

Chapter 3	"Interactions of mutually incoherent self-trapped beams of white light in a photopolymerisable medium", Kasala, K.; Saravanamuttu, K. *Appl. Phys. Lett.,* **2008**, 93, 051111
Chapter 4	"A black beam borne by an incandescent field self-traps in a photopolymerizing medium", Kasala, K.; Saravanamuttu, K., minor revisions requested, *Journal of American Chemical Society*, 20 July **2012**, ja-2012-05671b
Chapter 5	"Optochemical self-organization in spatially modulated white light beams: a single-step route to polymer lattices assembled from dark and bright waveguides", *manuscript submitted*
Chapter 6	"Optochemical self-organisation of white light in a photopolymerisable gel: a single-step route to intersecting and interleaving 3-D optical and waveguide lattices", Kasala, K.; Saravanamuttu, K. *J. Mater. Chem.*, **2012**, 22, 12281
Chapter 7	"Coaxial self-trapping of white and gray regions of an incandescent field: a bright core with a dark cladding," Kasala, K.; Saravanamuttu, K., *Physics Research International: Advances in Novel Optical Materials and Devices(Invited)*, **2012**, 798906
Other Publications	"Self-trapping of spatially and temporally incoherent white light in a photochemical medium", Zhang, J.; Kasala, K.; Rewari, A.; Saravanamuttu K. *J. Am. Chem. Soc.,***2006**, 128, 406
	"Self-trapped white light beams and their interactions in a photochemical system", Zhang, J.; Sakalauskas, M.; Kasala, K.; Saravanamuttu, K. *Polymer Materials Science and Engineering Preprints*, **2006**, 95, 875

2. Experimental setup

2.1. Sample Preparation

Organosiloxane samples were prepared by the acid-catalysed condensation of 17.6 g (7.08 x10^{-2} mol) of 3-(trimethoxysilyl) propyl methacrylate (MAPTMS Sigma-Aldrich, USA) with 1.08 g (5.40 x 10^{-5} mol) 0.05M HCl. The initial phase separated mixture was stirred until it became homogenous, clear and transparent. This was sensitized to visible light with 0.096 g (0.05 wt %, 1.79 x 10^{-4} mol) of photo-initiator bis(η5-2,4-cyclopentadien-1-yl)-bis(2,6-difluoro-3-(1H-pyrrol-1-yl)-phenyl) titanium(IV) (λ_{max}= 393 nm, 460 nm, Ciba Specialty Chemicals, Inc., Canada). The mixture was stirred in the dark for >16 hours and was filtered through a polytetrafluoroethylene (PTFE) membrane (0.2 μm pore size, Pall Corporation, USA) before use. The sol was placed in a plastic spectrophotometer cell, (path length 10 mm, 3.5 ml, 334–2500 nm) and irradiated uniformly with white light from a Quartz-Tungsten-Halogen lamp (7 min, 0.6 W Cole-Parmer 9741-50-series, IL, USA) with the aid of a rotating magnetic stir-bar and an illumination chamber. The illumination chamber is essentially a 15 cm x 4cm steel tube lined with aluminum foil for enhanced and uniform reflectivity. The sample cuvette was placed on a magnetic stirrer, the chamber was positioned on the cuvette, and an optical fiber cable from the lamp was positioned ~5cm above the chamber to allow for uniform illumination. This resulted in uniform partial polymerization of the sample.

2.2. **Experimental setup for threshold studies**

The optical assembly for these studies (section 9.1) consisted of an incandescent Quartz-Tungsten-Halogen lamp (ScienceTech 200 Series, adjustable range 0-250W, ScienceTech Inc., USA) with a pinhole as the white light source (Figure 21). A pair of plano-convex lenses (L1, 25cm & 7.5cm focal lengths) focused this source beam onto an organosiloxane sample (S) (this is the nonlinear medium). This focal plane is the entrance face of the propagating beam in the nonlinear medium. The beam then propagates and diffracts through the length of the cuvette (10 mm path length). The imaging system consists of a CCD camera attached to a pair of plano-convex lenses (L2, 25cm & 25cm focal lengths) that can image any desired transverse cross section plane of the propagating beam throughout the length of the cuvette. This CCD system is set to image a plane 5.5mm from the entrance plane − this is the exit face of the beam. CCD camera (WinCamD^{TM} 14-bit digital camera,1360 x 1024 pixels, 4.65 μm squares, Data Ray Inc., USA), was driven by a beam-profiler software DataRay© (Version 5.0). The software calculates beam diameter (FWHM, $1/e^2$), relative peak intensity, generates 2 and 3-D intensity profiles. The CCD-lens system (CCD-L1-L2) had an effective magnification of 1.017. All imaging optical components were mounted on carriers that could be translated along the optic axis z with a resolution of 0.25 mm. The cell was additionally mounted on a micrometer stage which could be translated along z with a resolution of 0.5 μm. Six different pinholes (20μm, 30μm, 40μm, 50μm, 75μm and 100μm) were used as light sources in otherwise identical experiments. The source lamp intensity was adjusted at the beginning for each beam size, so that the beam power was nearly constant for each

different pinhole at ~10% of the CCD saturation value. Observations were then recorded every second for at least 3500 seconds on camera, with images being taken every 5 seconds.
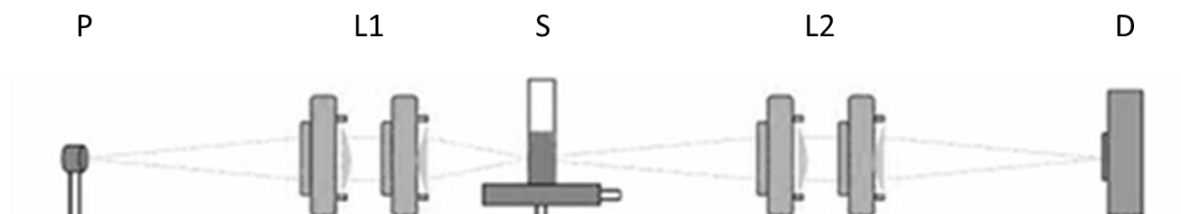
Figure 21. A diagram of the optical assembly shows light from an incandescent source passing through a pinhole (P) and focused (through plano-convex lenses L1) onto the entrance face of a cuvette filled with organosiloxane (S). Intensity profiles of beam after propagating 5.5mm in the cuvette are imaged onto the CCD camera-lens system (D-L2).

2.3. **Parallel beam interaction studies**
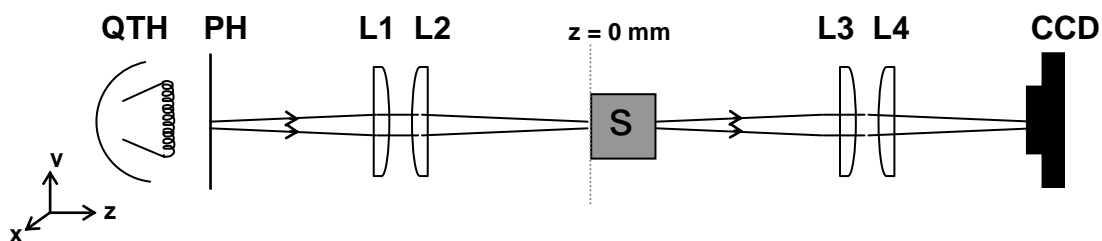
Figure 22. Scheme of the optical assembly. Light emitted by a quartz-tungsten-halogen (QTH) lamp was passed through two co-planar pinholes (PH) and focused through a pair of plano-convex lenses (L1, L2) onto the entrance face (z = 0 mm) of a cuvette containing the organoxiloxane (S). Profiles of the beams at z = 8 mm were focused through a second pair of plano-convex lenses (L3, L4) onto a CCD camera. Inset is the actual cross-sectional profile of the beam pair at z = 0 mm; parameters used to characterize beams in experiments are indicated.

Figure 22-Figure 23 are schemes of optical assemblies used for self-trapping interaction studies. The incoherent white light source was a power stabilized, quartz-tungsten-halogen lamp (ScienceTech 200 Series, range 0-250W, ScienceTech Inc., USA). The beam was first passed through a thin metal sheet with a pair of 50 μm pinholes (Lenox Laser Inc., USA) and then focused by a pair of plano-convex lenses (L1 = 25.6 cm, L2 = 7.56 cm) onto the entrance face (z = 0 mm) of a glass cuvette containing the organosiloxane medium. The peak-to-peak separation of the beam pair at z = 0 mm was adjusted by employing pinholes separated by different distances. Each beam at z = 0 mm had a width of ~40 μm and a power of 148 ± 10 nW (measured with a FieldMaster GS, Coherent Inc, USA). A second pair of plano-convex lenses (L3, L4 = 25.6 cm) imaged the beams at z = 8 mm with a magnification of 1 onto a CCD camera (WinCamD^{TM} 14-bit digital camera,1360 x 1024 pixels, 4.65 μm squares, Data Ray Inc., USA). The camera and optical components were identical to the assembly in Figure 21.

Proof of fusion of the two beams
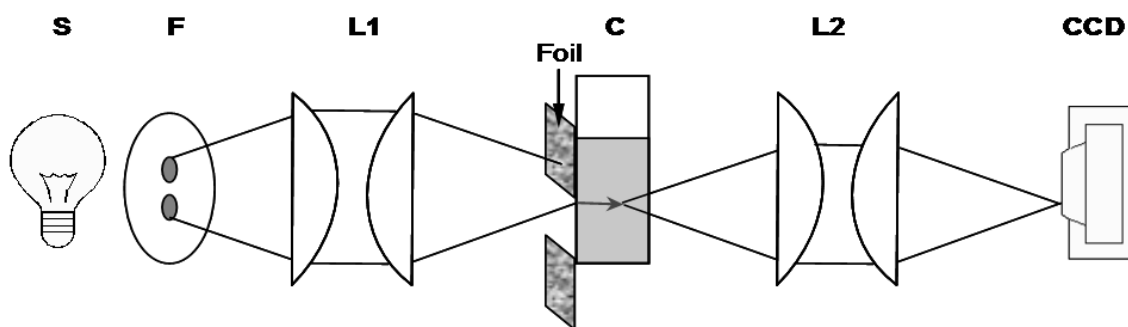
Figure 23. A schematic of the modified optical assembly used to generate single probe beams for interaction studies is shown above. Light from the incandescent source (S) is focused onto the organosiloxane cuvette (C). The output plane of the two beams is

monitored using a camera lens system (CCD-L2). A blocking mechanism is inserted at the input position of the two beams and can selectively block any one input beam while allowing the other beam to pass through.

In order to verify two beam fusion conclusively, it is essential to be able to distinguish each beam independently within the resulting single fused peak. The optical assembly was modified slightly, (as shown in Figure 23 above), to introduce a blocking mechanism that could selectively block either of the two input beams A and B. By choosing to selectively block only beam B, the profile of beam A can be mapped individually within the peak resulting from the interactions, and vice versa. These images were acquired once the single merged beam was observed. Each beam was blocked in turn while the other was imaged. Measurements were made quickly within a time period (4 s) that was much smaller than the response time of the medium, thus ensuring that significant refractive index changes did not occur during this time.

2.4. **Angular interactions assembly**

Large angle beam collision studies

Light from an incandescent Quartz-Tungsten-Halogen lamp source (S) is coupled into two multimode optical fibers (F) of 50 μm diameter each (Figure 24). Light from the cleaved ends of the two fibers are focused with a pair of plano-convex lenses (L1) onto the inner wall of an organosiloxane filled cuvette (C). The cuvette is 1cm x 1cm x 3.5 cm in dimensions, and its walls are 1 mm thick. The lenses in (L1) each have a focal length of 25 cm, and each pair (L1) along with its corresponding fiber tip, is mounted on a

rotating arm pivoted at the cuvette wall (C). The two arms (shown with the blue dotted arrow at L1) can rotate from a minimum angle of 80 up to 180^0. Each lens pair (L1) has a 1:1 magnification and launches a 50 micron wide incoherent white light beam at the inner wall of the cuvette (C).

The imaging side of the assembly consists of another pair of plano-convex lenses (L2) of focal lengths 1.9 cm and 3.8 cm respectively. The imaging assembly L2-CCD is also mounted on a rotating arm that is pivoted about the cuvette wall (C), and can rotate about it. It can therefore be rotated to image each beam individually, or even both beams simultaneously provided their angular separation is small.
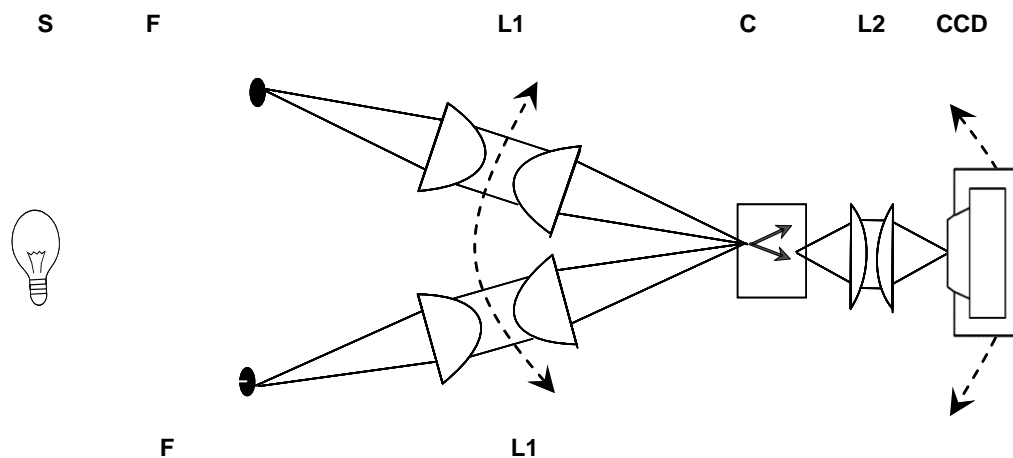
Figure 24. "Large angle assembly": Two self-trapping beams are generated by using light coupled into two optical fibers (F) from an incandescent source (S). The light is focused onto a cuvette (C) containing the organosiloxane sample using a pair of plano-convex lenses (L1). Each assembly of the light source and lenses (F-L1) can be rotated freely about an angle, in order to generate self-trapping beams at angles within the cuvette (C).

The imaging assembly consists of another pair of plano-convex lenses (L2) and a CCD camera.

Small angle collisions assembly

In order to study angular collisions smaller than 8 degrees, the constraints imposed by the lenses in the large angle assembly had to be eliminated. The small angle assembly (Figure 25) achieves this by using the fibers to directly illuminate and generate two white light beams within the cuvette. It consists of the same incndescent source (S) with two optical fibers (F) to generate the two beams as before, but without the lenses (L1) of the large angle assembly. The imaging side is identical to large angle assembly and consists of two plano-convex lenses (L2) and a CCD camera. The cuvette in this case is made by using two thin glass cover slips. Each micrometer stage (M1 and M2) controls a needle glued to the optical fiber in order to orient it in space. Using 2D micrometer stages (M1) gives sufficient flexibility to orient the two fibers at small relative angles to one another.
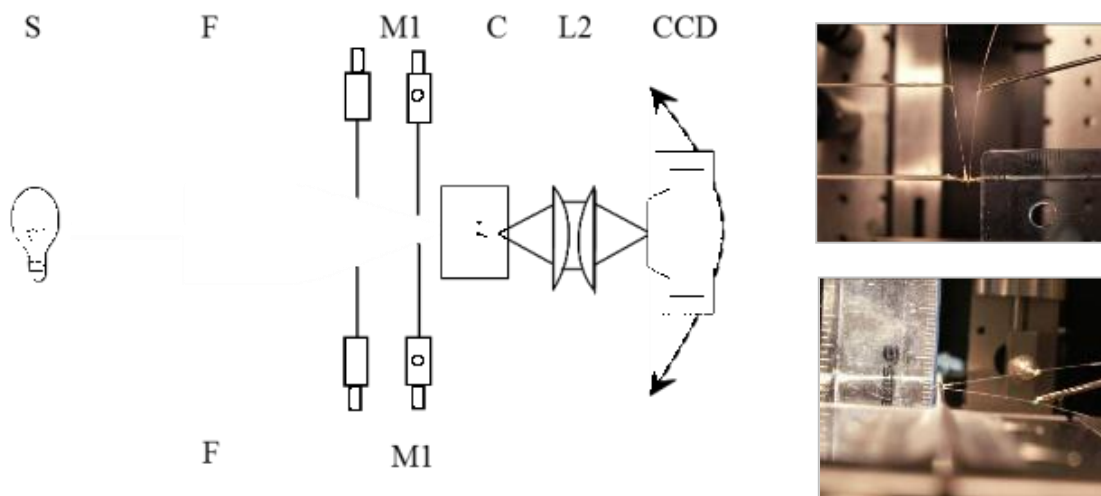
Figure 25. "Small angle assembly": Two self-trapping beams are generated by using light coupled into two optical fibers (F) from an incandescent source (S). The light is directed onto a thin cuvette wall (C) directly from the optical fibers (F). Two micrometers (M1-M2) are used to orient each fiber along a desired angle. Each assembly of the light source and lenses (F-L1) can be rotated freely about an angle, in order to generate self-trapping beams at angles within the cuvette (C). The imaging assembly consists of another pair of plano-convex lenses (L2) and a CCD camera. The photographs on the right show the tips of the fibers used to generate the two beams at an angle.

2.5. **Generating dark self-trapping beams with white light**
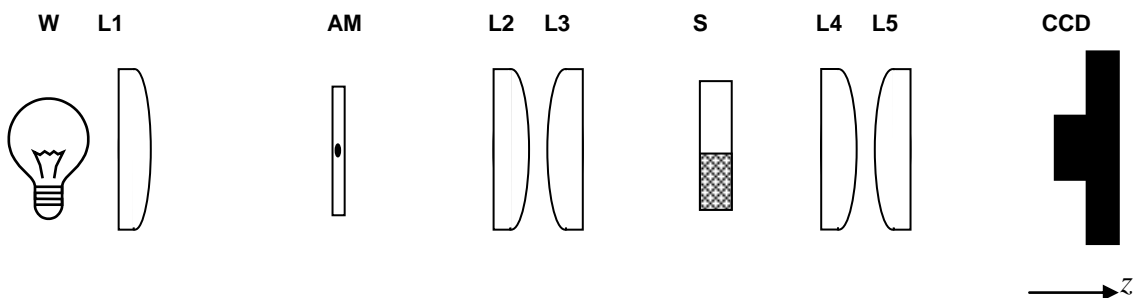
Figure 26. A schematic diagram of the optical assembly used to generate the dark beams is shown. Light from a Halogen lamp-Lens assembly (W-L1) illuminates an amplitude mask with a dark spot (AM), which is in turn imaged onto the inner wall of an organosiloxane filled cuvette (S) using a pair of plano convex lenses (L2-L3). The imaging setup consists of a CCD and a pair of lenses (L4-L5) that can be moved together, to focus on any plane within the cuvette.

Optical assemblies in Figure 26 and Figure 27 were used to generate dark self-trapping beams. In a typical experiment, white light (380 nm – 1168 nm) emitted by a power stabilized, quartz-tungsten-halogen lamp (**W**) (ScienceTech Inc., USA) was collimated with a planoconvex lens (**L1**, F = 25 cm) and passed through an amplitude mask (**AM**), which introduced a weak, circular depression ~100μm in the optical field. The white beam (henceforth referred to as the background beam) bearing the dark circular notch was then focused through a pair of plano-convex lenses (**L2**, F.L = 5 cm, **L3**, F.L = 2.5 cm) onto the entrance face (z = 0.0 mm) of a cuvette containing the organosiloxane gel (**S**). The cuvette holder was mounted on a micrometer stage, which could be translated along z with a resolution of 0.5 μm. The image of the dark spot diffracts along its propagation path through the cuvette. The profile of the beam at z = 6.0 mm was imaged

through a second pair of planoconvex lenses (**L4**, FL = 25 cm **L5**, FL = 25 cm) and focused onto a CCD camera (WinCamD^{TM} 14-bit digital camera,1360 x 1024 pixels, 4.65 μm squares, Data Ray Inc., USA). The camera was driven by the software DataRay© (Version 5.0), which calculates parameters including beam diameter (FWHM, $1/e^2$) and relative peak intensity. All optical components were mounted on a rail with carriers that could be translated along the beam propagation direction (z) with a resolution of 0.5 mm. The rail itself was mounted on an optical table (flatness of ± 0.13 mm) with tuned damping to isolate the assembly from vibrations. All optical and mechanical components of the assembly were purchased from Newport Corporation, CA, USA. In case of the single dark beam studies, the single beam self-trapping experiment was done with an additional diffuser placed between the source (S) and lens (L1), in order to provide a uniform optical field.
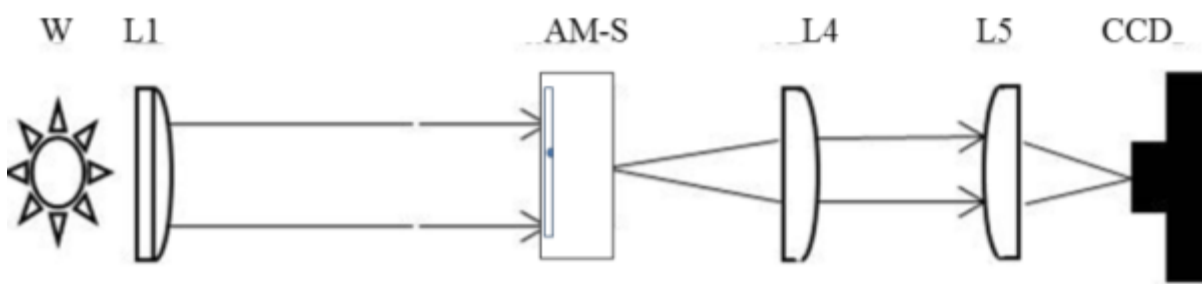
Figure 27. Assembly#2: An alternate assembly to generate a dark self-trapped beam is shown. This simplified assembly uses a thin amplitude mask made of 35 mm film slide with printed dots or patterns, *which is actually placed at the inner wall within the cuvette.* Light from a Halogen lamp (W) illuminates an amplitude mask with a dark spot (AM), of an organosiloxane filled cuvette (S), therefore eliminating the need for a pair of plano-convex lenses (L2-L3) used in the previous setup. The imaging setup (L4-L5-CCD) is

otherwise identical to Figure 26. This assembly was made in order to provide for self-trapping arrays of dark waveguides by printing patterns of dark dots on the mask (AM).

In the simplified setup, patterns used for the masks were designed in Microsoft powerpoint, and printed out either on a regular A4 transparency (low resolution, high contrast) or were sent as JPG files for printing on 35 mm film slides (high resolution, low contrast).The mask was cut to size and inserted into the cuvette before organosiloxane was poured into the cuvette for illumination.

Simulations of an incoherent dark beam

Simulation studies were done using BeamPROP^{TM} software of the RSoftCAD^{TM} suite. A combination of coherent Gaussian waves was used to simulate the average intensity profile of a dark self-trapping beam in 2D. Each iteration consisted of simulating the propagation of the beam from an input to an output plane through an index profile of the medium. A photopolymer type saturating refractive index gradient (depending on previous intensity experienced in the medium) was also simulated with a C programme at each iteration.

2.6. **Optochemical self-organization with white light beams**

Optical assemblies shown in Figure 28 and Figure 29 using amplitude masks were used to generate 2D, 3D photonic templates as well as woodpile lattices in an organosiloxane photopolymer described in Chapters 5-6. On illumination, the mask casts a pattern of bright and dark areas of light in the organsiloxane. This induces optical self-trapping and waveguide formation in the bright areas. In order to generate structures, the simplified dark beam setup was used, with masks consisting of printed patterns of dots. Masks of low resolution were made with office transparencies printed with patterns designed in Microsoft Word and printed with desktop printers. Higher resolution masks were made by printing scaled patterns onto 35 mm film slides.
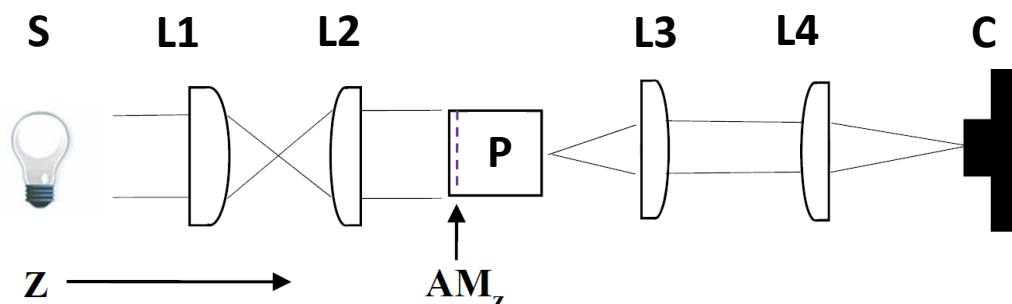
Figure 28. A scheme of the assembly employed for generating self-organized arrays using a single white light beam (in Chapters 5-6) is shown above. The assembly shown in Figure 28 was modified slightly in order to generate multiple dark or bright filaments simultaneously along z axis. Similar to Figure 28, a white light excitation source was (450 nm – 800 nm) emitted by a power stabilized, quartz-tungsten-halogen lamp (**S**) (ScienceTech Inc., USA) was used. The source beam was collimated with a pair of planoconvex lenses and launched onto the entrance face ($z = 0$ mm) of a cuvette containing the organosiloxane (**P**). An amplitude mask (**AM$_Z$**) was positioned at the entrance face inside the cuvette. The imaging setup is otherwise identical to Figure 26.
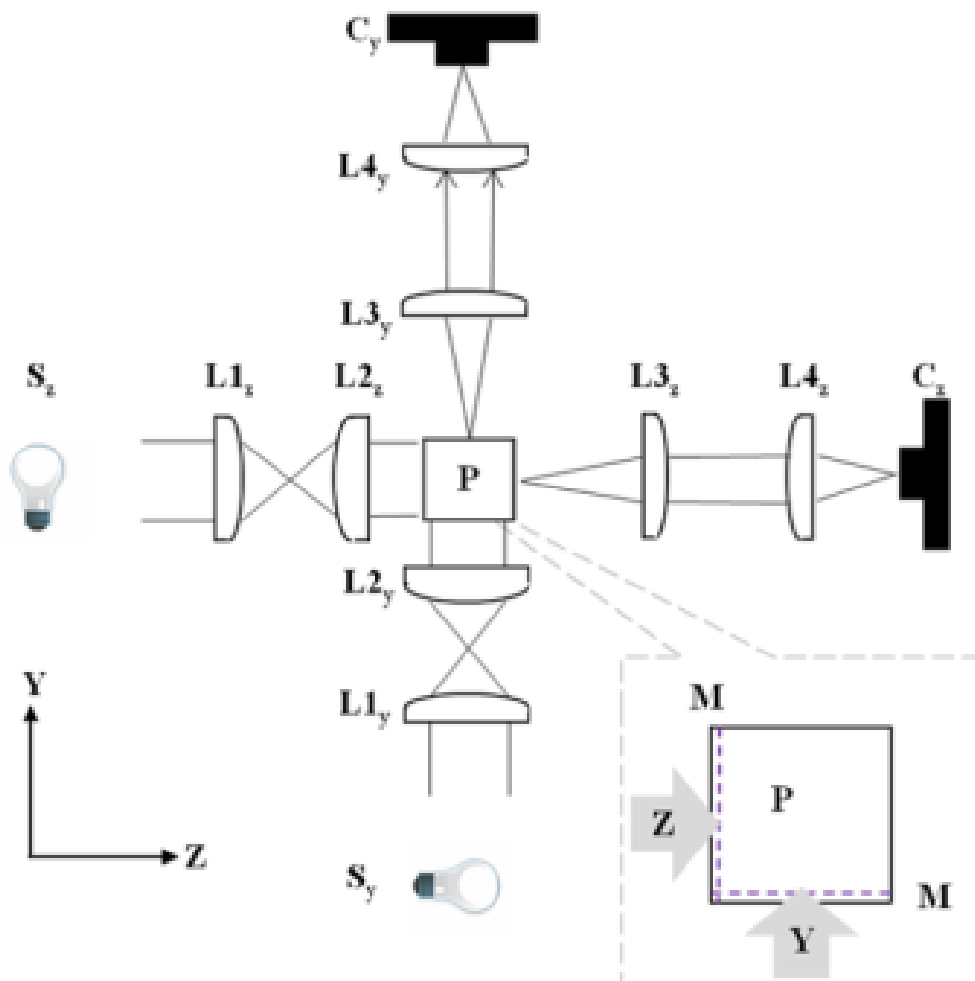
Figure 29. The optical assembly used to generate 3-D optical and microstructural lattices (in Chapters 5-6) using an orthogonal pair of white light beams emitted by two separate quartz tungsten halogen lamps is shown above. Each beam is individually identical to the setup in Figure 28. Each beam Y and Z were each collimated with a pair of plano-convex lenses and passed through an amplitude mask, which imposed a very weak (noise-like[206]) honeycomb pattern of dark rings on the optical field. The two patterned beams were simultaneously launched into the entrance face ($x = 0.0$ mm, $y = 0.0$ mm) of a transparent glass cuvette (10 mm x 10 mm x 10 mm) containing the organosiloxane photopolymer. The consequent changes in the spatial intensity profile of each beam that lead to lattice formation were simultaneously monitored at a propagation distance of 6.0 mm with two CCD cameras.

Optical Assembly for the white light beam along Y axis

Experiments on self-trapping of dark beams were carried out with the assembly depicted in Figure 29. The excitation source was white light (450–900 nm) emitted by a power stabilized, quartz-tungsten-halogen lamp (**W**) (ScienceTech Inc., USA). The white beam (henceforth referred to as background beam) was collimated with a pair of plano-convex lenses (**L1**, F.L = 7.5 cm, **L2**, F.L = 7.5 cm) onto the entrance face ($z = 0$ mm) of a cuvette containing the organosiloxane gel (**S**).An amplitude mask (**AM**) (made from 35 mm film slides) is positioned at the entrance face inside the cuvette. The optical assembly used for imaging is identical to the previous section (Figure 28).

Optical Assembly for the white light beam along Z axis

In the z direction, the assembly used is identical to the y direction assembly. The Z excitation source was white light (380–725 nm) emitted by a quartz-tungsten-halogen lamp (**W$_y$**) (41720 Series, Cole Parmer Inc., USA). The beam was focused through a pair of plano-convex lenses (**L1$_y$**, F.L = 8.8 cm, **L2$_y$**, F.L = 6.3 cm) onto the entrance face ($y = 0$ mm) of the cuvette containing the organosiloxane gel (**S**).Two separate amplitude masks (**AM$_z$,AM$_y$,**) were positioned at the entrance face inside the cuvette, for each propagation direction, y and z.

The beam profiling assembly, consisting of **L3$_y$-L4$_y$** and the CCD (**C$_y$**) was identical to the 2D array assembly for both, y (described above) and z directions. Beam powers along y were also adjusted to match levels along the z direction, and were identical to powers for the 3D array beams. The intensity of the background beam was 1.4

mWcm^{-2} measured at the input plane (532 nm with a FieldMaster GS power meter, Coherent Inc, USA) for the y and z directions.

Mask preparation

Masks were made identical to the method of Figure 29. The patterns used for the masks were designed in Microsoft PowerPoint, and printed out either on a regular A4 transparency (low resolution, high contrast) or were sent as JPG files for printing on 35 mm film slides (high resolution, low contrast). The mask was cut to size and inserted into the cuvette before organosiloxane was poured into the cuvette for illumination. For orthogonal masks that were employed in Figure 29, a single larger mask was initially printed along with a dotted guide, and the mask was folded along this line to form two separate masks. The folded booklet shaped mask was then cut to size and inserted into the cuvette before organosiloxane was poured into the cuvette for illumination. This method of folding a single mask into two parts enabled designing an orthogonal mask with the precise offsets required for woodpile lattices (Chapter 6). Mask patterns used are shown in the appendix section.

Interleaved vs intersecting lattices

For intersecting masks, a double sized mask was printed with a uniform pattern and folded like an 'open-book' to resemble two perpendicular masks. Each side therefore had an identical pattern. For interleaving masks, first, Y and Z patterns were printed on each half of the double sized mask, with a precise 1/4th period offset separated by a guide line. This sheet was then again folded at the guide line to form an 'open-book'

shape resulting in two perpendicular masks with ~1/4th period offset in 3D. This was then inserted into the cuvette to generate two orthogonal lattices, one with each side of the mask.

Micrographs of longitudinal profiles

Micrograph images were taken after completion of each experiment (t>2000 s). A high resolution microscope (SteREO Discovery.V12, maximum magnification 400x, Carl Zeiss Ltd., Canada) was used for the purpose. The sample was extracted from the cuvette by breaking it open very carefully so as to preserve its shape. Micrographs were taken both, from a top down view, as well as the input and output faces of the sample. Optical images were also taken with a commercial digital camera for several samples.

Simulations of theoretical photonic band gaps

Simulation studies were done using BandSolve™ software of the RSoftCAD™ suite. Photonic lattices with a background index of 1.46 and of geometries similar to the experiment (including dimensions) were designed with the RSoftCAD™ suite and their theoretical bandgaps were calculated using BandSolve™. Gradient index waveguides were not considered in simulations under the assumption that after substantial illumination, waveguides assume a flat profile index in experiments.

2.7. **Self-trapping bright and dark ring beams**

Experimental assemblies used for generating embedded beams were identical to the simplified assemblies used for dark beams as well as lattices shown in Figure 28. Ring patterns used for the masks were designed in Microsoft powerpoint, and printed out either on a regular A4 transparency (low resolution, high contrast) or were sent as JPG files for printing on 35 mm film slides (high resolution, low contrast).The mask was cut to size and inserted into the cuvette before organosiloxane was poured into the cuvette for illumination.

Simulations of an incoherent dark ring beam

Simulation studies were done using BeamPROP^{TM} software of the RSoftCAD^{TM} suite and parameters were chosen to correspond with previous simulations of single dark beams. A combination of coherent Gaussian waves was used to simulate the average intensity profile of a dark ring self-trapping beam in 2D. Each iteration consisted of simulating the propagation of the beam from an input to an output plane through an index profile of the medium. A photopolymer type saturating refractive index gradient (depending on previous intensity experienced in the medium) was also simulated with a C program at each iteration.

3. Interactions of self-trapping beams of incoherent white light

3.1. Introduction

Chapter 1.3 details an in-depth review of studies of interactions between two self-trapped beams. Here, results of studies of (a) interactions between a pair of parallel propagating white light beams at varying separation distance and (b) interactions between self-trapped beams at an angle are described.

Self-trapped light beams form in a wide variety of materials[45] and exhibit diverse forms of interactions that range from elastic collisions in planar Kerr waveguides[111,113,114,207,208,209] to complex 3-D trajectories in bulk materials with saturable nonlinearities.[90, 210] Such interactions can be classified by the *relative* coherence of beams[210], which if mutually coherent undergo interference effects that result in fusion[91,93,211] annihilation[94] or birth of solitons.[92] If mutually incoherent, they can superpose to produce an intensity increase that causes fusion[88,89,95,98,212,213] and under certain conditions, repulsion[214] or spiraling.[212] Recent studies elucidated that the interactions of self-trapped *incoherent* beams are entirely distinct from those of coherent self-trapped beams (including mutually incoherent ones). This was elegantly demonstrated by an experiment that switched attraction between coherent beams to repulsion (and *vice versa*) simply by rendering both beams incoherent.[104] Other examples include coherence cooling - an increase in spatial correlation - of an incoherent beam upon collision with dark self-trapped beams[121] and shape transformation upon collision

with each other.[50,55] Spiraling of elliptical incoherent beams colliding within the same plane - unexpected because of the absence of initial angular momentum – was also reported.[54]

While the above studies involved partially (spatially) incoherent light, self-trapped beams of white light, which is both spatially *and* temporally incoherent[33,34,215] were discovered by Mitchell and Segev in 1997.[12] Self-trapping of this weakly correlated wavepacket was theoretically described in terms of spatial correlation[33], shape[34], frequency distribution[31], behavior in media with nonlocalized responses,[7] response to intensity fluctuations,[215] propagation in nonlinear lattices[216] and susceptibility to modulation instability.[33] These studies raise intriguing questions about interaction dynamics and consequent changes to the statistical coherence structure of white light beams. While their collisions were modeled by extending the coherent density approach,[217] there has previously been no experimental study of the interactions of self-trapped white light beams, which can be difficult to generate as they form only in materials with a photoresponse that is noninstantaneous and saturable.[12] These respectively average out phase fluctuations over time and facilitate growth of a multimode waveguide.[215] Such conditions were realised at low intensities (nW) in a photorefractive crystal[12] but as our group recently showed, are inherent to free-radical photopolymerization systems, which enables white light self-trapping across a wide intensity range.[63,65] Exploiting this route, interactions of two parallel propagating and mutually incoherent self-trapped white light beams can now be studied experimentally.

Interactions of two parallel propagating and mutually incoherent white light beams were examined in a photopolymerisable organosiloxane. Three types of interactions were identified: the beams fused when separated by a distance corresponding to the width of each beam but at separation distances much greater than the beam width, formed two discrete self-trapped beams that repelled each other. At separation distances smaller than the beam width, the beams suffered filamentation due to modulation instability but ultimately fused into a single self-trapped beam. This study also opens accessible routes to extend studies of the interactions of self-trapped white light beams, which until now have only been studied theoretically.

Angular collusions

Collisions and the resulting interactions between self-trapped beams are their most fascinating features. These collisions have a striking similarity to both elastic and inelastic particle collisions pointing to a possible fundamental relationship between self-trapped beams and the deBroglie wave-particle duality[90]. Two beam collisions have been studied extensively between coherent and partially coherent beams in recent times. Previous studies of collusions of self-trapping beams have shown the two beams interact at angles less than 8 degrees. Above this angle, light from colliding beams is unable to refract and couple into each other, resulting in two beams simply passing through one another.[89] At smaller angles, the two beams are able to exhibit various interacting phenomena.

Coherent colliding beams have been shown to exhibit varied phenomena such as fusion[91,93], fission[92] and annihilation[93] between the interacting beams. However, because such interactions are strongly dependent on the relative phase between the colliding beams, certain interactions such as spiraling – that require a very careful balance of inter-beam forces– can only be achieved transiently.[90,115] Unlike coherent beams, mutually incoherent beams simplify this problem as they can only exhibit attractive interactions in close proximity, and they have shown relatively stable spiral orbiting.[98] Such beams can be generated using coherent sources; however their relative phase varies much faster than the response time of the medium, resulting in a response "blur" i.e. any response of the medium to their interaction gets averaged over all the possible relative phases between the two beams.

The previous section showed three types of interactions between parallel propagating self-trapping incoherent white light beams. These studies were extended to examine the properties of self-trapping beams that propagate at an angle to each other. Two types of angular interactions were also studied, (i) large angle interactions at angles $>8^0$) and small angles interactions at angles $<8^0$.

3.2. **Results – Parallel propagating beams**

White light in the spectral range 400 nm-800 nm and with random polarization emitted by a quartz-tungsten-halogen bulb was passed through apertures to generate two parallel-propagating beams (Figure 22), which were focused onto the entrance face (z=0 mm) of a glass-cuvette containing photopolymerizable organosiloxane.[63] At z=0 mm, the beams each had a power of ~150 nW, full width at half maximum (*fwhm*) of ~40 μm and peak-to-peak separation (Δx) of 74 μm, so selected to approximate their $1/e^2$-width of ~78 μm. At these settings, ~0.05 of each beam's cross-sectional area overlapped with the other. Because the beams were *mutually* incoherent,[218] they did not interfere but produced an intensity increase[219]; the relative intensity (~30 %) at their overlap-midpoint was approximately the sum of their individual intensities at the same position (~13 %). These are described in the sections below.

Control Experiment

In organosiloxane without photoinitiator (in the absence of photopolymerization), each beam broadened (diffracted) to ~190 μm at z=8 mm and remained unchanged when monitored over ~4 hrs. The beams were confirmed to *individually* self-trap in the organosiloxane sensitized to visible wavelengths (λ_{max}=393 nm, 460 nm)[63] by blocking each in turn at z=0 mm and allowing the other to initiate polymerization along its propagation path. Its consequent self-trapping was observed at z=8 mm by a ~3-fold decrease in width and corresponding intensity increase (Figure 30).
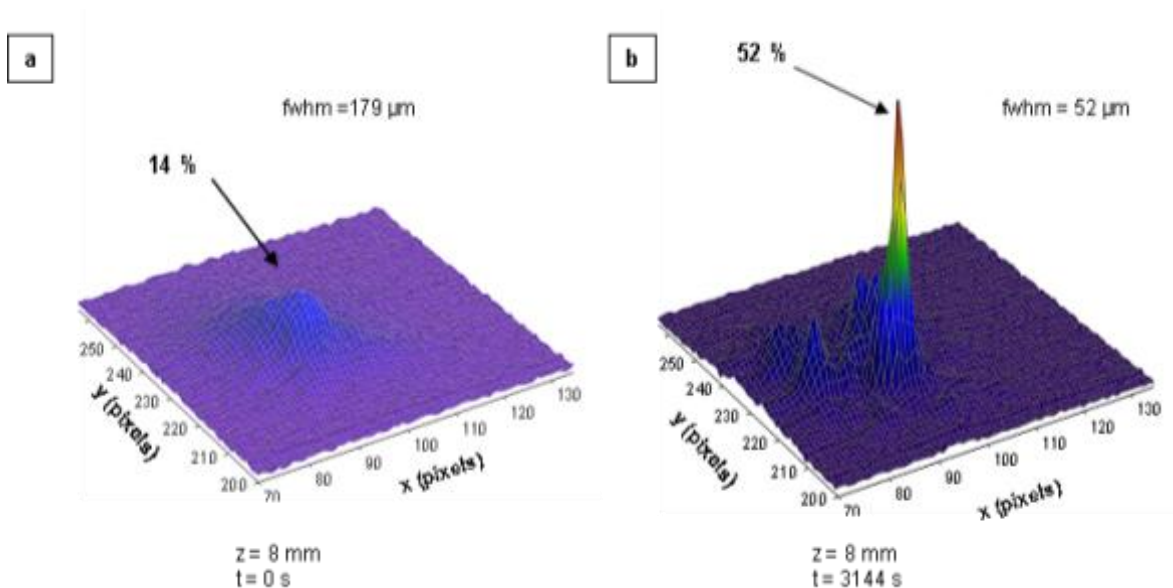
Figure 30. Evidence of the self-trapping of an individual beam of incoherent white light. Spatial intensity profiles of (a) the initially diffracted and (b) subsequently self-trapped beam. Both profiles were acquired at z = 8 mm. Relative peak intensities and beam widths (fwhm) are indicated. 1 pixel = 9 μm

3.3. **Two beam fusion at 74 μm**

To study their *interactions*, the beams were launched simultaneously and monitored at z=8 mm. Typical results in Figure 31 show that the beams could not *coexist* as discrete self-trapped beams but merged into one that was stable for >3500 s. Merging is characteristic of mutually incoherent beams in general[210] and current results confirm that despite its polychromaticity and incoherence, this is also the case for white light.

Figure 31 further reveals that merging is a *competitive* process where one beam selectively stabilizes by depleting intensity from its counterpart: initially, both beams (A and B) were diffracted with only minor (~1 %) intensity differences (1c-d). However, at 300 s, the intensity of A was greater by 5 %; this small intensity difference became

amplified over time. At ~500 s, A increased in intensity by >2-fold while B grew only by ~0.5-fold (Figure 31f) as each beam underwent self-trapping. At ~600 s, B was unchanged while A had grown by 1.4-fold (Figure 31g) and continued to grow even as B weakened and ultimately disappeared. At ~800 s, only a single self-trapped beam remained.
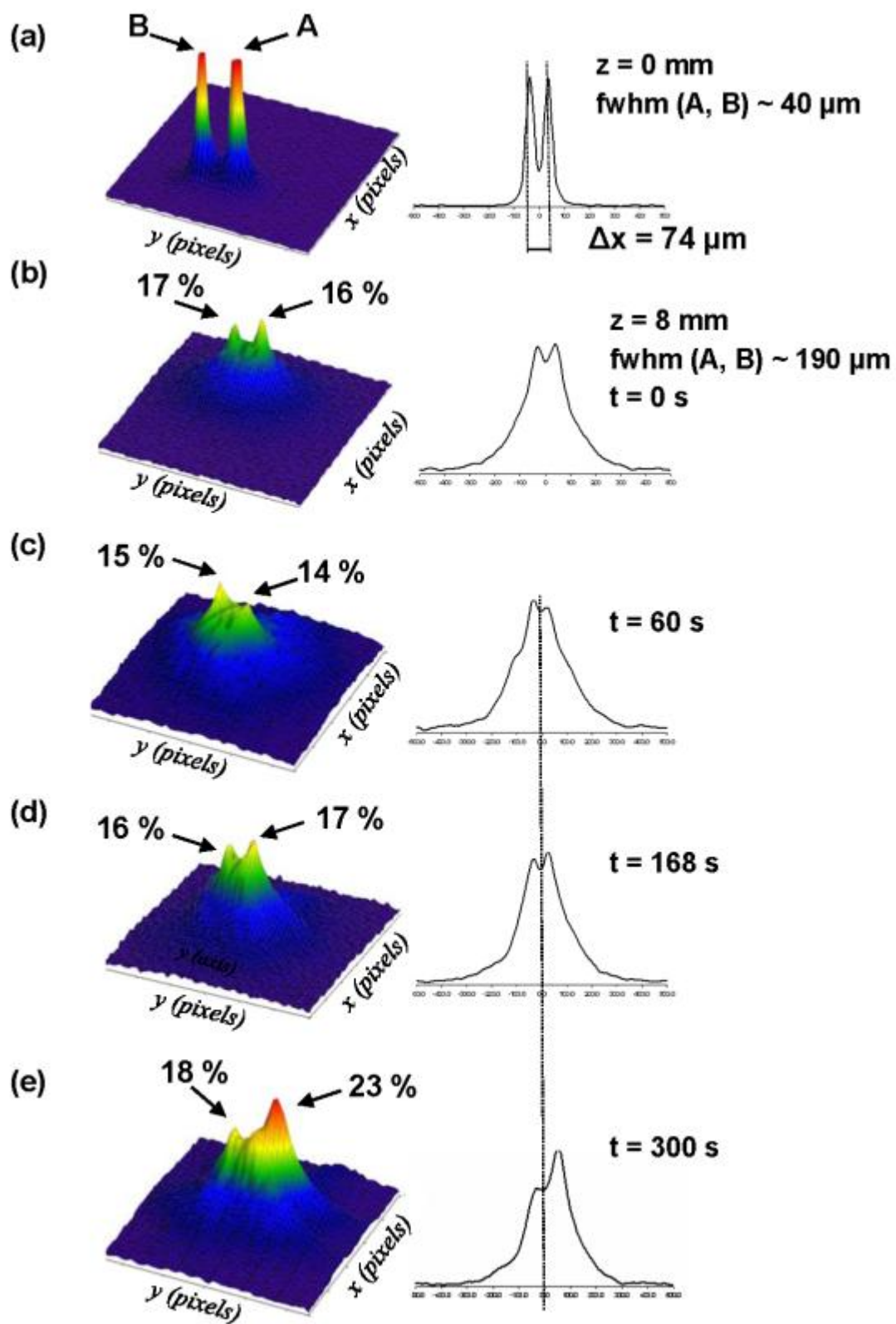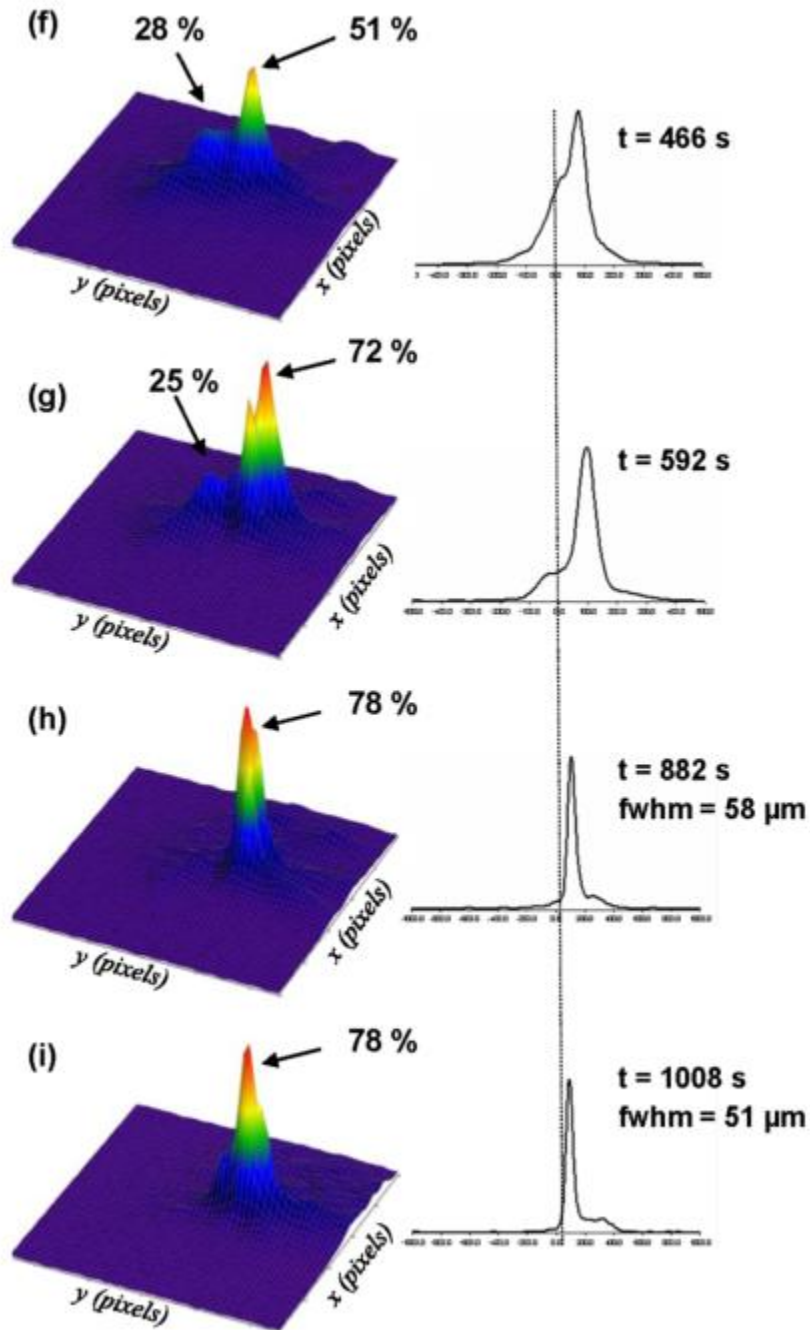
Figure 31. Interactions of a pair of parallel propagating self-trapped beams of incoherent white light with a peak to peak separation (Δx) = 74 μm. 3-D and corresponding normalized cross-sectional intensity profiles are given for the beam pair at (a) z = 0 mm and (b) z = 8 mm. (c-j) trace the temporal evolution of the beam pair at z = 8 mm.

Relative peak intensities (%), beam widths (fwhm) and time (s) are indicated. Dotted lines are placed through the origins of cross-sectional profiles as a guide to the eye. For clarity, the intensity scale of 3-D profiles in (b-e) is magnified by x2 relative to (f-i). 1 pixel = 9 µm.

Selective imaging of the merged peak in Figure 31i was carried out to confirm that it consisted of intensity from both A and B. The images in Figure 32 were acquired once the single merged beam was observed. Each beam was blocked in turn while the other was imaged. Measurements were made within a time period (4 s) that was much smaller than the response time of the medium, thus ensuring that refractive index changes did not occur during this time.
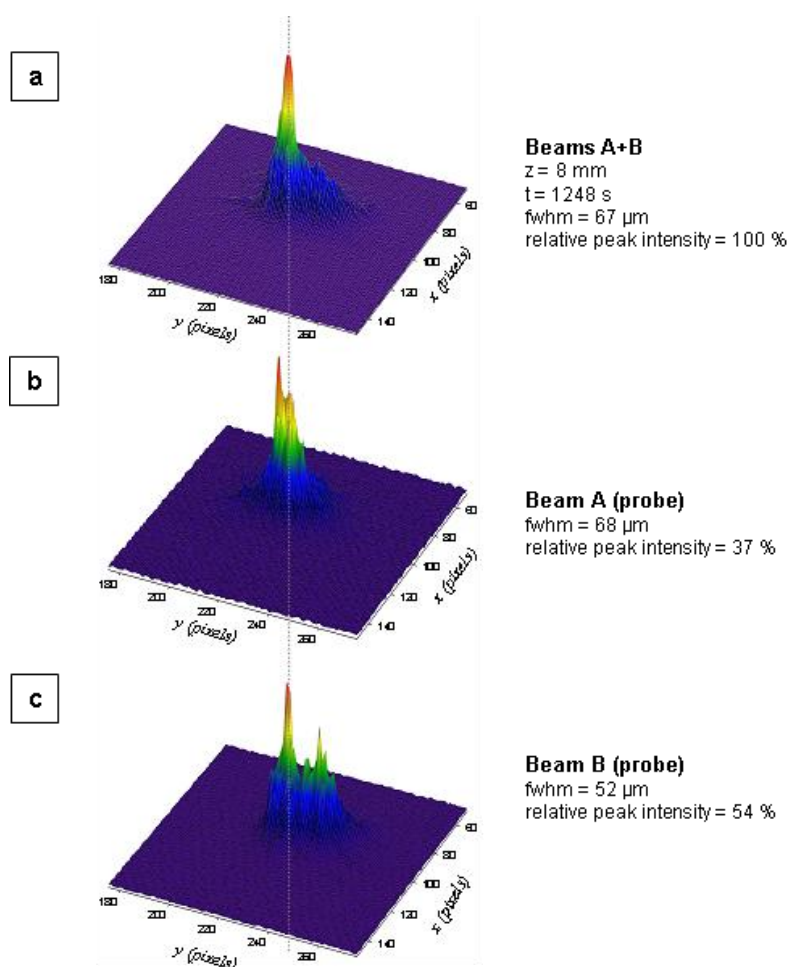
Figure 32. (see also Figure 31i in text) Evidence of merging of beams A and B with an initial peak to peak separation (Δx) = 74 µm into a single self-trapped beam. *Normalized 3-D spatial intensity profiles at z = 8 mm are provided for (a) the merged beam (A+B) and its individual components (b) A and (c) B. A dotted line is placed through the centre of the merged beam as a guide to indicate the relative positions of individual beams (b, c) to the merged beam (a). Relative peak percentages (%), beam widths (fwhm) and time of measurement are provided. *Note that while there is residual intensity at beam B's original position, the maximum intensity of beam B is located in the position of the merged beam.* (1 pixel = 9 µm)

Separately, experiments at z=6 mm showed that beam-merging took place for at least the final 2 mm of propagation in the medium (Figure 33).

103
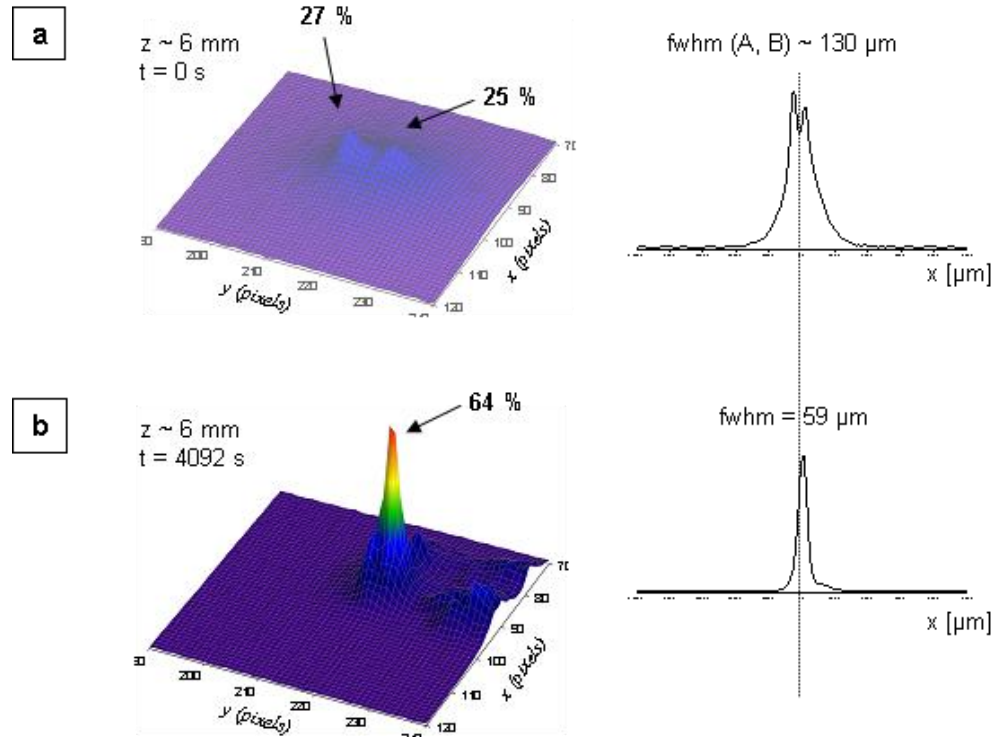
Figure 33. Merging of two parallel-propagating self-trapped beams of white light with a peak-to-peak separation (Δx) = 74 μm monitored at z = 6 mm. 3-D spatial intensity profiles and corresponding normalized cross-sectional profiles are provided (a) before and (b) after merging. Relative peak intensities (%), beam widths (fwhm) and times (s) of measurement are provided. A dotted line is placed through the origin of the cross-sectional profiles as a guide to the eye. (1 pixel = 9 μm)

3.4. **Discussion**

Competitive growth that leads to merging of beams A and B in Figure 31 can be understood through the nonlinear Schrödinger expression [equation 3-1], which describes self-trapping of a beam with diameter $a \gg \lambda/2\pi$ as:

$$ik_0 n_0 \frac{\partial \varepsilon}{\partial z} + \frac{1}{2}\nabla_t^2 \varepsilon + k_0^2 n_0 \Delta n \varepsilon + \frac{i}{2} k_0 n_0 \alpha \varepsilon = 0 \qquad [3\text{-}1]$$

Here, ε is the electric field amplitude and α, the attenuation coefficient of the medium at wavelength λ corresponding to free space wavenumber, $k_0 = \omega/c$.[38] Equation [3-1] shows that the interaction between light intensity and refractive index change (Δn) creates a waveguide that traps and guides the beam along its propagation path (z). Under these conditions, the *slightly* more intense A induces a waveguide with a slightly greater index, which traps more intensity from its surroundings (including B) and in turn, increases in index. As A strengthens, the slightly *less* intense B weakens and ultimately disappears as its intensity leaks into A's waveguide. A previous study of beams with *deliberately* introduced power differences showed that the trajectory of the most powerful beam dominated during self-trapping.[125] In the current study, both beams were initially equivalent; their minor intensity differences at early times originate from *random noise* inherent to the medium, making it equally probable that either beam stabilized by depleting the other.

3.5. **Two beam repulsion at larger separations**

This 50 µm increase in Δx is unexpected as repulsion, with one exception[214], has previously only been observed with mutually coherent, out-of-phase beams. These destructively interfere upon overlap to create a dark region that shifts the centroids[210] of both beams, which thus appear to repel. The only previous example of repulsion of *mutually incoherent* beams was engineered through the anisotropic response of a photorefractive crystal.[214] Polymerization-induced index changes however are isotropic; in this system, each self-trapped beam increases the index and therefore, the extent of polymerization within its own waveguide. The resulting gradient in the concentration of polymerizable methacrylate substituents could trigger diffusion of oligomeric siloxanes bearing unsaturated methacrylates towards each self-trapped beam. Concentration-driven diffusion in photopolymers exposed to non-uniform optical fields is well-understood in photolithographic[220] and self-focusing[221] processes. In the case of the beams at Δx=430 µm, diffusion creates the *equivalent* of a dark region in between them, resulting in repulsion. The beams also formed separate, equivalent self-trapped beams at Δx=120 µm (Figure 34a-c). Here, the extremely small beam overlap ($\sim 4 \times 10^{-4}$ % of each beam's cross-section) induced index changes sufficient to localize significant intensity ($\sim$4-fold increase relative to linear conditions) (Figure 37c). The concentration gradient was therefore weaker, resulting in less diffusion and an increase in Δx of only 10 µm.
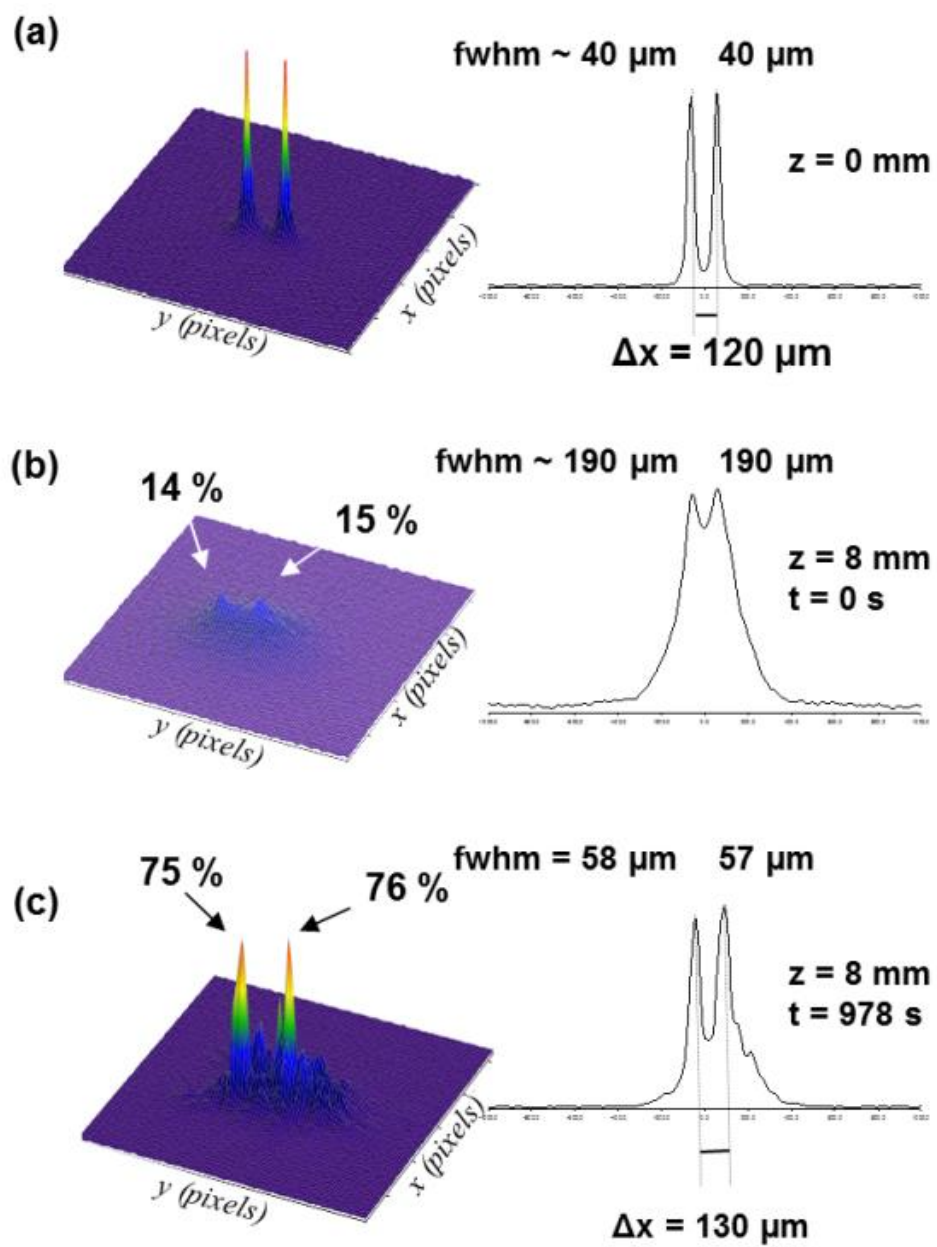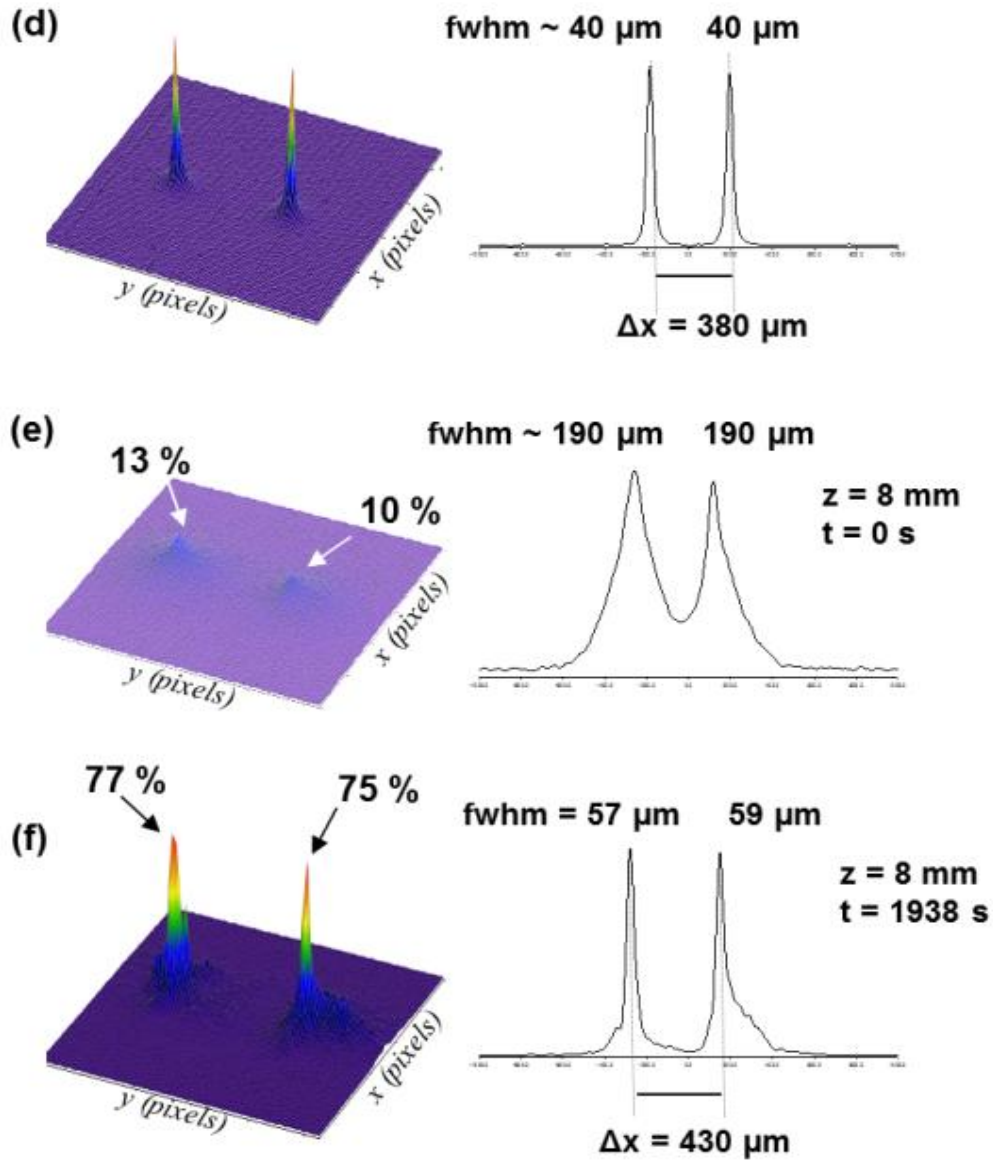
Figure 34. Behavior of a pair of parallel-propagating self-trapped beams of incoherent white light with peak to peak separations (Δx) of (a-c) 120 µm and (d-e) 380 µm. 3-D and corresponding normalized cross-sectional intensity profiles are given for each beam pair at (a, d) z = 0 mm. Profiles at z = 8 mm are provided (b, e) before and (c, f) after self-trapping. Relative peak intensities (%), beam widths (fwhm) and time (s) are indicated. 1 pixel = 9 µm. At Δx=380 µm (>>$1/e^2$ beam width), the beams did not overlap and formed separate, near-identical self-trapped beams with Δx=430 µm (Figure 34d-f).

3.6. **Two beam fission at smaller separations**

Interactions of the beams at Δx=56 μm ($<1/e^2$ width) were also examined (Figure 35). At ~500 s, both divided into multiple self-trapped filaments, which at ~1000 s merged into a dominant, self-trapped beam (Figure 35-Figure 36). Although the number and intensity distribution amongst filaments varied between repeat-experiments, they always ultimately merged over time into a single self-trapped beam with width ~58 μm. Like repulsion, fission was previously considered possible only with mutually coherent beams where interference fringes induced multiple waveguides (>2) causing the beams to divide.[211] Filamentation of the mutually incoherent beams in this study however originates from modulation instability (MI), where random noise seeds spontaneous division of a *broad* beam.[61] MI occurs in beams wider than the optimum self-trapped beam-width, which in organosiloxane ranges from 50 μm-60 μm (Figure 30). At Δx=56 μm, overlap between the beams is sufficiently large (~0.16 of each beam's cross-section) that they behave as a *single* beam with an effective (*fwhm*) width of ~100 μm and thus suffer MI. Whereas filaments formed through MI in a uniform beam (without an intensity gradient) are extremely stable[61], those formed through superposition of the two narrow beams in this study always coalesced into a single self-trapped beam (Figure 35-Figure 36).
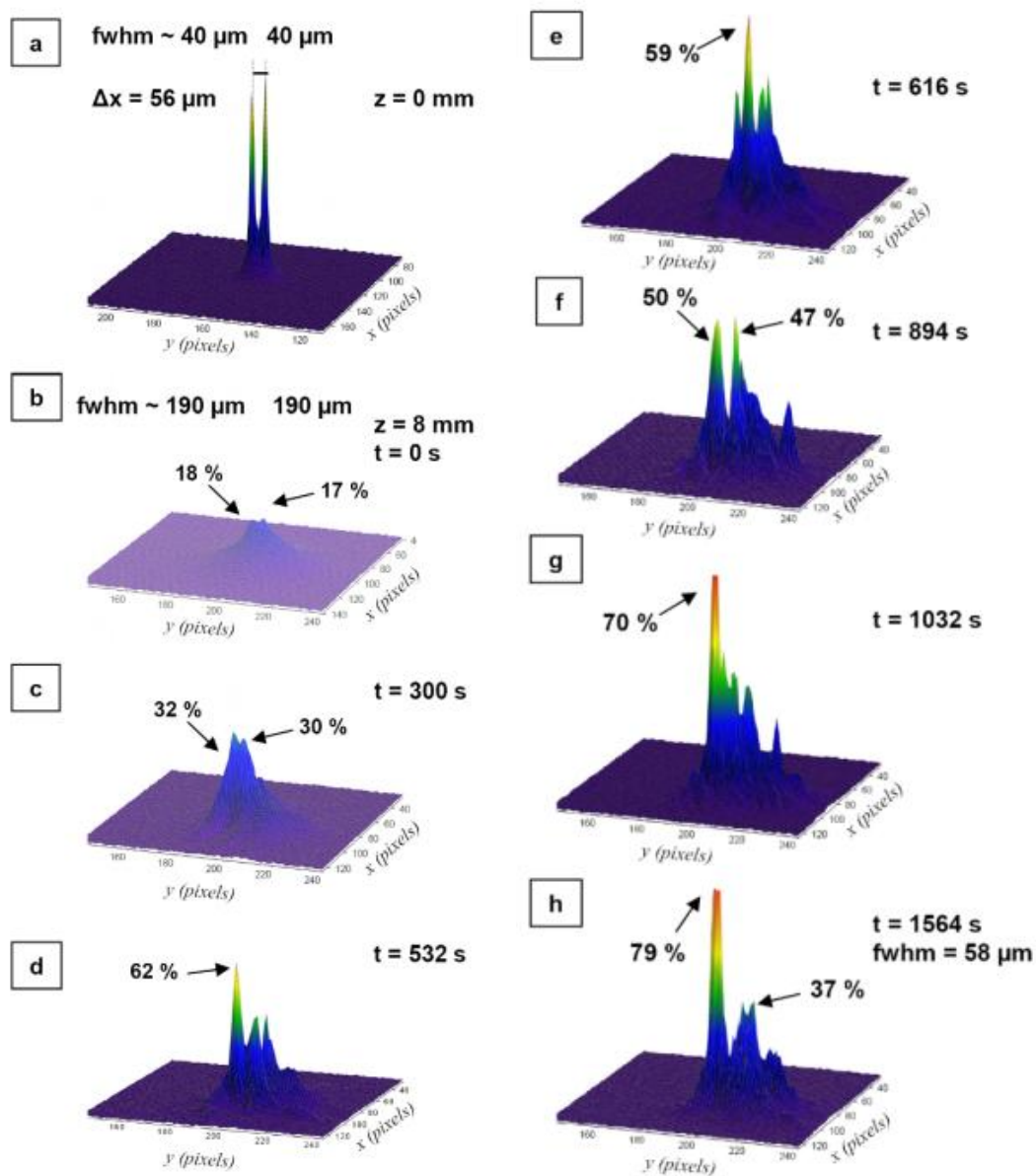
Figure 35. Interactions of a pair of parallel propagating self-trapped beams of incoherent white light with a peak to peak separation (Δx) = 56 µm. 3-D spatial intensity profiles are given for the beam pair at (a) z = 0 mm and at (b) z = 8 mm. (c-h) trace the temporal evolution of the beam pair at z = 8 mm. Relative peak intensities (%), beam widths (fwhm) and time (s) are indicated. 1 pixel = 9 µm
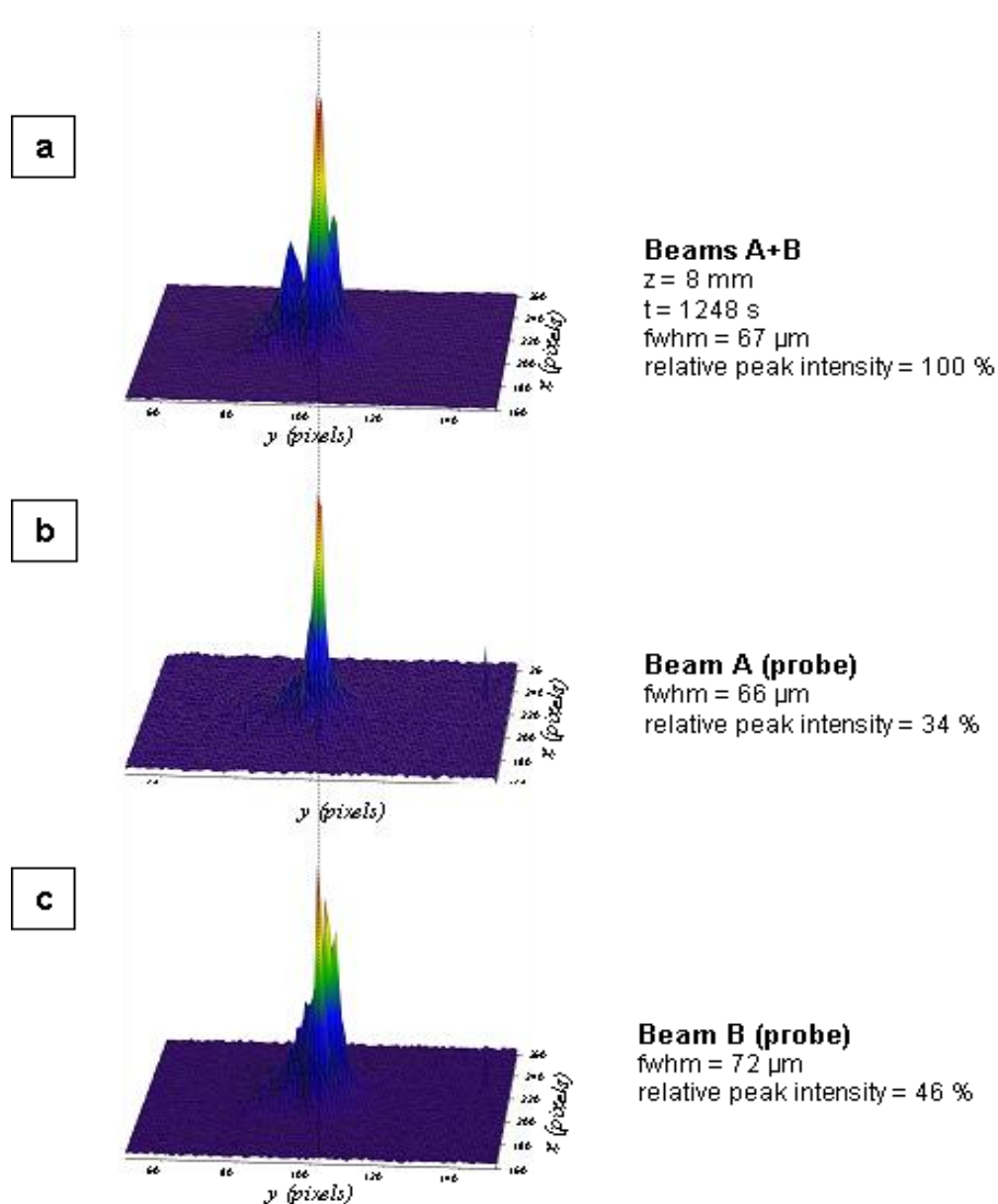
Figure 36. (see also Figure 35) Evidence of merging of beams A and B with an initial peak to peak separation (Δx) = 56 μm into a single self-trapped beam. *Normalized* 3-D spatial intensity profiles at z = 8 mm are provided for (a) the merged beam (A+B) and its individual components (b) A and (c) B. A dotted line is placed through the center of the merged beam as a guide to indicate the relative positions of individual beams (b, c) to the merged beam (a). Relative peak percentages (%), beam widths (fwhm) and time of measurement are provided. (1 pixel = 9 μm)

3.7. **Conclusion**

In summary, parallel-propagating and mutually incoherent white light beams exhibit merging, repulsion and filamentation behavior depending on their initial separation distance. The interactions were found to be reproducible by repeating each interaction at least three times. Repulsion (with one exception[214]) and filamentation were previously not shown with mutually incoherent white light beams.[210] Such interactions between the mutually incoherent beams observed in this study originate from concentration gradient-driven diffusion and modulation instability, respectively. Future work may include theoretical modeling of such interaction phenomena as well as their effects on the coherence structure of white light.

Profiles at z = 0 mm	Δx [μm]	M	A
	56	0.65	0.16
	74	0.27	0.05
	121	0.08	0.0004
	381	0.007	0

LEGEND

Δx = peak to peak separation
M = relative intensity at overlap midpoint
A = overlap area (fraction) of each beam
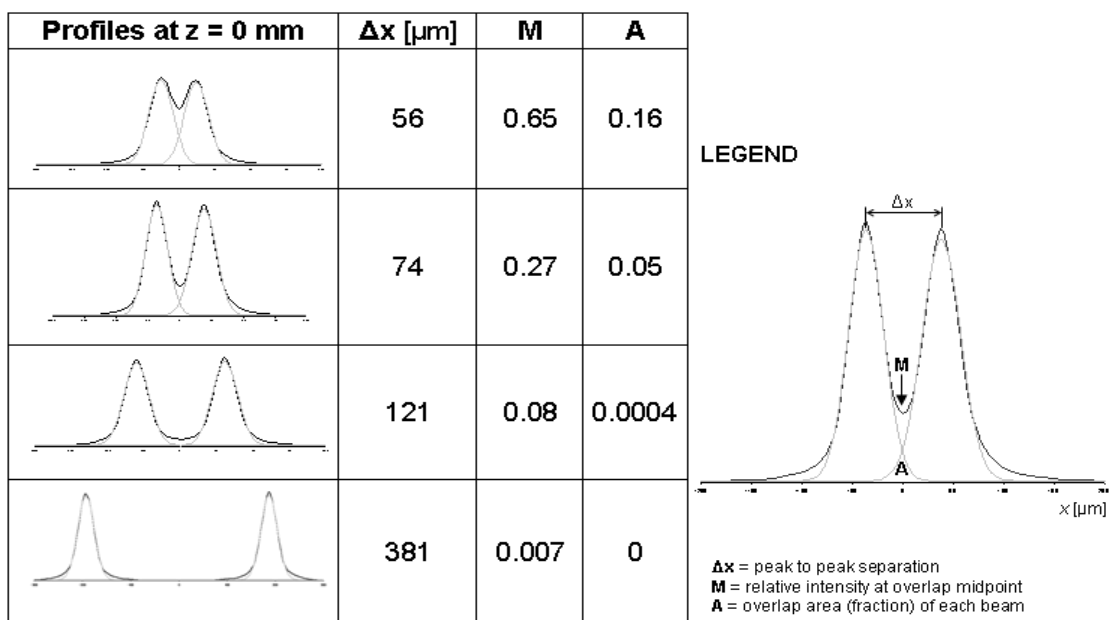
Figure 37. A summary of the cross-sectional profiles and corresponding parameters of the beam pair at z = 0 mm for the peak-to-peak separations of 56 μm, 74 μm, 121 μm and 381 μm.

3.8. **Angular Interactions**

Objectives

The principal objective is to study in detail the behavior of self-trapping beams propagating with angular separation. These first time experiments will establish the fundamental forms of interactions between self-trapping beams of spatially and temporally incoherent light. Through comparison with previous studies of equivalent studies with coherent and partially coherent light, features that are unique to white light, including the consequences of interactions on their statistical coherence structure, will be established. The other objectives of the work are as follows:

Both, copropagating incoherent self-trapping beams and beams colliding at very small angles have been predicted to fuse together. The former has been demonstrated in the previous section for the case where $\Delta x \approx 1/e^2$. The first objective is to investigate whether small angle collisions between such beams also lead to fusion. At large angles, coherent and mutually incoherent self-trapped beams simply pass through one another. Is this also the case with incoherent white light self-trapping beams? Between the above two extreme cases of small angle fusion, and no interaction at large angles, mutually incoherent beams have a threshold region, where they do not fuse, but can still couple light into one another. This threshold is defined by their total internal reflection angle, and above it, even cross-coupling of light into each other's waveguide is not possible. The third objective is to study the existence of such a threshold region with white light beams. Any coupling of light at such a threshold region can be studied by using for example,

different polarization filters or color filters for each of the two beams at their source, and measuring them after their collision. Any study where components of the two input beams can be distinguished (e.g. by using two different polarization filters) additionally provides a good insight into the coherence behavior of the beams after collision. The study can also be repeated with two beam fusion, to study coherence modification under complete fusion. Deflections are possible with incoherent beams, where one beam can influence and alter the path of another one in its proximity. In order to investigate whether this is possible with incoherent white light beams and to what extent, two beams of different intensities can be used. Their proximity and angle (0^0-180^0) in space can also be varied to study deflections. The possibility of spiraling interactions can also be determined. Interaction between counter propagating white light beams can also be studied to determine if waveguides can fuse when in proximity. Any resulting waveguide can also be studied for its coherence and transmission characteristics.

Results and Discussion

Two different optical assemblies were built – one to study large angle ($>8^0$) collisions, and another to study small angle ($\sim8^0$) collisions. At large angles, two beams were found to pass un-deviated through one another.[89] In the second optical assembly, built to launch two incoherent white light beams at tunable small angles, the two beams were launched by using two optical fibers with 50 μm cores, and aligning them at an angle relative to one another (see appendix). With this setup, under linear conditions, the beams were found to cross one another at a minimum angle of 8^0. Under photopolymerization conditions, each beam was found to self-trap along its original path.

No measurable deflection was observed in either of the two beams for this angle. This corresponds well to theoretical studies predicting that two self-trapping beams cannot interact beyond a certain critical angle.[93] It was not feasible to generate angles smaller than 8^0 using incoherent white light through 50 µm optical fibers, using existing equipment due to the following unresolvable issues: (i) Very strong divergence of white light, (ii) loss of intensity and reflections at a 1mm thick cuvette interface, (iii) coupling fibers and light into a flowing liquid medium (gelation of the liquid makes the fibers useless, requiring splicing, setup and alignment of fibers again).

3.9. **Large angle collisions**

Control Experiment - linear conditions

The images shown in Figure 38 clearly show two beams launched at angles and crossing one another inside the cuvette (linear conditions). Angles can be determined by measuring the physical angle between the two movable arms in the optical assembly (8 degrees) as well as from the calibration (linear conditions). Two beams are observed to cross over approximately 0.75 mm within the cuvette under linear conditions.
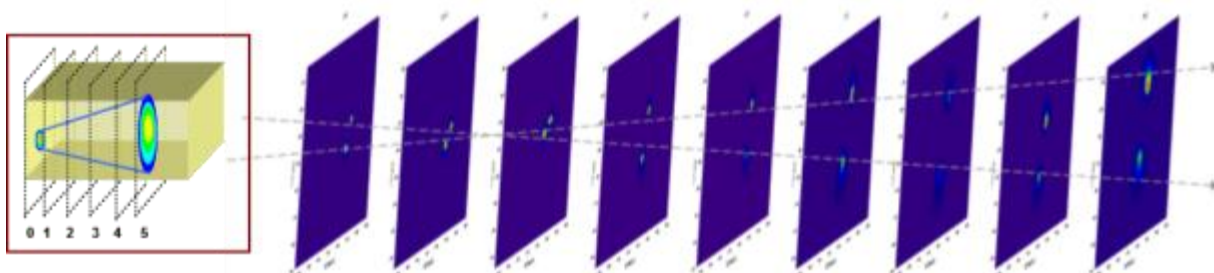
Figure 38. Two self-trapping beams at an angle are generated in an organosiloxane filled cuvette using incandescent light focused from two optical fibers. Images taken at the wall

of the cuvette, the focus, 0.5 mm, 1 mm, 2 mm, 3 mm, 4 mm, 5 mm and 6 mm respectively, are shown in the skewed 2D beam profiles above. The two arrows show the propagation directions of the two diffracting beams under linear conditions. Their (unskewed) 2D and 3D profiles are shown below.

a   b   c   d   e   f   g   h   i   j
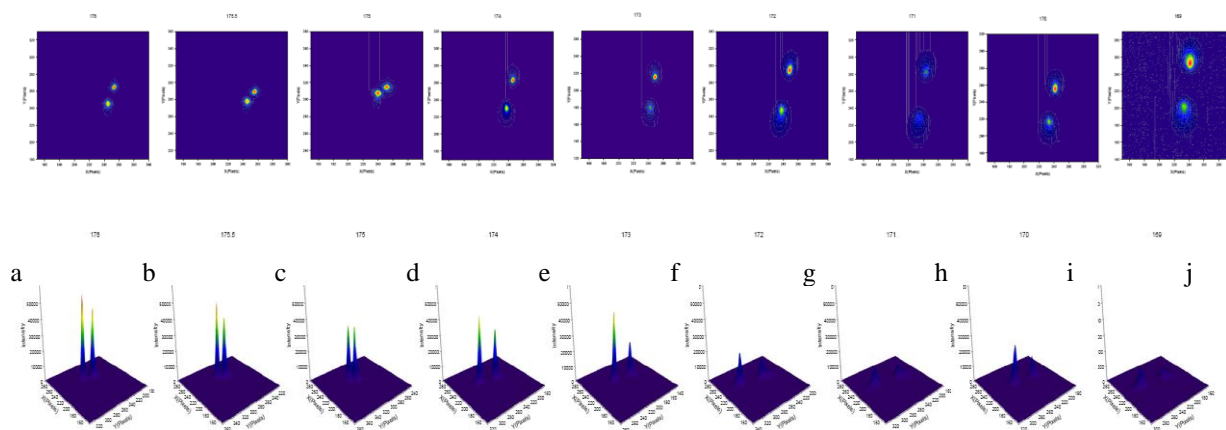
Figure 39. Two self-trapping beams at an angle are generated in an organosiloxane filled cuvette using incandescent light focused from two optical fibers. Images taken at the wall of the cuvette, the focus, 0.5 mm, 1 mm, 2 mm, 3 mm, 4 mm, 5 mm and 6 mm respectively, are shown in the 2D and 3D beam profiles above. The beam intensities decrease and their widths increase as they propagate along the cuvette under linear conditions.

Interactions under self-trapping conditions

Under nonlinear self-trapping conditions, the two beams self-trap. Their 2D and 3D profiles are shown in

Figure 40, at t=0s (a), 322s (b), 638s (c), 1270s (d), 1902s (e) and 2534s (f) through the self-trapping process.

The two beams appear elliptical at t=0s because the imaging system (CCD and plano-convex lens pair) is oriented at neither beam exactly. Instead, it is aligned towards the middle of the two beams, so that it can monitor light from both beams simultaneously. Each beam's temporal evolution can be monitored independently when necessary, by simply rotating the imaging arm to point directly towards it. Self-trapping results in an intensity rise apparent by 322 s in (b), and increases as the beams self-trap in (c), (d) and (e). It subsequently decreases as photopolymerization progresses to completion in (f) by 2534s.
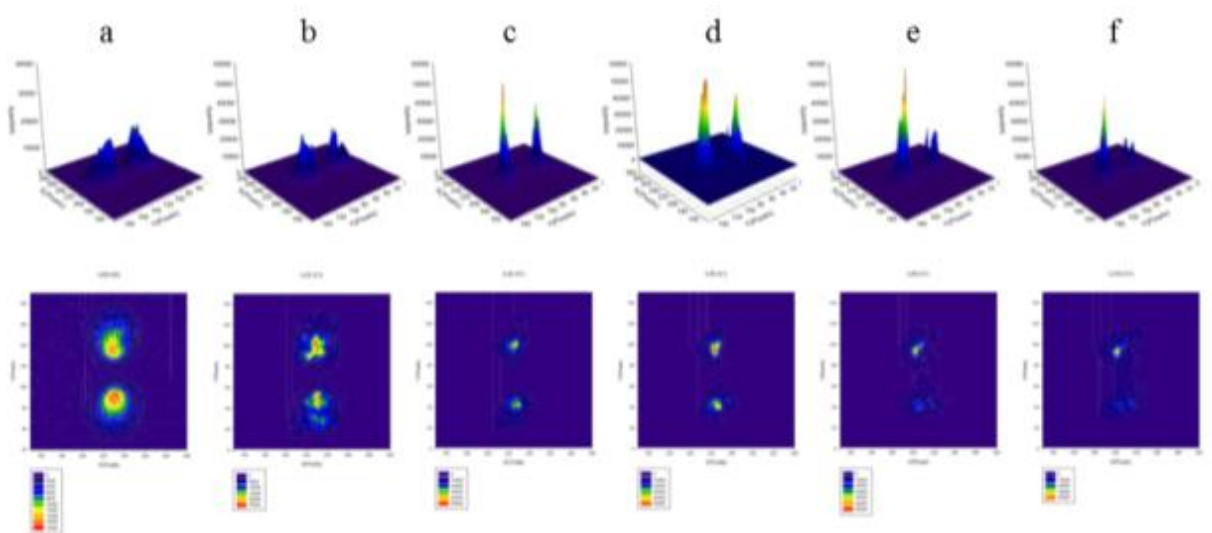
Figure 40. Two self-trapping beams at an angle are generated in an organosiloxane filled cuvette using incandescent light focused from two optical fibers. Under nonlinear self-trapping conditions, the two beams self-trap. The 5 mm plane is monitored over time for changes in the two beams. Above, the 2D and 3D temporal beam profiles at this plane are shown. The beam intensities increase and their widths decrease as they self-trap over time. Towards the end of the self-trapping process, the intensity of the beams falls again.
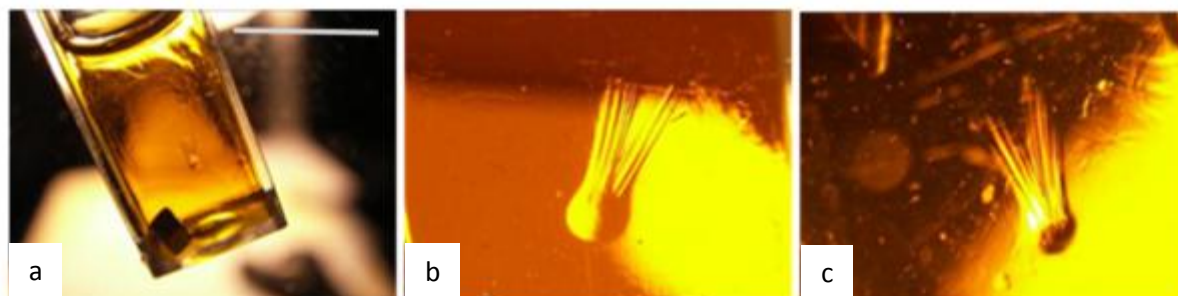
Figure 41. Two self-trapping beams at an angle are imaged in an organosiloxane filled cuvette after the self-trapping experiment using assembly #1. The digital images show the waveguides at an angle in (a), and at a close up in (b) and (c). Scale bar in (a) is 9 mm.

3.10. **Small angle collisions**

Interactions under self-trapping conditions

Under nonlinear self-trapping conditions, the two beams self-trap. Their 2D and 3D profiles are shown in Figure 42 at t=0s (a), 322s (b), 1902s (c), 3482s (d), through the self-trapping process. The two beams are slightly distorted at t=0s due to distortion at the input position of the cuvette. The light from the cleaved ends of the optical fiber diffract and fall at an angle onto the outer wall of the cuvette, resulting in distortion due to diffraction and reflection at the surface. Subsequent self-trapping results in an intensity rise apparent by 322 s in (b), and increases as the beams self-trap in (c). It subsequently decreases as photopolymerization progresses to completion in (c) and (d) by 3482s.
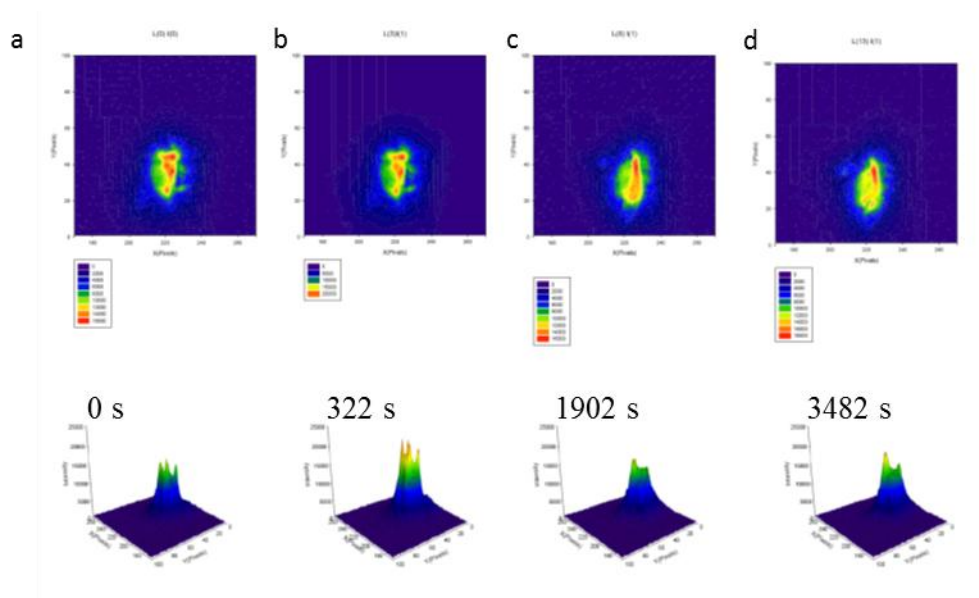
Figure 42. Two self-trapping beams at an angle are generated in an organosiloxane filled cuvette using incandescent light focused directly with two optical fibers. Under nonlinear self-trapping conditions, the two beams self-trap. The 5 mm plane is monitored over time for changes in the two beams. Above, the 2D and 3D temporal beam profiles at this plane are shown. The beam intensities increase and their widths decrease as they self-trap over time. Towards the end of the self-trapping process, the intensity of the beams falls again.
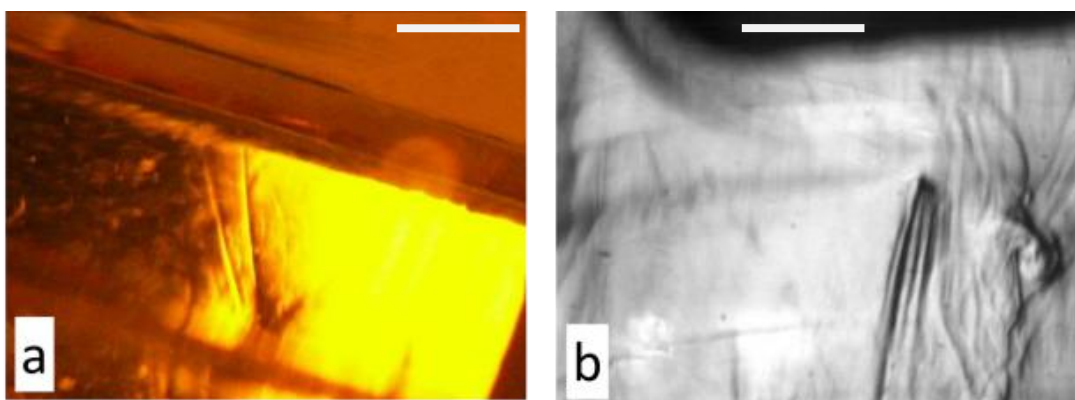
Figure 43. Two self-trapping beams at an angle are imaged in an organosiloxane filled cuvette after the self-trapping experiment using assembly #2. (a) Digital photograph of

the waveguides at an angle and (b) corresponding micrograph are shown. Scale bar is 9 mm in (a) and (b).

Discussion: Features and constraints of large angle (>8^0) assembly

This optical assembly (Figure 24) has a minimum limiting angle directly determined by the physical dimensions of the lenses (L1). At their closest approach, the two lenses, each of 1" diameter and focal length of 25 cm, touch one another and have an angle of approximately 8 degrees between them. This angle can be further reduced by either decreasing the lens diameters or to some extent, by increasing their lens focal lengths. Smaller sized lenses with either equal or larger focal lengths were not available.

The best suited lens (also with the largest focal length) was chosen based on the following constraints: (i) The largest possible focal length of the imaging lens of the pair (L1) was desirable for the smallest possible angle. (ii) The fiber optic light sources used were 50 µm in diameter. A 1:1 or lower magnification of the pair of lenses (L1) had to be preserved in order to generate a beam less than 50 µm diameter necessary for single self-trapping. (larger diameter beams were found to induce fragmentation and multiple filaments through modulation instability.[180] Therefore the focal length of the imaging lens of L1 had to be less than, or equal to that of the object lens of L1. (iii) Keeping the incandescent source (W) too far away from the lens pair (L1) failed to generate sufficient light intensity necessary for self-trapping, and the smallest focal length of the object lens of the pair (L1) was desirable. (iv) Using both plano-convex lenses of the pair (L1) of focal lengths 25 cm each was found to be optimal and satisfied all three constraints.

A study of small angle collisions with an angle <8 degrees was found to be necessary in order to study objectives 1 and 3 described above, and an alternate optical assembly was built to study these collisions as described in the next section.

Features of Small angle assembly (<8^0)

This assembly (Figure 25) was constructed to study small angle collisions (<8^0). It consisted of two mounted cleaved optical fibers as light sources into a cuvette. The fibers were glued to rods mounted on micrometer stages, and adjusting the stages led to a change in the angle between the two fibers. This assembly also proved to be more difficult to control in order to generate small angle collisions. Small angles between beams could not be quantified directly or accurately because of the delicate assembly and the small angle involved.

Further, <1mm gap between the fibers and the cuvette entrance face caused in significant diffraction and back reflections and the beams were launched with a size larger than 50 µm. In order to compensate for the diffraction through the cuvette wall and the resulting error in launch size of the two beams, hand-made customized cuvettes were built using very thin cover slips. These were significantly thinner compared to the 1 mm cuvette wall in the large angle assembly. The two fibers, when placed in contact with the cover slip were still able to generate two incoherent white light beams sufficiently close to the desired size of 50 µm. Keeping the cuvette walls in constant contact with the fibers on the other hand, was found to damage the fiber tips significantly after repeated use. The tunability of the two fibers is limited by the free motion of the micrometer stages

used (2.5 mm). A minimum angle of ~ 12 degrees between the two beams at launch was

achievable.

Conclusion

It was not feasible to generate angles $< 8^0$ using incoherent white light through 50 μm

optical fibers, using either optical assembly built with the existing equipment (even after

working on it for over a year). Colliding beams in angular collisions $>12^0$ were found to

simply pass through one another. Very strong diffraction of white light, loss of intensity

and reflections at a 1mm thick cuvette interface, coupling fibers and light into a flowing

liquid medium (gelation of the liquid makes the fibers useless, requiring splicing, setup

and alignment of fibers again) were the main issues that could not be resolved.

4. Self-trapping of an incoherent black beam in a photopolymer

4.1. Introduction

Both coherent as well as incoherent light waves undergo natural divergence as they propagate along their path. Divergence of incoherent waves becomes apparent, for example, in shadows cast by objects in daylight. With increasing distance, shadows blur, fade away and finally disappear with increasing distance behind the object. This chapter shows that a photopolymerisation process reverses the blurring of a shadow in an incandescent field. A weak shadow borne by an incandescent beam propagating through a photopolymerising medium remains sharply focused and turns black with increasing distance. This *self-trapped* black beam inscribes a permanent channel in the medium, which remains impenetrable to visible light.

Self-trapped waves, including solitons, travel without distortion over long distances in space or time. This nonlinear form of propagation occurs in a range of chemical, physical and biological processes; examples include excitations along polymer chains[222,223], nonlinear chemical waves in reaction-diffusion systems[224], thermal solitons that drive biochemical cycles[225], vibrations along proteins[226], pulses along nerves[227] and within the heart[228], sound[229], potentially catastrophic ocean waves[230], rolling clouds[231] and magnetosonic structures in space plasma.[232] Although they span stunning diversities and echelons of natural systems, nonlinear waveforms are unified by mathematical expression and therefore unsurprisingly, exhibit similar internal dynamics and interactions.[233] Self-

trapped *light* waves, which can be generated and probed under precisely controlled laboratory conditions, are invaluable models of less tractable systems ranging from Bose Einstein condensates[234] to rogue waves in oceans.[235,236] The discovery in 1997 of self-trapping with spatially and temporally incoherent white incandescent light broke three decades of assumption that nonlinear propagation was the exclusive behaviour of coherent light fields.[12] Importantly, self-trapped incoherent beams promise greater fidelity to localised wavepackets in natural systems, which subject to inherent thermal or quantum fluctuations must be composed of waves that are poorly correlated in space and time.[182]

Spatially self-trapped incoherent beams that are *dark* comprise a non-divergent core of reduced intensity that is embedded in an incoherent, bright background beam. Discovered and studied predominantly in photorefractive crystals, self-trapped dark incoherent beams emerge under self-defocusing conditions.[47,58, 106] Here, light intensity from the defocusing background leaks into and suppresses the natural divergence of the dark beam. Because they contain background light, dark beams are characteristically grey (*vide infra*) and as they are born in an incoherent field, are necessarily random in phase structure.[137] This chapter shows that a self-trapped black beam that is spatially *and* temporally incoherent forms spontaneously in a photoinitiated free-radical polymerisation system. The black beam emerges under the self-focusing conditions established by polymerisation-induced changes in the refractive index of the medium. Remarkably, the complete extinction of light intensity to generate self-trapped *black* beams could (until now) only be achieved with coherent optical fields.[137] By imaging the distribution of light

intensity in the medium and monitoring its evolution, an understanding of the mechanism underlying this seemingly counterintuitive discovery is obtained.

Preparation of methacrylate-substituted siloxane photopolymer

Organosiloxane sols were prepared by acid-catalysed condensation of 3-(trimethoxysilyl) propyl methacrylate with aqueous HCl as detailed in Section 2.1. The resulting sol was sensitised to visible light with photoinitiator bis(η5-2,4-cylcopentadien-1-yl)-bis(2,6-difluoro-3-(1H-pyrrol-1-yl)-phenyl) titanium(IV) (λ_{max}= 393 nm, 460 nm). The sol (3.5 ml) was placed in a plastic spectrophotometer cell (path length 10 mm) and irradiated uniformly with white light from a Quartz-Tungsten-Halogen lamp until the free-flowing sol transformed into a gel.

Optical assembly for studies of nonlinear propagation of dark beams

Optical experiments were carried out with the assembly described in Section 2.5 (Figure 26). In a typical experiment, white light (380 nm – 1168 nm) emitted by a quartz-tungsten-halogen lamp (**W**) was collimated with a plano-convex lens and passed through an amplitude mask (**AM**). This introduced a weak, circular depression in the optical field.

The white beam (henceforth referred to as the background beam) bearing the dark circular notch was then focused through a pair of plano-convex lenses onto the entrance face (z = 0.0 mm) of a cuvette containing the organosiloxane gel. The cuvette holder was mounted on a micrometer stage, which could be translated along z with a resolution of 0.5 μm. The profile of the beam at z = 6.0 mm was imaged through a second pair of planoconvex lenses and focused onto a CCD camera. The camera was driven by the

software DataRay$^{©}$ (Version 5.0), which calculates parameters including beam diameter (FWHM, $1/e^2$) and relative peak intensity.

Self-trapping experiments were carried out with three beam configurations corresponding to an effectively infinite, finite and small background beam. Table 1 lists the widths of the background and dark beams employed in each configuration. In each case, the intensity of the background beam was 1.4 mWcm^{-2} measured at z = 0.0 mm (FieldMaster GS power meter, Coherent Inc, USA). Variations in the profile of the dark and background beams at z = 6.0 mm were then monitored over time. The ambient room light intensity, which was measured at ~3 %, was not subtracted from any measurements.

Table 1. Widths of background and dark beams employed in self-trapping experiments. Widths were measured at the entrance face (z = 0.0 mm) of the sample.

	Background beam [μm]	Dark beam [μm]
infinite	5317	124
finite	1146	125
small	614	106

Characterisation of self-induced dark channel in the organosiloxane

The optical assembly in Figure 26 was modified to characterise light-guidance by the self-inscribed dark channels in the organosiloxane. For these measurements, a self-trapped dark beam was first generated and allowed to propagate in the organosiloxane for at least 4000 s, which ensured that the sample was completely polymerised along the path of the beam. The amplitude mask (AM) in the optical assembly (Figure 26) was then removed and a completely uniform, broad beam of white light was launched into the

sample containing the channel inscribed by the self-trapped dark beam. Light transmitted by the sample at $z = 6.0$ mm was measured with the CCD camera. To ensure that the probe beam did not induce additional changes in the medium, the transmittance was monitored for at least 300 s and determined to be constant over this time. Optical reflectance micrographs of the self-inscribed dark channel were acquired with a STEREO Discovery.V12 microscope (Carl Zeiss Ltd., Canada).

Simulations of the self-trapping of dark beams in a photopolymer

The formation and evolution of dark self-trapped beams were modelled through a beam propagation method that was previously developed by the Saravanamuttu group.[66]

Results and Discussion

A weak, noise-like depression (*dip*) in a uniform beam of incoherent white incandescent light spontaneously narrowed, deepened and transformed into a self-trapped black beam as it propagated in a photopolymer. Under linear conditions (in the absence of polymerisation), the dip was negligible noise that rapidly disappeared with propagation distance due to the characteristically large divergence[219] of the background white light. By contrast, when the dip-embedded beam initiated free-radical polymerisation as it propagated through the medium, the system was pushed off-equilibrium into a nonlinear regime. Under these conditions, the dip amplified into a dark beam, which spontaneously rejected light until it transformed into a self-trapped black beam. Because it was embedded in an optical field that was spatially and temporally incoherent, the black beam was extremely poorly correlated in phase and amplitude in space and time. The self-

trapped black beam permanently inscribed a channel in the photopolymer, which rejected white light even under linear conditions.(The channel was intact until the sample disintegrated over a few days).

Selecting a medium for the nonlinear propagation of incoherent white light

Incoherent beams self-trap under very specific conditions:[12] unlike coherent laser radiation, incandescence from the sun or a tungsten filament bulb suffers random variations in phase and amplitude, typically at the femtosecond timescale. A white light beam from an incandescent source can be considered an ensemble of rapidly fluctuating intensity speckles. This chaotic[237], spatially and temporally incoherent wavepacket can self-trap in a medium that undergoes a photoinduced index change over an interval that greatly exceeds the femtosecond regime.[12] Such a *noninstantaneous* system - like the human eye for example - responds to the time-averaged (smoothed) intensity profile of a white light beam and is unperturbed by the phase and amplitude fluctuations that would otherwise inhibit self-trapping.[238] The photoinduced index change must moreover saturate over time and be sufficiently large to self-consistently guide the multiple optical modes that constitute white light.[45] Should these prerequisites be satisfied, then an incoherent beam self-traps as a whole, conserving energy and spectral composition.[63, 65]

Based on the previous findings that self-trapping[63] and other forms of nonlinear propagation of *bright* incoherent light[180,181,239] can be elicited through photoinitiated free-radical polymerisation, we intuited that the same chemical process could also host *dark* incoherent beams. The organosiloxane photopolymer selected for the dark beam

experiments satisfies the requirement of a noninstantaneous, saturable and large photoresponse[63] when exposed to white light in the presence of a photoinitiator, methacrylate substituents of the organosiloxane undergo free-radical polymerisation (Figure 6), which produces a local increase in refractive index (Δn).

The timescale of Δn changes, which is determined by the polymerisation rate, varies from seconds to minutes over the course of the reaction. This translates into a photoresponse time that is at least 13 orders of magnitude greater than the femtosecond fluctuations of incandescent light. As polymerisable moieties are depleted in the medium, index change in organosiloxane reaches a maximum value of ~0.006[240], which is sufficient to support all the modes of white light.[63]

4.2. **Experimental evidence of self-trapped black beam**

To generate the incoherent self-trapped dark beam, a broad, collimated beam of white light emitted by a quartz-tungsten-halogen lamp was passed through an amplitude mask, which introduced a weak, circular depression in the optical field (see Materials and Methods). The dip-containing beam was focused onto the entrance face of a transparent cuvette containing the organosiloxane photopolymer, which was sensitised to visible wavelengths with a titanocene photoinitiator. At the entrance face of the sample, the dip had a width ($1/e^2$) of 124 µm while the background beam was 5317 µm-wide and therefore considered to extend infinitely in the vicinity of the dip (henceforth referred to as the *infinite* background beam). The dip, with a relative intensity of 66 %, was slightly weaker in intensity than the background beam, which had an intensity of 77 %. The dip

broadened and increased in intensity as it propagated through the medium under linear

conditions. This is a consequence of the inherently large divergence of the incoherent

background beam.[229] After a propagation distance (z) of 6.0 mm, the dip was extremely

faint with a diameter of approximately 400 μm and a relative intensity of 67 % making it

nearly indistinguishable from the background beam, which had decreased in intensity to

72 %. To study the effect of free-radical polymerisation on the propagation dynamics of

the dip and its consequent transformation into a self-trapped black beam, the spatial

intensity profile of the dip-embedded beam at a propagation distance (z) of 6.0 mm with a

CCD camera was monitored.

Typical experimental results are shown as temporal plots of width and intensity of

the dip at z = 6.0 mm (Figure 44 a). Corresponding spatial profiles (Figure 44 b-e) are

also presented. The dip underwent a sequence of striking changes when polymerisation

was initiated along the propagation path of the beam: within 90 s, the dip became visible

at z = 6.0 mm, narrowing by almost half from 400 μm to 220 μm and darkening from a

relative intensity of 67 % to 56 %. Over the next 180 s, the dip darkened to 23 % and

reached a minimum width of 152 μm, which was comparable to its width of 124 μm at z

= 0.0 mm. This signified the transformation of the dip into a *self-trapped* dark beam,

which travelled through the medium without significant broadening. In the next 200 s, the

self-trapped dark beam widened to 200 μm but continued to reject light until its relative

intensity decreased to an average value of 4 %. This value, being indistinguishable from

the dark noise (3 %) of the CCD detector, meant that the self-trapped beam was now

effectively *black*. The self-trapped black beam widened to 250 μm over the next 460 s but

remained stable at this width *without reverting to its original divergent form* (400 µm) and remained black for as long as it was monitored (~4000 s).

The self-trapped black beam inscribed a permanent cylindrical channel from the entrance to the exit face of the photopolymer. Optical microscopy revealed the 150 µm-wide structure, which appeared black in an otherwise uniformly polymerised bright medium (Figure 45 a). Remarkably, this channel was black and was impenetrable to white light even under linear conditions. To quantify its exclusion of light, a broad and entirely *uniform* white light beam was launched into the sample and monitored at $z = 6.0$ mm. The beam propagated in all regions of the sample but was selectively excluded from the black channel. The relative intensity transmitted through the channel was 5 %, which was nearly indistinguishable from the dark noise (3 %) of the CCD camera (Figure 45 c).
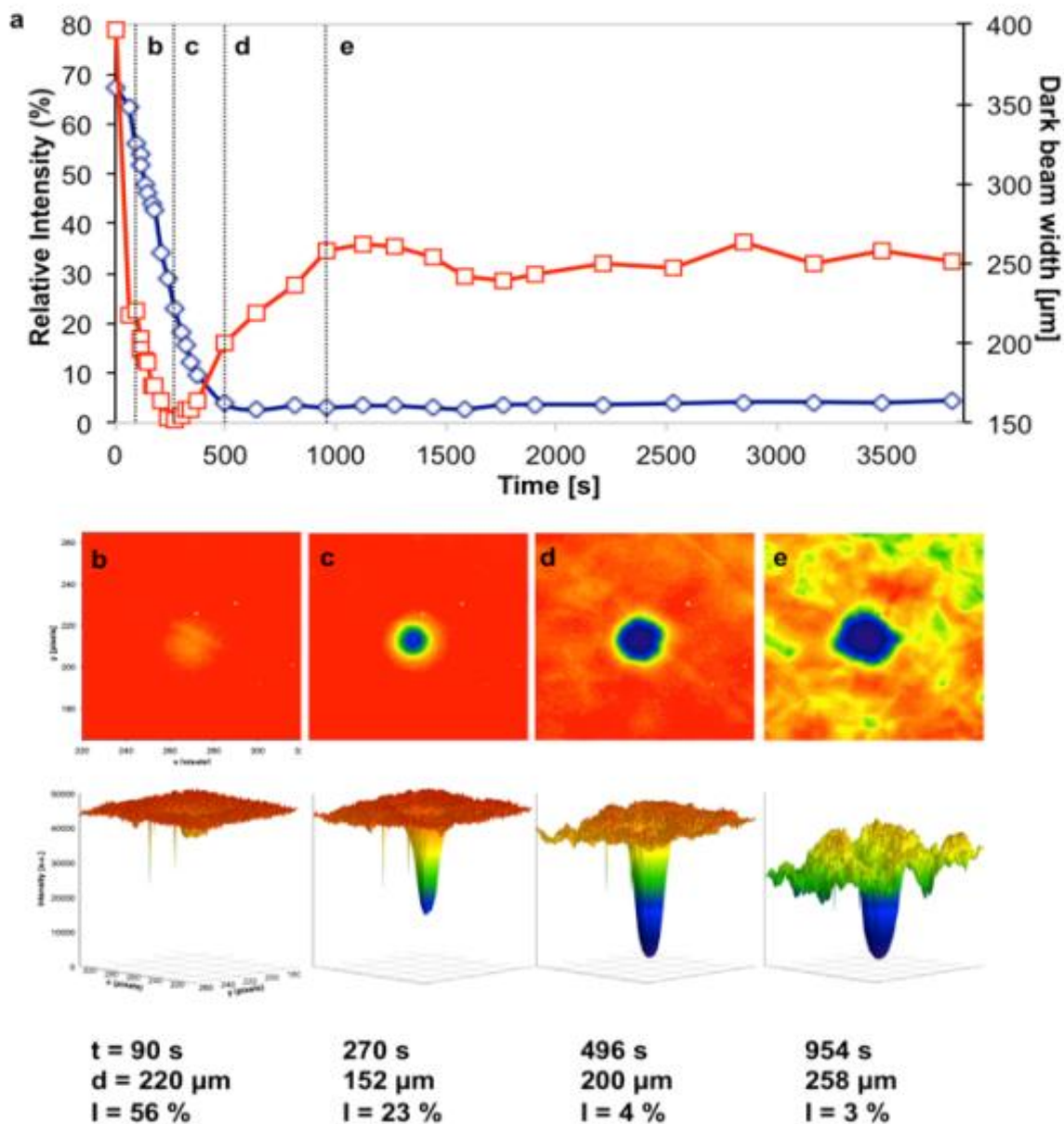
Figure 44. Formation and evolution of self-trapped black beam due to photoinitiated free-radical polymerisation in the organosiloxane observed through (a) temporal plots of relative intensity (diamond) and width (square) at $z = 6.0$ mm. Gray lines correspond to 2-D and 3-D spatial intensity profiles of the black beam acquired at $z = 6.0$ mm at (b) 90 s (c) 270 s (d) 496 s and (e) 954 s at $z = 6$ mm. The black beam width (fwhm) and relative intensity at each time is indicated. The scales employed in (b) apply to (c-d).
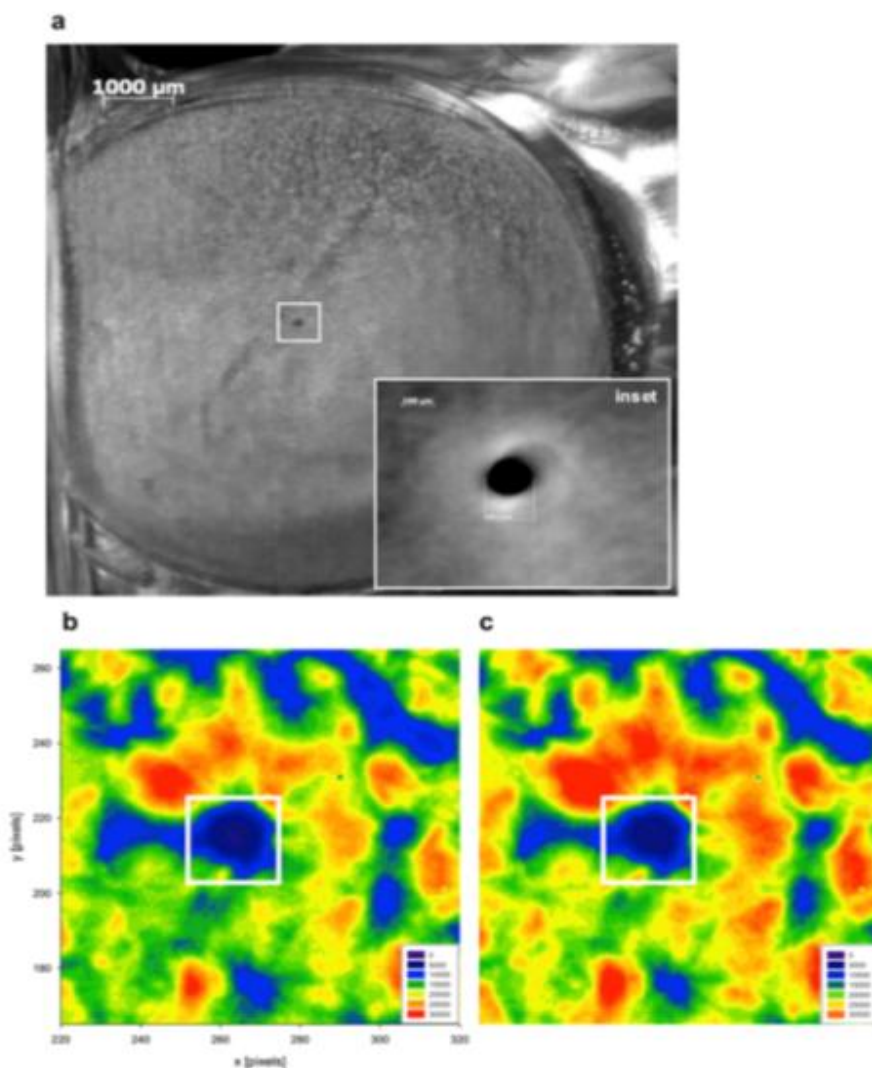
Figure 45 (a) Optical micrograph of self-induced black channel in the organosiloxane. The 150 µm-wide channel (Inset) is embedded in an otherwise uniformly photopolymerised area, which corresponds to the background beam. Comparison of the spatial intensity profiles at $z = 6.0$ mm of the (b) self-trapped dark beam at t = 3798 s and a broad white light beam launched into the (c) corresponding self-inscribed channel show negligible differences: the relative intensity (width) of the self-trapped black beam (b) and channel (c) were 4.5 % (251 µm) and 5 % (235 µm), square. Intensity variations across the background beam in (b) and (c) are due to modulation instability of the background beam, which emerges at late times in the experiment.

4.3. **Proposed mechanism of self-trapped black beam formation**

The origin and evolution of the self-trapped black beam is understood by considering the refractive index changes induced along the path of the dip-embedded background beam. Index changes due to photoinitiated free-radical polymerisation in the organosiloxane vary in space and time according to[43]

1-11

[1-11]

Where Δn_0 is the maximum index change (at saturation), U_0, the critical energy required to initiate polymerisation, τ, the monomer radical lifetime and $E(t)$, the electric field amplitude of the optical field. Equation [1-11] must be combined with the general expression for beam propagation in a photoresponsive medium, which is given by the nonlinear paraxial wave equation[241]:

$$ik_0 n_0 \frac{\partial \varepsilon}{\partial z} + \frac{1}{2}\nabla_t^2 \varepsilon + k_0^2 n_0 \Delta n \varepsilon + \frac{i}{2} k_0 n_0 \alpha \varepsilon = 0 \qquad [4\text{-}1]$$

where α is the attenuation coefficient of the medium at wavelength λ corresponding to the free space wavenumber, $k_0 = \omega/c$. Equation [4-1] describes the reciprocal interactions between a beam and self-induced refractive index changes along its propagation path. Solutions of Equation [4-1] show that the natural divergence of a beam in the directions orthogonal to its propagation path (represented by the transverse Laplacian term) is suppressed by self-induced refractive index changes (Δn) along its propagation path. This *positive* nonlinearity (self-focusing conditions), as extensively demonstrated by theory

and experiment[241,66], enables self-trapping of *bright* beams. Below, a mechanism is proposed on why the same positive nonlinearity can elicit the converse species - a self-trapped black beam.

The proposed mechanism is that the self-trapped black beam forms through the following sequence of events (then proven through experiment and simulation): the dip introduces a weak inhomogeneity in the otherwise uniform rate of polymerisation and consequent Δn across the background beam. According to Equation [1-11], Δn induced by the background beam at early times marginally exceeds that induced by the dip. Because light preferentially propagates in regions of even weakly elevated index[47,106], the dip-induced perturbation in refractive index triggers the efflux of intensity from the dip to the background. As light concentrates in the regions of the background beam, the local refractive index increases further causing additional outflow of intensity from the dip. Continually depleted in this way, the dip turns black as the background intensity reaches maximum. Simultaneously, Δn of the background becomes sufficiently strong to effect self-trapping of the *background* beam through the nonlinear process described by Equation [4-1]. The self-trapped and therefore non-divergent background beam in turn suppresses the broadening of the embedded dip by "holding" it in focus along the propagation path. During this process, the background continually increases in refractive index and withdraws intensity from the dip. Once polymerisable methacrylate units in the background are depleted and Δn saturates, the system equilibriates and both background and self-trapped black beams becomes stable.

4.4. **Experimental verification of mechanism**

To prove the proposed mechanism, the experiment is repeated by replacing the infinite background beam with one of smaller width (henceforth, the finite background beam). This enabled quantitative correlation of the spatial intensity profiles of the background and dip. Because its width (1146 μm) exceeded that of the dip (125 μm) by an order of magnitude, the background beam could still be considered uniform in the dip's vicinity.
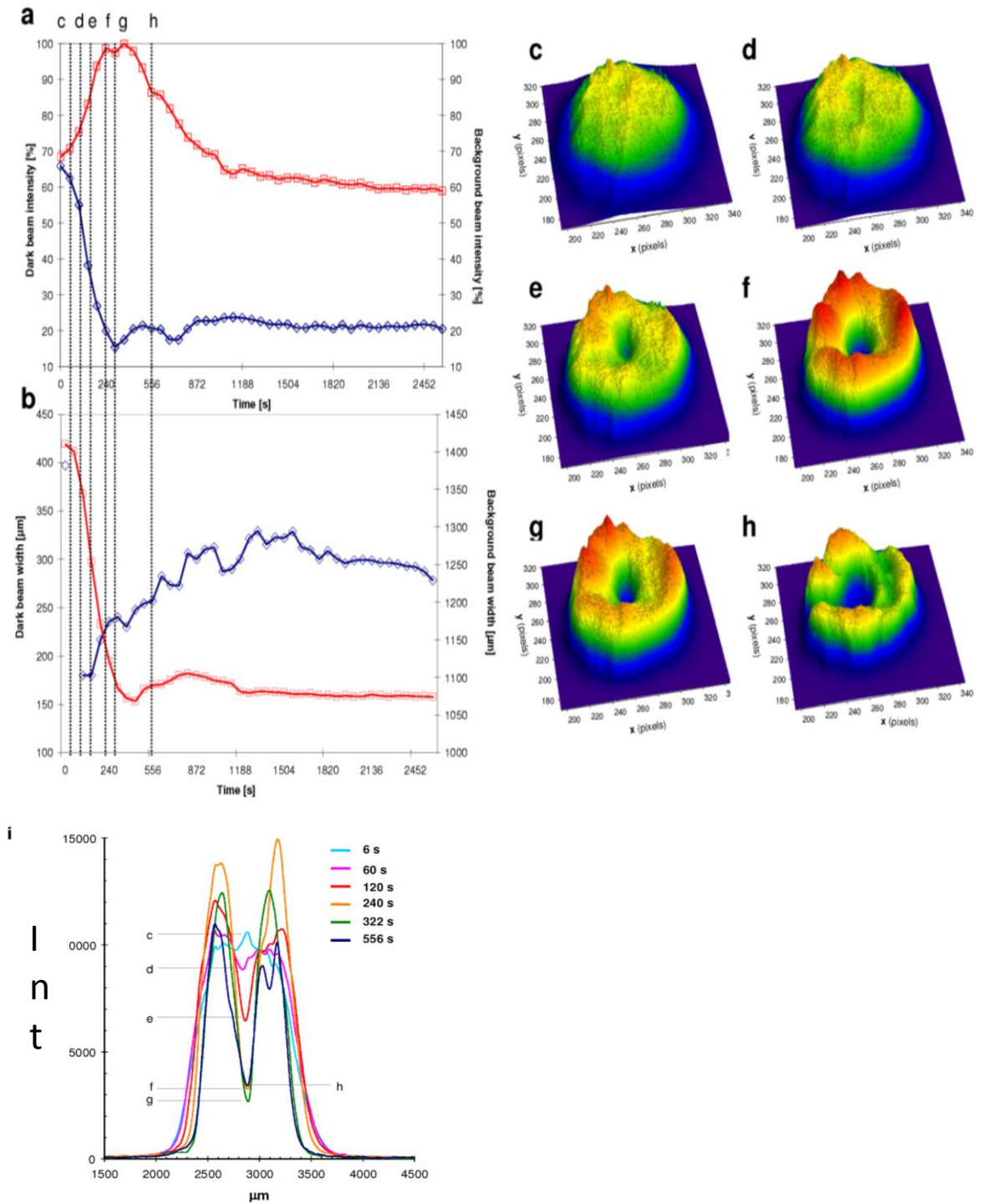
Figure 46. Formation and evolution of self-trapped dark incoherent beam in a background beam of finite width (1146 μm) observed through temporal plots of (a) relative intensities

and (b) widths of the dark beam (diamond) and background beam (square) at z = 6.0 mm. Dotted lines correspond to spatial profiles of the beam acquired at z = 6.0 mm at (c) 6 s, (d) 60 s, (e) 120 s, (f) 240 s, (g) 322 s and (h) 556 s. Corresponding 1-D profiles in (i) clearly trace the deepening and widening of the self-trapped dark beam over time.

First, it was confirmed that a self-trapped dark beam could be generated with this new configuration and that it followed similar dynamics as with the infinite beam (Figure 46). Then, temporal plots of widths (Figure 46 a) and intensities (Figure 46 b) of the background and the dip at z = 6.0 mm were compared to test the validity of the proposed mechanism.

Experimental results were in excellent agreement with the proposed mechanism: within 120 s, the predicted self-trapping of the background beam was detected by its decrease in width from 1400 μm to 1343 μm and increase in relative intensity from 68 % to 76 %. Self-trapping of the background suppressed the divergence and caused *simultaneous* self-trapping of the dip, which narrowed substantially (from 400 μm to 180 μm) with a concurrent decrease in relative intensity (66 % to 55 %). Once self-trapped, the dark beam widened to 217 μm at 180 s (the same trend was observed with the infinite background in Figure 45). During the same time, the background beam narrowed further to 1171 μm. The cause of dark beam-widening is evident in the sequence of 1-D spatial profiles (Figure 46 i). At early times, narrowing of the background beam was sufficient to almost exactly counter the natural divergence of the embedded dip. However, as its local Δn continued to rise, the background beam began to self-focus. While the outer diameter of the background beam decreased, its inner boundaries were drawn away from the

centre, effectively widening the dark beam. Although it widens slightly after reaching a minimum width, the dark beam remains self-trapped and is significantly narrower compared to its original width.

In the proposed mechanism, dark beam formation is governed by the outflow of intensity from the dip to the background. Accordingly, a precise reciprocity in intensity transfer between the dip and background beam was observed (Figure 46 a): the rate of increase of background intensity exactly matched the rate of decrease of dip intensity; the background and dip intensities maximised and minimised, respectively at ~ 322 s. At long times (~1200 s), as the rate of polymerisation and refractive index changes became negligible, the system reached equilibrium and light transfer from the dark to the bright regions ceased. The dark beam stabilised with an average width of 305 μm, remained dark (relative intensity of ~21 %) and did not revert to its original divergent form for as long as it was monitored (~3500 s).

Although the self-trapped dark beam generated with the finite background beam became significantly dark (relative intensity of ~21 %), it did not turn completely black. In fact, we repeated the experiment with an even smaller background beam (614 μm) and found that although a self-trapped dark beam formed (Figure 47), its minimum intensity was 31 % (Table 1). For the infinite background beam, the dip is the only region of depressed intensity in an otherwise uniform field. It is therefore the only source from which intensity is withdrawn during self-focusing of the background beam and is ultimately rendered black. A smaller background beam can withdraw intensity from the dip as well as the regions surrounding its outer boundary (these regions initially contain

intensity due to the divergence of the background beam with propagation distance). Refractive index changes in the background therefore saturate and the system reaches equilibrium before the intensity of the dip is entirely depleted. This accounts for the residual intensity in the self-trapped dark beam in the case of the finite and small background beams. Self-trapping parameters for the three different background beams are presented for comparison in Table 1. Self-trapping of the dip, which was observed in all cases, followed the same dynamics, initially decreasing to a minimum width and showing a slight increase as the background beam continued to self-focus.

4.5. **Effect of background beam on self-trapping dynamics**
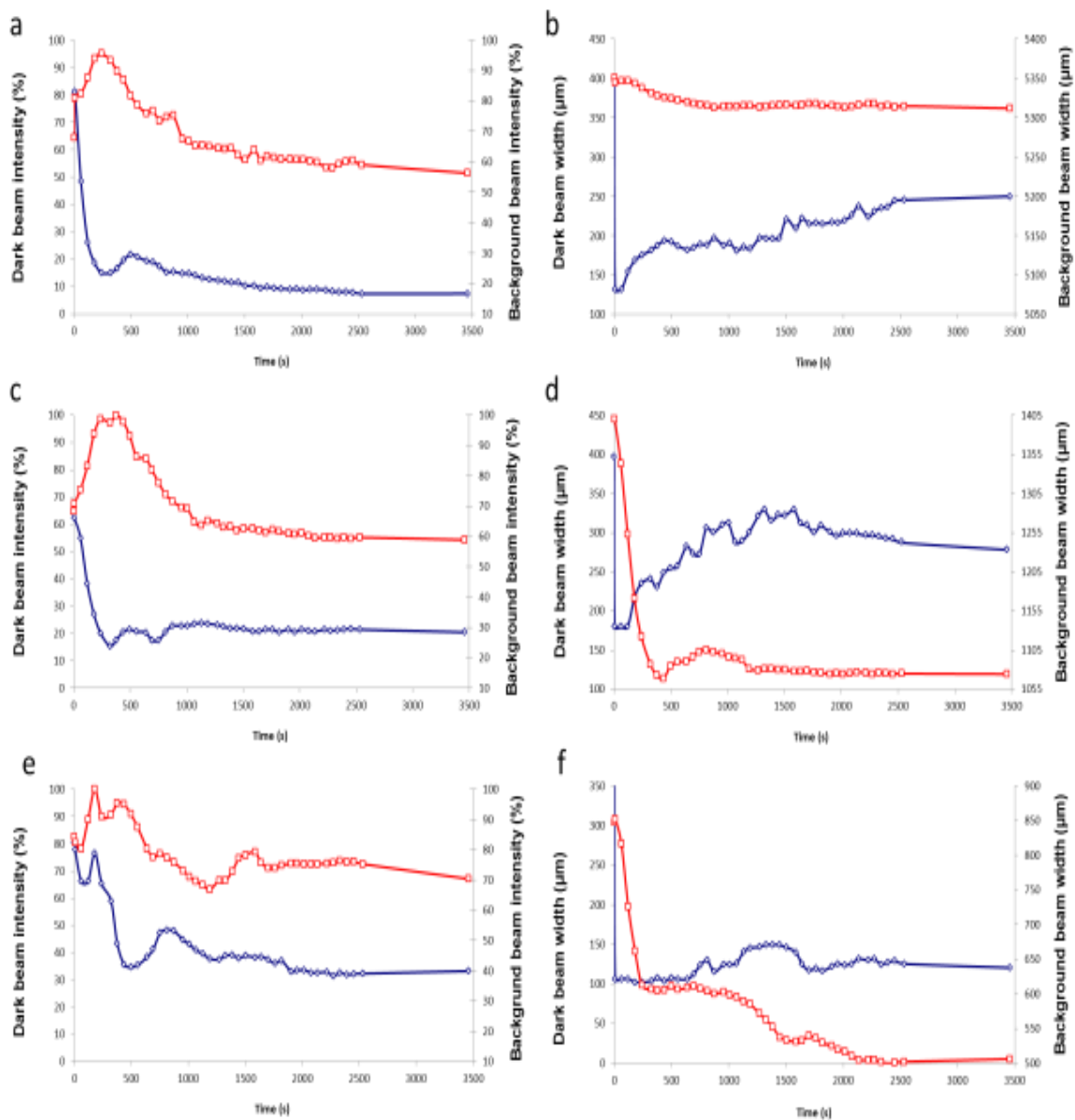
Figure 47. Effect of background beam width on self-trapping dynamics Temporal plots of relative intensity and width of the dark (blue diamond) and corresponding bright background (red square) beams during self-trapping. Plots correspond respectively, to dark and background beam widths of (a, b) 124 µm, 5317 µm, (c, d) 125 µm, 1146 µm and (e, f) 106 µm, 614 µm. Plots (c,d) are presented as Figure 46 in the article but are included here for ease of comparison.

Table 2. Experimental parameters of self-trapped black and dark beams in the organosiloxane photopolymers (z=6 mm)

Background beam width at $z = 6$ mm [μm]	Time of dark beam self-trapping [s]	Minimum dark beam width [μm]	Corresponding background beam width [μm]	Minimum dark beam intensity [%]	Final dark beam width [μm]	Final bright beam width [μm]
5351	270	152	n/a	3	251	n/a
1410	120	180	1254	21	279	1075
848	120	102	662	31	118	515

Comparison with self-trapped incoherent dark beams in photorefractive crystals

The self-trapped black and dark beams generated in the organosiloxane differ fundamentally from the only other known self-trapped dark *incoherent* beams, which form in photorefractive crystals through the electro-optic effect.[47] These studies have predominantly employed partially spatially incoherent, quasi-monochromatic laser light although the interactions between a pair of self-trapped spatially and temporally incoherent dark beams have been examined.[267] Self-trapped dark beams in appropriately biased photorefractive crystals emerge from a *negative* nonlinearity (self-defocusing conditions): in contrast to the photopolymer system, the greatest changes in refractive index are induced by the dip embedded in a background beam. The inner boundaries of the background beam therefore expand as they gravitate into the higher-index dark region. This shrinks the diffracted dark beam profile, reducing it in spatial width. This self-*defocusing* of the background beam compensates for the divergence of the dark beam, enabling it to self-trap. Incoherent dark beams formed in this way necessarily contain light intensity and thus are always grey, *i.e.*, contain more light intensity than the

dip at the input face of the crystal. Until now, it was assumed that self-trapped *black* beams could only be generated with coherent laser beams.

4.6. **Proof of concept: Simulated self-trapped black beams form due to self-focusing nonlinearity**

Finally, numerical simulations were performed to support the counterintuitive finding that self-trapped dark beams originate from the positive self-focusing nonlinearity of a photopolymerisation process. A previously developed method to simulate nonlinear light propagation in a photopolymer was employed to model the formation and evolution of dark self-trapped beams; there is excellent agreement between results obtained through this approach with those obtained by solving the nonlinear paraxial wave equation [4-1]. Briefly, simulations were carried out through an iterative method that combined calculations of the propagation of the optical field by applying the beam propagation method (BPM) with updates of photoinduced refractive index changes in the medium.[66] BPM was applied through the software package BeamPROP[TM] (RSoft Design Group, Inc.) and refractive index changes along the propagation path of the beam were calculated through a home-written external subroutine.

The objective here was to provide proof of the concept that a dark dip propagating through a medium with a positive self-focusing nonlinearity could self-trap and exhibit the dynamics observed experimentally. Therefore using single wavelength light for simplicity, the propagation of a dip embedded in a finite background beam in a medium with a photoresponse expressed by Equation [4-1] was simulated. Results presented in

Figure 48 confirmed that a dip in a finite background beam evolves into a self-trapped dark beam; the dynamics of the process were in excellent agreement with experiment.

Spatial intensity profiles showed that at early times, self-focusing background beam leads to simultaneous self-trapping of the dip (Figure 48 c-f). The corresponding narrowing of the background and dark beams are evident in temporal plots of widths calculated at $z = 6.0$ mm (Figure 48 b). Reciprocity in temporal plots of intensity of the background and dark beams indicate the outflow of intensity from the dip to the background beam (Figure 48 a). The simulations even captured the slight widening of the dark beam that takes place as the background beam continues to self-focus. Both background and dark beams stabilise in width and intensity at long times as photoinduced refractive index changes in the medium approach saturation. Simulations of the self-trapping of the dark beam with the infinite and small background beams were also carried out and found to correspond with experiment (Figure 49-Figure 50, Table 3.
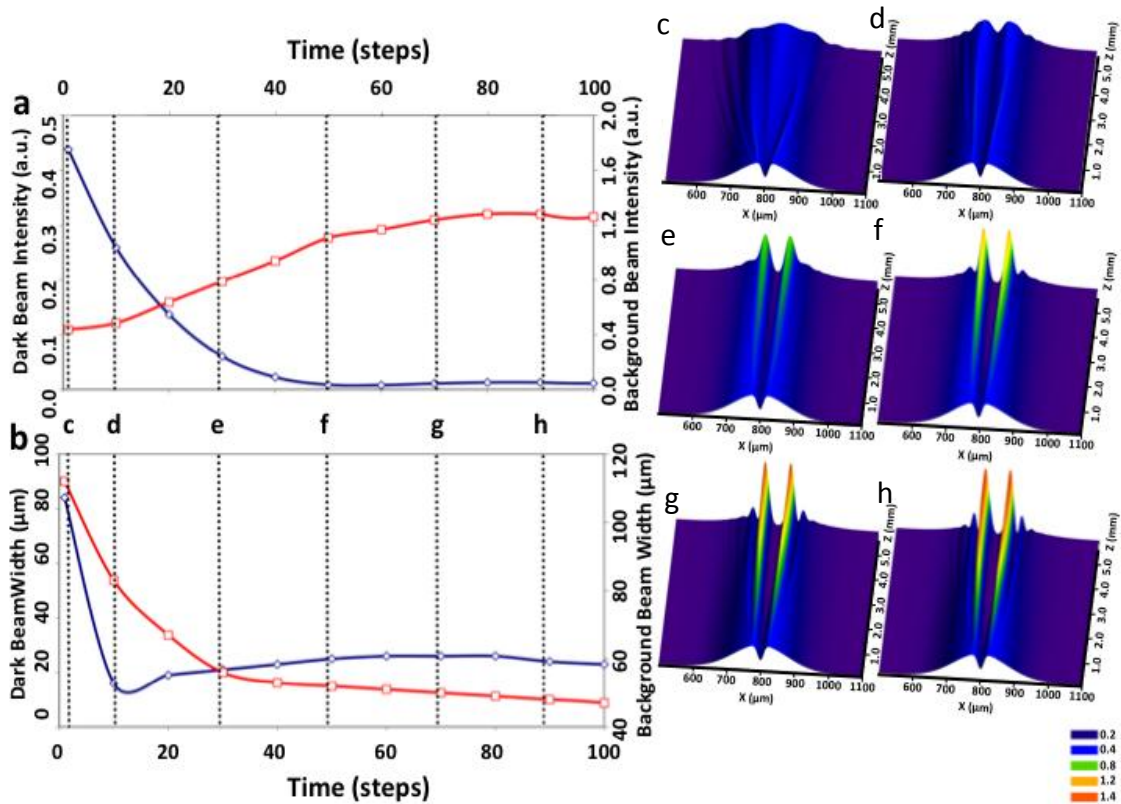
Figure 48. Beam propagation simulations of the formation and evolution of a self-trapped dark   beam in a photopolymer. Results are presented as temporal plots of (a) relative intensities and (b) widths of the dark (square) and background (diamond) beams at $z = 6.0$ mm. Time is represented as steps, which correspond to each iteration of the simulation. Dotted lines correspond to spatial profiles along the propagation path ($z = 0$ mm to 6 mm) at (c) 1 step (d) 10 steps (e) 30 steps (f) 50 steps (g) 70 steps and (h) 90 steps. For simplicity, simulations were carried out with continuous wave, 532 nm light. The dark beam and background beam widths were 11 μm and 97 μm, giving a ratio of 0.11 that corresponded to the experiment with the medium background beam (Figure 46).

Table 3. Widths of dark and background beams measured at $z = 0.0$ mm in experimental and simulated studies of dark beam self-trapping.

	Experiment			Simulation		
	dark beam [μm]	background beam [μm]	dark beam/ background beam	dark beam [μm]	background beam [μm]	dark beam/ background beam
Infinite	124	5317	0.02	11	470	0.02
Finite	125	1146	0.11	11	97	0.11
Small	106	614	0.17	10	58	0.17

In the simulations, the ratios of the widths of the dark beam to the background beam were set to correspond to the three different experimental beam configurations as tabulated in Table 3. In a typical simulation, the dark dip containing Gaussian beam was launched along the 6.0 mm path-length of a medium with refractive index (1.46) corresponding to the non-polymerised organosiloxane. The propagation of the beam under linear conditions was calculated and a map of the resulting electric field amplitude along the propagation length. The external subroutine was then employed to calculate the map of refractive index changes induced by the optical field based on Equation [1-11]. The updated refractive index map of the medium was now fed into BeamPROP^{TM} and the amplitude map of the optical field in the modified medium was recalculated. This process was iteratively performed (usually to a maximum of 100 steps) until subsequent changes to the results were constant ($< 1\%$).
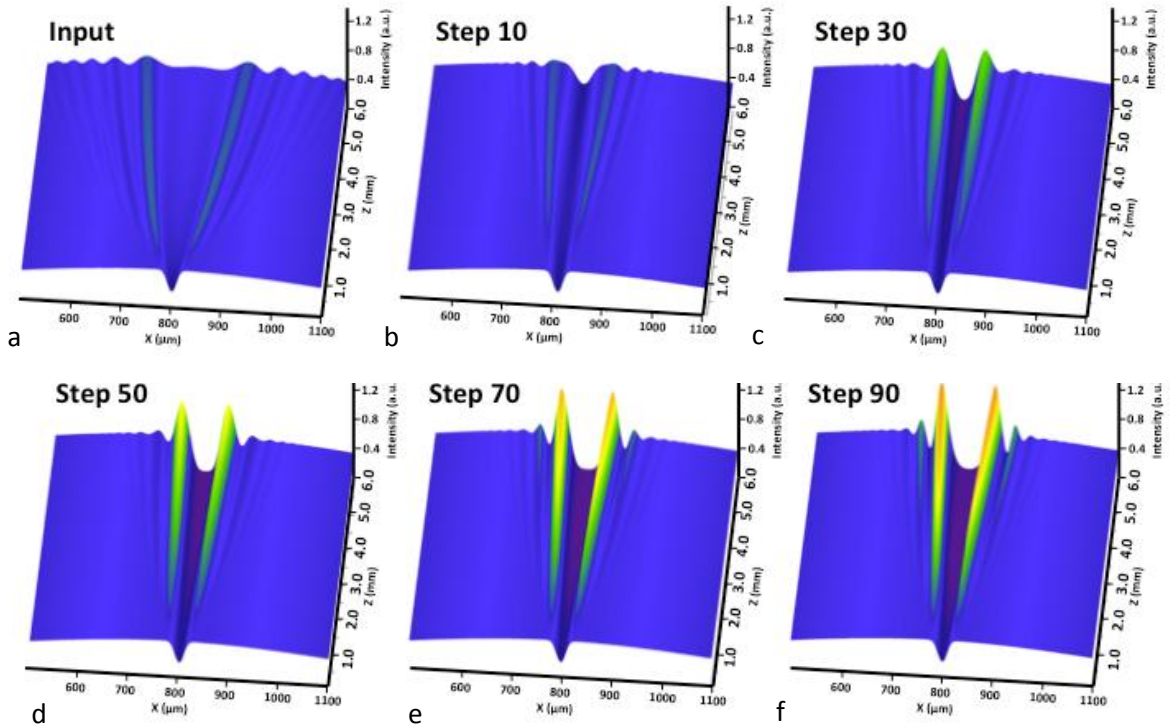
Figure 49. Simulations of dark beam self-trapping with an infinite background beam. Beam propagation simulations of the formation and evolution of a self-trapped dark beam in a photopolymer. Results are presented as spatial intensity profiles along the beam propagation path (from $z = 0$ mm to 6 mm). Time is represented as steps, which correspond to each iteration of the simulation and profiles are presented at intervals of 10 steps from 1 to 100 (a-k). The dark beam and background beam widths were 11 μm and 470 μm, respectively giving a ratio of 0.02 that corresponded to the experiment with the infinite background beam (Table 3).(Note: Unlike experiments, fringes appear in the simulation at later stage due to the use of a coherent background beam).
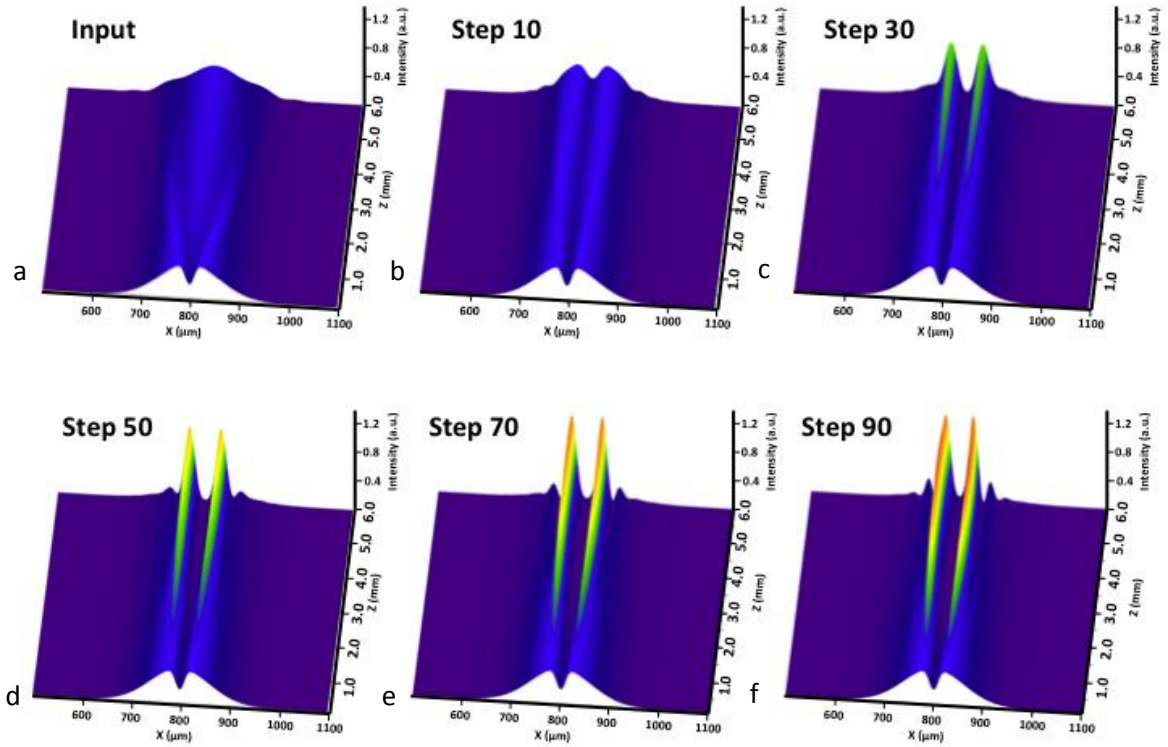
Figure 50. Simulations of dark beam self-trapping with a small background beam. Results are presented as spatial intensity profiles along the beam propagation path (from $z = 0$ mm to 6 mm). Time is represented as steps, which correspond to each iteration of the simulation and profiles are presented at intervals of 10 steps from 1 to 100 (a-k). The dark beam and background beam widths were 10 μm and 58 μm, respectively giving a ratio of 0.17 that corresponded to the experiment with the largest background beam (Table 3).
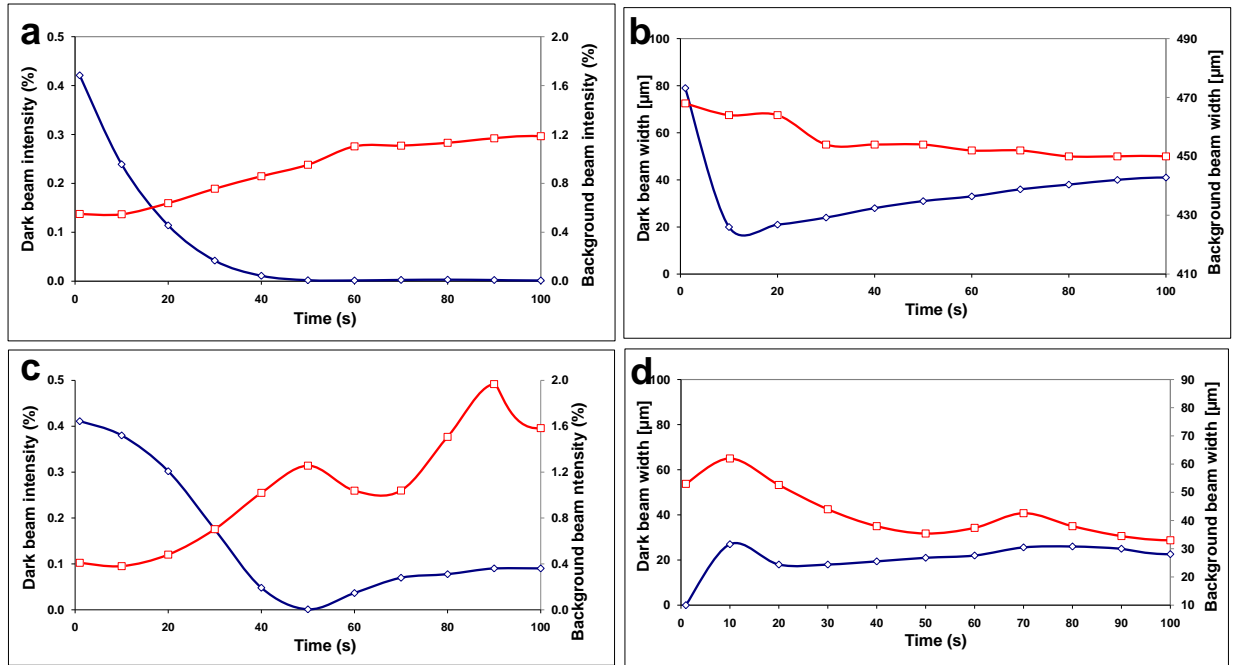
Figure 51. Calculated temporal plots of relative intensity and width of the dark (blue diamond) and corresponding bright background (red square) beams at $z = 6.0$ mm. Plots (a) and (b) correspond to dark and background beam widths of 11 µm and 470 µm, respectively. Plots (c) and (d) correspond to dark and background beam widths of 10 µm and 58 µm, respectively.

Table 4. Simulated parameters of dark beam self-trapping corresponding to experimental parameters in Table 3. All of the simulated self-trapped beams were nearly black whereas in experiments, a black self-trapped beam was generated only in the case of the largest background beam.

Dip width (z=0.0 mm)	Background beam width (z=0.0 mm)	Time of dark beam self-trapping [steps]	Minimum dark beam width [µm]	Corresponding background beam width [µm]	Minimum dark beam intensity [%]	Corresponding background beam intensity [%]	Final dark beam width [µm]	Corresponding bright beam width [µm]
11	470	4	20 (step 10)	464	0.001(step100)	1.186	41	450
11	97	4	16 (step 6)	105	0.008(step 60)	1.168	23	47
10	58	16	20 (step 20)	53	0.001(step 50)	1.256	23	33

4.7. **Summary and outlook**

Photopolymerisation provides an accessible route to self-trapped dark beams including black beams that are spatially and temporally incoherent. These fundamentally new optical species form because of the specific way in which refractive index changes due to polymerisation evolve over space and in time. Our findings bring together research into the nonlinear propagation of both chemical and optical waves. Although traditionally disparate research areas, both share the objective of gaining insight into the dynamics of nonlinear waves: a self-trapped beam is in fact a spatially localised reaction field that exhibits nonlinear propagation. While nonlinear chemical waves can be excited in reaction-diffusion systems[224,242] the nonlinear propagation of polymerisation waves in our system is established through the reciprocal interactions between a light beam and a photochemical medium. By deliberately modifying the spatial profile of the optical field, *i.e.*, by introducing a dip, it is possible to precisely control the spatial and temporal evolution of the reaction field. Because light is a participant in the reaction, optical imaging provides sensitive insight into the kinetics and 3-D spatial evolution of the reaction field that would otherwise be impossible to acquire.

The random phase structure of the black beam embedded in the incandescent field is an intriguing optical paradox as until now, self-trapped black beams necessarily had precisely defined phase structure.[263] Staging collisions between self-trapped incoherent black beams with bright/dark and incoherent/coherent beams could provide insight into their phase structure and also open possibilities to deliberately change the coherence of

colliding beams, which would be extremely important in designing active photonic devices.[45]

Channels induced by self-trapped dark beams typically possess greater indices of refraction relative to their surroundings and therefore, behave as conventional waveguides that confine and guide light.[261] By contrast, the channels induced by self-trapped black beams in our system suppress the transmission of visible light over long distances (>> Rayleigh length). This is particularly important as dark features in incoherent beams (like shadows cast by daylight) suffer significant blurring and become grey after very short propagation distances. The self-induced black channels therefore provide a powerful alternate mechanism to control the flow of light through selectively *suppressing* light transmission over long distances. Most significantly, these mechanisms could be applied to light from inexpensive and miniaturised incoherent sources such as LEDs, which are critical in the development of microphotonics and integrated-optics devices.

5. Optochemical self-organization in a spatially modulated incandescent field: a single-step route to black and bright polymer lattices

5.1. Introduction

A rich and often unexpected diversity of patterns emerge when thin films are driven away from equilibrium through exposure to gradients in temperature or electric field.[165] Such patterns, if elicited in polymeric[167, 243, 244, 245, 246] or polymerizable systems[247,168 248], can be permanently "frozen" into the medium through photo- or thermal curing for example, generating a range of polymer microstructures. The work presented in this article exploits the *optical* analogue of pattern formation seeded by instability. In this process, termed modulation instability,[45] a broad, uniform beam travelling through a photoresponsive system becomes unstable due to self-induced changes in refractive index (Δn). Above a critical value of Δn, the beam stabilizes by dividing spontaneously into a large ensemble of light filaments. Each filament induces Δn along its propagation path, inscribing and becoming entrapped in a cylindrical channel – an *optical waveguide* – which guides it over long distances without suffering attenuation or changing its spatial profile. In this way, modulation instability yields a large population of waveguides, each of which efficiently guides a fraction of the beam through the medium. Modulation instability has been predominantly studied in nonlinear optical materials such as photorefractive crystals[60, 61, 249] in which Δn originates from the excitation of high order

dielectric tensors. Consequently, in the absence of the excitation source, the system

relaxes to its original state and all traces of Δn eventually disappear.

Our group previously demonstrated that Δn produced by a chemical reaction -

photoinitiated free-radical polymerisation - satisfies the prerequisites for optical self-

trapping of both coherent laser[66] and incoherent incandescent light.[63, 65] In this case, a

narrow light beam becomes entrapped within a self-induced cylindrical channel and

propagates through a photopolymerizable organosiloxane medium without diverging (as

it would under linear conditions). These experiments also showed that due to the

irreversibility of the polymerisation reaction, the cylindrical waveguide induced by the

beam was permanently inscribed into the medium. Knowing that optical self-trapping of a

narrow beam occurs under the same conditions as modulation instability of a broad,

uniform beam[180,181] next, an incandescent beam was then demonstrated to spontaneously

undergo filamentation when launched into a methacrylate-derivatised organosiloxane sol.

The resulting pattern of self-trapped filaments inscribed the corresponding microstructure

into the medium, transforming it from a homogeneous, isotropic sol into a solid array of

uniaxial, cylindrical waveguides.

The above-described process will be termed optochemical self-organization[250] to

signify the reciprocal roles played by the photochemical reaction and the optical field, as

well as the spontaneity of the filamentation process. Optochemical self-organization

occurs through the following sequence of events: when a broad, uniform white light beam

emitted by a quartz-tungsten-halogen lamp is launched into the organosiloxane, it initiates

free-radical polymerization of methacrylate substituents along its propagation path. Δn

originating from polymerization pushes the system into a nonlinear regime, where weak and normally negligible noise in the optical field become greatly amplified. This triggers the division of the beam into thousands of self-trapped light filaments (typical sample volume = 10 mm^3).[180]Because Δn is irreversible, cylindrical waveguides induced by the filaments are indelibly imprinted into the medium. Significantly, these filaments propagate over very long distances without attenuation, resulting in 3-D polymer microstructures that span large volumes, limited only by the dimensions of the sample cells (10 mm x 10 mm x 20 mm)[250] employed in our experiments. Importantly, these are functional polymer microstructures, which even under linear conditions, serve as lattices of polychromatic, multimoded waveguides. Extending this technique to an orthogonal pair of beams, the spontaneous generation of 3-D lattices constructed from intersecting waveguide arrays was also demonstrated. These previous experiments focused on generating specific lattices of bright beams with nearly-square[181], nearly-cubic[181], b.c.c. and woodpile[250] symmetries.

The previous chapter showed that the same free-radical polymerization process that elicits self-trapped bright beams and modulation instability also gives rise to self-trapped black beams - narrow channels that propagate through the medium and are impenetrable to the visible spectrum.[251] It was also shown (Chapter 7) that it is possible to simultaneously elicit self-trapped bright and dark regions of an optical field by demonstrating the formation of a hybrid beam, which comprised a self-trapped dark core with a self-trapped bright cladding.[252] Exploiting this property, a new generation of optochemically self-organized lattices consisting of ordered arrays of black beams with

the interstitial regions occupied by bright filaments is introduced. This approach is to elicit modulation instability in a beam embedded with a pattern of dips. Intensity differences between the bright and dark regions become greatly amplified under the nonlinear conditions generated through photopolymerization so that modulation instability and filamentation are strictly confined to the bright regions. The dips play a critical role in controlling the spatial organization of the bright filaments. As the bright regions increase in Δn, they deplete the adjacent dips of intensity until they are rendered black and evolve into dark cylindrical channels. The strong contrast in Δn ensures that light is strictly confined to the high-index bright regions and does not leak into the dark channels as it would under linear conditions. By systematically varying the size, type and organization of the dips imposed on the optical field, it is possible to precisely control the population and spatial positioning of both the bright waveguides and the dark channels.

Optical Assembly

An optical assembly described in section 2.6 was used to generate 2D arrays of dark self-trapping beams in a photopolymer (Figure 28). This assembly also consisted of a quartz-tungsten-halogen lamp as an incandescent white light source, to illuminate a 10 mm of an organosiloxane filled cuvette (S) with collimated light. A patterned 2D amplitude mask (AM) which was placed inside the cuvette itself at the entrance face. On illumination, the mask casts a pattern of bright and dark areas of light in the organsiloxane. This induces optical self-trapping and waveguide formation in the bright areas. Filamentation and dark waveguides also form under certain conditions. A CCD and

a pair of lenses were mounted on a rail beyond the exit face of the cuvette in order to monitor the output profile of the beam over time. An identical assembly was set up in a perpendicular direction around the same cuvette in order to generate 3D lattices (Figure 29). Amplitude masks of various patterned geometries were used to generate the lattices listed below:

1. Hexagonal 2D lattices

2. Square 2D lattices

3. ABAB type square 2D lattice

4. Square 3D lattice

5.2. **Optochemical self-organization of an incandescent beam embedded with a hexagonal array of dips**

In a typical experiment, a broad incandescent beam was launched, patterned with a hexagonal array of dark dots into a transparent cuvette containing the photopolymerizable organosiloxane. At the input face ($z = 0.0$ mm) of the sample, the relative intensities of the background and dips were ~64 % and ~3 %, respectively. The dips were ~180 μm in diameter and separated (centre-to-centre) from their nearest neighbours by ~410 μm. Typical results in Figure 52 (a-f) trace the temporal evolution of the optical field at $z = 6.0$ mm in the medium. Because the extent of photopolymerization and corresponding changes in the refractive index (Δn) of the medium were negligible at very early times (1 s), the beam initially diverged as it propagated from the entrance to the exit face of the medium; the spatial profile of the optical field acquired at $z = 6.0$ mm

158

after 1 s (Figure 52a) showed that although the background intensity remained approximately the same (67 %) as at the input (64 %), divergence of the background caused an increase in the average diameter of the dips from 180 μm to 195 μm. Broadening of the background and consequent leaking of intensity into dark regions led to an increase in the intensity of the dark spots from 3 % at the input to 13 % at $z = 6.0$ mm (Figure 52a). The significant divergence of the beam over the relatively short distance of 6.00 mm is understandable as compared to coherent laser light, incandescent light suffers considerably greater broadening due to its rapid (10^{-13} s) and random fluctuations of phase and amplitude and its small coherence length (~300 nm).[219]

   As the extent of photo-initiated polymerization increased along its propagation path, the beam underwent a striking sequence of spatial reorganization and redistribution of intensity. Results presented in Figure 52(a-f) show that over time, the dark spots increased in diameter and decreased significantly in intensity. Simultaneously, the bright interstitial regions in-between the dark spots became unstable and spontaneously divided into multiple bright filaments. These changes originate from refractive index changes caused by photopolymerization, which elicit two distinct but interrelated forms of nonlinear light propagation: (i) self-trapping of the bright interstitial regions and their subsequent (ii) modulation instability[180] and division into discrete and stable self-trapped filaments of light.
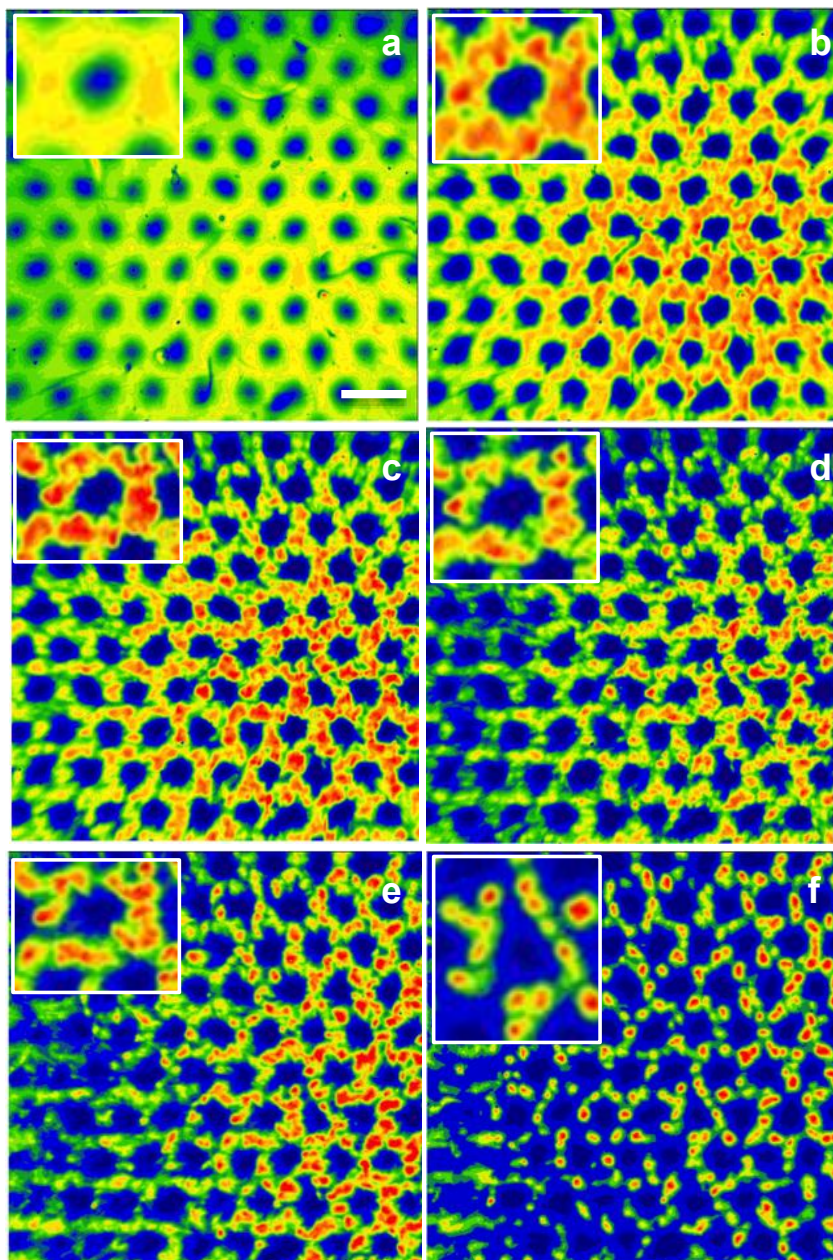
Figure 52. Optochemical self-organization of a broad incandescent beam patterned with a hexagonal array of dips. Spatial intensity profile of the beam were acquired at z = 6.0 mm at (a) 1 s, (b) 60 s, (c) 120 s, (d) 180 s, (e) 322 s and (f) 1336 s. Scale bar ~ 400 μm applies to all images.

5.3. **Mechanism of optochemical self-organization**

Nonlinear phenomena (i) and (ii) can be understood as follows: because the rate of free-radical polymerization is intensity-dependent, the corresponding values of Δn maximize in the bright interstitial regions and minimize in the dips (*vide infra*). Our group previously showed that Δn in the organosiloxane is sufficiently large to suppress the divergence of an individual narrow incandescent beam. This enables its propagation over long distances as a non-diverging, self-trapped beam. The behavior is described by the nonlinear paraxial wave equation[241]:

$$ik_0 n_0 \frac{\partial \varepsilon}{\partial z} + \frac{1}{2}\nabla_t^2 \varepsilon + k_0^2 n_0 \Delta n \varepsilon + \frac{i}{2} k_0 n_0 \alpha \varepsilon = 0 \qquad \text{[4-1]}$$

where α is the attenuation coefficient of the medium at wavelength λ corresponding to the free space wavenumber, $k_0 = \omega/c$. Equation [4-1] describes the dynamic competition between the natural tendency of a light beam to diverge in the directions orthogonal to its propagation path (expressed by the transverse Laplacian term) and focusing due to self-induced Δn changes, which are described through[43]:

$$\Delta n(r, z, t) = \Delta n_s \left\{ 1 - \exp\left[-\frac{1}{U_0} \int_0^{t-\tau} |E(t)|^2 \, dt \right] \right\} \qquad \text{[1-11]}$$

Where Δn_s is the maximum index change (at saturation), U_0, the critical energy required to initiate polymerization, τ, the monomer radical lifetime (assumed to be negligible) and $E(t)$, the electric field amplitude of the optical field.

Solutions of equation [4-1] correspond to narrow self-trapped beams, which propagate without divergence over long distances (>> Rayleigh range), as extensively demonstrated through theory and experiment.[241] In the current experiment, the same photoinduced Δn resulted in the self-trapping and divergence-free propagation of the entire interconnected network of bright interstitial regions. Self-trapping was evidenced by the decreasing thickness of the interstitial regions with a corresponding increase in their average intensity from 67 % (t = 0 s) to 75 % (t = 60 s) (Figure 52c). Narrowing of the bright interstices caused an effective increase in the average diameter of the dips from 195 μm to 255 μm. During this time, the dips also decreased in intensity from 13 % to 5 %. This is because once self-trapped, the interstices no longer diverged and leaked intensity into the dark regions, which therefore retained approximately the same intensity as at the entrance face of the medium (3 %).

As Δn increased, the self-trapped bright regions, which were initially uniform in intensity (Figure 52c), developed weak inhomogeneities (Figure 52d) that amplified over time (Figure 52e) and ultimately divided into discrete filaments (Figure 52f). This sequence of noise amplification followed by filamentation is consistent with the modulation instability of broad unstructured beams of incandescent light. The average width of the bright filaments in Figure 52(f-h) also consistent with the characteristic diameter of filaments (~80 μm) generated with an unpatterned incandescent beam.[180] Whereas in the unpatterned beam, the filaments would be uniformly (although randomly) distributed in space, in the current example they were spatially confined to the interstices of the dips (Figure 52f-h).

5.4. **The critical role of dips**

The dips embedded in the input beam play an important role in controlling the spatial positions of the self-trapped filaments. Because Δn is greater in the bright interstices, there is a spontaneous transference of light intensity from low (dark) index to adjacent high (bright) index regions. These reciprocal changes in intensity are evident in Table 5; as the bright interstices self-trapped and increased in intensity to a maximum of 86 %, the dips were depleted of intensity until at long times (> 1330 s), they were rendered black with a relative intensity of only 1 %, which was comparable to the background noise of the CCD detector.

Table 5. Temporal evolution of the relative intensity of the bright interstices and dips during optochemical self-organization measured at $z = 6.00$ in the photopolymerizable organosiloxane. Corresponding changes to the average dip diameter are also listed.

Time [s]	Bright interstitial intensity [%]	Dip diameter [µm]	Dip intensity [%]
1	67	195	13.2
60	75	256	4.9
120	86	259	3.5
180	83	248	2.0
322	68	293	2.9
1336	48	303	1.0

The significance of the black channels becomes clear when comparing the propagation of dips embedded in a broad beam under *linear* conditions (*i.e.*, in the absence of polymerization). Here, the dips gain intensity with propagation distance due to

the natural divergence of the beam (Figure 52a). However, in the nonlinear regime generated by photopolymerisation, the contrast in Δn between the bright interstices and black channels ensures that light selectively propagates in the higher-index regions from the input to the output face of the medium. As a result, the self-trapped filaments are confined to the interstitial regions over the entire propagation distance through the medium. The result is the transformation of the optical field into a hexagonal lattice of dark cylindrical channels with interstitial regions occupied by tightly packed but randomly positioned filaments (Figure 52f). Figure 53a,b shows the simultaneous formation of both black and bright channels in bottom-up and top-down views of the lattice, respectively.
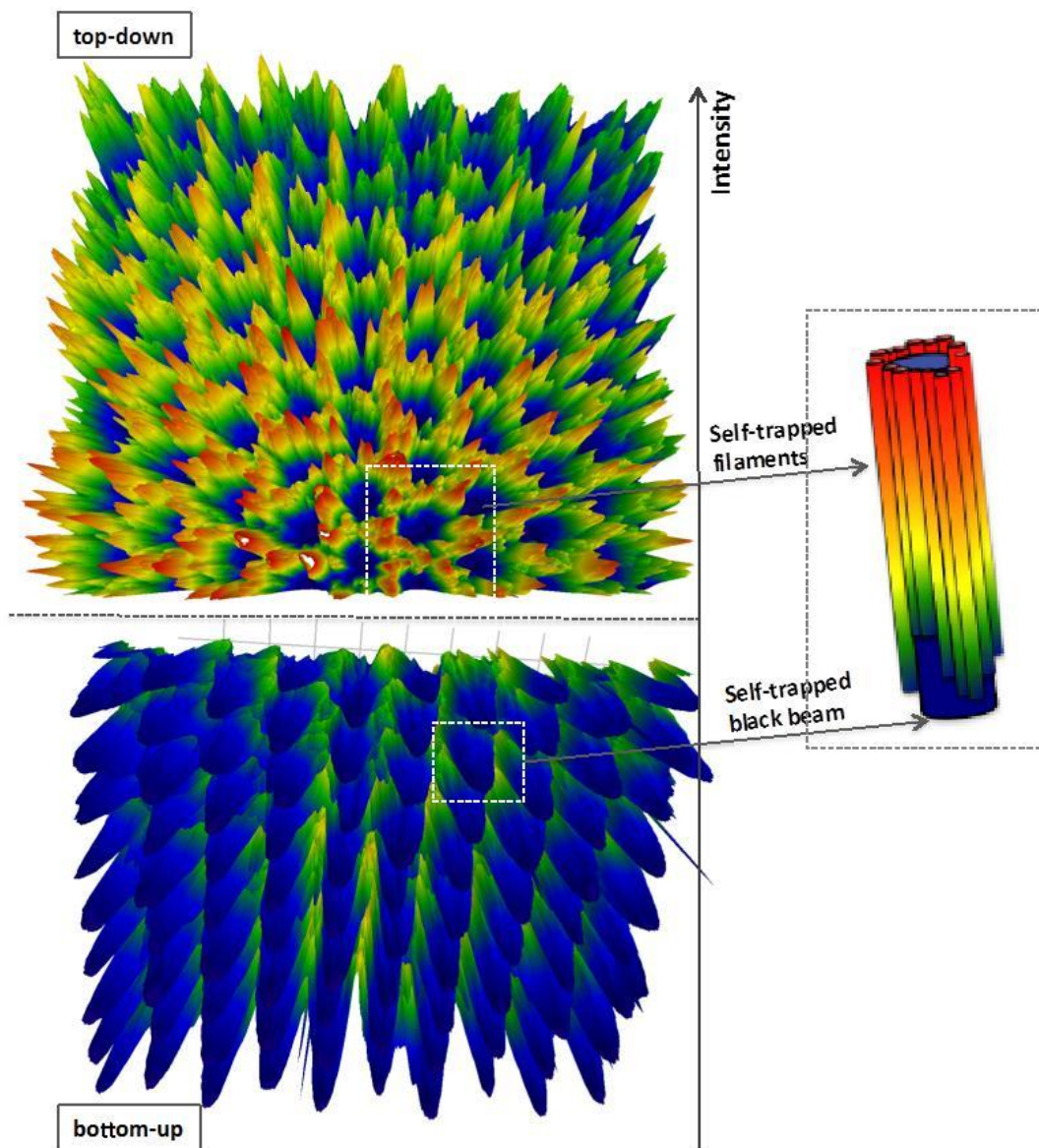
Figure 53. 3-D spatial intensity profiles showing the co-existence of bright filaments and black beams in an optochemically self-organized lattice. The bottom-up view shows the periodic array of amplitude depressions corresponding to the self-trapped black beams while the top-down view shows the self-trapped filaments. The spatial intensity profile was acquired at z = 6.00 mm at 322 s and corresponds to Figure 52e. The accompanying cartoon is a guide to the eye, which shows how each black beam is surrounded by bright self-trapped filaments.

5.5. **Controlling the spatial positions of self-trapped filaments**

We carried out experiments with incandescent beams bearing a hexagonal array of dips with average diameters ranging from 170 μm, 270 μm and 290 μm to 315 μm with a constant centre-to-centre separation distance of 425 μm. In this way, the interstitial width between neighbouring dips was tuned from 255 μm, 155 μm, and 135 μm to 110 μm. Spatial intensity profiles of the polymer waveguide lattices induced under these different conditions are collected in Figure 54; corresponding parameters are tabulated. 3-D spatial intensity profiles have been included as Figure 57.
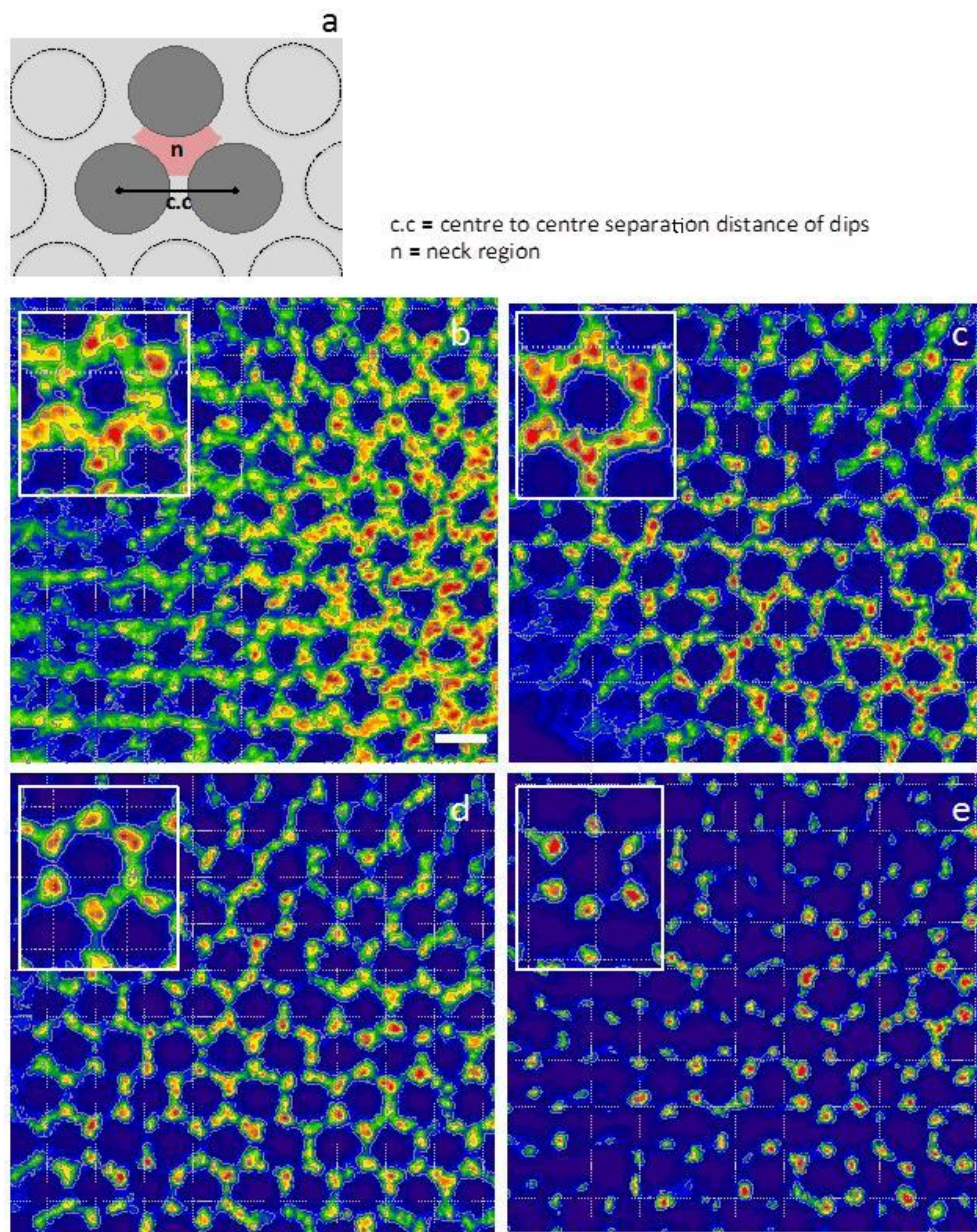
Figure 54. Optochemically self-organised lattices generated from incandescent beams patterned with a hexagonal array of dips with the same center-to-center separation (a) of 425 μm and diameters ranging from (b) 170 μm, (c) 270 μm and (d) 290 μm to (e) 315 μm. Spatial intensity profiles were acquired at z = 6.0 mm at 322 s. Corresponding parameters are listed in Table 6. Scale bar = 360 μm applies to all images. Magnified images are presented as insets. (See also Figure 57).

Table 6 Widths and relative intensity of self-trapped black beams generated with dips of different diameters acquired z = 6.0 mm. All measurements were made at 322 s.

Dip input diameter [µm]	170	270	290	315
Dark beam diameter at 322 s[µm]	245	312	291	313
Output intensity at 322 s [%]	2.9	3.0	1.4	1.8

Optochemical self-organization was observed for all dip diameters; the dynamics of the process in each case followed the temporal evolution described in Figure 52. In all cases, the dips were depleted of intensity until rendered black with relative intensities ≤ 3 %. However, the spatial organization of filaments in the final stable lattice showed significant differences. In the case of the greatest interstitial width of 255 µm, multiple, randomly positioned and tightly packed filaments occupied the interstitial regions surrounding the dips (Figure 54b). The filament population decreased significantly when the interstitial width was decreased to 155 µm; in this case, single filaments occupied some interstices although clusters of filaments were also observed. A critical threshold appeared to be crossed when the interstitial width was decreased by another 20 µm to 135 µm. In this case, clusters were not observed; instead, the interstices were occupied by a single file of filaments, which encircled each dip as a continuous ring. By contrast, the smallest interstitial width of 110 µm gave rise to a sextet of discrete filaments, which were positioned with azimuthal symmetry about each dip; in this case, the long-range arrangement of the filaments corresponded to a hexagonal lattice.

The differences in the lattices presented in Figure 54 are understood by considering the characteristic diameter (d_f) of modulation instability-induced filaments in the photopolymer, which is determined by the coherence of the incident optical field. The incandescent field employed in the current experiments has a spatial coherence length of 300 nm, which results in $d_f \approx 80$ μm. An interstitial width of 255 μm, being 3-fold greater than the d_f, was sufficiently large to support multiple filaments. As in the case of an unpatterned beam, the filaments generated in the interstitial regions were randomly positioned in space (Figure 54b). When reduced to 155 μm, the interstitial area was sufficiently large to support at least one filament but at the threshold of being able to support two. In this case, both single filaments as well as filament clusters were observed in the resulting lattice (Figure 54c); the latter preferentially occupied the "necks" (Figure 54a) formed by each triad of dips. The necks had a larger area than the interstitial region between two adjacent dips and could therefore support more than a single filament. Single filaments predominantly occupied the regions between two adjacent dips. An interstitial width of 135 μm, being significantly smaller than $2d_f$, could only support single filaments, which formed rings around each dip (Figure 54d). At the smallest interstitial width of 110 μm, filaments preferentially occupied the necks and in this way, formed an azimuthally symmetric sextet around each dip (Figure 54e).

Experimental results presented in Figure 55 with corresponding parameters collected in Table 7 show that this approach could also be applied to a square array of square-shaped dips. (3-D spatial intensity profiles have been included as Figure 58 corresponding to the temporal evolution of lattices in Figure 55a and Figure 55c. Here

too, multiple, randomly positioned filaments occupied the interstices when its width was set at 235 μm, greater than twice the filament diameter (Figure 55a). When the interstitial width was decreased to 150 μm, just below twice the filament diameter, both individual and clusters of filaments coexisted in the resulting lattice (Figure 55b). At an interstitial width of 80 μm, which corresponded to the filament diameter, the filaments preferentially occupied the corners of each square dip, forming a lattice with long-range square symmetry.
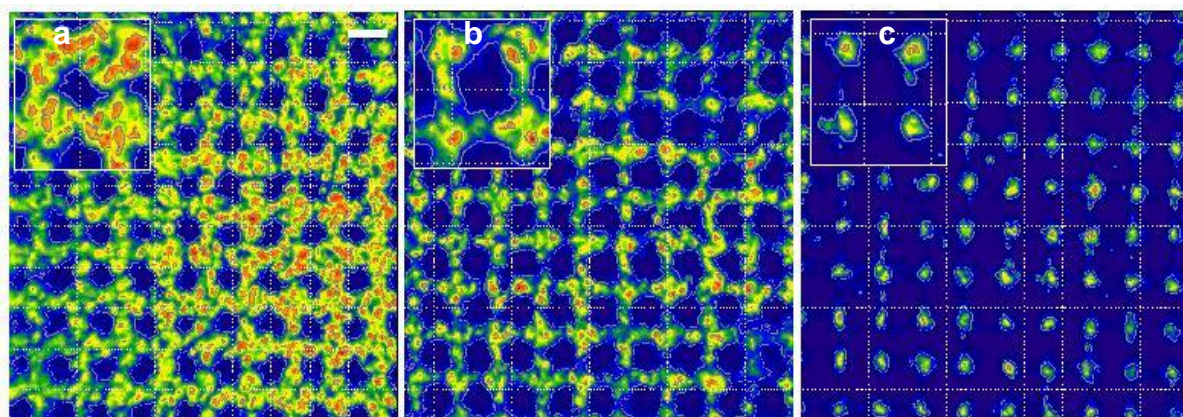
Figure 55. Optochemically self-organised lattices generated from incandescent beams patterned with a square array of dips with the same centre-to-centre separation of 410 μm and diameters ranging from (b) 175 μm, (c) 260 μm and (d) 330 μm. Scale bar = 360 μm applies to all images. Magnified images are presented as insets. (See also Figure 58.

Table 7. Widths and relative intensity of self-trapped black beams generated with dips of different diameters acquired z = 6.0 mm. All measurements were made at 322 s.

Dip input radius (μm)	175	260	330
Dark beam diameter at 322 s (μm)	237	285	410
Output intensity at 322 s (%)	1.4	1.6	0.7

Figure 56b is the spatial intensity profile of an optochemically self-organized square lattice, in which each lattice point consisted of a pair of filaments. The filament pairs were oriented alternatingly at $+45^{o}$ and -45° throughout the lattice. To generate this structure, the incandescent beam was patterned with a square array of dips with alternating diameters of 820 μm and 620 μm, which were positioned edge-to-edge. The resulting bright interstitial regions were rectangular in shape (~350 μm x 190 μm) and oriented alternatingly at $+45^{o}$ and -45°. In this case, filamentation preferentially occurred along the long axis of each bright rectangle resulting in a doublet of filaments, which were organized in the long-range with square symmetry. This example highlights the possibility of generating unique lattices through the optochemical self-organization approach through deliberate design of the pattern of dips imposed on the incandescent beam. The lattice presented in Figure 56b would be extremely difficult to generate through conventional lithographic techniques.
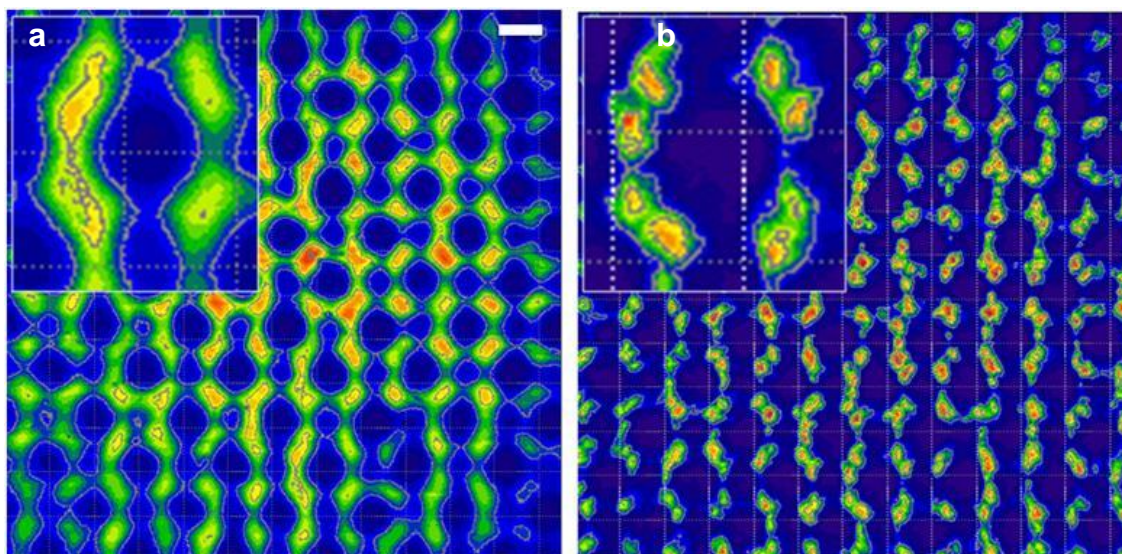
Figure 56. Optochemically self-organized lattices from an incandescent beam embedded with dips of alternating diameters. Spatial intensity profiles acquired at z = 6.00 mm at (a) 0 s and (b) 332 s show that the interstitial regions undergo filamentation to generate a lattice of filament doublets. Scale bar = 360 μm.
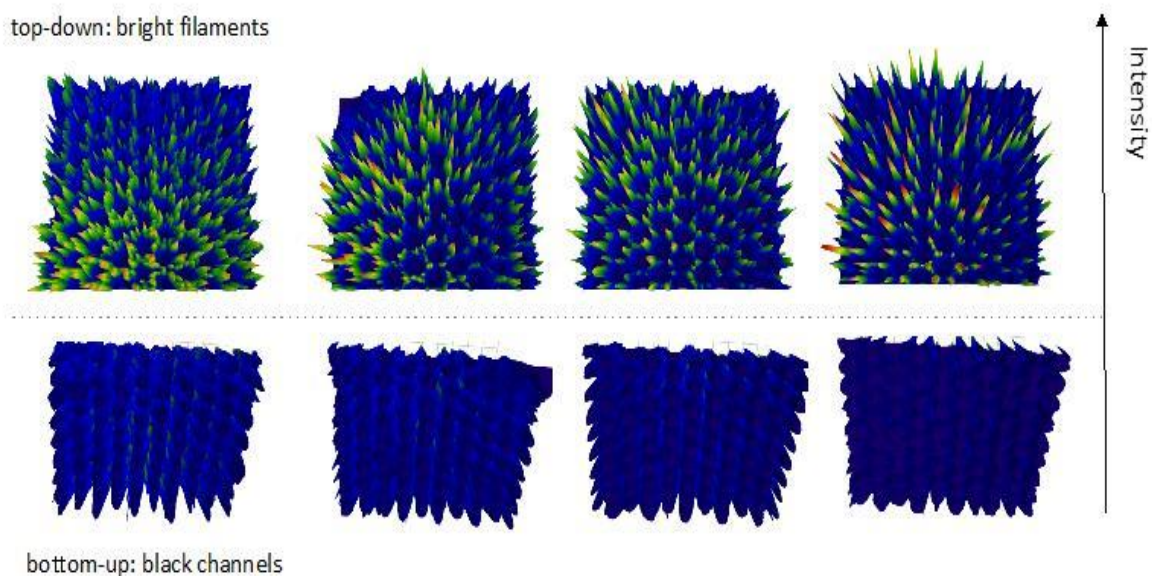
Figure 57. 3-D spatial intensity profiles showing the co-existence of bright filaments and black beams in optochemically self-organized lattices generated with an incandescent beam patterned with a hexagonal array of dips with the same center-to-center separation

of 425 µm and diameters ranging from (a) 170 µm, (b) 270 µm and (c) 290 µm to (d) 315 µm. Spatial intensity profiles were acquired at z = 6.0 mm at 322 s. Corresponding images and parameters are found in Figure 54 andTable 6, respectively. The bottom-up view shows the periodic array of amplitude depressions corresponding to the self-trapped black beams while the top-down view shows the self-trapped filaments.
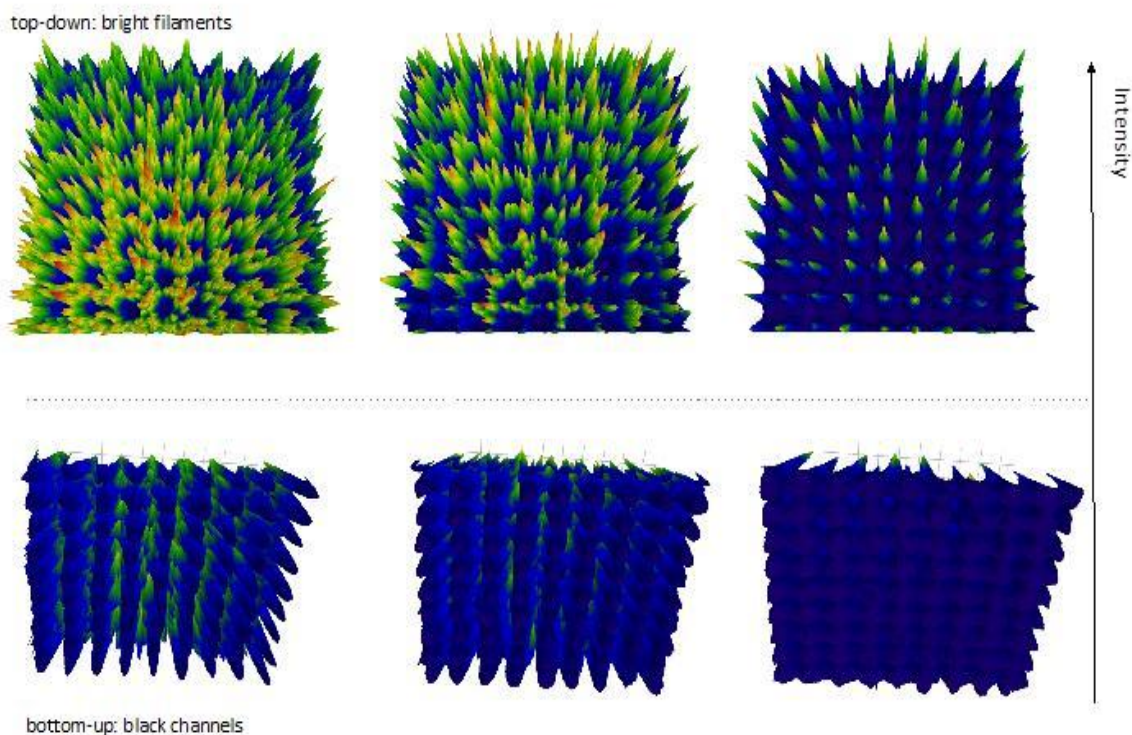
Figure 58. 3-D spatial intensity profiles showing the co-existence of bright filaments and black beams in optochemically self-organized lattices generated with an incandescent beam patterned with a square array of dips with the same centre-to-centre separation of 410 µm and diameters ranging from (b) 175 µm, (c) 260 µm and (d) 330 µm. Spatial intensity profiles were acquired at z = 6.0 mm at 322 s. Corresponding images and parameters are found in Figure 55 and Table 7, respectively. The bottom-up view shows the periodic array of amplitude depressions corresponding to the self-trapped black beams while the top-down view shows the self-trapped filaments.

5.6. **3-D lattices induced by two orthogonal white light arrays**

Lattices shown in the previous section utilize a single mask and a single white light beam to fabricate a 2D structure. By using an identical additional mask and a second beam of white light orthogonal to the first beam (as described in section 2.6) a full 3D dark lattice is possible, consisting of two orthogonal 2D lattices. The pair of orthogonal masks consisted of a square packed array of transparent dots on a black background. Consequently, these masks only allowed arrays of bright self-trapping beams to form in organosiloxane. Each output face of the resulting structure shows a 2D lattice with a square geometry (Figure 59).
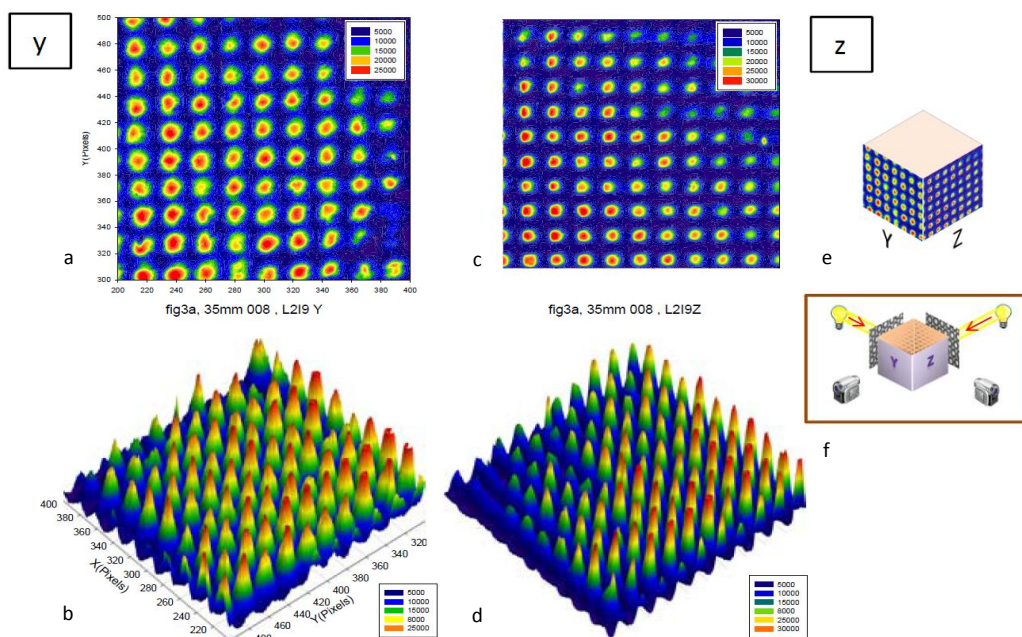
Figure 59. Profiles along Y and Z output faces show evidence of a 3D lattice fabricated using a white light beams and mask along each direction (as shown in the cartoon above). 2D (top) and 3D profiles (bottom) show individual self-trapped beams of 90 µm width and with a spacing of 209 µm at 322s. The mask was designed to generate only bright beams.

5.7. **Calculations of photonic band gaps in self-organised structures**

Simulated index gradient lattices were studied for (i) 2D lattices of HCP and (ii) square dark beam lattices. Bright beams in interstitial regions of the largest and smallest ratios were also considered for each case. Waveguides were assumed to have a uniform index profile and a circular cross section (infinite out-of-plane). Dark beams were assumed to have a maximum possible negative index gradient while bright beams were assumed to have a positive index gradient in comparison to the background index of 1.46. By varying the positive index gradient, (and the ratios of dark beams in some cases) bandgaps open up for some of the lattices (Figure 60) and summarized in Table 8.

With regard to simulations, a uniform index per waveguide and saturated maximum index changes was assumed for simplicity. Simulations assume a constant circular index profile in 2D for each cylindrical waveguide filament. Background index is assumed to be 1.46, with a higher index for bright filaments and lower one for dark filaments. Simulated index gradient lattices were studied using BeamPROP software of the RsoftCAD Suite. Waveguides were assumed to be of circular cross section and of infinite length for the 2D simulations, and cylindrical rods for 3D simulation.

Simulated index gradient lattices were studied for (i) 2D lattices of HCP and (ii) Square dark beam lattices. Bright beams in interstitial regions of the largest and smallest ratios were also considered for each case. Waveguide filaments were assumed to be having a uniform index profile and a circular cross section (infinite out-of-plane) for 2D simulations, and cylindrical rod profiles for 3D simulations. Dark beams were assumed to

have a maximum possible negative index gradient while bright beams were assumed to have a positive index gradient in comparison to the background index of 1.46. By varying the positive index gradient, (and the ratios of dark beams in some cases) bandgaps open up for some of the lattices as shown in Table 8.

Simulations of hexagonal and square geometry lattices
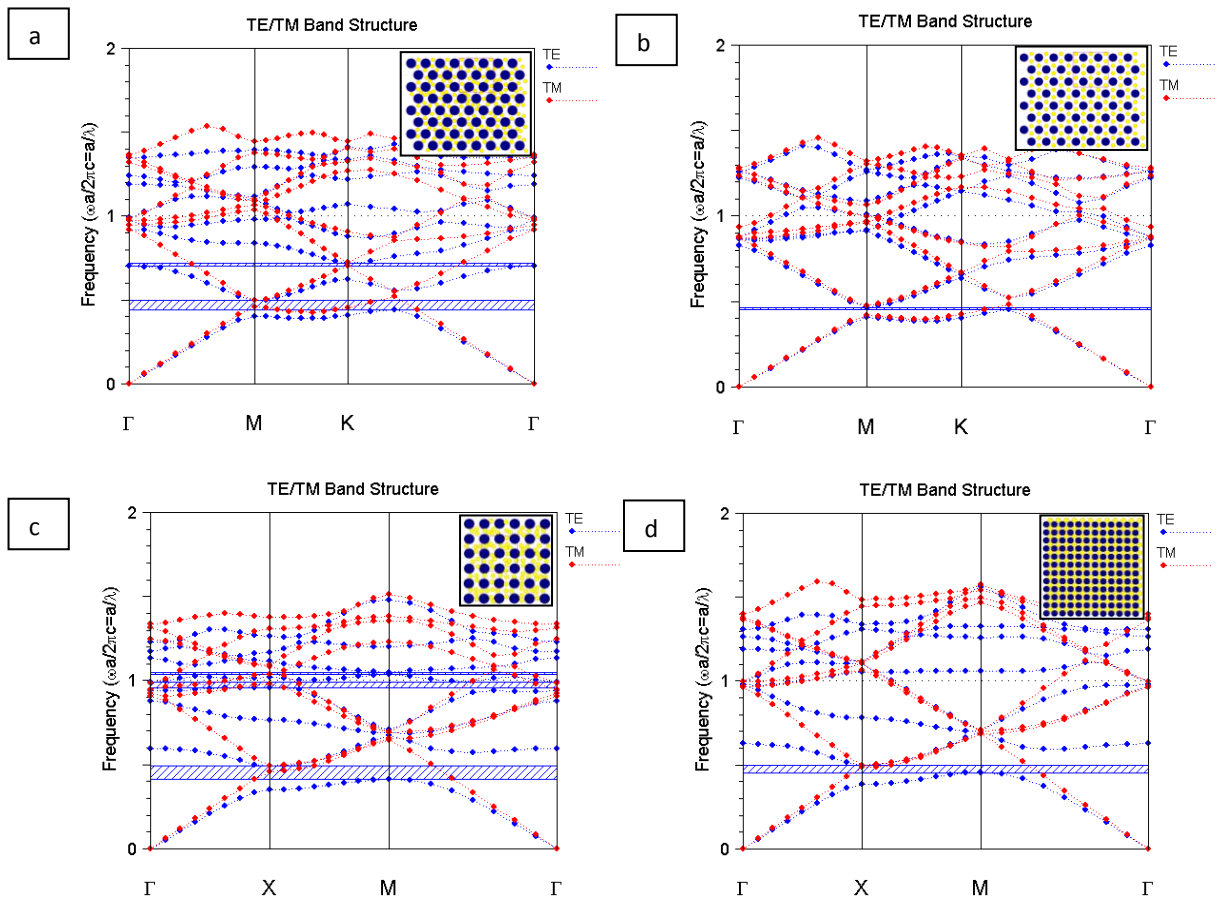
Figure 60. Photonic bandgaps above show up for 2D lattices (inset) corresponding to experimental geometries (Figure 57 and Figure 58) (a) hexagonal lattice with R=0.3, (b) hexagonal lattice with R=0.9, (c) square lattice with R=0.3 and (d) square lattice with R=0.9. Here, R is the ratio of dark spot radius/lattice spacing used in the mask template for experiments. Index contrasts of 2.5-3.0 are necessary, as shown in data shown in

Table 8. Bandgaps range from 250-600 μm, corresponding to frequencies of 1.2 THz – 500 GHz (FIR-EHF, Far infrared-Extremely high freq. radio waves).

Table 8. The table shows bandgaps open up for simulated polymeric optical lattices corresponding to experimental profiles for ratios 0.3 and 0.9 (Figure 57 and Figure 58), at index contrasts of 2.5-3.0. Results correspond to bandgap diagrams of Figure 60. Background index = 1.46, Δn= -0.46 for dark filaments and lattice period = 250 for these simulations. All bandgaps are in 250-600 μm range, corresponding to frequencies of 1.2 THz – 500 GHz (FIR-EHF, Far infrared-Extremely high freq. radio waves).

	Corresp. Exptal ratio	Lattice type	Δn (bright filaments)	bright beam radius	dark beam radius	Number of gaps	Gap frequencies a/λ	Frequency/Gap width	λ (μm)
a	0.3	HCP	2.5	57	145	2	0.71	0.01	352
b	0.9	HCP	3	57	120	1	0.46	0.02	543
c	0.3	Square	2.5	64	144	3	0.45	0.19	555
							0.98	0.04	256
							1.05	0.01	239
d	0.9	Square	3	138	170	1	0.48	0.1	521

Some of the key differences between "white light lithography" vs. traditional lithography are the complexity involved in setting up a traditional 3D lithography setup. Holographic lithography, for instance, involves a complex setup requiring a high degree of precision in order to get accurate interference between 4 laser beams for a 3D structure. In comparison, white light lithography requires only 2 beams for a full 3D structure, with a relatively simple setup, such as an incandescent source and cheap printable masks. Additionally, 1D defects can be incorporated easily with white light lithography by simply modifying the mask pattern.

The only current major limitation is the resolution with such a setup. Currently, lowest resolution is limited by printable mask features, the intensity and quality of the source white light beam and MI in the medium to ~70 μm. Lowering mask sizes reduces the contrast ratio between bright and dark areas significantly due to the use of broadband incoherent white light, resulting in lower fabrication quality. However, separate MI studies[259] indicate that partially incoherent light may significantly scale down features by atleast an order of magnitude. Even so, large feature lattice structures could find many potential applications in GHz and MHz wavelengths.[260,261,262, 263, 264]

Our results also demonstrate that entire arrays self-trap in a stable manner, with no apparent interaction between filaments. In contrast, our previous studies show interactions between neighboring bright self-trapping beams can occur up to a range of 300 μm. This is likely a result of geometric arrangement of neighboring filaments cancelling their mutual interactions on a common neighbor.

In lattices with dark beams, results strongly suggest dark beams appear to stabilize bright beams and limit interactions. Neighboring bright filaments are spaced ~180μm in Figure 57-d, which is within an attractive and repulsive interaction spacing.[239] In order for neighboring bright beams to interact, a suitable refractive index gradient has to be induced within their region of overlap – higher index for attraction and lower one for repulsion. However, previous studies show dark beams evolve significantly faster than corresponding bright beams and create permanent index changes (~300 s vs. 900 s). Once permanent index changes are created, even bright beams within an interaction distance cannot change their spatial position.

Another common question that arises is whether Y and Z direction filaments of 3D lattices are interleaved or intersecting. The 3D lattices fabricated above were made non-specific – they were neither made to specifically intersect or to specifically interleave. Specifically interleaved 3D lattices are discussed in a separate publication.

 Experimentally, organosiloxane photopolymer currently achieves low index gradients of about 0.006. Very high theoretical index gradients may possibly be achieved by doping such lattices with either metal or suitable high index particles. Alternatively, etching methods may be useful to dissolve unpolymerized regions and infiltrate the lattice with high index materials, and dissolving the polymerized regions subsequently for low index regions to give an inverse structure. Suitability of such materials will depend upon their transparency to the bandgaps wavelength.

5.8. **Summary and outlook**

This chapter demonstrated that optochemical self-organization could be elicited in a spatially modulated incandescent field to yield a diverse range of new polymer waveguide architectures comprising black and bright waveguides. The lattices consisted of hexagonal or square arrays of black channels, which suppressed transmission of white light while their interstitial regions were occupied by multimode polychromatic waveguides, which could efficiently trap and guide incandescent light. Due to the irreversibility of polymerization, the waveguides inscribed by the optical field were permanently inscribed in the medium. The coexistence of dark and bright waveguides in the lattices is particularly significant as the large contrast in refractive index between the

two enhances the efficiency of light confinement and guidance within the bright waveguides. By varying the dimensions of the interstices with respect to the filament diameter, the positioning of the bright waveguides could be tuned from random organization to periodic hexagonal or square lattices. By employing anisotropic interstitial regions such as the bright rectangles generated by a square array of dips with alternating diameters, it was possible to generate square lattices of waveguide doublets. Optochemical self-organization is a single-step, inexpensive route to bright and black waveguide lattices, which only requires an incandescent lamp and amplitude mask.
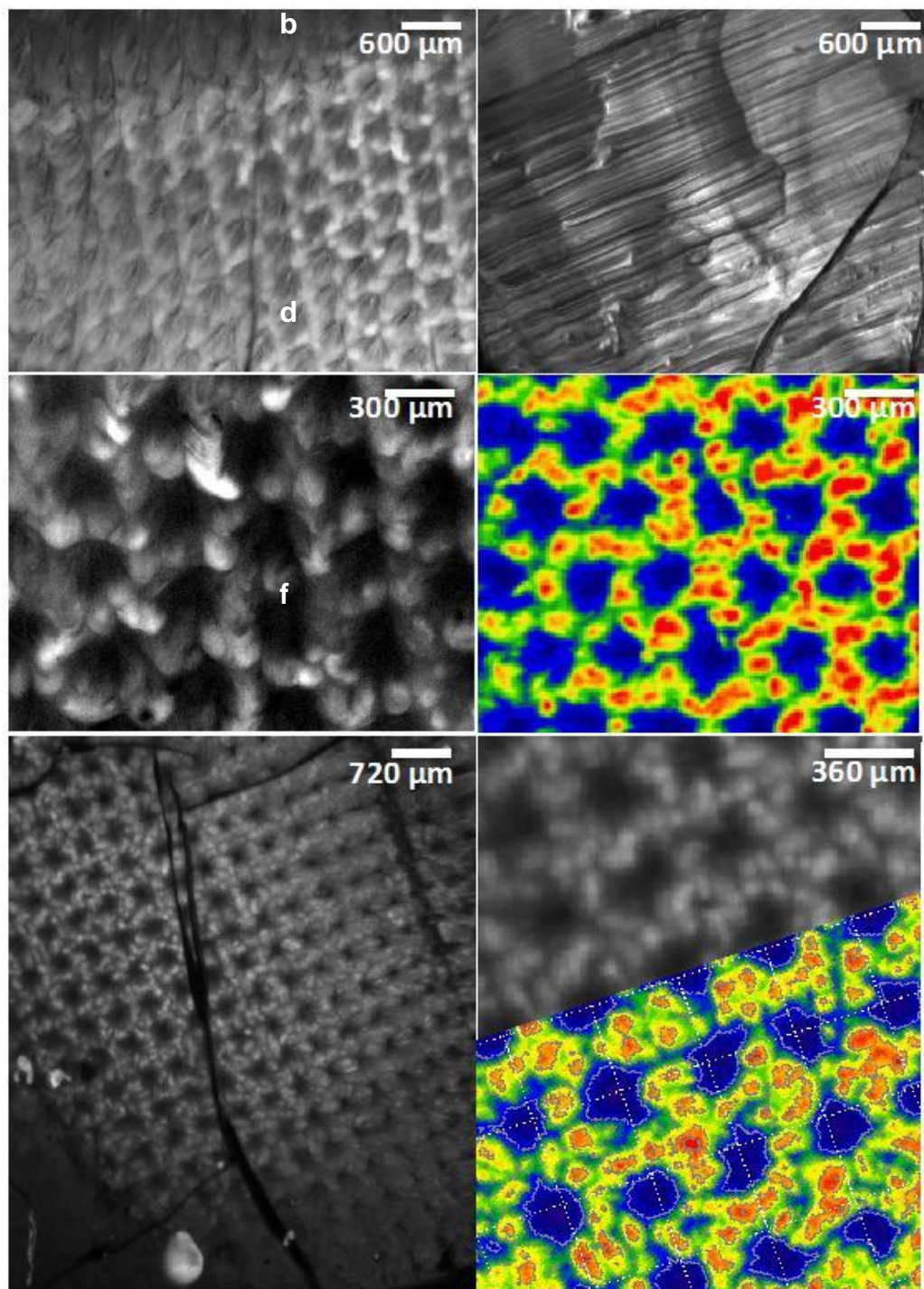
Figure 61. Transmission optical micrographs of optochemically self-organized waveguide lattices of (a) transverse and (b) longitudinal cross-sections of a hexagonal array of dark waveguides with interstitial regions occupied by bright waveguides. A magnified image

(c) shows the close correspondence between the polymer microstructure and the (d) spatial intensity profile of the self-trapped dark beams and bright filaments. (e) Self-organized lattice of a square array of dark waveguides with interstices occupied by randomly positioned bright waveguides. A magnified image (f) corresponds closely to the lattice of self-trapped dark beams and bright filaments.

The examples described in this article showcase its potential to yield a large range of complex structures through variations of the symmetry and dimensions of the pattern of dips imposed on the optical field. In the current examples, the lattice periodicity is determined by the characteristic filament diameter. However, we have previously shown that it is possible to control the characteristic filament width through the spatial coherence of the optical field,[253] which could in turn enable the generation of lattices with smaller periodicities. The waveguide lattices possess residual, unsaturated methacrylate moieties and therefore, upon irradiation undergo further changes in refractive index. Based on this property, we are investigating their application as a new type of nonlinear photonic crystals, which offer opportunities to manage light diffraction in micro-optical systems through the generation of lattice solitons.[185, 186, 182, 175, 172]

6. Optochemical self-organisation of white light in a photopolymerisable gel: a single-step route to intersecting and interleaving 3-D optical and waveguide lattices

6.1. Introduction

This chapter shows a route to fabricate 3-D optical and microstructural waveguide lattices, which combines the elegant spontaneity of self-organisation, to the precision and directionality of photolithography. This method exploits the inherent instability, known as modulation instability,[45] of a broad, uniform beam of white light propagating in a photopolymer and its consequent division into identical filaments of light.[180] By imposing spatially controlled noise on the white light beam (using an amplitude mask), the self-organising MI-induced filaments can be guided into 2-D and 3-D[181] lattices. Because light-induced changes in the photopolymer are irreversible, optical lattices formed in this way permanently inscribe the corresponding microstructure in the medium. Each element of such an *optochemically self-organised* lattice is a cylindrical, multimode waveguide that can trap and guide polychromatic light. This method provides a rapid (seconds to minutes-long), single-step, room temperature route to dense 2-D and 3-D lattices comprising thousands of cylindrical waveguides[180] – such structures are impossible to construct through conventional lithographic processes. This technique does not require lasers but employs incoherent white light emitted by inexpensive incandescent lamps. The

resulting structures have potential applications as dense interconnect arrays for optical fibers as well as nonlinear photonic lattices, which can be considered the next generation of photonic crystals.[171]

The optochemical self-organisation of lattices is based on the understanding of the nonlinear propagation[63,65] and specifically, instability[180] of incoherent white light beams propagating in a photopolymer. This is fundamentally different from holographic lithography, which relies on the interference of 3 or 4 mutually coherent beams to generate 2-D and 3-D optical lattices, respectively[159]. A white light beam in a photopolymer suffers modulation instability (MI) because of self-induced refractive index changes originating from photopolymerisation along the beam-path. These index changes drive the system into a nonlinear regime where noise - normally negligible spatial fluctuations in intensity and index - becomes greatly amplified.[254] Rendered unstable by such perturbations, the beam spontaneously divides into identical white light filaments with a characteristic diameter (which depends on monomer diffusion properties).[180] Akin to the nonlinear propagation of solitary waves such as self-trapped beams or solitons[255], the filaments travel without diverging over long distances (>> Rayleigh length). Because they originate from noise, MI-induced filaments - although densely packed - are randomly positioned in space. It was previously found that by imposing a controlled noise-form such as a weak 1-D periodic modulation (bright and dull stripes), the filaments could be selectively confined to the bright stripes and thus coaxed into a square lattice. When two orthogonal and mutually incoherent (and therefore non-interfering[219]) beams are launched into the photopolymer, they simultaneously underwent MI and created an

intersecting pair of square lattices. This was in effect a 3-D near-cubic optical lattice,[181] which permanently inscribed the corresponding lattice of cylindrical waveguides in the medium.

This chapter shows that optochemical self-organisation can be extended beyond square and near-cubic arrays to complex optical and structural lattices: white light beams embedded with noise in the form of an array of dark rings suffer MI and transform into hexagonal lattices. Two cross-propagating and mutually incoherent white light beams simultaneously undergo MI to generate an orthogonal pair of hexagonal lattices. When made to *intersect*, these lattices generate a body-centred cubic (BCC) lattice and made to *interleave*, produce a woodpile lattice.

Experimental Section, 2.6 (Figure 29) outlines a scheme of the optical assembly employed to generate 3-D lattices[180]: two white light beams (Y, Z) emitted by separate quartz-tungsten-halogen lamp sources (S) were each collimated with a pair of plano-convex lenses (L1, L2) and passed through an amplitude mask (M), which imposed a weak hexagonal pattern of dark rings on the optical field. This pattern can be referred to as a *controlled noise-form*[181] because under linear conditions, it weakens and disappears with propagation distance due to the natural divergence of the white light beams, which effectively appear uniform at a propagation distance of 6.0 mm. The noise-patterned beams were simultaneously launched at 90º to each other onto the entrance faces ($y = 0.0$ mm, $z = 0.0$ mm) of a transparent glass cuvette containing a free-radical organosiloxane photopolymer (P), which was sensitised to visible wavelengths ($\lambda_{max} = 398$ nm, 470 nm) with a titanocene photoinitiator.[63] Because they originate from separate incandescent

sources, the beams were mutually incoherent and therefore superimposed within the photopolymer to produce an overall, homogeneous increase in intensity (*i.e.*, they did not suffer optical interference).[219] Both beams initiated free-radical polymerisation and corresponding changes in refractive index as they propagated through the photopolymer. Consequent changes in the spatial intensity profiles of both beams were simultaneously monitored at a propagation distance of 6.0 mm with two separate CCD cameras.

6.2. Self-organisation of 3-D optical lattice

Typical experimental results are presented in Figure 62. (Both beams Y and Z behaved identically. For clarity, the transitions of only beam Z are shown in Figure 62 while the final stable lattice induced by both beams are included.) Each ring of the noise-pattern imposed on beams Y and Z at the entrance face of the photopolymer had outer (*o.d.*) and inner diameters (*i.d.*) of 270 μm and 172 μm, respectively and was separated (centre to centre) from its nearest neighbours by 340 μm (Figure 62a). The noise-pattern had weak contrast with relative intensities of 55 % and 45 % in its dark and bright regions, respectively. Under linear conditions (when polymerisation was negligible), the characteristically large divergence of white light caused the noise-pattern to broaden and weaken so that each beam was effectively uniform at $z = 6.0$ mm (Figure 62b). However, as the beams initiated polymerisation and corresponding index changes along their respective propagation paths, their spatial profiles underwent the same, striking sequence of changes traced in Figure 62.
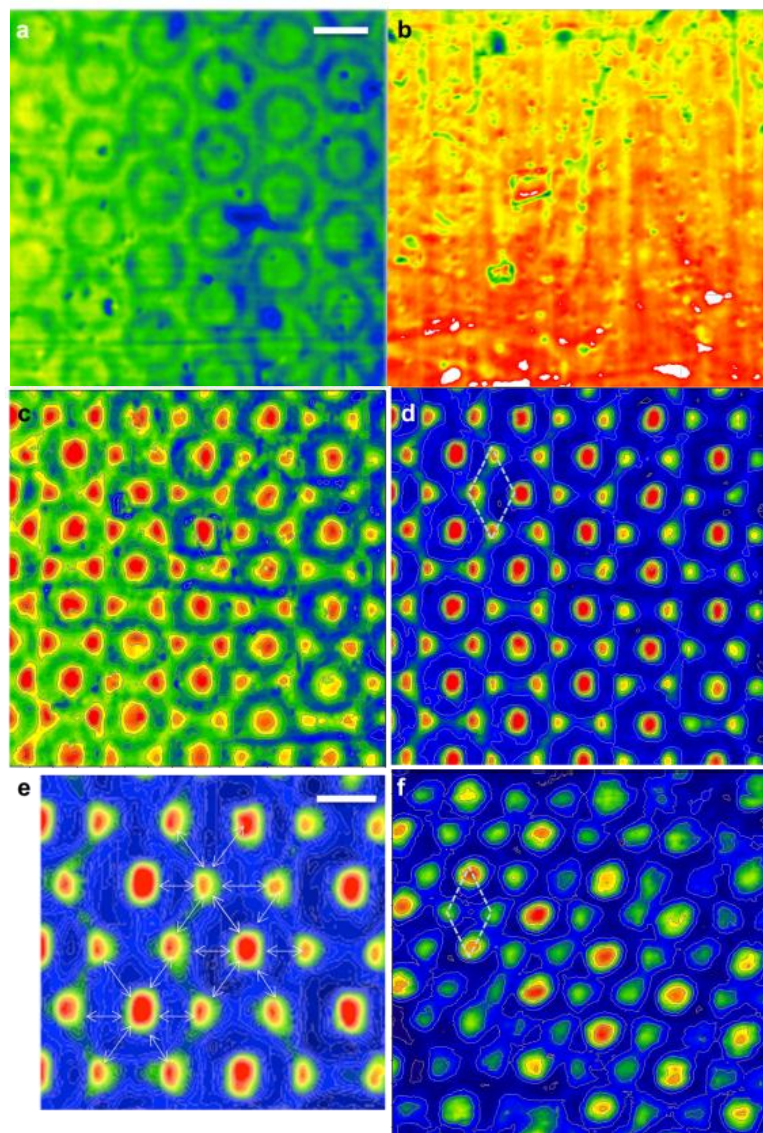
Figure 62. Self-organisation of 3-D optical lattice. 2-D spatial intensity profiles show that (a) the weak hexagonal array of dark rings imposed on the beam (Z) at the input face of the cuvette becomes negligible at (b) a propagation distance of 6.00 mm but (c) emerges in sharp contrast after 42 s of polymerization. The pattern subsequently undergoes MI and forms a (d) stable hexagonal array of bright dots. The rhombus in dotted white corresponds to the unit cell of the hexagonal lattice. Beam Y simultaneously undergoes identical transitions to form a (f) hexagonal lattice of self-trapped filaments (at 84 s). The scale bar in (a) applies to images in (a-d) and (f).

As the beams initiated polymerisation and corresponding index changes along their respective propagation paths, their spatial profiles underwent the striking sequence of changes traced in Figure 62 b-d. Within 42 s, the weak honeycomb pattern of dark rings self-trapped and emerged in sharp focus at a propagation distance of 6.0 mm (Figure 62c). The outer diameter of the dark rings was ≅300 µm, which was comparable to its value of ≅275 µm at the entrance face (Figure 62a). The significant decrease in the internal diameter of the ring from ≅200 µm to ≅ 100 µm was caused by self-trapping of the bright region within the ring into an intense, narrow beam. These changes collectively indicated that refractive index changes due to polymerisation along the beam path now suppressed the natural divergence of the noise-pattern, enabling it to propagate as a *self-trapped* pattern (*vide infra*). Consistent with self-trapping, the pattern at $z = 6.0$ mm relative was stronger in contrast than the input noise-pattern at $z = 0.0$ mm: the decrease in intensity of the dark rings (from 45 % at $z = 0.0$ mm to 23 % at $z = 6.0$ mm) was accompanied by an approximately 1.6-fold increase in the intensity of the bright interstices between the dark rings (from 55 % to 86 %). The intensity of the self-trapped beam centred *within* each dark ring increased from 63 % to 90 %.

With time, the self-trapped pattern of dark rings suffered MI and divided into filaments (Figure 62d-f): at 42 s, the bright interstices between the dark rings developed high-intensity nodes, which self-organised with azimuthal symmetry about each dark ring (Figure 62 c). The nodes amplified by depleting intensity from their immediate

surroundings and by 66 s, transformed into a sextet of discrete, filaments of average width $\cong$ 65 µm (Figure 62d). The filaments were symmetrically positioned about the bright region contained *within* each dark ring. The central bright region did not suffer MI but remained a stable self-trapped beam of width $\cong$ 90 µm. As the local environment of the dark rings self-organised in this way, beams Y and Z were each transformed into a lattice of filaments with long-range hexagonal symmetry and an average filament-to-filament separation of $\cong$ 200 µm.

Beams Y and Z transformed simultaneously into hexagonal lattices, the intensity output of which was observed even after they had propagated in orthogonal directions over 6.00 mm in the photopolymer (Figure 62d, f). This proved that the lattice pair intersected each other at 90° over a volume of 10 mm x 10 mm x 6 mm without suffering distortion to their hexagonal symmetry. Consequently, they formed a 3-D lattice composed entirely of self-trapped white light filaments, which was stable for as long as it was monitored (3600 s). The optical lattice permanently inscribed the corresponding microstructural lattice of waveguides in the photopolymer. The hexagonal arrangement of waveguides is evident in optical micrographs of the transverse cross-section of the lattice (Figure 63a). The multiple intersections between cross-propagating waveguides induced by beams Y and Z are evident from a top-down view (Figure 63b). Considering, based on previously established convention,[180] the intersection between an orthogonal pair of filaments as a lattice point, the intersecting pair of 2-D hexagonal lattices gives rise to a 3-D lattice with BCC symmetry (as depicted in Figure 63c-e).

The lattice-formation described above originates from the self-trapping and subsequent modulation instability (MI) of the noise-pattern imposed on the white light beams. These related phenomena are expressed by variations of the nonlinear paraxial wave equation[45]:

$$ik_0 n_0 \frac{\partial \varepsilon}{\partial z} + \frac{1}{2}\nabla_t^2 \varepsilon + k_0^2 n_0 \Delta n \varepsilon + \frac{i}{2} k_0 n_0 \alpha \varepsilon = 0$$

[4-1]

,which describes the competition between the natural divergence of the beam in the transverse (x, y) directions (transverse Laplacian operator) and refraction due to photoinduced index change (Δn). The attenuation coefficient is α at wavelength λ (free space wavenumber, $k_0 = \omega/c$).[241] Spatial and temporal variations of the photoinduced index changes in the photopolymer is described through equation[1-11].

$$\Delta n'(x, y, z, t) = \Delta n_o' \left\{ 1 - \exp\left[-\frac{1}{U_o} \int_0^{t-\tau} |E(t')|^2 \, dt' \right] \right\}$$

1-11]

where $\Delta n_o'$ is the index difference between the monomer and polymer, $|E(t')|^2$ is the optical field intensity , τ is the monomer radical lifetime and U_0 is the critical exposure needed to initiate polymerization. As previously shown,[43,66] coupling of equations [4-1] and [1-11] leads to self-trapping and the consequent divergence-free propagation of a narrow Gaussian beam. Results in Figure 62b show that the *same* mechanism of self-induced refractive index changes gives rise to self-trapping of the weak noise-pattern embedded in each beam (Figure 62b). The significant increase in contrast of the pattern (Figure 62c) is characteristic of self-trapping and originates from the weak gradients in intensity across the original noise-pattern (Figure 62b). At early times, Equation [1-11] shows that photoinduced refractive index changes would be

greater in the brighter areas of the noise-pattern. Because light preferentially propagates in regions of even marginally greater index, light initially contained within the darker regions of the pattern (*i.e.*, the rings) gravitates towards the brighter areas, which increase in index further. In this way, light intensity is continually redistributed from the dark to bright regions until maximum contrast is achieved.
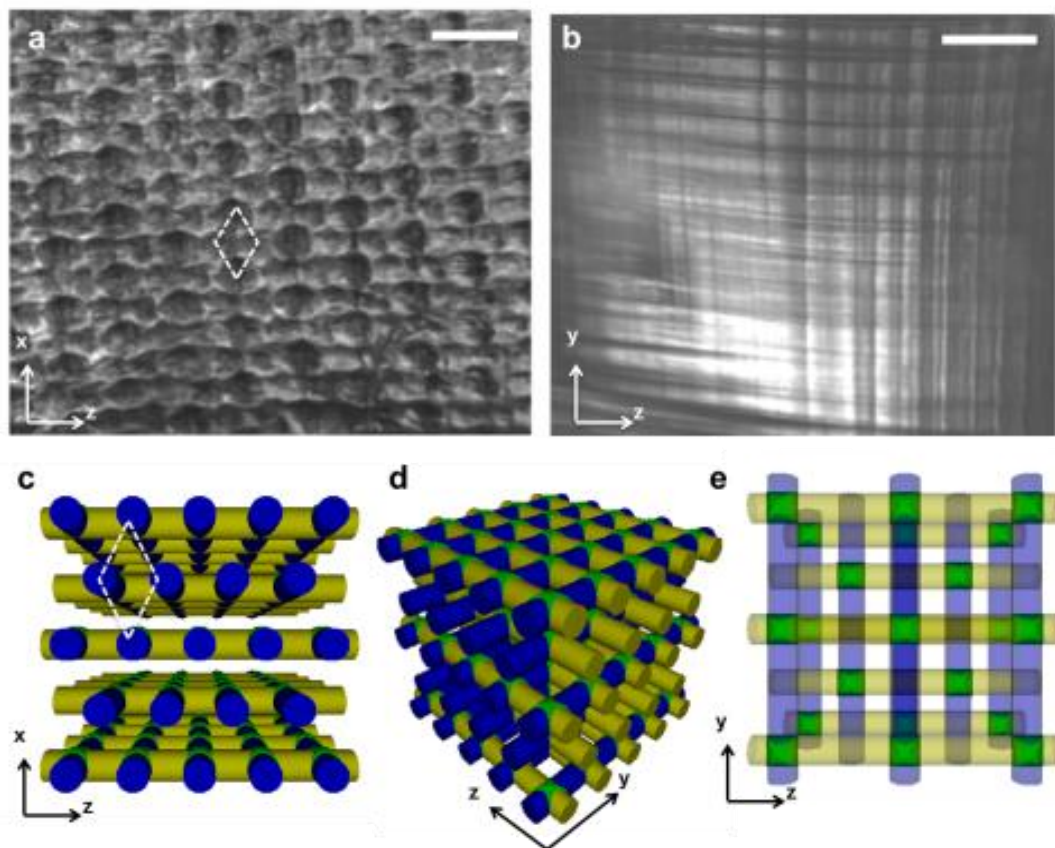
Figure 63. Reflection optical micrographs of the microstructure induced by the optical lattice in Figure 62 (a) The micrograph acquired at the exit face of beam Z shows a hexagonal array of waveguides and a (b) top-down view shows the intersections between the orthogonal hexagonal lattices. As a guide, cartoons of the 3-D lattice are presented in (c) to (e). The top-down view shows that the points of intersection between the orthogonal lattices assume b.c.c. symmetry.

The final transformation of each beam into a hexagonal lattice results from MI-induced filamentation of the self-trapped pattern. The mechanism of white light MI in photopolymers has been studied previously for making lattices[180] Briefly, the process is seeded by normally negligible, random variations of intensity or refractive index, which amplify through the same reciprocal interactions between the optical field and photopolymer described in Equation [1-11] and trigger filamentation.[256] MI occurs in broad beams with areas significantly greater than the characteristic size of the filaments. In an entirely featureless, uniform beam, the resulting monodisperse filaments are randomly positioned in space. In the current example, MI is restricted to the bright interstitial regions of the self-trapped dark ring pattern in beams Y and Z. These interstices were uniform in intensity and as they were interconnected, could support multiple filaments. However, the *thickness* of the interstices ($\cong 75$ μm) was deliberately set to be approximate the characteristic filament width (Figure 62a).[180] This ensured that only a *single* circle of filaments occupied the interstices of each dark ring (Figure 62d, f)). (A thickness $>> 70$ μm would result in multiple, randomly positioned filaments).[180] While MI occurred in the interstitial interconnected regions, the discrete bright regions *encircled* by each dark ring supported only a *single* self-trapped beam (Figure 62d, f).

Confined to the interstices of the dark rings, the white light filaments collectively self-organised into the most stable configuration: a lattice with hexagonal symmetry. Consistently forming in groups of six, the filaments spontaneously arranged themselves with azimuthal symmetry about the central self-trapped beam (Figure 62d). In the resulting long-range hexagonal symmetry of the lattice, the average filament-filament

distance was $\cong$ 200 µm. This separation distance falls within the range where an *individual* pair of self-trapped white light beams would fuse due to mutually attractive forces.[239] Each filament in the lattice however, is surrounded by a sextet of equivalent and azimuthally symmetric neighbours; the net cancellation of attractive interactions stabilises each filament and in this way, the entire lattice.

The hexagonal lattices induced by orthogonal beams Y and Z intersect each other to generate a 3-D optical lattice. The lattice is stable because the intersections of the orthogonal 2-D lattices neither disrupt the trajectory nor attentuate the intensity of their constituent filaments. These effectively inert collisions between orthogonal filaments is characteristic of the related species, solitons. When colliding at angles exceeding the total internal reflection angle of their self-induced waveguides, solitons traverse through each other unimpeded and without loss of intensity.[90] While collisions have previously been predominantly studied only with a single pair of solitons or self-trapped beams, each individual filament in the hexagonal lattices formed through MI is estimated to undergo approximately 30 periodically spaced intersections with orthogonal counterparts. Remarkably, the filament retains its spatial profile, intensity and trajectory throughout these multiple intersections.

6.3. **Interleaving hexagonal lattices**

Next, optochemical self-organisation was employed to generate 3-D lattices composed of an *interleaving* pair of 2-D lattices. In this case, beams Y and Z were weakly patterned with a hexagonal array of dark *holes* rather than dark rings. Each hole was $\cong 220$ μm wide and periodicially separated from its neighbours by $\cong 130$ μm. To achieve interleaving of the 2-D lattices, the patterns imposed on the two beams were offset by half a period (as described in section 2.6). Figure 64a is the spatial intensity profile of beam Z after lattice formation. The same mechanism of MI led to a sextet of filaments, each $\cong 65$ μm wide, positioned with azimuthal symmetry about each dark hole. The stability of the lattice can again be attributed to the net cancellation of attractive forces exerted on each filament by its 4 nearest equivalent neighbours as depicted in the magnified image in Figure 64b. The interleaving of the identical but out-of-phase pair of honeycomb lattices is evident in Figure 63a-b, which display the 2-D hexagonal lattice of filaments induced by beam Z but *also* contain the streaks of light scattered by the orthogonally propagating filaments induced by beam Y. These were visible through the dark holes of the lattice induced by beam Z.

The method of interleaving lattices was extended to generate a woodpile lattice of waveguides (Figure 64c-f). One of the most extensively investigated geometries for photonic band gaps[161,257], the woodpile is a stack of layers each consisting of parallel rods that are periodically separated by some length *a*. The long axes of rods contained in adjacent layers are perpendicular to each other while rods in alternate layers are parallel but offset from each other by a/2 (Figure 64e-f). Recognising this configuration to be a

pair of interleaved 2-D hexagonal lattices, this is a resultant woodpile structure, generated through optochemical self-organisation of beams Y and Z. Hexagonal lattices were generated by imposing a noise-pattern of dark rings on each beam. To achieve interleaving of the two hexagonal lattices, the noise patterns imposed on the beams were deliberately offset with respect to each other by half a period.

Beams Y and Z each generated hexagonal lattices of self-trapped filaments. This was confirmed through spatial intensity profiles at their respective exit faces (Figure 64 c-d). In contrast to the results described in Figure 62, the dimensions of the noise pattern selected for this lattice resulted in very intense central self-trapped 110 μm-beams with a sextet of relatively weak filaments. Although the weaker filaments could be observed in the spatial intensity profiles (Figure 4b, c), the corresponding microstructural lattice consisted predominantly of waveguides induced by the intense central beams (Figure 65).

The waveguides induced by the central self-trapped beams were themselves positioned with hexagonal symmetry. Because they were offset with respect to each other by half a period, the orthogonal pair of hexagonal lattices interleaved to generate a 3-D woodpile structure. Figure 65a is a photograph of a photopolymer monolith that was extracted from its sample cell after lattice formation; the entire 9 mm x 9 mm x 20 mm volume of this sample was imprinted with the woodpile structure. The magnified photograph in Figure 65b emphasizes that the lattice is composed entirely of individual waveguide elements: the intense, bright circular spots correspond to light from an incandescent lamp that was captured by and transmitted through a population of lattice

waveguides, each approximately 10 mm long. Significantly, orthogonal waveguides, which were *not* oriented in the direction of the incandescent lamp remained unlit. This is characteristic of optical waveguides, which have a very narrow range of coupling angles.[258]
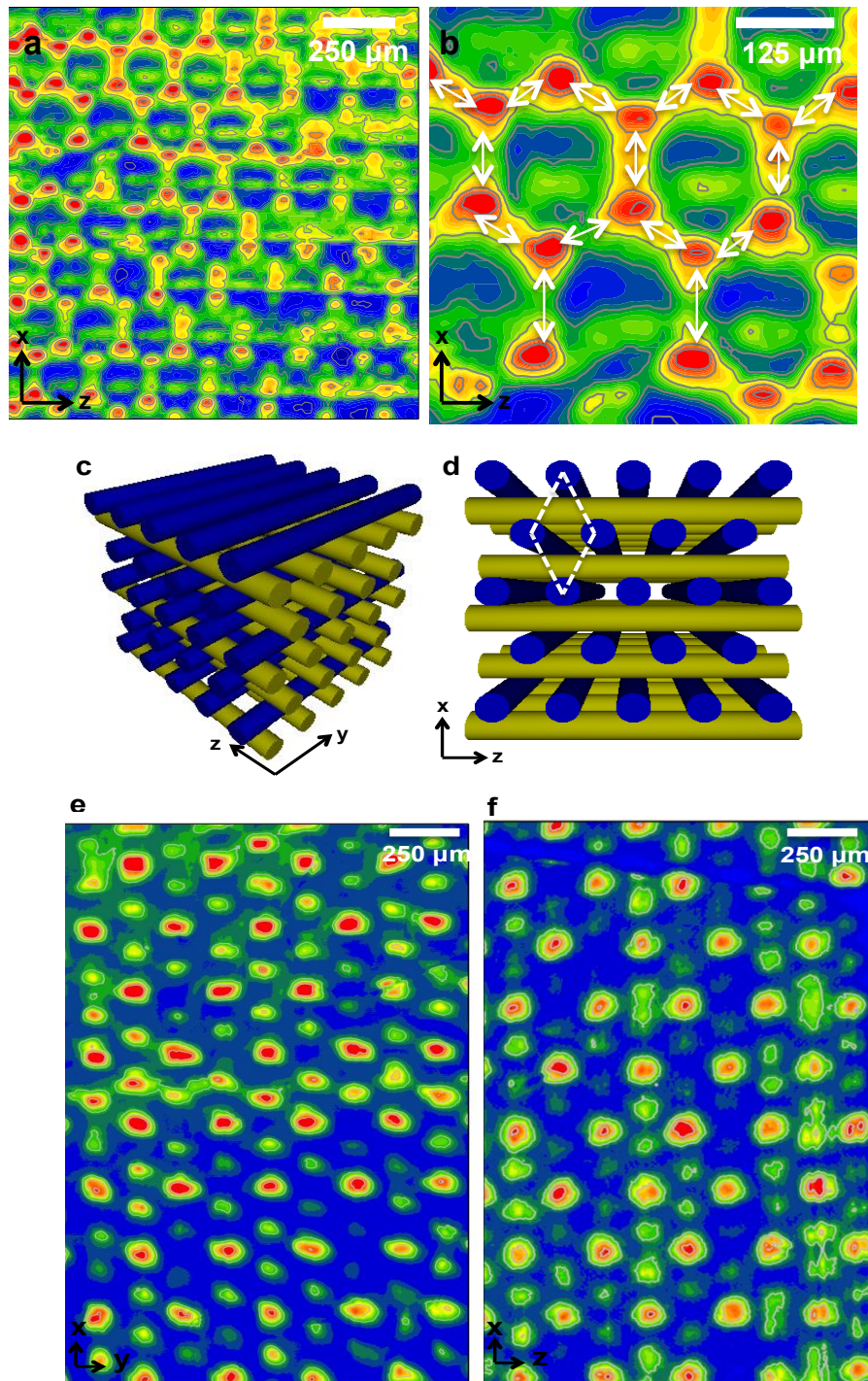
Figure 64. Self-organisation of interleaving lattices. (a) Spatial intensity profile at a propagation distance of 6.00 mm of a honeycomb lattice induced by beam Y bearing a weak hexagonal pattern of dark holes. Filaments simultaneously induced by beam Z are

visible propagating in the orthogonal direction (scale bar = 250 μm). (b) Arrows in the magnified image of the lattice indicate interactions between the self-trapped filaments (scale bar = 125 μm). Cartoons of a (c) woodpile lattice showing the (d) interleaving of an orthogonal pair of hexagonal lattices. Spatial intensity profile at a propagation distance of 6.00 mm of the hexagonal lattice induced by beams (e) Y and (f) Z.

The photograph in Figure 65c is a top-down view of the lattice, which shows the cross-propagating waveguide arrays induced by beams Y and Z. The interleaving of these two arrays is evident in magnified optical micrographs of the woodpile lattice (Figure 65d), which capture the tranverse cross-section of the lattice induced by beam Z and longitudinal cross-section of the lattice induced by beam Y. The former is evident as the hexagonal arrangment of circular waveguides; consistent with the woodpile geometry (Figure 64e-f), each layer of the hexagonal array is interleaved with the orthogonal array of waveguides induced by beam Y. To confirm that the longitudinal features were in fact waveguides induced by beam Y, we launched a uniform broad beam of white light into the structure along the *y* axis. The micrographs in Figure 65 e-f confirms that the light is selectively guided through the longitudinal interleaving waveguides; the output is seen as brightly lit regions only at the exit of the waveguides.
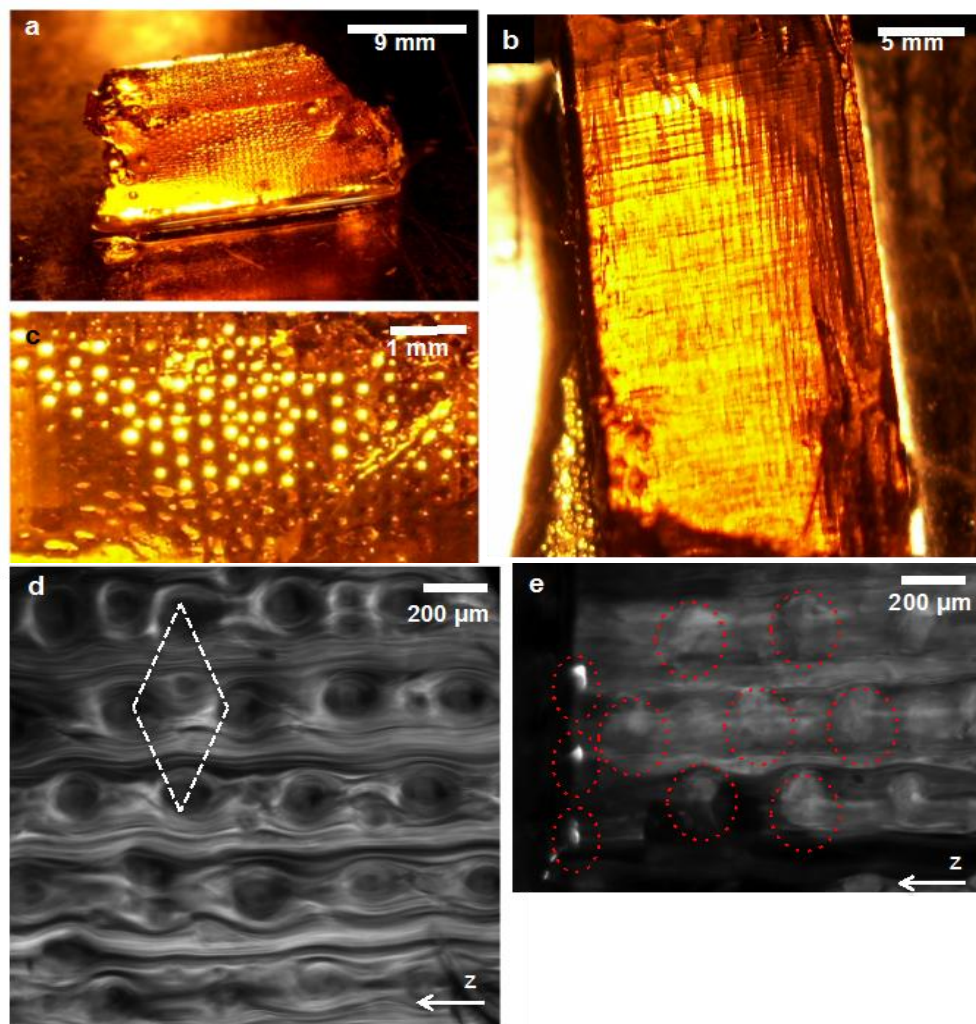
Figure 65 Photographs of 3-D microstructure induced by beams Y and Z show that (a) patterning occurs over a large scale. (b) A top-down view shows the cross-propagating waveguides. The magnified view (c) shows that each element of the woodpile lattice is a waveguide that traps and guides light. (d) The optical micrograph acquired at the exit face of beam Y shows the hexagonal array of waveguides interleaved with waveguides induced by the orthogonal beam Z. (e) Light shone into the lattice from the Z direction was captured and selectively guided through the waveguides oriented along this direction. Light at the exit of the Z waveguides and the waveguides induced by beam Y are circled in red as a guide to the eye.

6.4. **Control Lattices without self-organization**

Figure 66 demonstrates a 3D control lattice formed by perpendicularly oriented HCP lattices of bright self-trapping waveguides only. This provides an alternative route to fabricating structurally similar lattices avoiding self-organization of the waveguides. Control structures in Figure 66 (lattice spacing = 750 µm) and Figure 68 (lattice spacing = 190 µm) demonstrate that finer structures such as in Figure 64 can only be made with self-organized waveguides.

An identical optical assembly was used for lattices of Figure 66 and Figure 62 but with a different mask pattern, consisting of a black background with a lattice of transparent HCP dots. This results in the generation of a HCP lattice of bright self-trapping filaments only along the path of input beams while avoiding dark self-trapping beams and secondary rearrangements altogether. The lattice filaments may be forced to form either an interleaved or an intersecting lattice depending on the initial arrangement of the masks.

Figure 67 (b), (c) and (d) show reflection micrographs of structures formed as a result of self-trapping in Figure 66. Such structures can potentially be utilized to generate 3-D woodpile lattices as well, by forcing an interleaved structure analogous to Figure 64. Denser lattices with a smaller spacing can also be generated by altering the lattice spacing of the HCP grid on each mask to a lower value as shown in Figure 68. However resulting structures were of limited quality due to resolution limitations of the printers used to fabricate masks. Resulting masks had numerous interstitial defects as well as a lower contrast between black and bright regions, leading to formation of an increasing number

of smaller irregular bright filaments in interstitial regions of the lattice. Another potential method for scaling down lattice spacing is to utilize coherent light in order to generate finer resolutions.[259] Such lattices could potentially be employed for GHz and MHz wavelength applications.[260, 261,262, 263, 264]
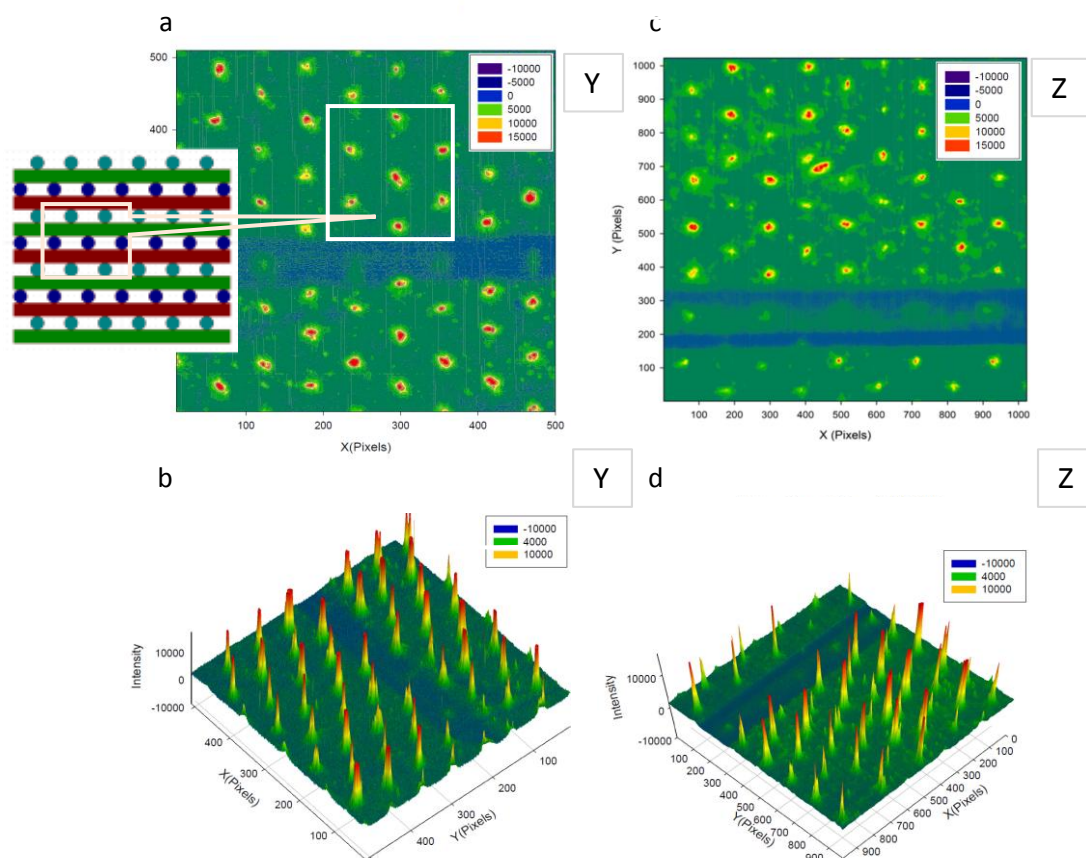
Figure 66. (Above) 2D profiles and (below) 3D profiles show Y (left) and Z (right) output faces of a fabricated 3D lattice without the use of dark beams. Profiles were recorded at 60 s of illuminating an organosiloxane sample in the optical assembly of Figure 29. Beams are of 70 μm widths and have a spacing of 750 μm between nearest beams. Transparent dots spaced apart in a HCP arrangement in an otherwise blackened mask were used to generate each beam at the correct lattice location. Inset (left) compares the experimental lattice to a 3D woodpile scheme.
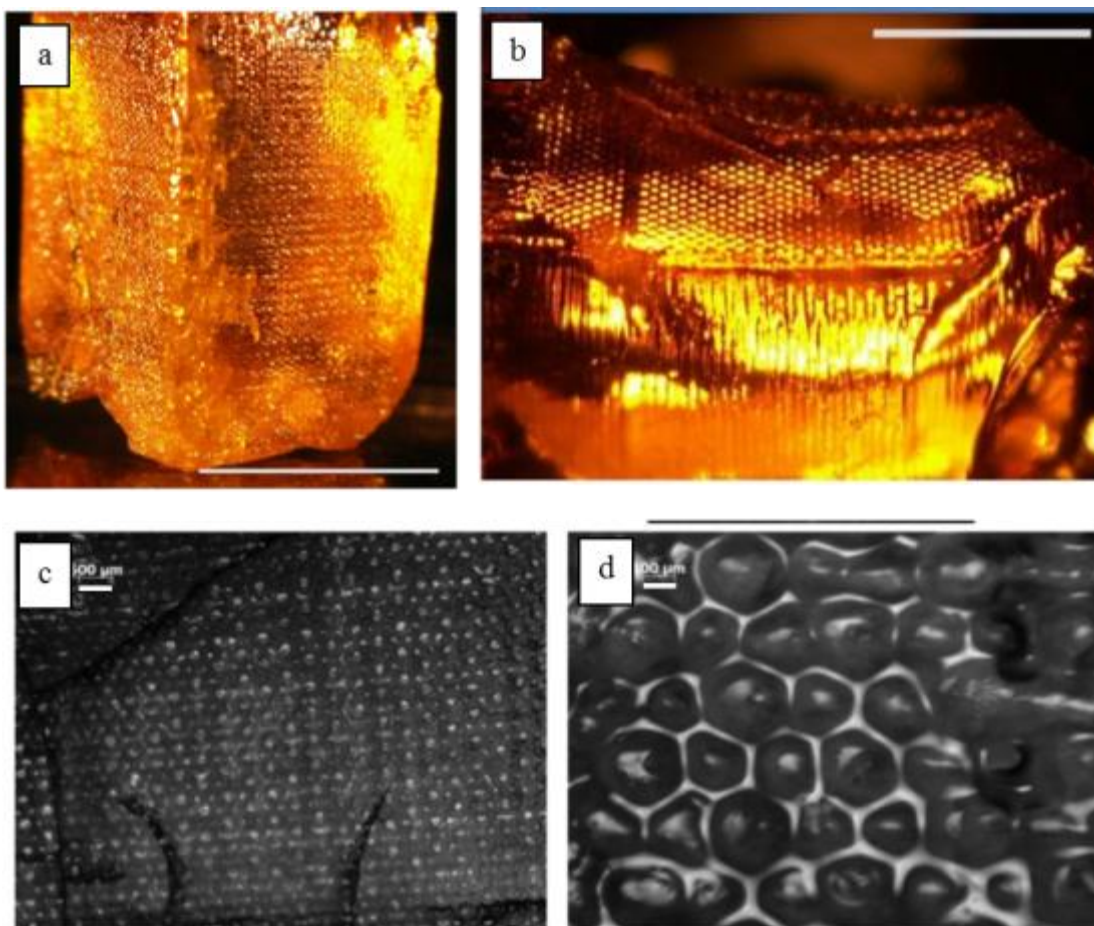
Figure 67. 3D control lattices resulting from self-trapping arrays of dark-self-trapping beams of Figure 62 (a). In comparision, 3D lattices made with bright self-trapping filaments only is shown in (b), (c) and (d). scale bar 9 mm (b). A micrograph of the HCP face of a lattice corresponding to the Y input is shown in (c), and is magnified (d). Scale bars are 500 μm (c) and 100 μm (d).
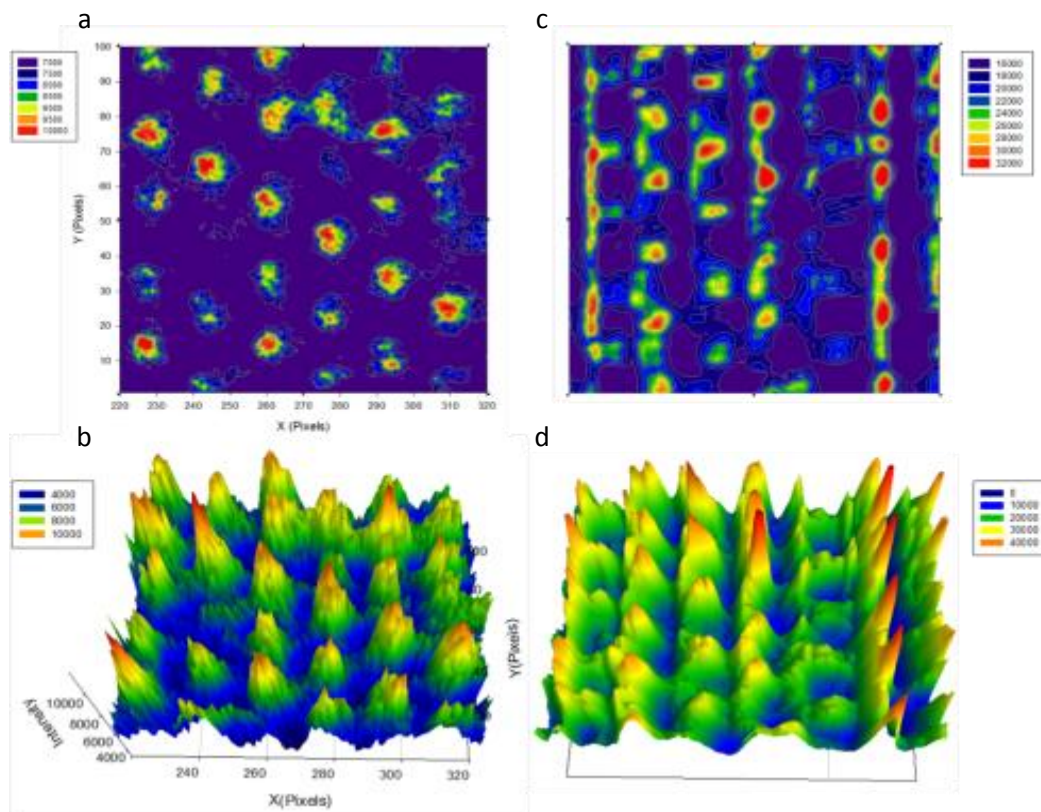
Figure 68. 2D (above) and 3D profiles (below) show Y (left) and Z (right) output faces of a 3D control lattice fabricated ((60s) using a method identical to Figure 66 but with a finer lattice spacing. Beams are of 70 μm widths and have a spacing of 190 μm between nearest beams. Reducing the lattice spacing from 750 μm to 190 μm leads to formation of defect regions, in part due to resolution limitations of the mask printing process.

6.5. **Simulation studies**

Simulated lattices with index gradients similar to Figure 63-Figure 66 were studied using BeamPROP software of the RsoftCAD Suite. Simulated index gradient lattices are presented for 2D HCP lattices of bright and dark filaments (similar to Figure 62) and separately, for 3D woodpile-like lattices of bright filaments (that may be obtained

from Figure 66) in Figure 69. For simplicity, waveguides were assumed to be circular in cross section and of infinite length out-of-plane (for 2D lattice simulations), and cylindrical rods (for 3D lattice simulations).Dark beams were assumed to have a theoretical maximum negative index gradient of -0.46 while bright beams were assumed to have a positive index gradient in comparison to the background index of 1.46. Simulations reveal that varying the positive index gradient of lattice filaments (and the ratios of dark beams in some cases) opens bandgaps for 2D HCP bright lattices as well as 3D woodpile lattices (Figure 69). While 2D bandgaps of a moderate 4% gap width /wavelength ratio were possible for index contrasts as low as 0.9, larger gaps of upto 6 % are possible for bright woodpile-like 3D lattices, but only with high refractive index contrast ratios of 2.0 between polymerized and unpolymerized regions.

Table 9. The table shows bandgaps open up for simulated polymeric optical lattices corresponding to experimental profiles for 2D dark & bright lattices, as well as 3D bright filament lattices. Δn = -0.46 for dark filaments and background index = 1.46.Results correspond to bandgap diagrams of Figure 69. 2D bandgaps are at 332 µm while 3D gaps are at 26 µm. These corresponding to frequencies of 903 GHz & 11.3THz respectively (Extremely high freq. radio waves & Far infrared).

Image name	Corresponding experimental ratio	Lattice type	bright filaments		Period	dark filament radius	Total gaps	Gap frequencies (a/λ)	Frequency /Gap width	λ (µm)
			Δn	radius						
2D HCP Bright lattice	0.9	HCP	0.9	34	250	86	2	0.75	0.03	332.23
								0.62	0.05	406.5
3D Woodpile lattice	0.35	wood pile	2	-	192	68	1	0.32	0.02	26.58
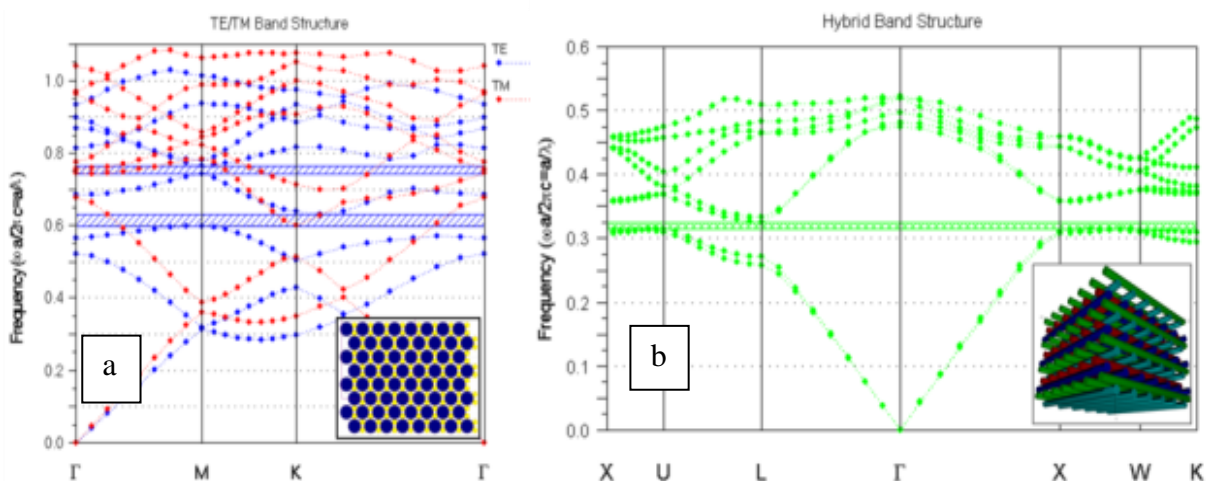
Figure 69. 2D photonic bandgap of a simulated lattice (left inset) of HCP dark beams (blue circles) with interstitial bright beams (yellow dots) is shown in (a). Dark filaments (84 µm width) and bright filaments (34 µm) are used in (a) whereas bright filaments (68 µm) are used in (b). 3D photonic bandgap of a simulated woodpile lattice (right inset) of interstitial bright beams is shown in (b) (filaments in interleaved layers are of red, green, blue and cyan colors). Filaments and band gap parameters are listed in Table 9

A limitation of current simulations of lattice structures is the assumption of a high index for bright filaments and lowest possible index for dark filaments. Experimentally organosiloxane photopolymer achieves index gradients of about 0.006 with current methods, however, higher index gradients up to 0.9 can be theoretically achieved using metallic dopants or other high dielectric particles in combination with etching.[151,152] Suitability of such materials will additionally require that such materials possess a high degree of transparency in the wavelength region of the bandgap they are intended for.

6.6. **Summary and outlook**

In summary, controlled noise-patterns in the form of a weak honeycomb array of dark rings imposed on a white light beam amplify significantly under the nonlinear conditions created by photopolymerisation and undergo a combination of self-trapping and MI to form a hexagonal lattice of filaments. Two orthogonal beams simultaneously transform into a pair of 2-D hexagonal lattices, which when intersecting give rise to a 3-D lattice with BCC symmetry and when interleaving, a 3-D lattice with woodpile symmetry. Corresponding structural lattices composed entirely of intersecting cylindrical waveguides were permanently inscribed in the photopolymer. Such structures are impossible to generate with conventional lithographic or self-assembly routes. Furthermore, relative to other lithographically fabricated or self-assembled structures, which typically span tens of microns, optochemical lattices occupy volumes of several millimeters (limited only by the sample cells employed in our experiments). Because the process is light-driven, the spatial and temporal variation in optical intensity offers a powerful means to visualise in 3-D, quantify and understand the mechanism of lattice formation. Optochemical self-organisation is an extremely facile, inexpensive single-step route to 3-D optical lattices and functional waveguide lattices, requiring only a pair of incandescent light bulbs. The lattices have valuable applications as efficient light-collecting and channelling systems including coatings for solar cells and separately, as nonlinear photonic lattices.[172]

7. Coaxial self-trapping of white and gray incoherent optical fields: a bright core with a dark cladding

7.1. Introduction

We report that a new self-trapped incoherent species – a hybrid beam – forms in a photocrosslinkable organosiloxane.[65] The finding is counterintuitive as self-trapped bright and dark optical fields have until now only been generated separately, under self-focusing[12] and self-defocusing[58] conditions, respectively. The hybrid beam is created with incandescent light, which is incoherent in space and time. Self-trapping of such a weakly correlated wavepacket, which was first discovered in 1997[12], raises intriguing questions about the spatial correlation[33], shape[34], frequency distribution[31] and susceptibility to modulation instability (MI).[34] White light self-traps in certain photorefractive crystals, which at low intensities, exhibit a noninstantaneous and saturable photoresponse.[12] These critical properties permit copropagation of the multiple modes of white light and time-average out its femtosecond phase fluctuations, respectively. We previously showed that a saturable and noninstantaneous photoresponse is inherent to (and accessible over a wide intensity range in) a photocrosslinkable organosiloxane. Studies in this photopolymer provide insight into the dynamics,[63] interactions,[239] MI[180] and spontaneously formed lattices of self-trapped white beams.[181] We now find that the photopolymer permits simultaneous, coaxial propagation of a bright core and dark sheath as a hybrid beam.

Previously, coherent ring dark solitons were initially studied numerically by Kivshar, et al., in 1994 with a self-defocusing nonlinearity.[202] Dark self-trapped ring solitons were

shown to either collapse to a minimum radius or diverge to decrease the contrast, depending on the initial soliton angle. Their equation for soliton amplitude was also shown to be identical to a common cylindrical KdV equation that represents cylindrical and spherical pulse solitons in plasmas and tsunami-shallow water waves as well. Subsequently, coherent dark ring soliton formation was experimentally demonstrated by Baluschev, et al., using an amplitude mask with dark dots and 50-250 µm lines.[203] Dark self-trapped beams were referred to as odd dark spatial solitons (where dark self-trapped rings were referred to as even dark spatial solitons), due to the number of phase flips across the soliton. A dark dot was shown to initially evolve as a dark self-trapped beam, followed by a bright central region and subsequently concentric bright rings. Parallel numerical studies indicated that such a bright central beam has a higher intensity than the background bright region. However, these experimental studies suffered significant interference lines from the input and output faces of the sample. Dark rings were also observed in other environments such as Bose-Einstein condensates.[204, 265] Such dark ring solitons have been thought to be useful for real-time reconfigurable applications involving light directing, switching, and multiplexing/demultiplexing for information transmission purposes.[266]

This work is the first experimental demonstration of incandescent white light based self-trapped dark ring waveguides. Additionally, the earlier chapter demonstrating dark waveguides in a photopolymer with a positive self-focusing nonlinearity has enabled self-trapping of such dark ring shaped waveguides without use of a self-defocusing (negative nonlinear) medium. We find that incoherent dark rings self-trap very differently

from previously studied coherent counterparts. The central bright region within the incoherent dark ring also self-traps along with the ring itself. Their simultaneous self-trapping results in the formation of induced permanent waveguides analogous to the core and cladding of an optical fiber with high and low index regions respectively. Both, the ring and central waveguide were found to have no instabilities through their evolution. No evidence of interactions or deviations of the central bright waveguide with bright filaments[239] induced through modulation instability in close proximity outside the dark ring were observed either.

7.2. **Temporal Evolution of a ring beam**

In a typical experiment, a broad, collimated beam of white light (background beam) from a quartz-tungsten-halogen lamp was passed through an amplitude mask (section 2.7, Figure 28), which introduced a weakly dark (gray) ring (Figure 70 a). The ring-embedded background beam was launched into a transparent cuvette containing an organosiloxane photopolymer.[63] At the entrance face (z = 0.0 mm), the gray ring had an outer diameter (o.d.) = 350 μm while its white core had a FWHM diameter of 220 μm. The relative intensity of the ring was 44 % while that of the core and background was 50 %. The beam profile at propagation distance (z) = 6.0 mm in the photopolymer was imaged with a CCD camera.

Experimental results in Figure 70 trace the striking evolution of the hybrid beam. At early times (when polymerization was negligible), the natural divergence of the background beam caused the ring and core to broaden with propagation from z = 0.0 mm to z = 6.0 mm. The concomitant decrease in intensity of the core diminished its contrast with the grey ring so that at z = 6.0 mm, the beam appeared effectively uniform with a relative intensity of $\cong$40 % (Figure 70b).

Polymerization and consequent refractive index changes (Δn) along the beam path caused self-trapping of the gray ring and white core. At 36 s, self-trapping of the ring was indicated by the emergence of a well-defined dark ring at $z = 6.0$ mm with o.d. $= 410$ µm and a decrease in relative intensity from 40 % to 31 % (Figure 70c). Self-trapping caused the core to narrow to 141 µm and increase in relative intensity from 40 % to 60 %. The dark ring and bright core propagated coaxially without significant divergence as a self-trapped hybrid beam. With time, the ring continued to darken further even as its core grew in intensity until their contrast maximized at 72 s at relative intensities of 12 % and 99 %, respectively (Figure 70e). At this time, the core was 105 µm-wide while the ring o.d. was 440 µm. Although the core later decreased in intensity with a slight increase in width (similar to self-trapped white beams),[63] both the ring and core remained self-trapped for as long as they were monitored (3000 s). To understand the formation of the hybrid beam and specifically, simultaneous self-trapping of gray and white regions, we consider the nonlinear propagation of a narrow bright beam in the photopolymer. This is expressed by the nonlinear paraxial wave equation[241]   Eq [7-1],

$$ik_0 n_0 \frac{\partial \varepsilon}{\partial z} + \frac{1}{2}\nabla_t^2 \varepsilon + k_0^2 n_0 \Delta n \varepsilon + \frac{i}{2}k_0 n_0 \alpha \varepsilon = 0$$

[7-1]

This describes the competition between the natural divergence of the beam in the transverse (x, y) directions (transverse Laplacian operator) and self-focusing due to photoinduced refractive index changes (Δn). The attenuation coefficient is α at wavelength λ (free space wavenumber, $k_0 = \omega/c$). Spatial and temporal variations of Δn in the photopolymer are described through[43]: Eq [1-11],

$$\Delta n^{'}(x, y, z, t) = \Delta n^{'}_{o}\left\{1 - \exp\left[-\frac{1}{U_{o}}\int_{0}^{t-\tau}\left|E(t^{'})\right|^{2} dt^{'}\right]\right\} \qquad \text{1-11]}$$

where Δn_0 is the maximum index change (at saturation), U_0, the critical exposure required to initiate polymerisation, τ, the monomer radical lifetime (assumed to be negligible) and $|E(t)|^{2}$, the square of the electric field amplitude of the incident optical field. Because Δn in the photopolymer is always positive, it is classified as a self-focusing medium. In this case, others[241] and our group[66] have shown that coupling Equations [7-1] and [1-11] gives self-trapped solutions for narrow, non-uniform (e.g. Gaussian) beams. Experimentally, we showed that the same mechanism applies to incandescent light beams.[63]

The above mechanism accounts for self-trapping of the bright core in the current study. The critical difference is that results (Figure 70) show that the same self-focusing conditions elicit self-trapping of the gray ring around the core. We reason that this process occurs as follows: Δn in the photopolymer is induced by the bright core and background. These bright regions, which have the same initial intensity at $z = 0.0$ mm, undergo comparable rates of polymerization. The corresponding Δn suppresses the divergence of the core and background. This is observed as a narrowing and increase in intensity of the core (Figure 70). Similar changes to the background beam are not evident as it illuminates nearly the entire sample and changes to its boundaries cannot be detected (*vide infra*). However, because the background propagates without divergence, it "holds" the embedded grey ring in focus along the propagation axis. No longer divergent, the ring effectively self-traps and therefore becomes visible at $z = 6.0$ mm (Figure 70). The dynamics and interactions between the ring and core of the hybrid beam are evident in the temporal plots of width and intensity (Figure 71).
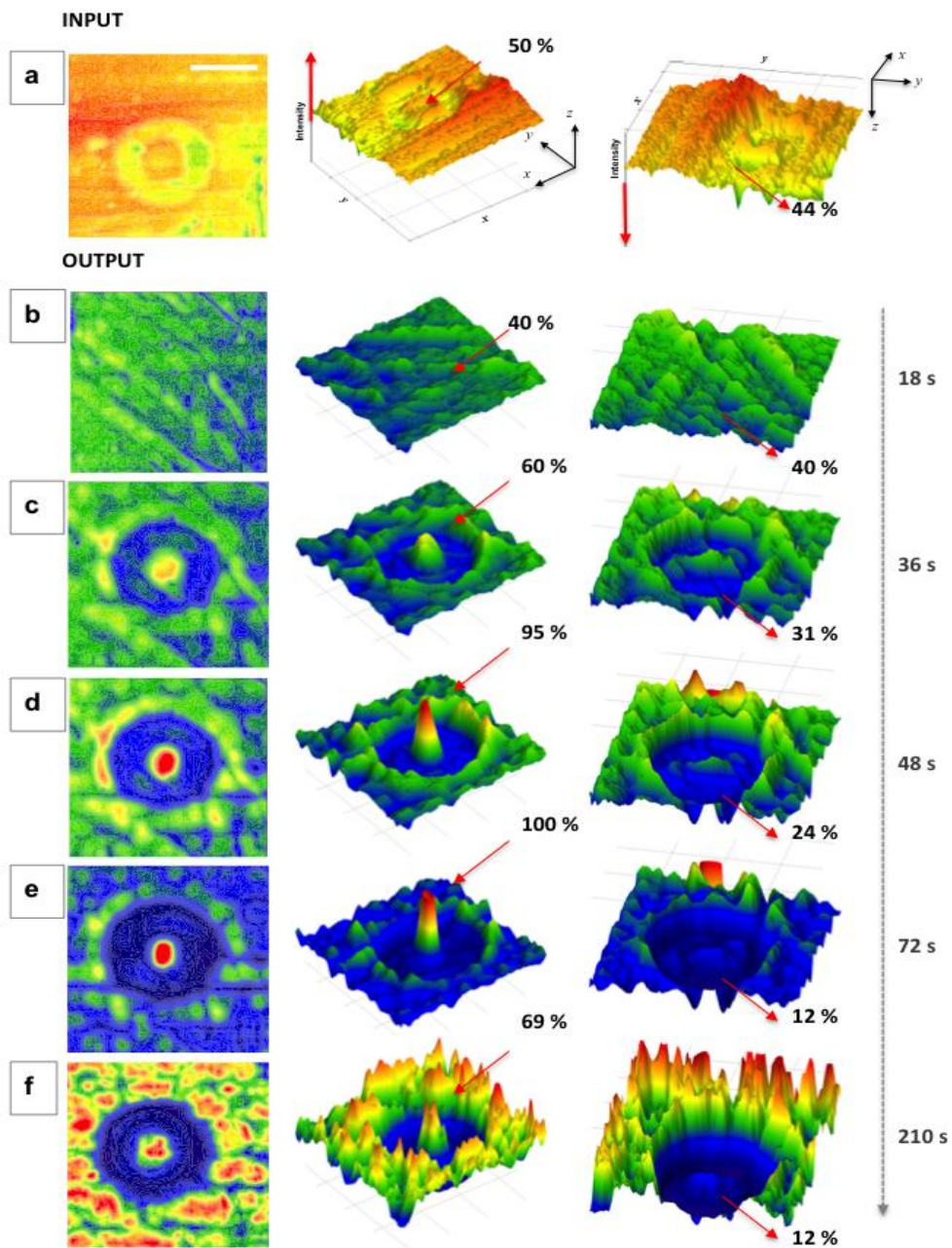
Figure 70. 2-D and 3-D spatial intensity profiles of the grey ring-embedded beam at $z = 0.0$ mm and its (b-f) evolution at $z = 6.0$ mm. The scalebar in (a) = 250 μm and applies to (b-f). Top and bottom perspectives of 3-D profiles show simultaneous self-trapping of the bright core and grey ring of the hybrid beam. Relative intensity scale ranges from blue (0 %) to red (100 %).
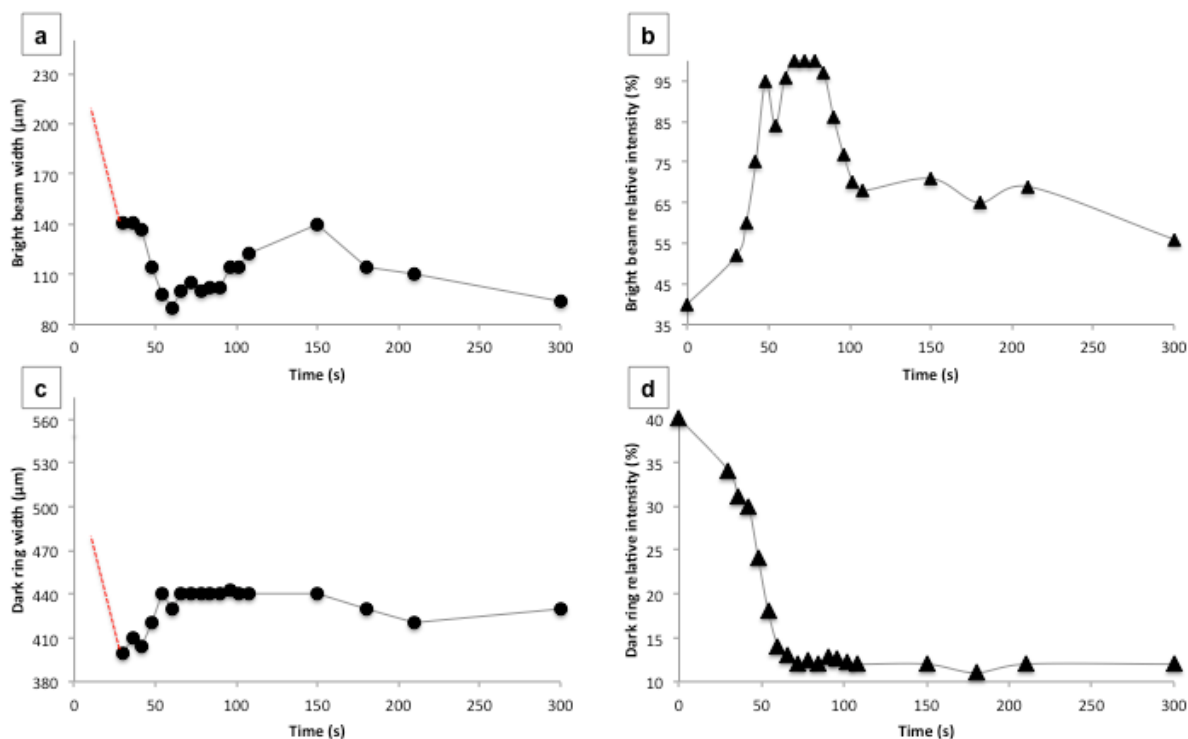
Figure 71. Temporal plots of width and relative intensity of the white core (a, b) and gray ring (c, d). Dotted lines indicate initial widths of ring and core could not be determined due to divergence.

7.3. **Ring beam existence within threshold widths**

Altering the widths of the self-trapping ring beams indicated that larger width beams as well as significantly smaller width beams cannot exist. Self-trapping dark rings of larger and smaller widths are shown in comparison with corresponding parameters in Figure 72. A larger beam (Figure 72a-A) is unstable due to MI induced fragmentation in its bright core. Decreasing the beam width makes it stable (Figure 72b-B,c-C). However, if it is too small, the bright core cannot sustain self-trapping when surrounded by a dark

ring (Figure 72d-D) unless it is larger than MI induced self-trapping filaments in its neighbourhood (Figure 72c-C).

Additionally, with larger rings, the mask is not completely black and there is light leakage, leading to minor filaments within the dark ring region itself. With smaller rings, the mask contrast is unchanged, but is still sufficient to prevent self-trapped filament formation inside dark regions.
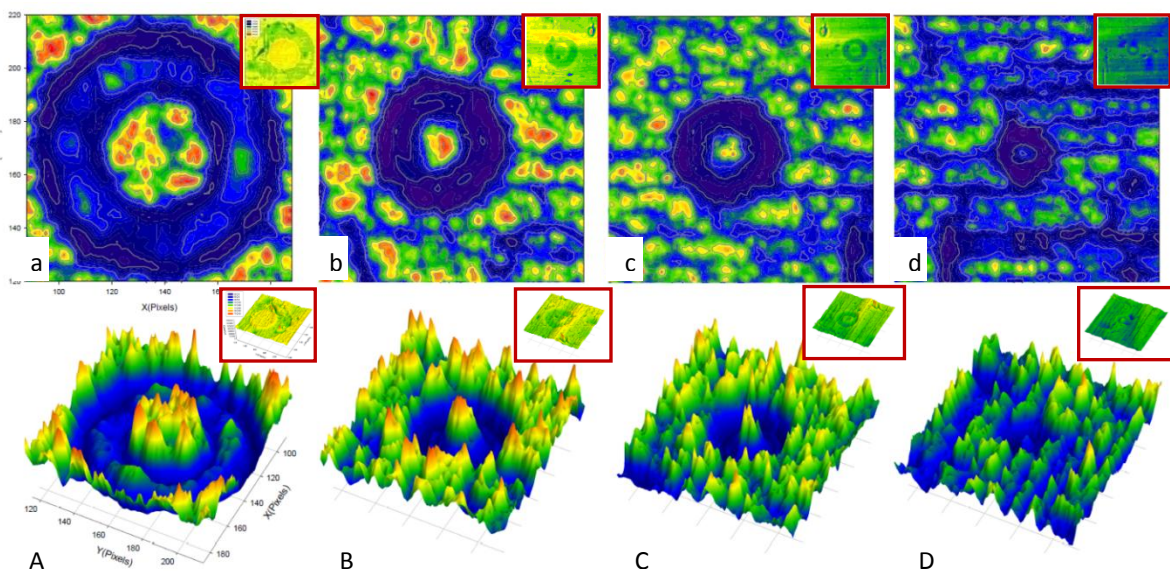
Figure 72. 2D (above) and corresponding 3D profiles (below) show self-trapped dark rings of decreasing widths at 72 s. Corresponding width and intensity parameters are listed in Table 10. Successively smaller width rings (a-d) have correspondingly smaller and lower intensity bright cores. Beam input profiles for each condition are shown in insets.

Table 10. Beam parameters corresponding to Dark self-trapping rings of decreasing widths of Figure 72 are shown above.

No. (72s)	Bright central beam width (µm)	Bright beam relative intensity (%)	Dark ring outer diameter (µm)	Dark ring annular width (µm)	Dark ring relative intensity (%)
A	380	95	1035	325	8.0
B	145	94	607	221	5.0
C	100	95	447	136	6.0
D	97	32	303	100	5.0
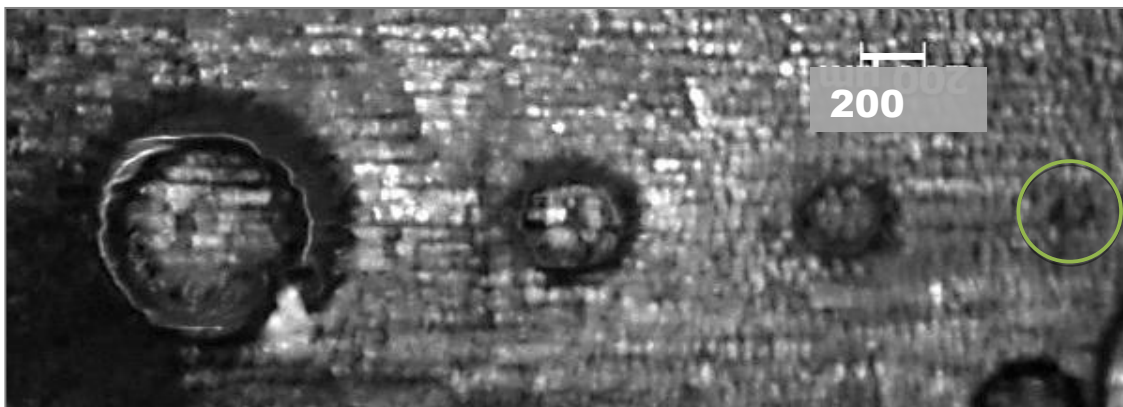
Figure 73. Micrograph (left to right) shows the output image profiles of self-trapped dark rings of increasing widths at >5000 s, and correspond to rings of small, medium, medium-2 and large widths respectively, of Figure 72.

7.4. Simulation of a 2D hybrid beam

Figure 71 (a-b) confirm that the ring and core self-trap simultaneously in the first 30 s when they both suffer the greatest decrease in width to 410 µm and 141 µm, respectively. The dark ring then reaches a stable value of 440 µm at 60 s. The core narrows further to 90 µm but widens slowly to 140 µm by 150 s. The ring and core then narrow slightly and remain self-

trapped. Figure 71 (c-d) show the complementary changes in intensity of the ring and core: at early times, the core increases in intensity from 40 % to 99 % by depleting the ring, which weakens from 40 % to 12 %. Intensity transfer originates from differences in the refractive indices: according to Equation 3-5, Δn in the photopolymer is intensity-dependent. As a result, Δn induced by the gray ring is smaller than that induced by the white core. This gradient triggers spontaneous intensity flow from the lower-index ring to the higher-index core. With increasing intensity, the core induces greater Δn and attracts even more intensity from the ring. A cycle is established in which the core grows by depleting intensity of the ring, which reaches a minimum intensity of 12 % at 72 s (Figure 70e, Figure 71d). Intensity transfer ceases when Δn of the core approaches saturation. At this time, similar to individual self-trapped white beams[63], the core intensity decreases together with a slight increase in its width. While the ring shows a corresponding increase in width, it remains dark and does not undergo any further significant changes.

The key property of the photopolymer, which gives rise to the hybrid beam, is its ability to simultaneously sustain bright and dark self-trapped beams. To provide additional proof, we carried out simulations based on a beam propagation method.[66] Using a continuous wave, visible beam (532 nm) for simplicity, we monitored the behavior of a broad beam bearing a grey ring from $z = 0.0$ mm to $z = 6.0$ mm in the photopolymer.
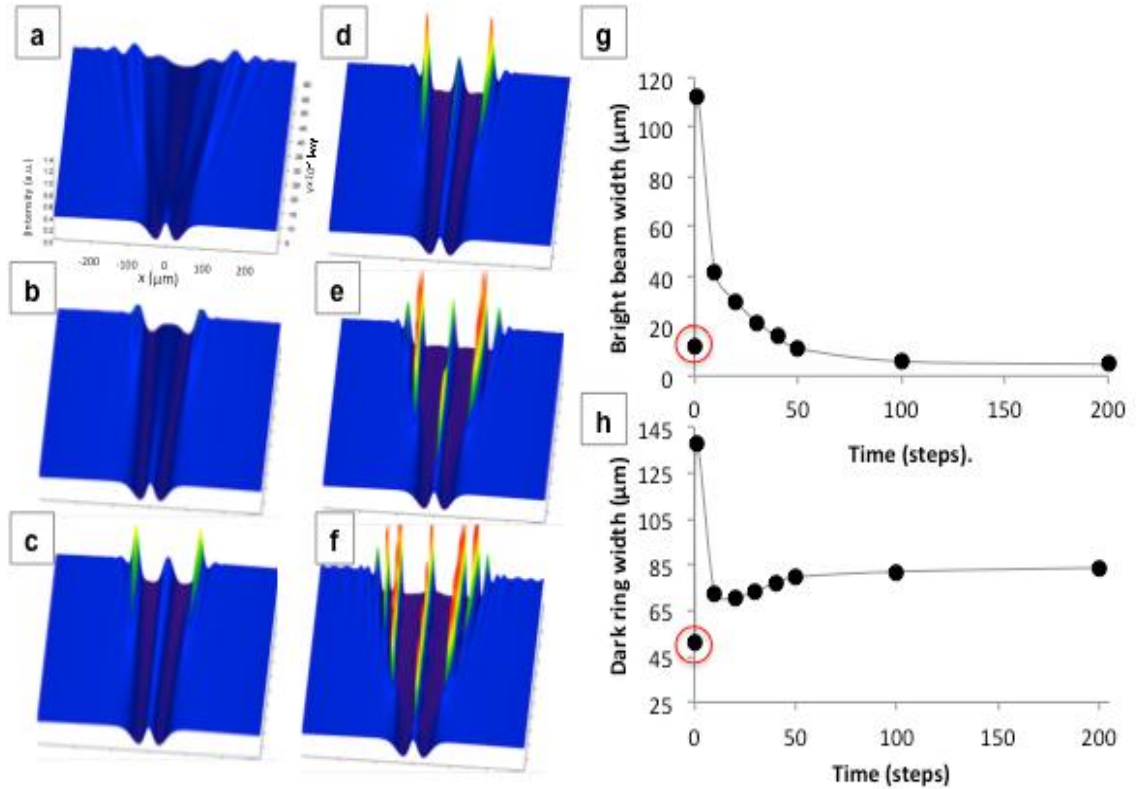
Figure 74. Simulated intensity maps of self-trapping of a grey ring and bright core at (a) 1 (b) 20 (c) 40 (d) 50 (e) 100 and (f) 200 steps. Scales in (a) apply to (b)-(f). Relative intensity scale ranges from dark blue (0 %) to red (100 %). Temporal plots trace diameters of (g) white core and (h) gray ring. Input widths are circled.

Results in Figure 74 show excellent agreement with experiment. Simulated intensity maps show that both the gray ring and white core self-trap into a hybrid beam over time. Consistent with experiment (Figure 70, Figure 71), the ring darkens as it self-traps while the core increases in intensity as it self-traps (Figure 74 a-f). (Intensity increase at the dark ring boundaries at later times is due to self-trapping of interference fringes in the coherent field. These are not observed in the experiment, which employs incoherent light). The dynamics of the simulated hybrid beam closely follow experiment; temporal plots of widths trace the simultaneous decrease in diameter, which signifies self-trapping

of the core and ring (Figure 74 g-h). Simulations also capture the slight widening of the dark ring observed at later times in the experiment (Figure 70).

Our experimental and computed findings indicate that the hybrid beam originates from simultaneous self-trapping and cooperative interactions of the gray ring and white core. The background beam, which also induces index changes in the photopolymer, undergoes an entirely different type of nonlinear behaviour, modulation instability (MI).[180] By 210 s, the uniform background spontaneously divided into multiple filaments (Figure 70f). The filaments, which are akin to individual self-trapped beams, were approximately 80 μm wide with ~74 % relative intensity. They originate from noise such as random, weak amplitude variations, which become amplified due to polymerization and render the beam unstable. The beam stabilises by spontaneously dividing into multiple filaments.[180] We note that although they originate in the same medium under identical conditions, MI-induced filaments form at a later time (210 s) than the self-trapped bright core (36 s). This is because the dark ring serves as a low-index sheath, which enhances light confinement in the core. This in turn would increase the rate and efficiency of self-trapping of the core relative to MI-induced filaments. Furthermore, although filaments immediately surrounding the dark rings were within interacting distance[239] with the self-trapped core (Figure 70e), no interactions (e.g. fusion) were observed. We previously showed that interactions between self-trapped white light beams rely on index changes induced by their overlapping optical fields.[239] In the current study, the smaller index of the dark ring inhibits such overlap and protects the core from interactions.

7.5. **Conclusion**

In summary, we experimentally demonstrated and supported through simulation, the first example of a self-trapped hybrid beam. This hybrid beam originates from simultaneous and cooperative self-trapping of a gray ring and its bright core embedded in a broad incandescent beam. The core grows by depleting intensity from the ring and the hybrid beam stabilizes when contrast between the two maximizes. Like the cladding of an optical fiber, the dark ring serves as a low-index sheath that enhances light confinement in the core and protects it from interactions. The hybrid beam opens opportunities to manipulate the confinement and interactions of self-trapped beams through designed introduction of gray and white regions in an optical field. Because of its spatial and temporal incoherence, the hybrid beam also raises fundamental questions about the coherence structure of the dark ring and its bright core. In terms of applications, hybrid beams would be readily accessible with other inexpensive and miniature incoherent light sources such as LEDs.

A higher index is induced in the core, while a lower index is induced in the surrounding simultaneously, which is structurally analogous to the core and cladding layers of an optical fiber. Such polymer waveguides may be studied for potential in optical glues for repairing and reattaching damaged optical fibers.

8. Conclusion and Future work

8.1. Conclusion

Self-trapping of incoherent white light is a subject pertaining to the field of nonlinear optics. Nonlinear waves are a special type of waves that violate the linear wave superposition principle (where the resultant amplitude of two waves is the linear sum of their amplitudes). Such waves are described by nonlinear wave equations (such as the nonlinear Schrödinger equation in optics) and exist in many other physical systems such as fluid dynamics and acoustics as well. Optically induced nonlinearity exhibits a wide range of phenomena such as harmonic generation, optical parametric amplification, self and cross-phase modulation, two photon absorption, modulation instability, self-trapping, etc. Of this rich variety of phenomena, optical self-trapping is one of the most fundamental, and is also described by the nonlinear Schrödinger equation. One of the most common effects of nonlinearity occurs when a very high intensity beam such as a laser passes through a material and simultaneously alters the refractive index of the material along its path depending upon the local intensity at that point. Such an index change can induce a feedback upon the original beam and either distort, focus or even defocus the original beam itself.

Self-trapping is a special phenomenon that occurs when the self-focusing tendency of a beam through an induced index gradient within a medium exactly balances out its natural divergence. Self-trapped beams can exist in both the temporal as well as the spatial domain; in the latter, they can be either of the bright or the dark type. Such beams

have been studied using coherent laser sources in a wide range of materials ranging from glass, sodium vapor, CS to photorefractive crystals, polymers, liquid crystals, semiconductors and even air. Previously, several theories have been modeled specific to various types of material nonlinearity such as Kerr or saturating nonlinearity, to describe each scenario of self-trapped beams.

Self-trapping beams are of particular interest for optical circuitry since such beams can both exhibit interactions when in proximity. Related phenomena such as modulation instability are also significant due to their ability to form complex periodic index gradient patterns. Advanced studies such as interactions between such self-trapped beams themselves hold vast potential for optical circuitry via interactions.

Incoherent self-trapping has also been shown to be possible, and theories have been extended to model this phenomenon. Previous research in our group has demonstrated and studied white light self-trapping for the first time in photopolymers. This thesis on white light self-trapped phenomena is a major step forward in our understanding of incoherently generated self-trapping beams in photopolymers. It is the first study of interactions and related complex phenomena with incoherent white light self-trapping beams. Previous studies were unable to generate multiple stable and robust self-trapping beams in order to study such complex phenomena. Because incandescent white light originates from the uncorrelated decay of excited states, white light suffers rapid and random phase fluctuations that prevent collective self-trapping.[33,34] The only previous study of such self-trapped beams, showed proof of principle of their existence using very low intensities (nW) in a photorefractive crystal.[12] Such studies can only be

generated in materials with a noninstantaneous and saturable photo response because they smooth (time-average) out phase fluctuations and allow collective self-trapping of an incoherent beam. Saturability and noninstantaneity are possible with free-radical photopolymerization reactions. We recently demonstrated self-trapping over a wide range of intensities in a polymerizable organosiloxane. Taking advantage of this accessible experimental route has enabled us to examine in detail for the first time, various phenomena with incoherent white light. Other new phenomena such as dark self-trapping beams as well as arrays of self-trapped beams have also been shown to exist with incoherent beams in photopolymers.

This research is additionally significant because it opens the possibility for material tuning with these polymer waveguides. Traditionally waveguides have been made in either crystalline materials or more recently, fabricated in Si based materials for easy integration with current opto-electronic devices. Existing technology based on inorganic crystals cannot access this. Polymers however, can be tuned so as to change the response wavelength, waveguide width, speed of polymerization, flexibility and durability of the material itself.

This thesis summarizes four chapters of interrelated phenomena that have been found to occur with white light self-trapping beams. These results have been grouped into parallel interactions of white light self-trapping bright beams, formation and dynamics of white light induced dark self-trapping beams, lattice structures formed using both bright as well as dark self-trapping beams and modulation instability, and formation of embedded self-trapping beams - bright beams encircled by dark beams and vice versa.

Supporting results also include simulation studies for dark self-trapping beams and embedded beams. Additional studies include threshold between single beam self-trapping and beam fragmentation through modulation instability, as well as trials of angular interaction phenomena between bright self-trapping beams and interactions between dark self-trapping beams.

Chapter 3 details the results of interactions between two co-propagating incandescently generated white light self-trapping beams. Previous studies of such interactions have all been performed on either coherent or partially coherent beams using laser sources. Such interactions strongly depend on the phase relationship of coherent beams. With incoherent white light, such a phase relationship does not exist and theoretical predictions indicate only fusion type interactions exist between such beams. Various fundamental questions regarding incoherent counterparts of coherent phenomena were explored, such as whether parallel incoherent beams *always* fuse at close separations, as theoretically predicted? Our research shows that incoherent beams can exhibit fusion, fission or even repulsion type interactions depending on the spatial separation between the beams.

At proximities less than their half-width, two self-trapping beams begin to self-trap as a single large beam and this beam undergoes fragmentation and fission. This occurs through a related phenomenon of modulation instability. In modulation instability, a single larger self-trapped beam profile undergoes filamentation due to random noise inherent in the system. At proximities comparable to their beam width, the two beams exhibit fusion, and merge into a single self-trapped beam. Any beam that happens to be

slightly lower than its neighbor due to random noise, decreases in intensity while the higher intensity beam dominates and increases at the expense of the neighbor. At larger separations, no significant interactions were found between the two self-trapping beams.

An unexpected result was also observed with two beams at about 5x their half widths – the two beams were found to exhibit repulsion type interactions. This type of interaction has not been observed or predicted theoretically previously. Such repulsion interaction is indicative of material drift through diffusion, resulting in a lower index region at the center. Additionally, such an interaction raises questions about the self-trapping behavior of a ring of such beams. Specifically, would such a ring of beams expand through mutual repulsions? This hints at formations of dark regions between bright self-trapping beams.

Next, in Chapter 4 dark self-trapping beams were shown to exist in photopolymer media. In the incoherent dark self-trapping beams, were conclusively proved to exist in photopolymer media and were characterized quantitatively. Dark beams are theoretically predicted to exist in negative nonlinear media only, since Gaussian-like light beams tend to self-defocus in such media. Negative nonlinear media undergo a decrease in refractive index with an increase in light intensity that self-defocuses light beams, where as positive nonlinear media undergo an increase in refractive index with an increase in light intensity that self-focuses light beams. Previous studies have also demonstrated dark beams in only negative nonlinear media, but never in positive nonlinear media. Incoherently generated dark beams have also been demonstrated in negative nonlinear media. The existence of dark self-trapped beams in photopolymer media that have a positive nonlinear

environment resulting in self-focusing of Gaussian-like light beams cannot be explained by current theory. Chapter 4 demonstrates self-trapping dark incoherent beams in organosiloxane which is a positive nonlinear medium – it undergoes photopolymerization and a refractive index increase with an increase in light intensity. Experiments were supported by theoretical simulations and detailed studies on their behavior and mechanism. The theoretical simulation study with photopolymerization nonlinearity confirms the experimental study. Self-trapping of such a dark beam was found to be dependent on the background light intensity, width of the background bright beam, as well as the width of the dark ring itself. This demonstration contradicts current theory that dark beams necessarily need a negative nonlinear medium to self-trap. Existence of such a beam was found to be possible due to an inherent property of photopolymer materials – material diffusion from dark to illuminated regions under photo-polymerization conditions, and the resulting decrease in index gradient in the dark regions enables self-trapping of such a beam in a positive nonlinear medium. This is a very interesting result from a fundamental nonlinear science perspective, and was shown both experimentally and with preliminary simulations.

Subsequently, self-trapping of multiple dark beams was studied and bundle of self-trapped dark filaments were also found to self-trap in a stable manner (Chapter 5). While similar arrays have been researched previously in nonlinear optical crystals, white light induced arrays in organosiloxane show evidence of intricate rearrangements in such waveguide arrays. When such dark beams were closely spaced, they induced

rearrangements among interstitial bright regions and formed additional ordered bright beams.

For instance, self-trapping 2D HCP arrays of dark beams result in formation of a spontaneous interstitial 2D HCP lattice of bright self-trapping filaments. This occurs when the dark beam lattice parameter is close to the width of each dark filament of the lattice. Additionally, if the lattice spacing was increased, the resulting larger interstitial bright regions were found to undergo filamentation through modulation instability. Altering the lattice geometry of the dark beams was therefore found to provide a novel means of controlling the geometry of interstitial bright filaments. Controlling the shape and width of bright regions accurately, for example, led to each bright region splitting into exactly two filaments through modulation instability.

These provided sufficient and robust control over the pattern formed and dark beams were therefore employed in controlling and directing interstitial bright self-trapped beams. This was done by using masks to generate multiple self-trapped beams - dark self-induced arrays as well as bright – of various geometries such as HCP and square lattices in each plane. These 2D lattices were found to be extendable to 3D as well. 2D as well as 3D lattices of a large variety of patterns were demonstrated using such beams.

These studies demonstrate an extremely simplified approach to creating complex 3D lattices previously made through laborious and expensive coherent optical assemblies. Traditional optical fabrication methods require accurate interference between four coherent beams to fabricate a full 3D geometry. This incoherent method requires only 2

beams for a full 3D geometry, and since each beam affects the medium independently, they do not require accurate assembling. Further, such rearrangements lead to geometries completely different from the masks used and hold significant potential in fabricating new types of lattices. These arrays are also extremely simple to fabricate, requiring a home-made printed mask and an incandescent white light source in comparison to alternative methods. This forms a 1-step, 2 beam process of white light lithography and is considerably simpler and cost effective than 4 interfering laser beam based fabrication methods traditionally used to make similar geometries.

Complex lattices corresponding to woodpile geometry can also be fabricated using rearrangement methods. Chapter 6 shows woodpile-like polymeric lattices can be fabricated in a single step with incandescent white light. Such a structure is significant for its 3D photonic bandgap since these geometries are commonly utilized in photonic crystals for light manipulating devices. Theoretical studies of simulated self-trapped arrays (using BandSolve® software) show such lattices do indeed possess potential band-gaps in the radio frequency and microwave range and can be employed to fabricate templates for photonic band gap materials if the index contrast is scaled up. Such higher index gradient structures can be made experimentally in future and optimized for specific photonic band gap applications. Additionally, a very wide range of white light based discrete self-trapping fundamental studies can now be done with white light self-trapped beams in various 2D as well as 3D lattices using these techniques.

The experiments on bright beams and dark beams also raise questions regarding whether such media would be able to support embedded waveguides. Embedded bright

beams consist of regular bright self-trapped beams with a dark self-trapping core, while embedded dark beams would consist of the converse - dark self-trapped beams with a bright self-trapping core. These beams are also have been previously studied with coherent beams in nonlinear optical crystals, but their white light counterparts have never been demonstrated before. In Chapter 7- dark ring beams, bright beams trapped in dark ring beams were demonstrated experimentally and supported with simulations. These beams essentially mimic an optical fiber's geometry – a cylindrical high index core with a low index cladding. These self-trapped ring beams were also essential to the creation of woodpile-like lattices. These are the first demonstration of incoherent white light generated ring beams.

Next, bright ring beams were also attempted (Figure 75). These beams were found to collapse into a single central bright beam forming a conical waveguide instead of self-trapping in a stable manner.
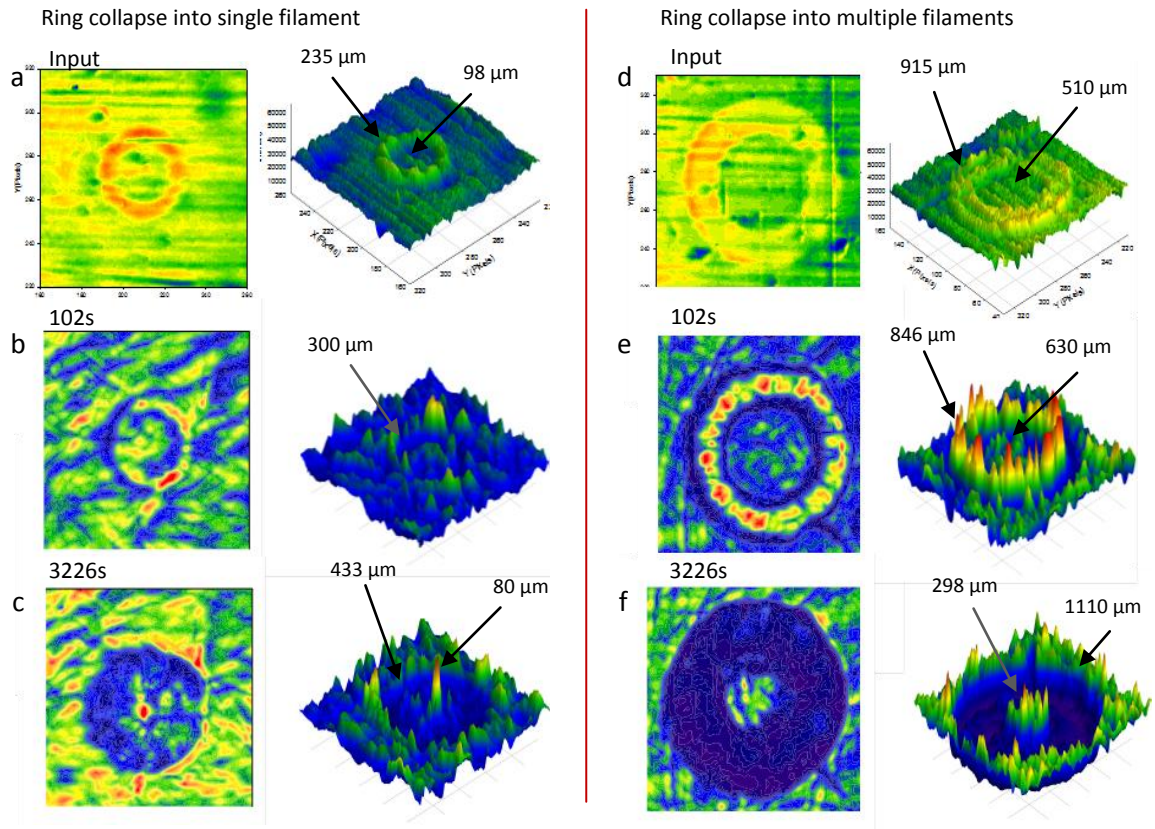
Figure 75. 2D profiles (left) and 3D profiles (right) show temporal evolution of a self-trapping ring shaped bright beam. Profiles shown were recorded at input before illumination, 102 s and 3226 s. Temporal evolution shows the bright self-trapping ring is unstable and collapses. A bright ring collapses into a single self-trapping filament (left row) or into a bundle of multiple filaments (right row) in case of a larger width ring.

In summary, this research has demonstrated four new classes of white light self-trapping phenomena, as follows: In *Chapter 3: Interactions* of two beams are characterized, demonstrating two beam fusion, fission as well as repulsion. Mutual repulsions between bright beams hints at dark regions which is explored in *Chapter 4: Dark self-trapping beams* with incoherent white light. This is supported by theoretical studies that demonstrate a dark beam can exist in a positive nonlinear environment. Next,

both bright and dark waveguides were employed in *Chapters* 5-6*: Fabricating lattices* for 2D and 3D structures. Woodpile structures were also demonstrated. The last *Chapter 7: on ring beams* demonstrates for the first time, the existence and self-trapping of embedded beams, which are white light counterparts of corresponding coherent self-trapping beams.

8.2. **Future Work**

Self-trapped beams and soliton formation is an area of fundamental research in the field of nonlinear optics. Nonlinearity results when a material's polarization is no longer a linear function of the electric field of an incoming light wave, and such a response can be utilized to make powerful light manipulating devices. The field of nonlinear optics came about with the invention and use of high intensity lasers capable of concentrating light to sufficiently high intensities to produce nonlinear effects in materials.

All current generation information technology hardware is based on a combination of mainly electronic and opto-electronic technologies. Current technology is also limited through cross conversions between optical and electronic devices since optical means are utilized mainly for transmission but not for processing. However, future solutions are projected to include a significant degree of optical technology in lieu of electronics. Unlike electronics, optical devices, besides avoiding conversion to electronic signals, are additionally capable of supporting vastly higher bandwidth though non-interfering parallel signals. Current trends are focused on building electronic device analogues with

optics, lowering power requirements and device sizes drastically by utilizing alternatives such as optical self-trapping, quantum dots, nanowires, as well as improved fabrication technology.

This study on optical self-trapping with incoherent light has been a major step forward in our understanding of incoherent white light self-trapping beams. White light self-trapping can potentially reduce power requirements while simultaneously increasing bandwidth by orders of magnitude in optical devices. Previous studies have focused mainly on laser-sourced partially incoherent light in inorganic crystals or separately, on laser sourced polymeric waveguide formations. This study details incandescent white light optical self-trapping phenomena utilizing such polymeric waveguides for the first time. Studies in this thesis have shown the first permanent polymer waveguides with incoherent white light that can be now used to manipulate and guide light in various ways.

This fundamental study also opens the possibility for material tuning with these polymer waveguides with white light. Traditionally waveguides have been made in either crystalline materials or more recently, fabricated in Si based materials for easy integration with current opto-electronic devices. Existing technology based on inorganic crystals cannot access such features. Polymers however, can be tuned so as to change the response wavelength, waveguide width, speed of polymerization, flexibility and durability of the material itself. Additionally, several new fundamental phenomena have been shown which can now be explored further theoretically as well as for applications.

Demonstration of Interactions between self-trapped beams (chapter 3) brings optical research a step closer to the possibility of all-optical control using white light beams. Optical beams to control the trajectory of neighboring optical beams can theoretically scale up to optical analogues of electronic circuitry, thereby eliminating intervening electronic processing devices in optical data transmission. Additionally, use of permanent polymer waveguides can potentially be used as an "optical glue" to repair damaged and sheared optical fibers.

Dark self-trapping waveguides formed with incoherent white light (chapter 4) is a new discovery in the field of white light self-trapping. Because such waveguides form within a positive nonlinear environment that have so far been thought to only support bright waveguides, this significantly our advances current theoretical understanding of dark waveguides. These waveguides additionally provides an alternative and potentially efficient means of guiding light in photopolymer media generating and studying fundamentally new phenomena with bright waveguides. Dark beams have been shown to guide white light, but their mechanism is not completely quantified. Theoretical studies on simulating white light self-trapping accounting for spatial, temporal as well as spectral incoherence would help explain how a dark self-trapping beam affects the coherence dynamics of an incoherent white light self-trapping beam.

Dark as well as bright beams of incandescent white light have been employed to fabricate lattices (chapters 5-6). The fabrication method used in these studies eliminates the complexity associated with current fabrication technologies that employ accurate interference between multiple laser sources or expensive fabrication masks. They can

generate complex structures that cannot be accessed by traditional means. Such customized patterned structures can be utilized for advanced studies of lattice solitons using both white light or coherent sources. These structures also closely mimic photonic band-gap materials and can theoretically be employed for their fabrication. Based on the currently achievable lattice spacing, these structures may be used to exhibit their bandgap properties for radio and microwave frequencies. Future studies can scale down the photonic structures to be effective at microwave and infrared light frequencies.

Ring self-trapping beams (chapter 7) are the white light analogues of corresponding coherent studies. This fundamental study shows interesting similarities as well as differences between such beams with their corresponding coherent counterparts. From a purely fundamental point of view, such beams are interesting due to their frequent instability and decay into symmetric shapes. These are an entirely new type of self-trapping waveguide, distinct from both bright and dark waveguides although they inherit some features of both types. Both, bright in dark as well as dark in bright waveguides can potentially guide light more efficiently than either bright or dark waveguides alone, due to their higher index gradient and increased light confinement. The instability and subsequent collapse of a dark in a bright waveguide into a tapering conical waveguide (Figure 75) is particularly interesting since such arrays of such structures have been employed for focusing beams of light in studies such as artificial insect eyes.

Previously both, parallel and angular interaction studies have been looked at in detail in our group. Future studies can progress to analyze two antiparallel beams (at 180 degrees to one another). Such incoherent white light counter propagating beams which

have been studied previously both theoretically[107,108] and experimentally[109] only with coherent and mutually incoherent beams). Further, beams may also interact at small angles ($<10^0$) as well. The possibility of gluing of two distinct closely spaced, but misaligned waveguides[267] with incoherent white light can possibly be verified with this setup. Mutually incoherent beams have a threshold region, where they do not fuse, but can still couple light into one another. This threshold is defined by their total internal reflection angle, and above it, even cross-coupling of light into each other's waveguide is not possible. A potential objective is to study the existence of such a threshold region with white light beams. This can be probed by any study where components of the two input beams can be distinguished (e.g. by using two different polarization filters) to provide a good insight into the coherence behavior of colliding beams.

This also follows from the effect seen in a completely different series of experiments studying 2D MI, where the individual beams of grids generated in two different dimensions always intersect.[181] However, the two grids were generated at 90^0 relative to one another.

Future studies may include measurements of index gradients in organosiloxane throughout the self-trapping, as well as quantifying diffusion and mass transfer of the photopolymer from dark to illuminated regions. Chemical studies for achieving high index gradients and making robust structures experimentally, and applications at radio-frequencies are also possible in the future. Chemical studies may also look at reversible index changes (using previous studies of cis-trans index gradients) as well. This could potentially be used for switching/non-permanent waveguides with white light.

Following up on several unexpected experimental results – such as white light beam repulsions, dark beams, and rearrangements within lattices - additional studies could include creating other types of lattice structures, multi-beam interactions, as well as interactions between different types, such as a bright and a dark beams. Other broad areas of future research include incoherent light simulations using multi-spectral beams, as well as experimental and theoretical studies of discrete self-trapping in optical lattices.

These studies also give rise to several new intriguing unanswered questions. Since bright and dark self-trapped beams both exist, what other equivalent phenomena of coherent beams can exist in photopolymer media with white light? Ring beams have already been shown as one such example. Theoretical studies could also analyze in-depth filamentation formed through MI leading to rearrangements and lattice formations with white light. Besides such fundamental studies, several areas of research directed at potential applications could also be explored.

Overall, studies of these phenomena take the field of incoherent self-trapping a significant step forward ranging from fundamental understanding of white light self-trapping to potential applications for various optical devices. incoherent light based devices such as LEDs can be used with such waveguides to lower costs, multiplexing to scale up bandwidth, lowering power requirements, shrinking device sizes thereby replacing current coherent laser sources. Studies of white light self-trapping and development of flexible and tunable photopolymer based devices will also complement other current approaches to nonlinear optical devices such as, photonic crystals, fibers,

plasmonics, new fabrication technology, nanowires, and quantum dots for new unique and more efficient devices.

9. Appendix

9.1. Single beam self-trapping and filamentation threshold

An experimental study was done to determine a threshold between incoherent white light self-trapping and MI phenomena in photochemical media. Self-trapping results from a single diffracted beam and MI from uniformly illumination in a nonlinear medium.[45] Both self-trapping and MI are related phenomena. Experimentally, it was found that the formation of a single self-trapped vs. multiple beams is governed by the relative width of the input beam entering the medium. Beams smaller than a threshold width (of 50 um) were found to induce single beam self-trapping, whereas larger beams were increasingly found to undergo filamentation. At the upper limit, a uniform beam of light induces an array of independent self-trapped filaments.

Each self-trapped beam is generated by focusing white light from a Quartz-Tungsten-Halogen lamp at the entrance face through a different pinhole - 20 to 100 μm diameters. Below, control experiments show input (z = 0 mm) and output (z = 5.5 mm) profiles of beams of increasing widths (20-100 um) under linear conditions. The profiles in Figure 76 are not normalized (narrow width beams diffract more, and have a higher intensity peak vs broader beams).

Linear input & output profiles
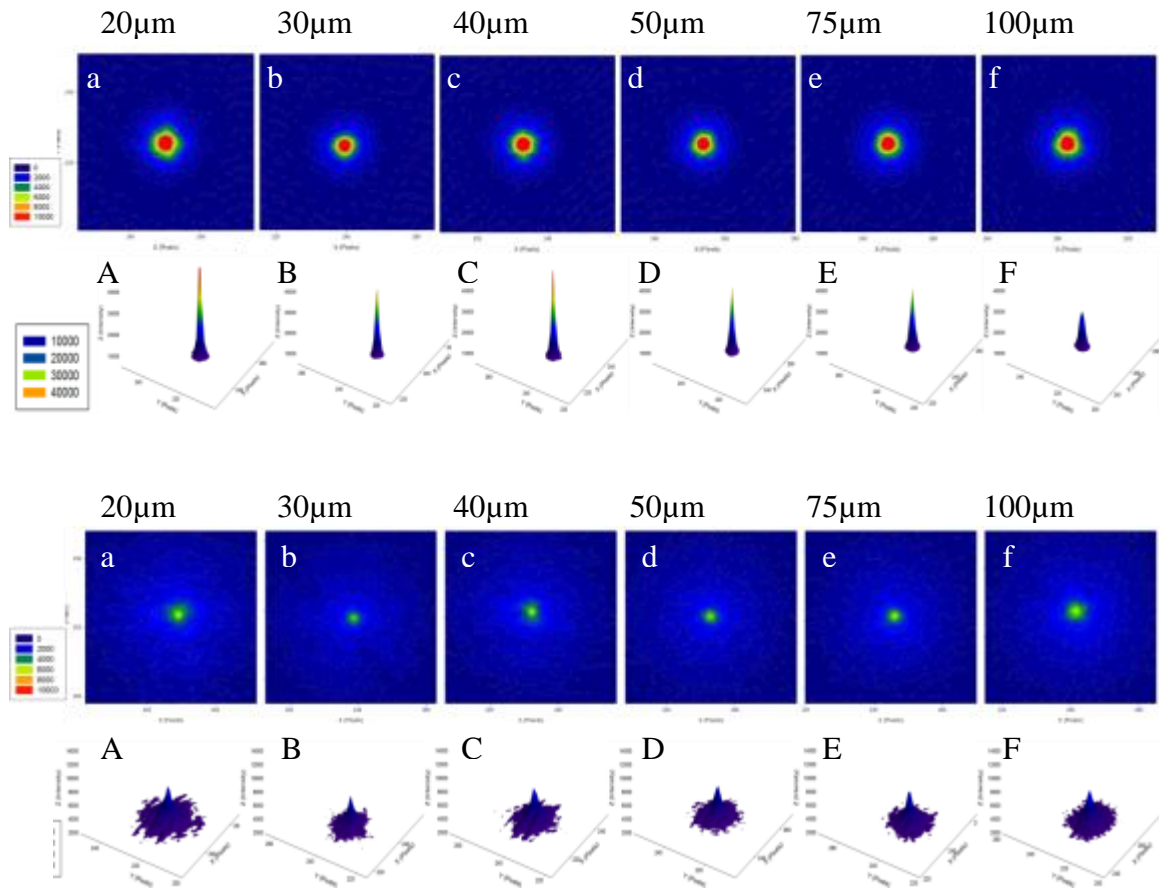
Figure 76. Above, 2-D (a-f) and 3-D (A-F) beam profiles at the entrance face are shown for input beams of widths 20, 30, 40, 50, 75 & 200 μm. BELOW: Corresponding output beam profiles at the exit face 2-D (a-f) and 3-D (A-F) are shown under linear conditions (3-D profiles scale is magnified for clarity). In beam profiles (A-F) width and intensity are nearly constant (10% relative intensity).
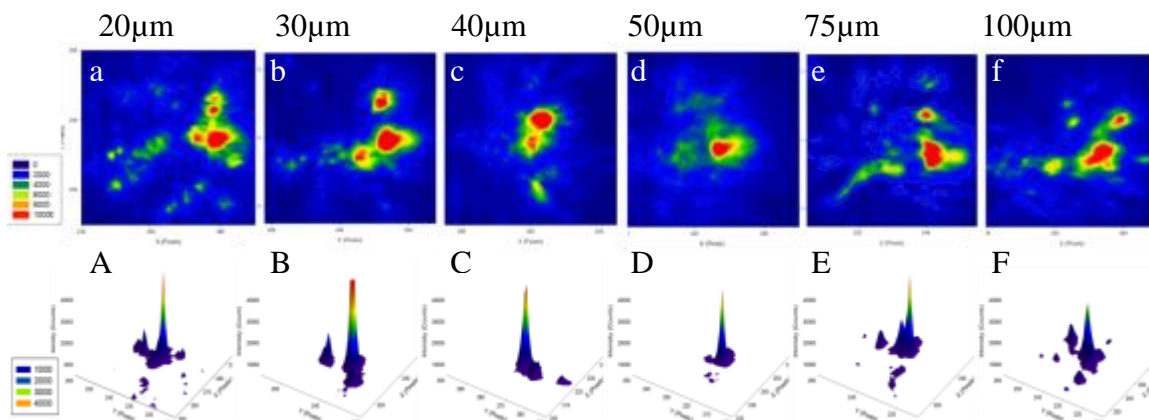
Figure 77. 2-D and 3-D beam profiles at the output face (after 5.5mm of propagation) under nonlinear self-trapping conditions are shown for input beam widths of 20, 30, 40, 50, 75 & 100 um. Wider input beams (75, 100 um) undergo fragmentation with secondary filaments being comparable to the largest filaments.   In smaller beams, (50 um), secondary filaments are either absent or less than 20% of the largest filaments.

Nonlinear photopolymerization conditions

Under nonlinear conditions, beam profiles (Figure 77) show beam fragmentation and multiple peak formations. for all except the 50 um beams. Although secondary filaments do form for smaller width beams (20 um, 30 um), their intensity is less than 20% of the largest filament's intensity. For larger width beam (100 um), the secondary filament has more than 50% of the largest filament's intensity. This is indicative of the transition to multiple beam formation through modulation instability.
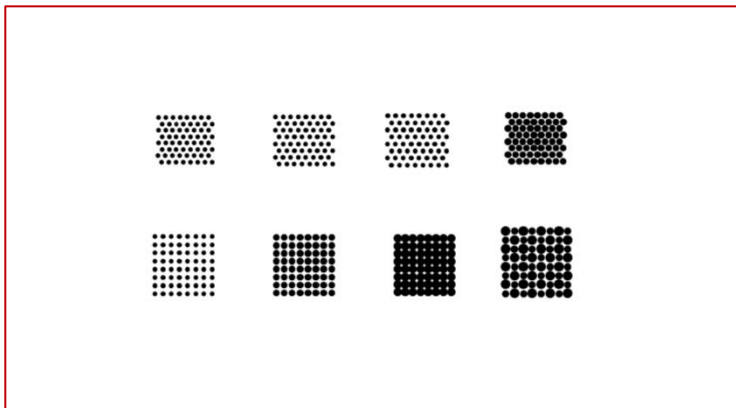
Figure 78. An image of the masks used for self-trapping experiments is shown here, corresponding to section 2.6. The image is scaled up 400% relative to the original, for clarity. These patterns were created in MS Word, printed onto slide transparencies, cut to size and inserted into sample cuvettes before illumination. For 35mm slides, images were sent for slide and film processing. to Burlington Camera, 489 Guelph Line South, Burlington, Ontario, Canada, L7R 3M2.

10. References

1 Królikowski, W.; Denz, C.; Stepken, A.; Saffman, M.; Luther-Davies, B. *Quantum Semiclass. Opt.*, **1998**, 10, 823

2 Hercher, M. *J. Opt. Soc. Am.*, **1964**, 54, 563

3 Chiao, R.Y.; Garmire, E.; Townes, C.H. *Phys. Rev. Lett.*, **1964**, 13, 15, 479

4 Bjorkholm, J.E.; Ashkin, A. *Phys. Rev. Lett.*, **1974**, 32,4,129

5 Segev, M.; Valley, G.C.;Crosignani, B.;DiPorto, P.;Yariv, A. *Phys. Rev. Lett.,***1994**, 73,24,3211

6 Bartuch, U.; Peschel, U.; Gabler, Th.; Waldhäus, R.; Hörhold, H-H. *Opt. Commun.,***1997**, 134, 49

7 Shen, M.; Wang, Q.; Shi, J.; Chen, Y.; Wang, X., *Phys. Rev. E,***2005**, 72, 026604

8 Aitchison, J.S.; Al-Hemiary, K.; Ironside, C.N.; Grant, R.S.; Sibbet, W. *Electron. Lett.,***1992**, 28, 1979

9 Lehner, T.; Auby, N. *Phys. Rev. E,* **2000**, 61,2,1996

10 Soljačić, M.; Segev, M. *Phys. Rev. A,* **2000**, 62, 4, 043817

11 Stegeman, G.I.; Christodoulides, D. N.; Segev, M. *Quantum Electron.,***2000**, 6, 6, 1419

12 Mitchell, M.; Segev, M. *Nature,***1997**, 387, 880

13 Kivshar, Y. S. *Opt.Quantum Electron.,***1998**, 30, 571

14 Akhmediev, N. N. *Opt.Quantum Electron.,***1998**, 30, 5355000

15 Conti, C.; Peccianti, M.; Assanto, G. *Phys. Rev. Lett.,***2004**, 92,113902

16 Mitchell, M.; Chen, Z.; Shih, M.; Segev, M. *Phys. Rev. Lett.,***1996**, 77, 3, 490

17 Christodoulides, D.N.; Coskun, T.H.; Joseph, R.I. *Opt. Lett.,***1997**, 22,14,1080

18 Christodoulides, D.N.; Coskun, T.H. *Phys. Rev. Lett.,***1997**, 78,4,646

19 Mitchell, M.; Segev, M.; Coskun, T.H.; Christodoulides, D.N. *Phys. Rev. Lett.,***1997**, 79,25,4990

20 Shkunov, V.V.; Anderson, D.Z. *Phys. Rev. Lett.,***1998**, 81,13,2683

21 Snyder, A.W.; Mitchell, D.J. *Phys. Rev. Lett.,***1998**, 80,7,1422

22 Segev, M.; Christodoulides, D. N. *Optics and Photonics News,***2002**, 13, 2, 70

23 Snyder, A. W.; Mitchell, D. J.; Kivshar, Y. S. *Mod.Phys. Lett. B,* **1995**, 9, 1479

24 Snyder, A. W.; Hewlett, S. J.; Mitchell, D. J. *Phys. Rev. Lett.,***1994**, 72, 1012

25 Lisak, M.; Helczynski, L.; Anderson, D. *Opt. Commun.,***2003**, 220, 321

26 Christodoulides, D.N.; Coskun, T.H.; Mitchell, M.; Segev M. *Phys. Rev. Lett.,***1998**, 83,11,2310

27 Królikowski, W.; Edmundson, D.; Bang, O. *Phys. Rev. E,***2000**, 61,3,3122

28 Christodoulides, D.; Eugenieva, E.; Coskun, T.; Segev, M.; Mitchell, M., *Phys. Rev. E,* **2001**, 63, 035601

29 Peccianti M.; Assanto, G. *Phys. Rev. E,***2002**, 65, 035603(R)

30 Shen, M.; Wang, Q.; Shi, J.; Hou, P.; Kong Q. *Phys. Rev. E,***2006**, 73, 056602

31 Buljan, H.; Segev, M.; Soljačić, M.; Efremidis, N.K.; Christodoulides, D.N. *Opt. Lett.,***2003**, 28,14,1239

32 Buljan, H.; Schwartz T.; Segev, M.; Soljačić, M.; Christodoulides, D.N. *J. Opt. Soc. Am. B,***2004**, 21, 2, 397

33 Buljan, H.; Šiber, A.; Soljačić, M.; Segev, M. *Phys. Rev. E,* **2002,** 66,3,035601

34 Buljan, H.; Šiber, A.; Soljačić, M.; Schwartz, T.; Segev, M.; Christodoulides D.N.*Phys. Rev. E,***2003**, 68, 3, 036607

35 Carvalho, M.I.; Coskun, T.H.; Christodoulides, D.N.; Mitchell, M.; Segev, M. *Phys. Rev. E,* **1999** 59,1,1193

36 Shen, M.; Shi, J.; Wang, Q. *Phys. Rev. E,***2006**, 74, 027601

37 *Elements of Photonics, Volume II: For Fiber and Integrated Optics*, Iizuka, K., John Wiley & Sons, Inc., New York, **2002**

38 Snyder, A.; Mitchell, D. *Science*,**1997**, 276, 1538

39 Shi-Gen, O.; Qi, G.; Sheng, L.; Li-Jun, W., *Chinese Phys. Lett.*, **2007**, 16, 8, 2325

40 Henninot, J. F.; François, J. F.; Warenghem, M. *J. Opt. A Pure Appl. Opt.*, **2007**, 9, 20

41 Hu, W.; Zhang, T.; Guo Q. *App. Phys. Lett.*, **2006**, 89, 071111

42 Blach, J. F.; Henninot, J. F.; Petit, M.; Daoudi, A.; Warenghem, M. *J. Opt. Soc. Am. B*, **2007**, 24, 5,1122

43 Kewitsch, A. S.; Yariv, A. *Opt. Lett.*, **1996**, 21, 1, 24

44 Taya, M., et. al., *Phys. Rev. A*, **1995**, 3095, 52

45 *Spatial Solitons,*Trillo, S.; Torruellas, W. Springer: New York, **2001**

46 Cohen, O.; Buljan, H.; Schwartz, T.; Fleischer, J. W.; Segev, M. *Phys. Rev. E*, **2006**, 73, 1, 015601

47 Coskun, H.; Christodoulides, D.N.; Segev, M. *Opt. Lett.*, **1998**, 23,6,418

48 Bronski, J. C.; Segev, M.; Weinstein, M. I. *PNAS*, **2001**, 98, 23, 12872

49 *Optical Waveguide Theory*, Snyder, A. W.; Love, J. D. Chapman, Hall, London, **1983**

50 Akhmediev, N.; Królikowski, W.; Snyder, A.W. *Phys. Rev. Lett.*, **1998**, 81,21,4632

51 Carmon, T.; Anastassiou, C.; Lan, S.; Kip, D.; Musslimani, Z. H.; Segev, M., *Opt. Lett.,***2000**, 25, 15, 1113

52 Ponomarenko, S. A. *Phys. Rev. E*, **2002**,65,5,055601

53 Katz, O.; Carmon, T.; Segev, M.; Christodoulides, D. N. *Opt. Lett.*, **2004**, 29, 11, 1248

54 Eugenieva, D.; Christodoulides, D.N.; Segev, M. *Opt. Lett.*, **2000**, 25, 13, 972

55Ankiewicz, A.; Królikowski, W.; Akhmediev N. N. *Phys. Rev. E*, **1999**, 59,5,6079

56 Coskun, H.; Christodoulides, D.N.; Segev, M. *Phys. Rev. Lett.*, **2000**, 84,2374

57 Makris, K. G.; Sarkissian, H.; Christodoulides, D. N.; Assanto, G..,*Quant. Electron. and Laser Sci. Conf. (QELS)*, **2005,** 1, 395

58 Chen, Z.; Mitchell, M.; Segev, M.; Coskun, T. M.; Christodoulides, D. N., *Science*, **1998**, 280, 889

59 Christodoulides, D.N.; Coskun, T.H.; Mitchell, M.; Chen, Z.; Segev, M. *Phys. Rev. Lett.*, **1998,** 80, 23, 5113

60 Kip, D.; Soljacic, M.; Segev, M.; Eugenieva, E.; Christodoulides, D.N. *Science*, **2000**, 290, 495

61 Schwartz, T.; Carmon, T.; Buljan, H.; Segev, M. *Phys. Rev. Lett.*, **2004**, 93, 22, 223901

62 Chen, Z.; Asaro, M.; Ostroverkhova, O.; Moerner, W. E.; He, M.; Twieg, R. J.,*Opt. Lett.,***2003**, 28, 24, 2509

63 Zhang, J.; Kasala, K.; Rewari, A.; Saravanamuttu K. *J. Am. Chem. Soc.,***2006**, 128, 406

64 Zhang, J.; Sakalauskas, M.; Kasala, K.; Saravanamuttu, K. *Polymer Materials Science and Engineering Preprints*, **2006**, 95, 875

65 Zhang, J.; Saravanamuttu, K. *J. Am. Chem. Soc*., **2006**, 128, 14913

66 Villafranca, A. B.; Saravanamuttu, K *J. Phys. Chem. C*, **2008**, 112, 44, 17388

67 Monro, T. M.; de Sterke, C. M.; Poladian, L. *Opt. Commun.*,**1995**, 119, 523

68 Monro, T. M.; de Sterke, C.M.; Poladian, L. *J. Opt. Soc. Am. B*, **1996**, 13, 2824

69 Monro, T. M.; Poladian, L.; Sterke, C. M. d., *Phys. Rev. E*, **1998**, 57, 1, 1104

70 Kewitsch, A. S.; Yariv, A. *Appl. Phys. Lett*., **1996**, 68, 455

71 Soppera, O.; Barghorn, C.C. ; Lougnot, D.J. *New J. Chem.*, **2001**, 25, 1006

72 Degirmenci, M.; Onen, A.; Yagci, Y.; Pappas, S. P.,*Polymer Bulletin,***2001,** 46, 443

73 Dulay, M. T.; Choi, H. N.; Zare, R. N., *J. Sep. Sci*., **2007**, 30, 2979

74 Saravanamuttu K.; Andrews M. P. *Chem. Mater*., **2003**,15,025652w,14

75 Chung, Y.; Dagli, N. *IEEE J. Quantum Electron*., **1990**, 26,1335

76 Sun, L.; Yip, G. L. *Opt. Lett*. , **1993**, 18, 1229

77 Bachelot, R.; Ecoffet, C.; Deloeil, D.; Royer, P.; Lougnot, D.-J.*Appl. Opt.,***2001**, 40, 32, 5860

78 Hocine, M.; Fressengeas, N.; Kugel, G.; Carré, C.; Lougnot, D. J.; Bachelot, R.; Royer, P., *J. Opt. Soc. Am. B,* **2006**, 23, 4, 611

79 Achilias, D. S.; Kiparissides' C. *Macromolecules,* **1992**, 25, 3739

80 Zhao, G.; Mouroulis, P. *J. Modern Opt.,* **1994**, 41, 10, 1929

81 Sheridan, J. T.; Downey, M.; O'Neill, F. T. *J. Opt. A: Pure Appl. Opt.,* **2001**, 3, 477

82 Kelly, J.; Gleeson, M.; Close, C.; O'Neill, F.; Sheridan, J.; Gallego, S.; Neipp, C.,., *Opt. Exp.,***2005**, 13, 18,6990

83 Wu, S. D.; Glytsis, E. N., J. Opt. Soc. Am. B, **2004**, 21, 1722

84 Mitchell, M.; Segev, M.; Christodoulides, D.N. *Phys. Rev. Lett.*, **1998**, 80, 21, 4657

85 Segev, M. *Optical and Quantum Electronics*, **1998**, 30, 503

86 Tikhonenko, V.; Christou, J.; Luther-Davies, B. *Phys. Rev. Lett.*, **1996**,76, 2698

87 Garca-Quirino, G. S.; Iturbe-Castillo, M. D.; Vysloukh, V. A.; Sánchez-Mondragón, J. J.; Stepanov, S. I.; Lugo-Martinez, G.; Torres-Cisneros, G. E., *Opt. Lett.*, **1997**, 22, 154

88 Shih, M.; Segev, M.; Salamo G. *Phys. Rev. Lett.*, **1997**, 78,13,2551

89 Shih M.; Segev M. *Opt. Lett.*,**1996**, 21, 1538

90 Stegeman, G.I.; Segev, M. *Science*, **1999**, 286, 1518

91 Gatz, S.; Herrmann, J. *IEEE J. Quantum Electron*, **1992**,28, 1732

92 Krolikowski, W.; Holmstrom, S. A. *Opt. Lett.*, **1997**,22, 369

93 Snyder, A. W.; Sheppard, A. P. *Opt. Lett*., **1993**, 18, 482

94 Krolikowski, W.; Luther-Davies, B.; Denz, C.; Tschudi, T. *Opt. Lett.*, **1998**,23, 97

95 Stepken, A.; Belic´, M. R.; Kaiser, F.; Królikowski, W.; Luther-Davies, B.., *Phys. Rev. Lett.*, **1999**, 82, 3, 540

96 Rasmussen P. D.; Bang, O.; Królikowski, W. *Phys. Rev. E*, **2005**, 72, 066611

97 Ye, F.; Kartashov, Y. V.; Torner, L., *Physical Review A*, **2007**, 76, 033812

98 Buryak, A. V.; Kivshar, Y. S.; Shih, M.-f.; Segev, M., *Phys. Rev. Lett.*, **1999**, 82, 1, 81

99 Krolikowski, W. *Appl. Phys. B*, **1999**, 68, 975

100 Guo, R.; Huang, C.; Liu, S. *J. Opt. A: Pure Appl. Opt.*, **2006**, 8, 695

101 Chun-Fu, H.; Qi, G.,*Chin. Phys. Lett*., **2007**, 24, 5,1279

102 Chun-Fu, H.; Guo, R.; Liu, S.M.; Liu, Z.H. *Opt. Commun.*, **2007**, 269, 174

103 Chun-Fu, H.; Guo, Q. *Opt. Commun*., **2007**, 277,414

104 Ku, T.; Shih, M.; Sukhorukov, A.A.; Kivshar, Y.S. *Phys. Rev. Lett.*, **2005**, 94, 063904

105 Królikowski, W.; Saffman, M.; Luther-Davies, B.; Denz, C., *Phys. Rev. Lett.*, **1998**, 80, 15, 3240

106 Zhao-Hong, L.; Si-Min, L.; Ru, G.; Yuan-Mei, G.; Tao, S.; Nan, Z.; Di, Q..,*Chin. Phys. Lett.*, **2007**, 24, 2, 446

107 Cohen, O.; Uzdin, R.; Carmon, T.; Fleischer, J.; Segev, M.; Odoulov, S. *Phys. Rev. Lett.*, **2002**, 89, 13, 133901

108 Johansen, S.K.; Bang, O.; Sørensen, M. P. *Phys. Rev. E*, **2002**, 65, 2, 026601

109 Rotschild, C.; Cohen, O.; Manela, O.; Carmon, T.; Segev, M. *J. Opt. Soc. Am. B*, **2004**, 21, 7, 1354

110 Aitchison, J. S.; Weiner, A. M.; Silberberg, Y.; Oliver, M. K.; Jackel, J. L.; Leaird, D. E.; Vogel, E. M.; Smith, P. W. E.,*Opt. Lett.*, **1990**, 15, 471

111 Zakharov, V. E.; Shabat, A. B. *Sov. Phys. JETP*, **1972**, 34, 62

112 Kelley, P. L. *Phys. Rev. Lett.*, **1965**, 15, 1005

113 Reynaud, F.; Barthelemy, A. *Europhys.Lett.*, **1990**,12, 401

114 Aitchison, J. S.; Weiner, A. M.; Silberberg, Y.; Leaird, D. E.; Oliver, M. K.; Jackel, J. L.; Smith, P. W. E.,*Opt. Lett.*, **1991**, 16, 15

115 Mitchell, D. J.; Snyder, A. W.; Polodian, L. *Opt. Commun.*, **1991**, 85, 59

116 Tikhonenko, V.; Chirstou, J.; Luther-Davies, B. *J. Opt. Soc. Am.*, **1995**, 12, 2046

117 Agarwal, G. P. *Phys. Rev. Lett.,***1990**, 64, 21, 2487

118 Chen, Z.; Segev, M.; Christodoulides, D. N. *J. Opt. A: Pure Appl. Opt.*, **2003**, 5S389

119 Christodoulides, D. N.; Singh, S. R.; Carvalho, M. I.; Segev, M. *Appl. Phys. Lett.*, **1996**, 68, 1763

120 Chen, Z.; Segev, M.; Conskun, T.H.; Christodoulides, D. N.; Kivshar, Y. S.; Afanasjev, V. V, *Opt. Lett.*, **1996**, 21, 22, 1821

121 Coskun, T. H.; Grandpierre, A. G.; Christodoulides, D. N.; Segev, M. *Opt. Lett.*, **2000**, 25, 826

122 Huang, C.-F.; Guo, R.; Liu, S.-M.; Zhu, N.; Wang, D.-Y.; Gao, Y.-M.; Lu, Y., *Optics Communications*, **2005**, 248, 4, 449

123 Morin, M.; Duree, G.; Salamo, G.; Segev, M. *Opt. Lett.,* **1995**, 20, 2066

124 Shih, M.; Chen, Z.; Mitchell, M.; Segev, M.; Lee, H.; Feigelson, R.; Wilde, J., J., *J. Opt. Soc. Am. B*, **1997**, 14, 3091

125 Shoji, S.; Kawata, S.; Sukhorukov, A. A.; Kivshar Y. S. *Opt. Lett.,* **2002**, 27, 3, 185

126 Dorkenoo, K.; Crégut, O.; Mager, L.; Gillot, F.; Carre, C.; Fort, A., *Opt. Lett.,* **2002**, 27, 20, 1782

127 Shoji, S.; Kawata, S. *Appl. Phys. Lett.,* **1999**, 75, 5, 737

128 Guo, A.; Henry, M.; Salamo, G. J.; Segev, M.; Wood, G. L., *Opt. Lett.,* **2001**, 26, 16, 1274

129 Klotz, M.; Crosser, M.; Guo, A.; Henry, M.; Salamo, G. J.; Segev, M.; Wood, G. L., *App. Phys. Lett.,* **2001**, 79, 10, 1423

130 Hirose, N.; Ibaragi, O. *IEEE Electronic Components and Technology Conference,* **2002**, 268

131 Segev, M.; Shih, M.; Valley, G. C. *J. Opt. Soc. Am. B*, **1996**, 13, 4, 706

132 DelRe, E.; Tamburrini, M.; Segev, M.; Pergola, R. D.; Agranat, A. J., *Phys. Rev. Lett.,* **1999**, 83, 10, 1954

133 Zakharov, V. E.; Shabat, A. B.; *Sov. Phys. JETP,* **1973**, 37, 823

134 Swartzlander, Jr., G. A.; Andersen, D. R.; Regan, J. J.; Yin, H.; Kaplan, A. E., *Phys. Rev. Lett.,* **1991**, 66, 12, 1583

135 Skinner S.R.; Allan, G. R.; Andersen, D. R.; Arthur, L., *IEEE J. Quant Electron.,* **1991**, 27, 9, 2211

136 Duree, G.; Morin, M.; Salamo, G.; Segev, M.; Crosignan, B.; Porto, P. D.; Sharp, E.; Yariv, A., *PhysRevLett.,* **1995**, 74, 11, 1975

137 Kivshar, Y.S.; Barry Luther-Davies, *Physics Reports,* **1998**, 298, 81

138 *Optical Solitons: From Fibers to Photonic Crystals,* Kivshar, Y.S.; Agrawal, G. P. Academic Press, London, **2003**

139 Kivshar, Y.S. *IEEE J. Quant. Electron.,* **1993**, 29, 1, 250

140 Snyder, A. W.; Mitchell, D. J.; Luther-Davies, B., *J. Opt.Soc.Am.B.*, **1993**, 10, 12, 2341

141 Chen Z.; Mitchell, M.; Shih, M.-f.; Segev, M.; Garrett, M. H.; Valley, G. C., *Opt. Lett.,***1996**, 21, 629; Chen, Z.; Segev, M.; Singh, S. R.; Coskun, T. H.; Christodoulides, D. N., *J. Opt. Soc. Am. B,* **1997**, 14, 1407

142 Castillo, M. D. I.; Sfinchez-Mondragon, J. J.; Stepanov, S. I.; Klein, M. B.; Wechsler, B. A., *Opt. Comm.,* **1995**, 118, 515

143 Jeng, C-C.; Shih, M.-F.; Motzek, K.; Kivshar, Y.., *Phys. Rev. Lett.,* **2004**, 92, 4, 043904-1

144 Dreischuh, A.; Neshev, D.; Petersen, D.; Bang, O.; Krolikowski, W., *Phys. Rev. Lett.,* **2006**, 96, 043901

145 Nikolov, N. I.; Neshev, D.; Królikowski, W.; Bang, O.; Rasmussen, J. J.; Christiansen, P. L., *Opt. Lett.,* **2004**, 29, 3, 286

146 Taya, M.; Bashaw, M. C.; Fejer, M. M.; Segev, M.; Valley, G. C., *Opt. Lett.,* **1996**, 21, 13, 943

147 Luther-Davies, B.; Yang, X. *Opt. Lett.,* **1992** , 17, 24, 1755

148 Chen, Z. *Opt. Lett.,* **1999**, 24, 16, 1160

149 Mamyshev, P. V.; Bosshard, C.; Stegeman, G. I.., *J. Opt. Soc. Am. B,***1994**, 11, 7, 1254

150 Zhang, X.; Liu, S.; Guo, R.; Gao, Y.; Wang, D.; Liu, Z.; Lu, Y., *Opt. Comm*., **2005**, 252, 84

151 Kennedy, S. R.; Brett, M. J.; Toader, O.; John, S. *Nano Lett*., **2002**, 2, 59

152 Cheng, C. C.; Scherer, A. *J. Vac. Sci. Technol. B*, **1995**, 13, 2696

153 Vlasov, Y. A.; Bo, X. Z.; Sturm, J. C.; Norris, D. J. *Nature*, **2001**, 414, 289

154 Blanco, A.; Chomski, E.; Grabtchak, S.; Ibisate, M.; John, S.; Leonard, S. W.; Lopez, C.; Meseguer, F.; Miguez, H.; Mondia, J. P.; Ozin, G. A.; Toader, O.; Driel, H. M. v., *Nature*, **2000**, 405, 437

155 Aoki, K.; Miyazaki, H. T.; Hirayama, H.; Inoshita, K.; Baba, T.; Shinya, N.; Aoyagi, Y..,*Appl. Phys. Lett*., **2002**, 81, 17, 3122

156 Fleming, J. G.; Lin, S. Y. *Opt. Lett.* , **1999**, 24, 49

157 Johnson, S. G.; Joannopoulos, J. D. *Appl. Phys. Lett.* **2000**, 77, 3490

158 Qi, M.; Lidorikis, E.; Rakich, P. T.; Johnson, S. G.; Joannopoulos, J. D.; Ippen, E. P.; Smith, H. I., A., *Nature*, **2004**, 429, 538

159 Campbell, M.; Sharp, D. N.; Harrison, M. T.; Denning, R. G.; Turberfield, A. J. *Nature*, **2000**, 404, 53

160 Yablonovitch, E.; Gmitter, T. J.; Leung, K. M. *Phys. Rev. Lett*., **1991**, 67, 2295

161 Noda, S.; Tomoda, K.; Yamamoto, N.; Chutinan, A. *Science*, **2000**, 289, 604

162 Jiang, P.; Bertone, J. F.; Hwang, K. S.; Colvin, V. L. *Chem. Mater*., **1999**, 11, 2132

163 Yin, Y.; Lu, Y.; Gates, B.; Xia, Y. *J. Am. Chem. Soc*., **2001**, 123, 8718

164 Yi, G.; Manoharan, V. N.; Michel, E.; Elsesser, M.; Yang, S.; Pine, D. *J. Adv. Mater*, **2004**, 16, 14, 1204

165 Zhihong, N.; Kumacheva, E. *Nature Materials*, **2008**, 7, 277

166 Srinivasarao, M.;Collings, D.; Philips, A.; Patel, S. *Science*, **2001**, 292, 79

167 Schaffer, E.; Thurn-Albrecht, T.; Russell, T. P.; Steiner, U. *Nature*, **2000**, 403, 874

168 Li, M.; Kumacheva, E. *Langmuir*, **2000**, 16, 7275

169 Efremidis, N. K.; Sears, S.; Christodoulides, D. N.; Fleischer, J. W.; Segev, M. *Phys. Rev. E*, **2002**, 66, 046602

170 *Nonlinear Optics and Applications* (Eds: H. A. Abdeldayem, D. O. Frazier), Ch. 5, Chen, Z.; Yang, J., Research Signpost, Trivandrum, Kerala, India, **2007**

171 Neshev, D.; Ostrovskaya, E.; Kivshar, Y. S.; Krolikowski, W. *Opt. Lett.*, **2003**, 28, 710

172 Fleisher, J. W.;Segev, M.;Efremidis, N. K.;Christodoulides, D. N.,*Nature (London)*,**2003**, 422, 147

173 Alvarado-Méndez, E.; Trejo-Durán, M.; Cano-Lara, M.; Huerta-Mascotte, E. *Appl. Phys. Lett.*, **2007**, 91, 191101

174 Neshev, D. N.;Sukhorukov, A. A.; Mitchell, A.;Rosberg, C. R.; Fischer, R.;Dreischuh, A.;Krolikowski, W.;Kivshar, Y. S. *Proc. of SPIE*, **2007**,6604, 66041B-1

175 a) Desyatnikov, A. S.; Ostrovskaya, E.; A. Kivshar, Y. S.; Denz, C. *Phys. Rev. Lett.*, **2003**, 91, 153902 ;
b) Martin, H.; Eugenieva, E. D.; Chen, Z.; Christodoulides, D. N. *Phys. Rev. Lett.*, **2004**, 92, 123902

176 Petter, J.; Schröder J.; Träger, D.; Denz, C. *Opt. Lett.*, **2003**, 28, 438

177 Desyatnikov, A. S.;Neshev, D. N.; Fischer, R.;Krolikowski, W.;Sagemerten, N.;Träger, D.;Denz, C.;Dreischuh, A.;Kivshar, Y. S. *Proc. of SPIE*, **2005**, 6023, 60230H-1

178 Chen, Z.; MaCarthy, K. *Opt. Lett.*, **2002**, 27, 2019

179 Desyatnikov, A. S.; Sagemerten, N.; Fischer, R.;Terhalle, B.; Träger, D.;Neshev, D. N.; Dreischuh, A.; Denz, C.;Krolikowski, W.; Kivshar, Y. S. *Opt. Exp.*, **2006**, 14, 7, 2851

180 Burgess, I.; Saravanamuttu, K. *J. Am. Chem. Soc.*, **2007**, 129, 15, 4738

181 Burgess, I.; Ponte, M.; Saravanamuttu, K. *J. Mater. Chem.*, **2008**, 18, 4133

182 Cohen, O.;Bartal, G.;Buljan, H.; Carmon, T.; Fleischer, J. W.;Segev, M.;Christodoulides, D. N. *Nature*, **2005**, 433, 3, 500

183 Martin, H.;Eugenieva, E. D.; Chen, Z.;Christodoulides, D. N. *Phys. Rev. Lett.*, **2004**, 92, 1226

184 Neshev, D.;Kivshar, Y. S.; Martin, H.; Chen, Z. *Opt. Lett.*, **2004**, 29, 486

185 Fleischer, J.W Carmon, T.;Segev, M.;Efremidis, N. K.;Christodoulides, D. N. *Phys. Rev. Lett.* , **2003**, 90, 023902

186 Bartal, G.;Manela, O.; Cohen, O.; Fleischer, J. W.;Segev, M. *Phys. Rev. Lett.*, **2005**, 95, 053904

187 Yang, J.;Makasyuk, I.;Kevrekidis, P. G.; Martin, H.;Malomed, B. A.;Frantzeskakis, D. J.; Chen, Z. *Phys. Rev. Lett.*, **2005**, 94, 113902

188 Pezer, R.;Buljan, H.;Bartal, G.;Segev, M.; Fleischer, J. W. *Phys. Rev. E*, **2006**, 73, 056608

189 Chen, Z.; Martin, H.;Bezryadina, A.;Neshev, D. N.;Kivshar, Y. S.;Christodoulides, D. N. *J. Opt. Soc. Am. B*, **2005**, 22, 1395

190 Wada, M.; Doi,Y.; Inoue, K.; Haus, J.W. *Phys. Rev. B,***1997**, 55, 10443

191 *Photonic Crystals:Molding the Flow of Light,*Joannopoulos, J. D.; Robert, D. M.; Joshua, N. W. Princeton University Press, **1995**

192 Kohn, W.; Rostoker, N. *Phys. Rev.*, **1954**, 94, 1111

193 Pendry, J.B.; MacKinnon, A. *Phys. Rev. Lett.*, **1992**, 69, 2772

194 *Computational electrodynamics :The finite-Difference Time-Domain Method,*2nd Edn,Taflove, A.; Hagness, S.C. Artech House, Boston, **2000**

195 *Quantum Theory of the Solid State,*Callway, J., Part B, NY, Academic Press, **2001**

196 Amemiya, K.; Ohtaka, Y. *J. Phys. Soc. Jpn*, **2003**, 72, 1244

197 Johnson, S.; Villeneuve, P.R.; Fan, S.; Joannopoulos, J.D.; *Phys. Rev. B*, **2000**, 62, 8212

198 Ho, K. M.; Chan, C. T.; Soukoulis, C. M. *Phys. Rev. Lett.*,**1990**, 65, 3152

199 Knight, J.C. *Nature*, **2003**, 424, 847

200 Yang, S.; Zhang, Y.; Peng, X.; Lu, Y.; Xie, S.; Li, J.; Chen, W.; Jiang, Z.; Peng, J.; Li, H., *Opt. Exp.*, **2006**, 14, 7, 3015

201 Knight, J.C.; Arriaga, J.; Birks, T. A.; Ortigosa-Blanch, A.; Wadsworth, W. J.; Russell, P. S. J., *IEEE Photon. Technol. Lett.*, **2000**, 12, 807

202 Kivshar, Y. S.; Yang, X. *Phys. Rev. E,***1994**, 50, R40

203 Baluschev, S.;Dreischuh, A.;Velchev, I.;Dinev, S.;Marazov, O. *Appl. Phys. B*, **1995**, 61, 121

204 Theocharis, G.;Frantzeskakis, D. J.;Kevrekidis, P. G.;Malomed, B. A.;Kivshar, Y. S.;*Phys. Rev. Lett.*, **2003**, 90, 120403

205 Kevrekidis, P.G.;Frantzeskakis, D.J.*Modern Physics Letters B*, **2004**, 18, 173

206 Definition of noise

207 Zabusky, N. J.; Kruskal, M. D., *Phys. Rev. Lett.*, **1965**, 15, 6, 240

208 Kang, J. U. ; Stegeman, G. I.; Aitchison, J. S.; *Opt. Lett.* 1996, 21, 189

209 Shalaby, M.; Reynaud, F.; Barthelemy, A.; *Opt. Lett.,* **1992**, 17, 778

210 *Transverse-Pattern Formation in Photorefractive Optics*, Denz, C;. Schwab M.; Weilnau, C.;.Springer Tracts in Modern Physics, Springer-Verlag Berlin Heidelberg, **2003**, 188, pp. 113-136

211 Meng, H.; Salamo, G.; Shih, M.-f.; Segev, M., *Opt. Lett.* **1997**, 22, 7, 448

212 Shih, M.; Chen, Z.; Segev, M.; Coskun, T.; Christodoulides, D. N., *Appl. Phys. Lett.,* **1996**, 69, 4151

213 Belić, M. R.; Stepken, A.; Kaiser, F. *Phys. Rev. Lett.* **1999**, 82, 544

214 Stepken, A.; Kaiser, F.; Belic, M. R.; Krolikowski, W., *Phys. Rev. E* , **1998**, 58, R4112

215 Ponomarenko, S. A.; Litchinitser, N. M.; Agrawal, G. P.; *Phys. Rev. E,* **2004,** 70, 015603

216 Pezer, R.; Buljan, H.; Fleischer, J.; Bartal, G.; Cohen, O.; Segev, M., *Opt. Exp.* **2005,** 13, 5013

217 Huang, C.-F.; Guo, R.; Liu, S.-M.; Liu, Z.-H., *Opt. Commun.* **2007,** 269, 174

218 Because the spatial coherence length of each beam was ~300 nm, 2 orders of magnitude smaller than the beam width or Δx.

219 *Principles of Optics,* Born M.; Wolf, E., Electromagnetic theory of propagation, interference and diffraction of light, 7th Edition, Cambridge University Press, UK., **1999**, Ch. 7

220 Lougnot D-J. ; Turck, C.; Helvetica Chimica Acta, **2002**, 85, 115

221 Zohrabyan, A.; Tork, A.; Birabassov, R.; Galstian, T., *Appl. Phys. Lett.,* **2007**, 91, 111912

222 Su, W. P.; Schrieffer, J. R.; *PNAS*, **1980**, 77, 5626

223 Tretiak, S.; Saxena, A.; Martin, R. L.; *PNAS,* 100, **2003**, 2185

224 Tuckwell, H. C. *Science*, **1979**, 205, 493

225 Careri, G.; Wyman, J. *PNAS*, **1984**, 81, 4386

226 Davydov, A. S. *J. Theor. Biol.*, **1979,** 66, 37

227 Heimburg, T.; Jackson, A.D., *PNAS,* **2005,** 102, 9790

228 Aslanidi, O.V. ; Mornev, O.A. *J. Biol. Phys.,* **1999**, 25, 149

229 Spadoni, A.; Daraio, C. *PNAS,* **2010,** 107, 7230

230 Witman, J. D.; Leichter, J. J.; Genovese, S. J.; Brooks, D. A. *PNAS,* **1993**, 90, 1686

231 Porter, A.; Smyth, N. F.; *J. Fluid Mech*., **2002**, 454, 1

232 Pokhotelov, O. A.; Onishchenko, O. G.; Balikhin, M.A.; Stenflo, L.; Shukla, P. K. *J. Plasma Phys.,* **2007**, 73, 981

233 *Nonlinear waves, solitons and chaos,* Infeld, E.; Rowlands, G., Cambridge University Press, **1990**

234 Proukakis, N. P.; Parker, N. G.; Frantzeskakis, D. J.; Adams, C. S. *J. Opt. B: Quantum Semiclassical Opt.* **2003**, 6, S380

235 Solli, D. R.; Ropers, C.; Koonath P.; Jalali, B. *Nature,* **2007**, 450, 1054

236 Kibler, B.; Fatome, J.; Finot, C.; Millot, G.; Dias, F.; Genty, G.; Akhmediev, N.; Dudley, J. M. *Nature Physics,* **2010**, 6, 790

237 Li, Y.; Krinsky, S.; Lewellen, J. W.; Kim, K-J.; Sajaev, V.; Milton, S. V. *Phys. Rev. Lett.,* **2003**, 91, 243602

238 Rotschild, C.; Schwartz, T.; Cohen, O.; Segev, M. *Nat. Photonics,* **2008**, 2, 371

239 Kasala, K.; Saravanamuttu, K. *Appl. Phys. Lett.,* **2008**, 93, 051111

240 Saravanamuttu, K.; Du, X. M.; Najafi, S. I.; Andrews, M. P. *Can. J. Chem.,* **1998**, 76, 1717

241 Monro, T. M.; De Sterke, C. M.; Poladian, L. *J. Mod. Opt.,* **2001**, 48, 191

242 Vanag, V. K.; Epstein, I. R. *Science*, **2001,** 294**,** 835

243 Wu, N.; Russel, W. R. *Appl. Phys. Lett.,* **2005**, *86*, 241912

244 Schäffer, E.; Harkema, S.; Blossey, R.; Steiner, R. *Europhys. Lett.,* **2002**, *60*, 255

245 Dutcher, J. R.; Dalnoki-Veress, K.; Nickel, B. G.; Roth, C. B. *Macromol. Symp.,* **2000**, 159, 143

246 Schäffer, E.; Harkema, S.; Roerdink, M.; Blossey, R.; Steiner, U. *Macromolecules,* **2003,** *36,* 1645

247 Xu, S.; Kumacheva, E. *J. Am. Chem. Soc.*, **2002**, 124, 1142

248 Grilli, S.; Coppola, S.; Vespini, V.; Merola, F.; Finizio, A.; Ferraro, P. *Proc. Natl. Acad. Sci.,* **2011**, 108, 15106

249 Chen, Z.; Klinger, J.; Christodoulides, D. N. *Phys. Rev. E.*, **2002**, 66, 066601

250 Kasala, K.; Saravanamuttu, K. *J. Mater. Chem.*, **2012**, 22, 12281

251 Kasala, K.; Saravanamuttu, K., *J. Am. Chem. Soc.*, **2012**, 134, 14195

252 Kasala, K; Saravanamuttu, K., *Physics Review International:Advances in Novel Optical Materials and Devices(Invited),* 2012

253 Shimmell, W. E., M.Sc. thesis, McMaster University, 2009

254, M.; Segev, M.; Coskun, T.H.; Christodoulides, D.N.; Vishwanath, A. *Phys. Rev. Lett.,* **2000**, 84, 467

255 Kip, D.; Soljăcíc, M.; Segev, M.; Eugenieva, E.; Christodoulides, D. N, *Science*, **2000**, 290, 5491, 495

256 Levi, L.; Schwartz, T.; Manela, O.; Segev, M.; Buljan, H.; *Opt. Exp.,* **2008**, 16, 7818

257 E.Yablonovitch, *J. Opt. Soc. Am. B*, **1993,** 10, 2, 283

258 *Optical Waveguide Theory*, Snyder, A. W.; Love, J. D., Springer, **1983**

259 Shimmell, W.; Saravanamuttu, K.; Filamentation through MI with partially coherent light in a photopolymer, *Unpublished results;* Villafranca, A.; Saravanamuttu, K.; Filamentation through MI with partially coherent light in a photopolymer.

260 Özbay, E.; Tuttle, G.; McCalmont, J. S.; Sigalas, M.; Biswas, R.; Soukoulis, C. M.; Ho, K. M. *Appl. Phys. Lett.*, **1995**, 67, 14, 1969

261 Iwayama, Y.; Yamanaka, J.; Takiguchi, Y.; Takasaka, M.; Ito, K.; Shinohara, T.; Sawada, T.; Yonese, M. *Langmuir*, **2003**, 19, 4, 977

262 Pralle, M. U.; Moelders, N.; McNeal, M. P.; Puscasu, I.; Greenwald, A. C.; Daly, J. T.; Johnson, E. A.; George, T.; Choi, D. S.; El-Kady, I.; Biswas, R. *Appl. Phys. Lett.*, **2002,** 81, 25, 4685

263 Brown, E. R.; Parker, C. D.; Yablonovitch, E. *J. Opt. Soc. Am. B*, **1993**, 10, 2, 404

264 Cheng, S. D.; Biswas, R.; Ozbay, E.; McCalmont, S.; Tuttle, G.; Ho, K.M. *Appl. Phys. Lett.*, **1995**, 67, 23, 3399

265 Anderson, B. P.; Haljan, P. C.; Regal, C. A.; Feder, D. L.; Collins, L. A.; Clark, C. W.; Cornell, E. A. *Phys. Rev. Lett.*, **2001**, 86, 14, 2926

266 Kivshar, Y. S.; Stegeman, G. I.; *Optics & Photonics News*, **2002**, 60

267 Kagami, M.; Yamashita, T.; Yonemura, M.; Matsui, T., *IEICE TRANSACTIONS on Electronics*, **2007**, E90-C 5, 1061